To the Graduate Council:

I am submitting herewith a dissertation written by Ke Zhao entitled "An Integrated Approach to Performance Monitoring and Fault Diagnosis of Nuclear Power Systems." I have examined the final electronic copy of this dissertation for form and content and recommend that it be accepted in partial fulfillment of the requirements for the degree of Doctor of Philosophy, with a major in Nuclear Engineering.

Belle R. Upadhyaya

Major Professor

We have read this dissertation and
recommend its acceptance:

J.W. Hines

J.F. Wasserman

A.R. Ruggles

Accepted for the Council:

Anne Mayhew

Vice Chancellor and Dean of Graduate Studies

(Original Signatures are on file with official student records.)

An Integrated Approach to Performance Monitoring and Fault Diagnosis of Nuclear Power Systems

A Dissertation

Presented for the Doctor of Philosophy Degree

The University of Tennessee, Knoxville

Ke Zhao

May 2005

Dedication

This dissertation is dedicated to my wife Hui Li for her always inspiring me and encouraging me to reach higher in my career.

Acknowledgments

I want to thank all those who have helped me in completing the Doctor of Philosophy degree in Nuclear Engineering at the University of Tennessee, Knoxville. I am especially grateful to Dr. B. R. Upadhyaya, the dissertation advisor, for giving me the opportunity of graduate study at UT and for encouraging me technically and spiritually all through the dissertation research. I would also like to thank Dr. J. W. Hines, Dr. A. R. Ruggles, and Dr. J. F. Wasserman for their invaluable comments and suggestions as doctoral committee members.

In addition, I would like to thank Dr. H. L Dodds and Dr. B. R. Upadhyaya for providing me with graduate research assistantship all through my graduate study.

Abstract

In this dissertation an integrated framework of process performance monitoring and fault diagnosis was developed for nuclear power systems using robust data driven model based methods, which comprises thermal hydraulic simulation, data driven modeling, identification of model uncertainty, and robust residual generator design for fault detection and isolation. In the applications to nuclear power systems, on the one hand, historical data are often not able to characterize the relationships among process variables because operating setpoints may change and thermal fluid components such as steam generators and heat exchangers may experience degradation. On the other hand, first-principle models always have uncertainty and are often too complicated in terms of model structure to design residual generators for fault diagnosis. Therefore, a realistic fault diagnosis method needs to combine the strength of first principle models in modeling a wide range of anticipated operation conditions and the strength of data driven modeling in feature extraction. In the developed robust data driven model-based approach, the changes in operation conditions are simulated using the first principle models and the model uncertainty is extracted from plant operation data such that the fault effects on process variables can be decoupled from model uncertainty and normal operation changes. It was found that the developed robust fault diagnosis method was able to eliminate false alarms due to model uncertainty and deal with changes in operating conditions throughout the lifetime of nuclear power systems.

Multiple methods of robust data driven model based fault diagnosis were developed in this dissertation. A complete procedure based on causal graph theory and data reconciliation method was developed to investigate the causal relationships and the quantitative sensitivities among variables so that sensor placement could be optimized for fault diagnosis in the design phase. Reconstruction based Principal Component Analysis (PCA) approach was applied to deal with both simple faults and complex faults for steady state diagnosis in the context of operation scheduling and maintenance management. A robust PCA model-based method was developed to distinguish the differences between fault effects and model uncertainties. In order to improve the sensitivity of fault

detection, a hybrid PCA model based approach was developed to incorporate system knowledge into data driven modeling. Subspace identification was proposed to extract state space models from thermal hydraulic simulations and a robust dynamic residual generator design algorithm was developed for fault diagnosis for the purpose of fault tolerant control and extension to reactor startup and load following operation conditions. The developed robust dynamic residual generator design algorithm is unique in that explicit identification of model uncertainty is not necessary.

Finally, it was demonstrated that the developed new methods for the IRIS Helical Coil Steam Generator (HCSG) system. A simulation model was first developed for this system. It was revealed through steady state simulation that the primary coolant temperature profile could be used to indicate the water inventory inside the HCSG tubes. The performance monitoring and fault diagnosis module was then developed to monitor sensor faults, flow distribution abnormality, and heat performance degradation for both steady state and dynamic operation conditions.

This dissertation bridges the gap between the theoretical research on computational intelligence and the engineering design in performance monitoring and fault diagnosis for nuclear power systems. The new algorithms have the potential of being integrated into the Generation III and Generation IV nuclear reactor I&C design after they are tested on current nuclear power plants or Generation IV prototype reactors.

Table of Contents

Chapter 1

Introduction 1

1.1 Background 1
1.1.1 Lessons Learned from TMI-II Accident 1
1.1.2 Position of Utilities on Performance Monitoring 3
1.1.3 Role of Fault Diagnosis in Generation-IV Nuclear Power Plants 4
1.2 Overview of Fault Diagnosis Techniques 5
1.2.1 Common Terminology Used in Fault Diagnosis 5
1.2.2 History of Model-Based Fault Diagnosis 6
1.2.3 Progress of Model-Based Fault Diagnosis in Other Industries 7
1.2.4 Status of Model Based Fault Diagnosis in Nuclear Industry 11
1.2.5 Trends in Fault Diagnosis for Industrial Application 11
1.3 Objective of the Dissertation: the Integrated Approach to Performance Monitoring and Fault Diagnosis 12
1.3.1 The Architecture of the Integrated Approach 12
1.3.2 Robust Data Driven Model Based Fault Diagnosis of the Integrated Approach 15
1.4 Contributions of the Dissertation 16
1.5 Outline of the Dissertation 17

Chapter 2

Basic Theory of Model Based Fault Diagnosis 19

2.1 Introduction 19
2.2 System Representation 19
2.3 Concepts of Residual Generator Design 24
2.3.1 Residual Generation for Fault Detection 25

2.3.2 Residual Generation for Fault Isolation 27
2.4 Residual Generation Techniques 29
2.4.1 Observer Based Residual Generation 29
2.4.2 Parity Space Approach 31
2.4.2.1 Parity Space Approach for Static Systems 31
2.4.2.2 Parity Space Approach for Dynamic Systems 36
2.4.3 Parameter Estimation Approach 37
2.5 Residual Evaluation Techniques 38
2.6 Robust Data Driven Model Based Fault Diagnosis 40
2.6.1 Motivation 40
2.6.2 Robust Parity Space Approach to Fault Diagnosis 43
2.6.3 Estimation of Model Uncertainty 45
2.6.3.1 Determination of Model Uncertainty Vector 46
2.6.3.2 Determination of Model Uncertainty Distribution Matrix 46
2.7 Summary 48

Chapter 3

Modeling and Simulation of the IRIS Helical Coil Steam Generator System 49

3.1 System Description 49
3.2 Description of HCSG Heat Transfer Mechanism and a Novel Approach to Level Measurement 52
3.3 Development of HCSG Steady State Model 54
3.3.1 Computation Algorithms 55
3.3.2 Heat Transfer Correlations 57
3.3.3 Pressure Drop Correlations 58
3.4 Steady State Results 59
3.5 Development of HCSG Dynamic Model 62
3.5.1 Model Assumptions 63

3.5.2 Nodalization 64
3.5.3 Primary Side Heat Balance Equations 64
3.5.4 Tube Metal Heat Balance Equations 66
3.5.5 Secondary Side Balance Equations 67
3.5.6 HCSG Pressure Controller 73
3.6 HCSG Transient Results 75
3.7 Summary 78

Chapter 4

Sensor Placement Design 80

4.1 Guidelines for Sensor Placement 82
4.1.1 Sensor Placement for Control 82
4.1.2 Sensor Placement for Performance Monitoring and Fault Diagnosis 83
4.2 Sensor Placement Design for Process Fault Diagnosis 84
4.2.1 Graph Representation of a Process 85
4.2.1.1 Sign Directed Graph 85
4.2.1.2 Directed Graph 89
4.2.2 Sensor Placement for Process Fault Detection 90
4.2.2 Sensor Placement for Process Fault Isolation 93
4.3 Redundancy and Observability Analysis 94
4.3.1 Variable Classification for Linear Systems 96
4.3.2 Variable Classification for Bilinear Systems 100
4.4 Sensitivity Analysis for Sensor Placement 105
4.4.1 Data Reconciliation 105
4.4.2 Basic Algorithm of Data Reconciliation 106
4.4.3 Sensitivity Analysis Procedure 109
4.5 Gross Error Detection and Identification 111
4.5.1. Gross Error Detection 111
4.5.2 Fault Identification 112

4.5.3 Fault Estimation 114
4.6 Application to HCSG system 115
4.7 Summary 132

Chapter 5

Fault Diagnosis during Steady State Conditions 133

5.1 Introduction 133
5.2 Principal Component Analysis for Fault Diagnosis 134
5.2.1 Motivation of Statistical Modeling 135
5.2.2 PCA Algorithm 137
5.2.3 Selection of the Number of Principal Components 141
5.2.4 Fault Detection 145
5.2.4.1 T^2 Statistics 145
5.2.4.2 Q Statistics 146
5.2.4.3 Conditions for Fault Detectability 147
5.2.5 Fault Isolation 149
5.2.5.1 Classification Based Approach 150
5.2.5.2 Contribution Based Approach 153
5.2.5.3 Reconstruction Based Approach 154
5.3 Application to the IRIS HCSG Systems 156
5.3.1 Data Generation and Model Development 156
5.3.2 Results of Single Fault Detection and Isolation 161
5.3.3 Results of Dual Fault Detection and Isolation 165
5.4 Hybrid PCA Model Based Fault Diagnosis 166
5.4.1 Motivation 166
5.4.2 Constrained PCA Algorithm 169
5.4.3 Application to the HCSG System 176
5.5 Robust PCA Model Based Approach to Fault Diagnosis 179
5.5.1 Identification of Model Uncertainty 179

5.5.2 Robust PCA Based Fault Detection 181
5.5.3 Robust PCA Model Based Fault Isolation 185
5.5.4 Identification of Fault Distribution Matrix 189
5.5.5 Application to the HCSG System 191
5.6 Summary 196

Chapter 6

Fault Diagnosis during Transient Conditions 198

6.1 Introduction 198
6.2 Theory of Subspace Identification 199
6.2.1 Block Data Equations 200
6.2.2 Recovery of System Matrices from State Sequence 202
6.2.3 Extractability of Kalman State Sequence from Input-output Data 203
6.2.3.1 System Decomposition 203
6.2.3.2 Extraction of Kalman State Vector 204
6.2.3.3 Extraction of Kalman State Sequence 209
6.2.4 Orthogonal Projection Methods 210
6.2.5 Oblique Projection Methods 212
6.3 Robust Dynamic Fault Diagnosis Algorithm 217
6.3.1 Robust Dynamic Fault Detection Algorithm 219
6.3.2 One-Step Robust Dynamic Residual Generator Design 222
6.3.3 Robust Fault Isolation Algorithm 227
6.4 Application to the HCSG System 229
6.4.1 Data Generation and Subspace Identification 229
6.4.2 Robust Fault Detection Design 232
6.4.3 Robust Fault Isolation Design 235
6.5 Summary 239

Chapter 7

Summary, Conclusions, and Recommendations for Future Research 240

7.1 Summary and Conclusions 240
7.2 Recommendations for Future Research 242

References 245

Appendices 258

Appendix 1 Matlab Code for HCSG Steady State Simulation 259
Appendix 2 Matlab Code for HCSG Transient Simulation 265
Appendix 3 Matlab Code for HCSG Bilinear Data Reconcilation 271
Appendix 4 Matlab Code for HCSG linear Data Reconcilation 283
Appendix 5 Matlab Code for HCSG Reconstruction PCA based FDI 292
Appendix 6 Matlab Code for HCSG Hybrid PCA Based FDI 297
Appendix 7 Matlab Code for HCSG Robust Data Driven Model based FDI for Steady State Operation Conditions 301
Appendix 8 Matlab Code for HCSG Robust Data Driven Model based FDI for Dynamic Operation Conditions 306

Vita 311

List of Tables

Table 2.1. Incidence matrix design for fault isolation 27
Table 3.1. Model parameters and steady state performance of dynamic HCSG modeling. 75
Table 4.1. Fault effect matrix..... 120
Table 4.2. Bipartite matrix to determine the minimum set of sensors for fault isolation. 121
Table 4.3. G matrix based on bilinear variable classification..... 124
to determine the redundant relationship between the measured variables (Case A) 124
Table 4.4. G matrix based on linearized variable classification 124
to determine the redundant relationship between the measured variables (Case A) 124
Table 4.5. G matrix based on linearized variable classification 124
to determine the redundant relationship between the measured variables (Case B)..... 124
Table 4.6. Physical redundant sensor placement based on sensitivity study 126
Table 5.1. Cross correlation coefficients of the generated data..... 158
Table 5.2. Determination of the number of Principal Components..... 160
Table 5.3. Minimum detectable fault magnitudes for sensor fault detection..... 162
Table 5.4. Cosine of the angle between the fault directions projected onto the residual space..... 164
Table 5.5. Reconstruction of simultaneous sensor faults T3 and W7..... 165
Table 6.1. The FDI indices of bias type sensor faults..... 238

List of Figures

Figure 1.1. Classifications of model based fault detection and isolation approaches..... 8
Figure 1.2. The performance monitoring and fault diagnosis in the I&C system. 13
Figure 1.3. The conceptual architecture of the integrated approach. 13
Figure 1.4. Robust data driven model based fault diagnosis. 15
Figure 2.1. Diagram of model based fault diagnosis. 20
Figure 2.2. Fault diagnosis for a closed-loop control system. 20
Figure 3.1. IRIS integral design. 50
Figure 3.2. IRIS steam generator layout. 51
Figure 3.3. A schematic of one pair of steam generators..... 53
Figure 3.4. HCSG design parameters at full power condition. 53
Figure 3.5. Fluid temperature versus tube length at 100% full power. 60
Figure 3.6. Fluid heat transfer coefficients on the primary side and the secondary side at 100% full power. 61
Figure 3.7. Steam quality versus tube length at 100% full power. 61
Figure 3.8. Pressure drop versus the tube length on the secondary side at 100% power. 62
Figure 3.9. Schematic of the nodalization for a helical steam generator. 65
Figure 3.10. Schematic of the helical coil steam generator control system. 74
Figure 3.11 (a). Steam temperature open-loop responses due to feed water flow and hot leg temperature transients. 77
Figure 3.11 (b). Cold leg temperature open loop responses due to feed water flow and hot leg temperature transients. 77
Figure 3.12 (a). Steam temperature closed-loop responses due to feed water flow and hot leg temperature transients. 79
Figure 3.12 (b). Cold leg temperature closed-loop responses due to feed water flow and hot leg temperature transients. 79
Figure 4.1. Procedure of sensor placement design for fault diagnosis. 81
Figure 4.2. SDG graph of a simple feedback control loop. 86
Figure 4.3. UTSG water level control system..... 87

Figure 4.4. SDG graph of nuclear UTSG system. 89
Figure 4.5. An illustration of the improved Greedy search algorithm. 92
Figure 4.6. Example system for variable classification. 98
Figure 4.7. Sensitivity analysis using data reconciliation. 110
Figure 4.8. The Directed Graph of one pair of HCSG system. 117
Figure 4.9. Bipartite Graph of one pair of HCSG system. 118
Figure 4.10. Determine the minimum set of sensors for fault detection 118
Figure 4.11 (a). Fault detection of W2 measurement error with redundant measurement. 128
Figure 4.11 (b). Fault detection of W2 measurement error without redundant measurement. 128
Figure 4.12 (a). Fault reconstruction of W2 measurement error without redundant measurement 129
Figure 4.12 (b). Fault reconstruction of W2 measurement error with redundant measurement. 130
Figure 4.13. Bilinear data reconciliation result of HCSG secondary flow rate. 131
Figure 4.14. Bilinear data reconciliation result of heat transfer rate. 131
Figure 5.1. The ratio of the variance of reconstructed error to the variance of the original data. 161
Figure 5.2. Detection of a fault with the minimum detectable fault magnitude. 162
Figure 5.3. Tracking the progression of the uneven flow distribution fault. 163
Figure 5.4. Isolation of the uneven flow distribution fault. 164
Figure 5.5. Identification of simultaneous dual faults (W7 and T3 sensor faults) 166
Figure 5.6. Comparison of fault detection between traditional PCA and constrained PCA using column information. 174
Figure 5.7. Fault detection and isolation of y1 sensor fault based on constrained PCA using column information. 174
Figure 5.8. Fault diagnosis of y2 sensor fault with a bias of 1.5 based on constrained PCA using row information. 175

Figure 5.9. Component decomposition of constrained PCA analysis using column information. 177
Figure 5.10. Fault diagnosis of a T5 sensor fault with 0.25% bias based on constrained PCA using column information. 177
Figure 5.11. Component decomposition of constrained PCA analysis using row information. 178
Figure 5.12. Fault diagnosis of a T3 sensor fault with 0.25% bias using constrained PCA with the constraint W7=W12. 178
Figure 5.13. Fault direction of tube blockage fault. 192
Figure 5.14. Direction of model uncertainty due to thermal degradation. 193
Figure 5.15. Comparison of robust detection algorithm with traditional method. 194
Figure 5.16. Isolation of HCSG tube blockage process fault 195
Figure 5.17. Fault reconstruction of a T3 sensor bias fault with a magnitude of 1.7 C. 195
Figure 6.1. Robust fault detection for the example case during normal operation condition. 226
Figure 6.2. The singular values of the projection matrix. 231
Figure 6.3. Model prediction of cold leg temperature. 231
Figure 6.4. Robust fault detection for cold leg temperature sensor fault. 232
Figure 6.5. Fault detection of feed water flow meter sensor fault during a reactor power transient. 233
Figure 6.6. Fault detection of steam pressure sensor fault. 234
Figure 6.7. Fault isolation of feed water flow meter sensor fault during a reactor power transient. 236
Figure 6.8. Fault isolation of steam pressure sensor fault. 237

Chapter 1

Introduction

1.1 Background

Performance monitoring and fault diagnosis has received increased attention in nuclear power systems since the 1970s, when economics, reliability and safety, and sustainability became increasingly important. After the Three Mile Island Unit 2 (TMI-II) accident, the U.S. Nuclear Regulatory Commission (NRC) recognized the importance of Fault Detection and Isolation (FDI) to prevent accidents and avoid human errors for accident treatment. As nuclear deregulation becomes inevitable, utilities have to reconsider the implication of using condition-based maintenance technologies including modern fault diagnosis methods to reduce plant downtime and save maintenance cost. Generation IV nuclear power systems are also awaiting emerging technologies for operation performance improvement and fault diagnosis for use in their advanced Instrumentation and Control (I&C) systems.

1.1.1 Lessons Learned from TMI-II Accident

The importance of fault diagnosis to the safety of nuclear power systems can be considered as a lesson learned from TMI-II accident in 1979.

The TMI-II accident was initiated by the mechanical failure of the main reactor feed water pump. After the reactor was automatically shut down, the pressurizer relief valve was triggered to open due to the loss of heat sink. The accident began when the valve failed to close because after the reactor pressure was relieved the operators were not able to determine the status of the valve position due to the inadequate parameter display in the control room. In the meantime, the emergency feed water was not opened until about eight minutes into the accident because a valve on the line was not reopened after a maintenance test. As voids began to form in the core when the pressure continued

to decrease, the pressurizer became full of water. The operators were confounded again by the level indication and stopped the operation of high-pressure safety injection system. From this point on, an anticipated operation event evolved into a severe accident resulting in the partial core melt and a limited amount of release of radioactivity into the environment.

An immediate lesson learned from the TMI-II accident is that a computer based operator support system would play a critical role in maintaining safe operation of nuclear power plants. Not long after the accident, the Nuclear Regulatory Commission issued a regulatory guide that a minimum set of parameters defining the safety status must be adequately displayed in the control room of nuclear power plants (NUREG-0585, 1979). Since then, computer based operator support system has become a basic licensing requirement of nuclear power plants and many research tasks have been launched to develop automatic systems for alarm processing and for emergency operation (Choi, Chung, and Lee, 1998), (Jae and Moon, 2002), (Kim, Kwon., Hwang., Lee, Park, Kim, and Lee, 2001), (Park and Seong, 2002).

Although a computer based operator support system with improved parameter display and computerized alarm processing is able to help operators to avoid human errors for accident treatment, its efficiency to improve plant safety is still limited without a supporting FDI system. On the one hand, if a fault can be detected and rectified at its incipient stage before abrupt failures occur, the possibility of some accidents can actually be eliminated. On the other hand, because optimal alarms and emergency operations are a sensitive function of the abnormal events, especially at early stages of transients before reactor scram, correct identification of an abnormal transient is of paramount importance for computerized emergency operation. For this reason, many investigations were reported on the development of fault diagnosis methods for transient identification (Bartlett and Uhrig, 1992), (Ohga and Seki, 1993), (Kim and Bartlett, 1994).

1.1.2 Position of Utilities on Performance Monitoring

In the early 1980s, performance monitoring and fault diagnosis was introduced by the Electric Power Research Institute (EPRI) in the context of condition-based maintenance to improve the operational safety and the economic performance of nuclear power plants (EPRI NP-2240, 1982). Because the functional status of sensors, actuators, and field devices are monitored on line, this makes it possible to perform maintenance tasks only when it is necessary. As a result, significant reduction in plant downtime, considerable maintenance cost savings, and reduction in maintenance errors can be expected.

Condition based instrument monitoring has been considered as an important advancement for safety improvement and higher autonomy in the control function of nuclear power plants. Some sensors are indicators for plant monitoring and others are used for closed-loop control. The sensor faults of the first type may force reactor operators to derate the power level and thus degrade the operation performance. It is reported that venturi feed water flow meter fault due to fouling is causing the amount of derated power ranging from 1% to 3% full power for Pressurized Water Reactor (PWR) plants in the U.S. (Kavaklioglu and Upadhyaya, 1994), (Gribok, Attieh, Hines, and Uhrig, 1999). The sensor faults of the second type may propagate their effects to the regulated variables and subsequently disturb other process variables through feedback control loops. The deleterious consequence of such disturbances is that the related actuators and plant equipment would not be able to operate at the designed optimal conditions and their expected lifetime may be shortened. In addition, both types of sensor faults may mislead operators to take incorrect actions and cause safety problems if they occur during abnormal transients.

On-line equipment performance monitoring was also an initial incentive when condition based maintenance was introduced to nuclear power plants. As early as the 1980s, neutron noise analysis was successfully performed to measure the vibration of reactor internals, which is now able to reach a resolution better than 0.025 mm. The cross-correlation between the neutron flux and the core exit temperature was used to

characterize the reactor core flow rate and detect any flow anomaly such as flow blockages, flow shifting, and other problems (Hashemian, 1998), (Hashemian, 2002). On-line monitoring of the thermal efficiency of nuclear steam generators has now become an industrial practice for many nuclear power plants. Because of fouling, the decline of steam generator thermal efficiency may force the reactor to reduce the steam generator operating pressure lower than the designed value and cause a lower electric output per unit reactor thermal power. In order to overcome this issue, on-line steam generator performance evaluation is used to trend the behavior of the overall heat transfer coefficient and predict their future behavior as a function of the secondary water chemistry.

1.1.3 Role of Fault Diagnosis in Generation-IV Nuclear Power Plants

After the TMI-2 accident, the design of nuclear power plants experienced two major changes. As compared with Generation-II operating commercial nuclear reactors, Generation-III reactors represented by advanced light water reactors — ABWR, System 80+, AP1000 — are characterized by passive safety design and the use of digital technology such as software based controls and computerized operation procedures. Generation-III design is evolutionary in the sense that it anticipated only a moderate performance improvement over the current design such that the licensing would not incur substantial additional effort. In fact, as far as instrumentation and control (I&C) is concerned, software based control is utilized solely for non-safety related systems and little effort is invested in making full use of the contemporary digital and computer technologies.

In order to strategically improve the technology in nuclear power system design and broaden the opportunity of the peaceful use of nuclear energy, the U.S. Department of Energy prompted the development of Generation-IV nuclear reactors, with an emphasis on the advances in economics, safety and reliability, and sustainability (Savage, 2001). For Generation- IV nuclear power systems, it is expected that the I&C design will see a revolutionary innovation. For the better use of the emerging I&C technologies,

such as smart sensing, automated monitoring and diagnosis systems, and computer simulations, the technical requirements of Generation- IV I&C design have been defined as follows (O'Hara, 2002):

In order to welcome the challenges arising from deregulation, the plant economic parameters will be monitored on-line and optimized with the constraints that the related nuclear safety regulations are rigorously satisfied. On-line monitoring, fault diagnosis, and response simulation will be available to support real time operation and maintenance decision-making. A higher autonomy of control will be utilized to maximize the human-machine efficiency and reliability. Real time risk monitoring will be improved to optimize plant surveillance testing and maintenance such that the risk due to off-normal alignments can be minimized. A more efficient human-machine interface will be developed such that the plant personnel in the control room can conveniently obtain adequate information in a concise manner for all the related operation tasks.

As evidenced by the above technical requirements, process performance monitoring and fault diagnosis plays a central role in the Generation- IV I&C design. The fault diagnosis system needs to provide information about the health status of sensors, actuators, and plant equipment to the operator support system or the plant surveillance system in the control room, thus assisting operators in making operation and maintenance planning. Under certain circumstances, the fault diagnosis system also needs to interface with plant control systems to implement advanced control such as adaptive control and fault tolerant control.

1.2 Overview of Fault Diagnosis Techniques

1.2.1 Common Terminology Used in Fault Diagnosis

With the increasing interest in the research and application of fault diagnosis in a variety of fields, a technical committee SAFEPROCESS on Fault Detection, Supervision, and Safety for Technical Process, was established within IFAC (International Federation of Automatic Control) in 1993. This committee standardized the definitions of the

terminology used in fault diagnosis (Simani and Fantuzzi, 2002), which are duplicated for use in this dissertation.

Fault

An unacceptable deviation of at least one characteristic property or parameter of the system from the acceptable, usual, or standard condition.

Fault Detection

Determination of faults present in a system and the time of fault occurrence.

Fault Isolation

Determination of the kind, location, and time of the occurrence of a fault.

Fault Identification

Determination of the size and the time-varying behavior of a fault.

Fault Diagnosis

Determination of the kind, size, location, and the time of the occurrence of a fault. It includes fault detection and identification.

Monitoring

A continuous real-time task of determining the conditions of a physical system, by recording information, recognizing and indicating anomalies in the system behavior.

1.2.2 History of Model-Based Fault Diagnosis

The simplest fault diagnosis method is to monitor the magnitude and the trend of individual signals. If the magnitude exceeds the design limit or the trend deviates the expected behavior, a fault is then detected. Although this scheme is simple, it can only be applied to simple processes with the aid of experienced operators for fault isolation.

Hardware redundancy is a traditional fault diagnosis design method that uses more than two components such as sensors, actuators, controllers, and computers to perform the same function. If one component does not perform its function as designed, a voting logic and a switching mechanism can be employed to detect, identify, and isolate

the malfunctioned component. Hardware redundancy is widely used in safety critical systems such as nuclear power plants and aircrafts. The major problem with the hardware redundancy design is the extra equipment and maintenance cost in addition to the extra space.

Modern fault diagnosis is based on analytical redundancy provided by the functional relationships governed by physical laws in a process system. Instead of using hardware redundancy, functional relationships are used to cross check process variables. The simplest scheme of consistency checking is to compare the measured values with the estimated values obtained from redundant relationships. The difference is called *physical residual*, which can be used as a fault signature for fault detection and isolation. In the context of analytical redundancy, model based fault diagnosis is defined as a systematic approach to generate residual quantities and analyze the residual properties such that the potential faults can be detected, identified, and isolated.

A novel advantage of model based fault diagnosis is that no additional hardware is needed for fault detection and isolation. Because the redundancy provided by functional relationships has the same reliability as a processing computer, its reliability is much higher than traditional hardware redundancy. The most significant contribution of analytical redundancy to fault diagnosis, which many researchers do not stress, is that the generated fault signatures are fully decoupled from the operation conditions if the developed functional relationships can cover entire operation regime. Although analytical redundancy is nothing but a principle, an overwhelming advancement has been seen in the field of fault diagnosis since the original work of Beard at MIT (Beard, 1971) along with the increasing power of computer technology.

1.2.3 Progress of Model-Based Fault Diagnosis in Other Industries

Many model based fault diagnosis techniques have been developed in a variety of industries in the past two decades under the principle of analytical redundancy

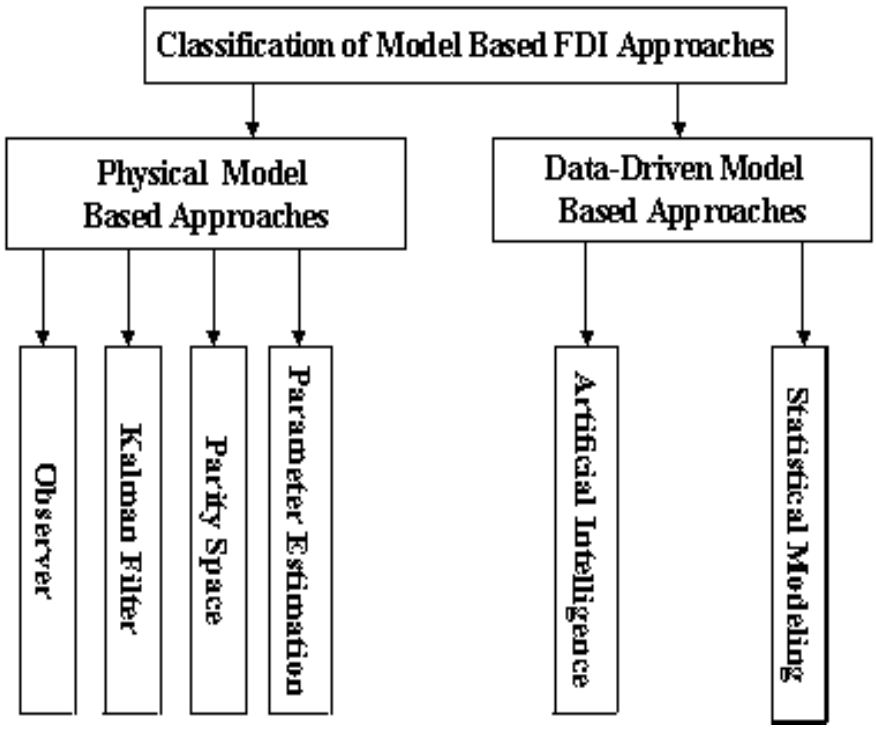

Figure 1.1. Classifications of model based fault detection and isolation approaches.

(Venkatasubramanian et al., 2003a, 2003b, 2003c). In a broad sense, these techniques can be classified according to what form of models are used. As shown in Figure 1.1, physical model based approaches use quantitative parametric models while data driven model based approaches use parametric or nonparametric models extracted from historic data.

The physical model based approaches were mainly investigated by control engineers in aircraft industry. Beard-Jones Fault Detection Filter was developed to generate directional residuals for fault diagnosis (Beard, 1971), (Jones, 1973). The innovation sequence generated by Kalman filter was tested on its statistical measures including the whiteness, mean and covariance for fault detection (Mehra and Peschon, 1971). The Generalized Likelihood Ratio Test (GLRT) on innovation sequence was used for fault diagnosis by Willsky and Jones, 1976. Sequential Probability Ratio Test (SPRT) was implemented by Upadhyaya for sensor incipient fault detection (Upadhyaya,

Wolvaardt, and Glocker, 1989). Multiple model adaptive filter approach based on multiple-hypothesis testing on the innovations generated by a bank of Kalman filters was proposed by Beric, 1998. Observer based fault diagnosis approach was first introduced to sensor fault detection and isolation by Clark, 1978. Parity space approach was proposed for fault diagnosis by Chow and Willsky, 1984. Parameter estimation approach was introduced for process fault diagnosis by Isermann, 1991a, and 1991b. A detailed description of these fault diagnosis methods, their industrial applications, and the performance comparison can be found in some recent survey papers by Frank, 2000, Isermann, 1997, Patton and Chen, 1997, and Patton and Chen, 1994. The robust issues of model based fault diagnosis were investigated by Chen and Patton via unknown input observers, eigen-structure assignment, optimal parity relations, and frequency domain design (Chen and Patton, 1999). The physical models used in model based fault diagnosis may take different forms including first-principle models such as macroscopic transport phenomena model (Himmelblau, 1978), input-output models (Gertler, 1998), and state space models (Chen and Patton, 1999) obtained from system identification through well-designed experiments (Ljung, 1999). Several signal validation methods were developed by Upadhyaya and his co-workers at The University of Tennessee (Erbay and Upadhyaya, 1997), (Holbert and Upadhyaya, 1990), (Holbert and Upadhyaya, 1994), (Upadhyaya, 1985), (Upadhyaya, 1987), (Upadhyaya, 1989), (Upadhyaya and Ferreira, 1999).

Data driven model based approaches were mainly developed by process engineers in chemical, refinery, and petrochemical industries. As digital technology becomes popular, thousands of measurements with strong spatial and serial correlations are routinely available. The principle of analytical redundancy motivated a better use of the redundant information contained in the historical data. The major data driven modeling techniques can be categorized as multivariate statistical modeling and artificial intelligence.

Principal Component Analysis (PCA) originated by Pearson, 1901, and Partial Least Squares (PLS) originated by Wold et al., 1984, are two most popular statistical modeling methods for process monitoring. The PCA approach to process monitoring was

investigated thoroughly by Qin's research group (Dunia, Qin, Edgar, and McAvoy, 1996a, 1996b) and the PLS approach to process monitoring was studied by MacGregor's group (Kresta, Marlin, and MacGregor, 1994). Qin and MacAvoy, 1992, proposed nonlinear PLS algorithms and Dong and MacAvoy, 1996, developed nonlinear PCA algorithm for fault diagnosis. The multiway PCA approach was developed by Nomikos and MacGregor, 1994, to monitor batch processes. In order to deal with a very large process, muiltiblock PLS algorithm was proposed by MacGregor et al., 1994. Discriminant analysis and PCA were combined by Raichand and Cinar, 1996, for better fault isolation. A survey of statistical model based process monitoring may be found in (Kourti and MacGregor, 1995), (Qin, 2002). The Group Method of Data Handling (GMDH) approach was developed for fault diagnosis of sensors and field devices (Upadhyaya et al., 1999, 2004).

Artificial Neural Networks (ANN) and Fuzzy Logic (FL) were studied for fault diagnosis in Artificial Intelligence community. The fault diagnosis was considered in the beginning simply as a classification problem using ANN classifiers (Watanabe et al., 1989). In order to explicitly reduce the feature space, Neural Networks were investigated as both a predictor and a classifier (Venkatasubramanian and Chan, 1989). Different Neural Network architectures were investigated to enhance the performance of modeling for fault diagnosis. Multi-layer feedforward Neural Networks with backpropagation training algorithms were used to develop static input-output characterizations (Venkatasubramanian et al., 1990). Recurrent Neural Network with neurons having intrinsic dynamic properties was used for dynamic fault diagnosis (Gan and Danai, 1999). Radial Basis Neural Network was introduced to fault diagnosis to address the issue of novelty identification (Simani and Fantuzzi, 2000). Self-Organizing Neural Networks represented by ART2 network were applied to fault diagnosis by Chen et al, 1998. A comparative study was performed (Ranaweera, 1994) for fault diagnosis with different Neural Network Structures. Physical model based fault diagnosis was compared with neural network-based fault diagnosis by Rengaswamy et al., 2001.

1.2.4 Status of Model Based Fault Diagnosis in Nuclear Industry

In parallel with other industries, analytical redundancy based FDI methods have also been extensively studied for nuclear power systems since three decades ago. Multivariate time series analysis, Neural Networks, and PCA were proposed for process monitoring and sensor fault diagnosis by Upadhyaya et al., 1980, 1992, 2001. The univariate and multivariate time series approach was successfully used to estimate the response time characteristics of thermometers (Hashemian et al., 1988), in-core flow dynamics (Sweeney, 1985), BWR stability (Upadhyaya and Kitamura, 1981), moderator temperature coefficient (Shieh et al., 1988), and sensor faults of PWR pressurizer subsystem (Upadhyaya and Skorska, 1984). Neural Network was applied to monitor the feed water flow rate and component thermal performance (Kavaklioglu and Upadhyaya, 1994). PCA was applied to detect and isolate nuclear plant sensors and actuator faults (Upadhyaya et al., 2003). Adaptive Neural Fuzzy Inference System (ANFIS) was proposed by Hines for sensor validation (Hines and Wrest, 1997). Multivariate State Estimation Technique was developed at Argonne National Laboratory (ANL) for process monitoring (Singer et al., 1996).

1.2.5 Trends in Fault Diagnosis for Industrial Application

Although many different fault diagnosis methods have been developed from various industries including nuclear power plants, there is no single method that is sophisticated enough to handle all the requirements for an engineering problem. The only pragmatic solution is to have a thorough investigation of the weaknesses of individual methods and build an application dependent method to fully utilize their strengths (Dash and Venkatasubramanian, 2000).

Except for a few, most researchers in fault diagnosis are paying more attention to the academic value than the engineering value. A hybrid of model based fault diagnosis and neural network was proposed by Hines, 1994. Bhushan et al., 2000, stressed the importance of instrument placement for maximal sensitivity of fault detection and best

resolution of fault isolation. Venkatasubramanian evaluated quantitative model based methods, qualitative model based methods, and historical data based methods for fault diagnosis with the conclusion that a hybrid approach is needed to overcome the limitations of individual methods (Venkatasubramanian et al., 2003a, 2003b, 2003c).

1.3 Objective of the Dissertation: the Integrated Approach to Performance Monitoring and Fault Diagnosis

The purpose of this dissertation is to develop appropriate procedures and methods of performance monitoring and fault diagnosis to improve the economics and safety of Generation-IV nuclear power systems. The developed performance monitoring and fault diagnosis system will be an integral part of the advanced digital I&C system as shown in Figure 1.2.

After digital control systems are used, a large amount of on-line measured data will be available on the field buses and the communication highway of nuclear power plants. The role of the developed performance monitoring and fault diagnosis system is to utilize the measured data to enhance the economics and safety of nuclear power plants. The information that can be obtained from the developed system will include the health status of sensors and actuators and the operation performance of critical components such as steam generators and reactor main pumps. On the one hand, this system will enable individual control loops to reset the setpoints to improve plant efficiency when operation performance degrades and to reconfigure the control actions when controlled variables have measurement faults. On the other hand, the obtained information can provide a technical basis for optimal maintenance management and optimal operation scheduling.

1.3.1 The Architecture of the Integrated Approach

An integrated approach to performance monitoring and fault diagnosis was developed in this dissertation research. Figure 1.3 illustrates the overall architecture of the integrated approach.

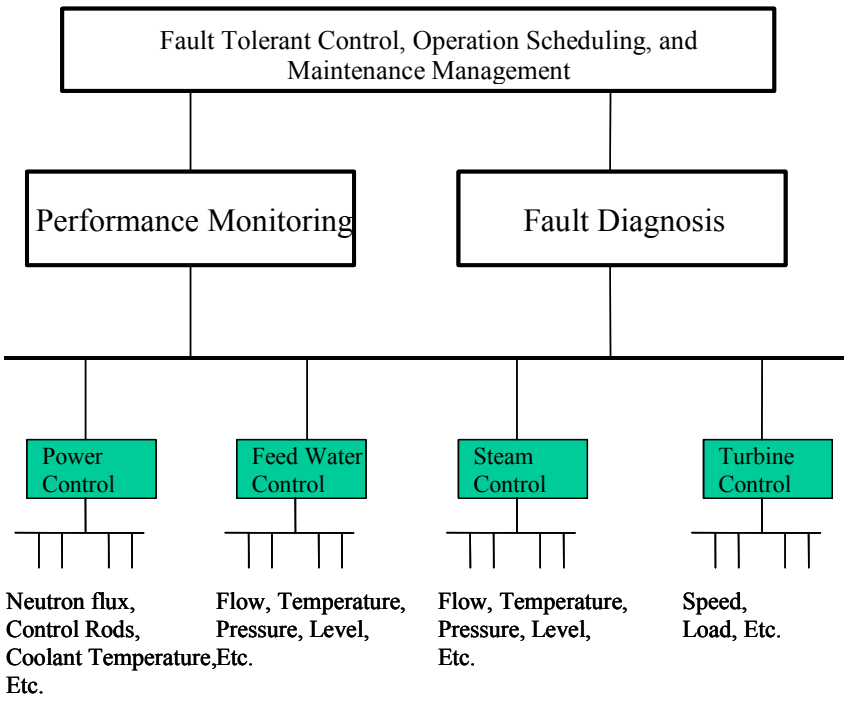

Figure 1.2. The performance monitoring and fault diagnosis in the I&C system.

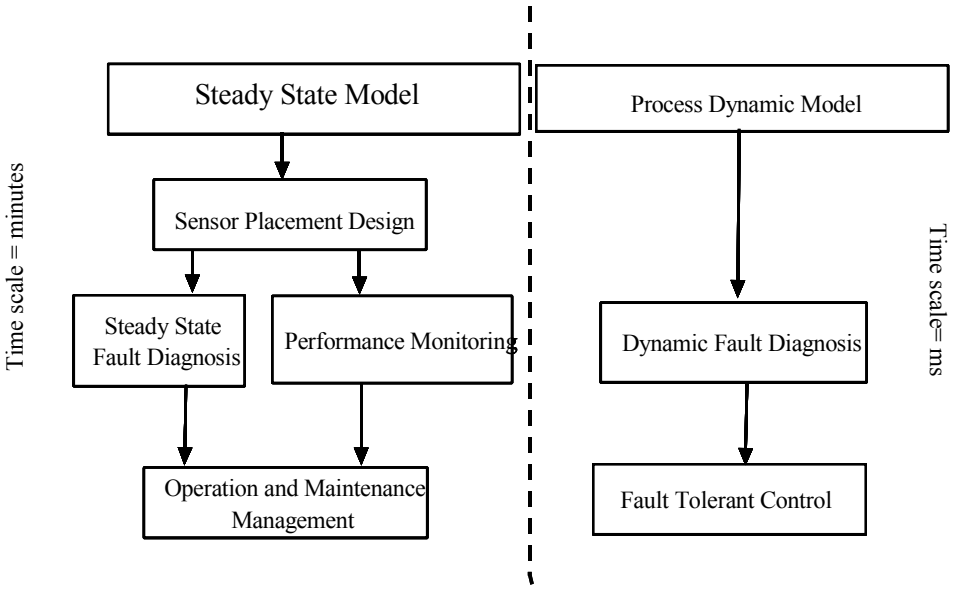

Figure 1.3. The conceptual architecture of the integrated approach.

The developed system consists of two paralleled subsystems shown in Figure 1.3. The subsystem based on steady state model such as plant-scale mass balance and heat balance equations are used to perform performance monitoring and steady state fault diagnosis. This subsystem provides plant monitoring in the time scale of minutes to days and is especially useful for operation scheduling and maintenance scheduling. For instance, the inferred values of measured variables based on balance equations can provide a basis for instrument calibration. The subsystem based on process dynamic models of individual components such as reactor core, pressurizer, steam generators, etc. is used to perform dynamic fault diagnosis. This subsystem is able to provide real time monitoring information during transient conditions, so it is appropriate for fault tolerant control.

The sensor placement design is emphasized in the developed integrated approach shown in Figure 1.3. In nuclear power systems, the consequence of an incorrect decision on fault diagnosis may be so adverse that the public cannot even accept a very low probability. For this reason, a fault diagnosis engineering system must be able to give reliable FDI results. Although the capability of an FDI system is method dependent, it is a much more sensitive function of sensor placement. Therefore, it is necessary to incorporate fault diagnosis into the instrumentation design phase.

Based on the presented architecture, the design of a performance monitoring and fault diagnosis system can be achieved by the following tasks:

1. Develop plant-scale steady state mass balance and heat balance models and dynamic simulation models for the control loops of nuclear power plants.
2. Determine the sensor placement requirements for efficient performance monitoring and fault diagnosis.
3. Develop steady state fault diagnosis algorithms for both sensor and process fault diagnosis.
4. Develop dynamic fault diagnosis algorithms, which are applicable to dynamic operation conditions such as reactor startup and load following.
5. Test the performance on the developed simulation models.

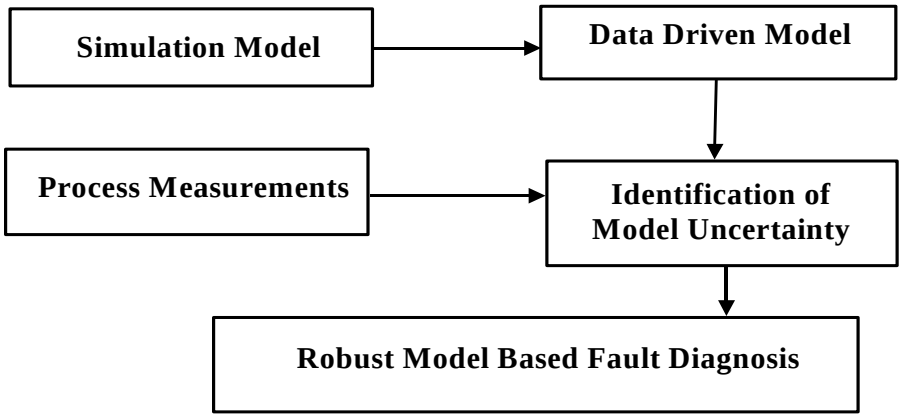

Figure 1.4. Robust data driven model based fault diagnosis.

1.3.2 Robust Data Driven Model Based Fault Diagnosis of the Integrated Approach

A robust data driven model based approach was developed in this dissertation to implement the presented architecture of performance monitoring and fault diagnosis. In this approach, shown in Figure 1.4, data are generated from the developed simulation model with well-designed simulation calculations. Because the data are generated with adequate input excitation, the developed data driven models will be able to cover the entire anticipated operation conditions. However, because the simulation model will always contain model uncertainty, robust fault diagnosis techniques must be applied to avoid false alarms.

The advantage of robust data driven model based approach is that the strength of historical data based approach and first principle model based approach, which are reviewed in Section 1.2, can be combined. A first principle model is able to represent the relationships among variables for all the operation conditions in a compact manner. However, the model may be too complicated for robust fault diagnosis design. On the contrary, data driven model based fault diagnosis usually has a relatively simple structure, which enables robust fault diagnosis design. However, the performance of data based approach depends strongly on the quality of collected data. For instance, the

degradation of steam generators and heat exchangers and the changes in operation setpoints are inevitable throughout the reactor lifetime, the past historical data would definitely not be able to characterize the inter-variable relationships for all the power levels at the most recent conditions of system configuration and component degradation. Therefore, a combination of the two types of approaches will be able to improve the performance of fault diagnosis in terms of reducing false alarms and avoiding misdiagnosis.

Linear model structure is pursued throughout the dissertation. Although nuclear power systems indeed have nonlinearity, this nonlinearity can be handled either by recursively updating a linear model or by using model uncertainty decoupling techniques for fault diagnosis design. Most importantly, linear state space model is the only class of systems tractable with rigorous theory.

1.4 Contributions of the Dissertation

The proposed integrated approach has provided a systematic solution to performance monitoring and fault diagnosis for nuclear power systems. The new architecture of fault diagnosis design is the first to emphasize the importance of sensor placement design for fault diagnosis and the importance of dynamic fault diagnosis for nuclear power systems. The developed robust data driven model based fault diagnosis algorithms for steady state conditions and dynamic conditions are a first effort to combine the strength of first principle model based fault diagnosis and the historical data based fault diagnosis.

The following original contributions are made in this dissertation:

1. The development of a simulation model of IRIS Helical Coil Steam Generator (HCSG) systems. Through the steady state thermal analysis, it is discovered that the primary coolant temperature profile can be used to indicate the HCSG tube inside fluid level.

2. The development of a new and complete algorithm based on causal graph theory and data reconciliation to perform sensor placement design for process and sensor fault detection, identification, and reconstruction.

3. The application of reconstruction based PCA approach to steady state fault diagnosis of IRIS HCSG system, which was able to deal with joint sensor and process faults based on subspace characterization of fault effects and quantify fault detectability and fault identifiability.

4. The development of a robust PCA model based approach for steady state fault diagnosis, in which PCA models were developed using data generated from simulation models while the model uncertainties were identified from plant measurements.

5. The development of a hybrid PCA model based approach for steady state fault diagnosis, which allowed the incorporation of partially known system knowledge into the PCA based fault diagnosis.

6. The development of a robust subspace model based approach for dynamic fault diagnosis. In this approach, a low order linear state space model was identified based on the data generated from well-designed simulation runs using widely available nuclear system analysis codes such as RELAP, RETRAN, TRAC, etc. A robust residual generation algorithm was then developed using measured data without directly identifying the model uncertainties.

1.5 Outline of the Dissertation

Chapter 2 reviews the state-of-the-art model based fault diagnosis techniques. The necessary conditions of fault detectability and isolability are emphasized. It is shown that the performance of fault diagnosis is a strong function of the fidelity of models used for residual generation. The robust issues of fault diagnosis are also discussed. In order to fulfill the requirements of fault diagnosis for an engineering system, the need to combine data driven modeling and fault diagnosis theory is motivated.

Chapter 3 develops both steady state and dynamic model for the IRIS HCSG systems. The steady state simulation study shows that the primary coolant temperature profile can be used to indicate the HCSG tube inside fluid level. The developed dynamic simulation model provides a platform to test the developed robust subspace model based dynamic fault diagnosis algorithm.

Chapter 4 presents a complete procedure and algorithm for sensor placement for fault diagnosis. The minimum sensor requirement is first determined for process fault diagnosis based on cause effect analysis. To ensure reliable process fault diagnosis, the minimum sensor requirement is then determined such that the related measured variables can still be reconstructed based on plant-scale mass balance and heat balance equations even if these sensors fail due to instrument faults. Finally, data reconciliation is used as a generic approach to perform the sensitivity analysis of a plant variable in the balance equations.

Chapter 5 presents PCA approach for steady state fault diagnosis. Reconstruction based PCA is first applied to deal with joint sensor and process fault diagnosis and determine the fault detectability and identifiability. Robust PCA model based algorithm is then developed to decouple the fault effects on the measurements from the model uncertainties. In order to improve the sensitivity of fault detection and interpretability of fault isolation, hybrid PCA approach is developed to incorporate the available system knowledge into PCA modeling.

Chapter 6 develops a robust subspace model based dynamic fault diagnosis algorithm. The theory of subspace identification is presented to determine a low order linear state space model from simulation data. A robust dynamic residual generator design algorithm is developed without directly identifying the model uncertainty. Finally, the developed algorithm is demonstrated through the application to IRIS HCSG systems for transient fault diagnosis.

Chapter 7 summarizes the dissertation and draws conclusions, along with recommendations for future work.

Chapter 2

Basic Theory of Model Based Fault Diagnosis

2.1 Introduction

Model based fault diagnosis is conceptually divided into two stages — residual generation and decision-making, as shown in Figure 2.1 (Chen and Patton, 1999). Residual generators transform the fault symptoms from measurement space to a lower dimensional feature space. Three major algorithms of residual generation are observer-based approaches, parity space approaches, and parameter estimation approaches. Decision-making performs appropriate statistical testing on the generated residuals to make a decision on fault diagnosis.

In this Chapter, a critical review is performed on the technical elements of model based fault diagnosis. The necessary conditions of fault detectability and isolatability are emphasized. It is shown that the performance of fault diagnosis is a strong function of the fidelity of models used for residual generation. In order to fulfill the requirements of fault diagnosis for an engineering system, robust data driven model based fault diagnosis approach is motivated to combine data driven modeling and fault diagnosis theory.

2.2 System Representation

In general, most of the components in an engineering process are operating in closed control loops. Figure 2.2 shows a standard closed-loop control system. In order to detect and isolate sensor faults, actuator faults, and process faults, mathematical models need to be developed to simulate the behavior of these process components and control devices.

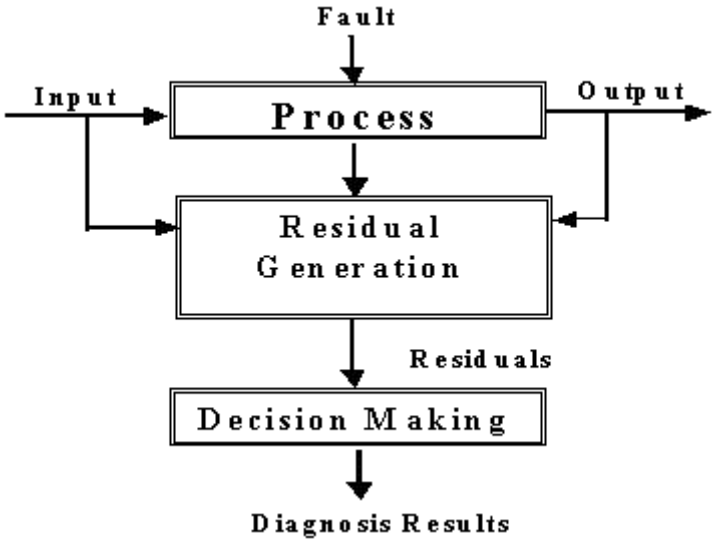

Figure 2.1. Diagram of model based fault diagnosis.

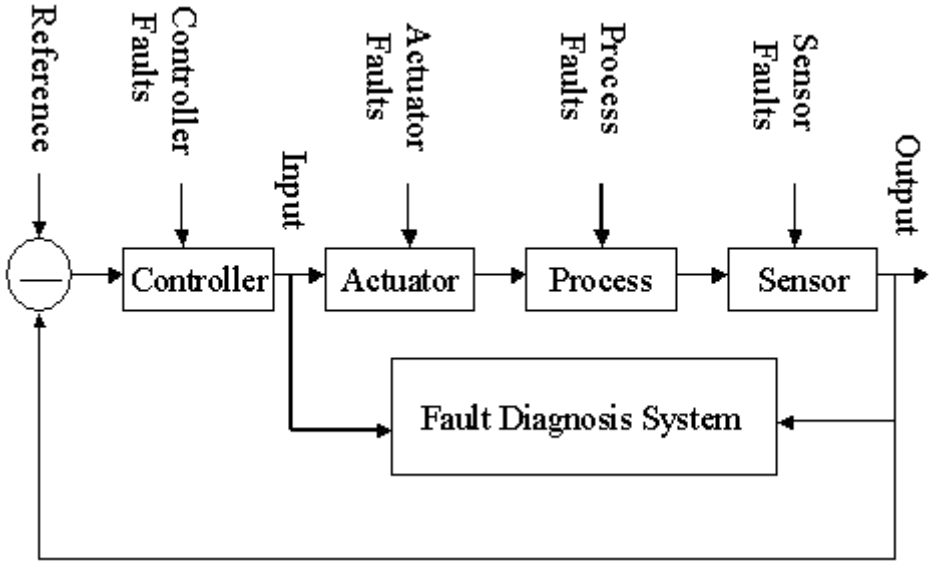

Figure 2.2. Fault diagnosis for a closed-loop control system.

As shown in Figure 2.2, a fault diagnosis system is not related to the controller design because the fault diagnosis system involves only the actuator input (or controller output) and the process output. If the actuator input is measured, an open loop system model is sufficient for fault diagnosis even if the physical system may operate in closed-loop conditions. However, if the actuator input is not available, a closed-loop model must be used, which involves the reference setpoint to calculate the error signal. Fortunately, the controller output is always known for a digital control system. In fact, the use of an open loop model can decouple the fault diagnosis from controller design and simplify fault diagnosis significantly (Chen and Patton, 1999).

For a linear dynamic system, the process dynamics is given by:

$$\begin{aligned} \dot{x}(t) &= Ax(t) + Bu^*(t) \\ y^*(t) &= Cx(t) + Du^*(t) \end{aligned} \tag{2.1}$$

where

$x(t)$ = the state vector.

$y^*(t)$ = the true system output.

$u^*(t)$ = the actuator output.

A, B, C, D = system matrices.

In model based fault diagnosis, the fault effects on the physical system are explicitly represented by appropriate fault models. This explicit representation of fault effects facilitates fault diagnosis such that the generated residuals will behave as designed. In fact, this is also the fundamental difference between model based fault diagnosis and signal based fault diagnosis such as spectral analysis and pattern recognition. For signal based fault diagnosis, fault signatures need to be extracted from representative fault data, which are difficult to obtain in most situations.

If the sensor dynamic is ignored, the fault model for a sensor fault is given by:

$$y(t) = y^*(t) + f_s(t) \tag{2.2}$$

where

$y(t)$ = the measured output.

$f_S(t)$ = the sensor fault vector.

If the actuator dynamics is ignored and the actuator output $u^*(t)$ is simplified to be equal to the actuator input $u(t)$, the fault model for an actuator fault is given by:

$$u^*(t) = u(t) + f_a(t) \tag{2.3}$$

where

$u(t)$ = the actuator input signal generated by controller output.

$f_a(t)$ = the actuator fault vector.

Obviously, the actual mapping between the actuator input $u(t)$ and the actuator output $u^*(t)$ can be easily represented by changing Equation (2.3) accordingly.

If a system input $u^*(t)$ is not a manipulated variable for control while it is a measured variable, the fault model for the input sensor is given by:

$$u(t) = u^*(t) + f_{is}(t) \tag{2.4}$$

where

$u(t)$ = the measured value of the system input $u^*(t)$ which is not used for control.

$f_{iS}(t)$ = the input sensor fault vector.

If a process fault results in a change in the system parameters, the model for the fault is given by:

$$\dot{x}(t) = Ax(t) + Bu^*(t) + f_c(t) \tag{2.5}$$

where

$f_c(t)$ = the process fault vector.

Considering all the possible sensor/actuator and process faults, the fault model can be given by:

$$\begin{aligned} \dot{x}(t) &= Ax(t) + Bu(t) + B(f_a(t) - f_{is}(t)) + f_c(t) \\ y(t) &= Cx(t) + Du(t) + D(f_a(t) - f_{is}(t)) + f_s(t) \end{aligned} \tag{2.6}$$

where

$u(t)$ = the process input variables including both the controller output and the measured input not used for control.

In Equation (2.6), the input and output of the dynamic system are all measured and the fault effects on the system dynamics are explicitly represented.

In general, the state space representation with different types of faults is given by:

$$\begin{aligned} \dot{x}(t) &= Ax(t) + Bu(t) + R_1 f(t) \\ y(t) &= Cx(t) + Du(t) + R_2 f(t) \end{aligned} \tag{2.7}$$

where R_1 and R_2 are known fault entry matrices which represent the fault effects on the dynamic system (Chen and Patton, 1999).

2.3 Concepts of Residual Generator Design

Residual generation plays an important role in model based fault diagnosis. The residuals are generated from a model covering the entire operation regime. Therefore, in the absence of faults, the residuals are only due to noise and disturbances and the magnitudes are small. In the presence of faults, the residuals should capture the inconsistency between the measured variables and the mathematical model for fault detection. Moreover, the generated residuals should respond to different faults in different manners for fault isolation. In fact, it is through appropriate residual generation that model based fault diagnosis is able to eliminate the shortcomings of traditional fault diagnosis methods, where operation condition dependent signal characteristics (e.g. amplitude, variation rate, and frequency) are used for fault diagnosis.

The simplest approach to residual generation is the parallel simulation scheme. The mathematical model used for residual generation is simply a simulation model of the physical system and the generated residual is nothing but the difference between the simulation output and the measured output. Because such a simulation model belongs to an open-loop architecture, the simulation output may become unstable if the physical system is unstable (Chen and Patton, 1999).

In general, model based fault diagnosis uses both the system input and the system output to generate residuals. The mathematical representation of residual generation is given by (in the Laplace domain):

$$r(s) = H_u(s)u(s) + H_y(s)y(s) \tag{2.8}$$

where

$H_u(s)$ = a linear transformation acted on the system input.

$H_y(s)$ = a linear transformation acted on the system output.

If input-output representation is used, the dynamics of the linear system with possible faults in Equation (2.7) is given by:

$$y(s) = G_u(s)u(s) + G_f(s)f(s) \tag{2.9}$$

where $G_u(s)$ and $G_f(s)$ are the matrix transfer functions between the system output and the system input and between the system output and the system fault, respectively. The two transfer functions are given by:

$$G_u(s) = C(sI - A)^{-1}B + D \tag{2.10a}$$
$$G_f(s) = C(sI - A)^{-1}R_1 + R_2 \tag{2.10b}$$

Combining Equations (2.8) and (2.9), the evolution of residual dynamics is as follows:

$$r(s) = (H_u(s) + H_y(s)G_u(s))u(s) + H_y(s)G_f(s)f(s) \tag{2.11}$$

2.3.1 Residual Generation for Fault Detection

Because residuals are used to check the consistency between the measurements and the system model, they must satisfy the following condition:

$$r(t) = 0 \qquad \text{if and only if} \qquad f(t) = 0 \tag{2.12}$$

To make the generated residuals decoupled from the operation conditions, all the residual generators must be able to produce a zero residual vector for fault free conditions. Based on Equation (2.8) and (2.9), a necessary condition of residual generation for fault detection can be obtained as follows (Chen and Patton, 1994):

$$H_u(s) + H_y(s)G_u(s) = 0 \tag{2.13}$$

In the meantime, the generated residual vector must be sensitive enough for fault detection. The dynamic response of a residual generator satisfying Equation (2.13) is as follows:

$$r(s) = H_y(s)G_f(s)f(s) = G_{rf}(s)f(s) \tag{2.14}$$

where
$G_{rf}(s)$ = the transfer function between the fault and the residual response.

Therefore, the fault detectability condition is that the transfer function between a fault and the residual response is not zero. To avoid the fault effects on the residual vector from disappearing when a fault still exists, it is necessary to define a stronger fault detectability condition, which is given by (Chen and Patton, 1994):

$$G_{rf}(0) \neq 0 \tag{2.15}$$

Considering an output sensor fault with $G_f(s) = \mathrm{I}$, if the residual generator is simply designed as $H_y(s) = \mathrm{I}$, and $H_u(s) = -G_u(s)$, the steady state gain of the transfer function between the residual response and the sensor fault will then be 1. Therefore, this simple residual generator design has strong fault detectability for output sensor faults.

Chen also proved that it is not always possible to design a residual generator to detect actuator faults (Chen and Patton, 1994). If an actuator fault has the fault transfer matrix $G_f(s) = G_u(s)$, then the transfer function matrix between the fault and the residual response $G_{rf}(s) = H_y(s)G_u(s)$ according to Equation (2.14). Again, according to the condition of residual generator for fault detection given by Equation (2.13), we must have $H_y(s)G_u(s) = -H_u(s)$. Therefore, if the transfer matrix

$H_u(s)$ is not well designed, there will be no physically realizable solution to $H_y(s)$ for this residual generator design because the solution might be noncausal.

2.3.2 Residual Generation for Fault Isolation

Multiple residual generators need to be designed for fault isolation. The designed residual generators have the property of fault isolation only if they respond to all the considered faults in different characteristic manners.

Structured residual design is one approach to residual generation for fault isolation. In this approach, each residual generator is designed such that it is sensitive to a subset of faults while insensitive to the remaining faults.

For structured residual design, the first step is to design an incidence matrix for fault isolation. Table 2.1 shows an example of incidence matrix design to isolate three faults. The columns of the incidence matrix correspond to the desired residual patterns for individual faults. The rows of the incidence matrix correspond to the responses of each residual generator to the considered faults. A "1" element of the incidence matrix indicates that the residual element of the residual generator is affected by the corresponding fault while a "0" indicates that it is not.

Table 2.1. Incidence matrix design for fault isolation

Residual generator	**Fault 1**	**Fault 2**	**Fault 3**
Residual generator 1	**0**	**1**	**1**
Residual generator 2	**1**	**0**	**1**
Residual generator 3	**1**	**1**	**0**

The simplest incidence matrix is that both the columns and the rows are canonical. For such an incidence matrix, the rows have equal numbers of zeros with different patterns and the columns have equal number of zeros with different patterns, too. The advantage of this canonical structure is that partial firing of one residual generator will not result in fault misclassification. Given that there are μ outputs of a system, ρ considered faults, a square incidence matrix with ρ residual generators and μ-1 zeros in each column always provides a solution to the canonical structured incidence matrix (Gertler, 1998).

The second step is to design residual generators such that the fault responses follow the designed incidence matrix. In this step, different residual generation techniques such as observer based approach and parity space approach may be used.

Fixed direction residual vector is an alternative approach to residual generation for fault isolation. In this approach, the residual generators are designed such that a directional residual vector lies in a fixed fault specific direction. Fault isolation is achieved by comparing the generated residual vector with the prespecified fault direction in residual generator design.

Considering sensor faults only, according to Equation (2.14), the residual generator sensitive to all faults but the ith sensor fault can be designed simply by making the ith columns of $H_y(s)$ equal to zero.

If actuator faults are considered, just like in the case of fault detection, because of the additional constraint $H_u(s) = -H_y(s)G_u(s)$, it is not always possible to find a realizable solution to $H_y(s)$ if the ith column of $H_u(s)$ is chosen to be zeros such that the residual generator is sensitive to all faults but the ith actuator fault. Therefore, actuator faults are not always isolatable (Chen and Patton, 1994).

2.4 Residual Generation Techniques

To generate residuals with the desired properties for fault detection and isolation, different residual generation techniques have been developed in the last two decades. Although these techniques are related to each other and become equivalent in certain cases, they do have very different characteristics in terms of the complexity, flexibility, and applicability. Three most representative residual generation methods, observer based approach, parity space approach, and parameter estimation based approach, are summarized in this section.

2.4.1 Observer Based Residual Generation

The basic idea behind observer based residual generation is to estimate the system output using Luenberger observers in a deterministic setting (Frank, 1990) or Kalman filters in a stochastic setting (Basseville, 1988). The weighted output estimation error is then used as residuals for fault detection and isolation (Chen and Patton, 1999).

For the purpose of fault diagnosis, only the output estimation is required while the state estimation is unnecessary. Therefore, a Lunenburger observer can be used for residual generation, which is given by:

$$\begin{aligned} \dot{z}(t) &= Fz(t) + Ky(t) + Ju(t) \\ r(t) &= L_1 z(t) + L_2 y(t) + L_3 u(t) \end{aligned} \tag{2.16}$$

where $z(t)$ is the state vector of the observer, and $F, K, J, L_1, L_{2,} L_3$ are matrices of appropriate dimensions.

The generated residual vector $r(t)$ in Equation (2.16) is related to the output estimation error. To be used for fault detection, the residuals must be zero in asymptotical sense for any initial states for a fault free system defined in Equation (2.1), that is:

$$\lim_{t\to\infty} r(t) = 0 \tag{2.17}$$

To obtain zero residuals in asymptotical sense with a full order observer, the matrices involved in the observer design must satisfy the following conditions (Chen and Patton, 1996). :

$$\begin{aligned} &z(t) = x(t) \\ &F = A - KC \\ &J = B - KD \\ &L_1 = -L_2 C \\ &L_3 = -L_2 D \\ &F \text{ must have stable eigenvalues.} \end{aligned} \tag{2.18}$$

If the residual generator, defined in Equation (2.16), is applied to the fault system defined in Equation (2.7), the residual dynamics can be derived as follows:

$$\begin{aligned} e(t) &= z(t) - x(t) \\ \dot{e}(t) &= Fe(t) - R_1 f(t) + KR_2 f(t) \\ r(t) &= -L_2 Ce(t) + L_2 R_2 f(t) \end{aligned} \tag{2.19}$$

The observer based residual generator exists for any dynamic system although stable state observer may not exist (Chen and Patton, 1996). Through appropriate choice of the matrices L_2 and K in Equation (2.19), the designed full order observers may generate residuals with a predetermined fault direction for fault isolation (Park et al., 1994a), (Park et al., 1994b). A Dedicated Observer Scheme (DOS) was suggested for sensor fault isolation in (Chen and Patton, 1994). In this scheme, multiple residual generators are designed with each observer excited by a single output. Therefore, each residual generator is sensitive to only one sensor fault. The Generalized Observer Scheme (GOS) also uses multiple residual generators for fault isolation. However, in this design scheme, each observer is excited by all the system outputs but one (Wuennengerg, 1990).

2.4.2 Parity Space Approach

The basic idea of parity space approach is to check the consistency of measurements for the monitored system in terms of some process constraints. The terminology of parity space was originated in digital data transmission using bits for error detection. If two groups of bits are the same, their sum is zero. If two groups of bits are different, a non-zero sum will be generated, which means that some transmission error has happened.

2.4.2.1 Parity Space Approach for Static Systems

The parity space approach to fault diagnosis was first proposed for steady state operation conditions, where there are more measurements than the number of state variables (Daly et al., 1979). An algebraic equation can be used to describe a general steady state system, which is given by:

$$y(k) = Cx(k) + f(k) + w(k) \tag{2.20}$$

where

$y(k)$ = the system measurements.

$x(k)$ = the system states.

$f(k)$ = the fault vector.

$w(k)$ = the measurement noise.

If the number of measurements m is greater than the number of independent state variables n, there exists a matrix V_0, which satisfies:

$$V_0 C = 0 \tag{2.21}$$

where V_0^T has $m-n$ columns of vectors that span the null space of C^T. In fact, Equation (2.21) consists of $m-n$ redundant equations relating the m measured variables.

The redundant equations in Equation (2.21) can be directly used as parity relations to generate residual vector $r(k)$, which is given by:

$$r(k) = V_0 y(k) = V_0 (f(k) + w(k)) \tag{2.22}$$

The generated residual vector is independent of the system states. The space spanned by the columns of the matrix V_0 is called parity space. A fault of the ith sensor will result in the largest magnitude along the direction of the ith column of the matrix V_0. Therefore, the m columns of the matrix V_0 can be directly used as the directional fault signatures of the m sensor faults for fault isolation.

Example 1.: Consider a system with four measured variables $\begin{bmatrix} y_1 & y_2 & y_3 & y_4 \end{bmatrix}^T$ and two state variables $\begin{bmatrix} x_1 & x_2 \end{bmatrix}^T$, which satisfies the following algebraic measurement equation:

$$\begin{bmatrix} y_1 \\ y_2 \\ y_3 \\ y_4 \end{bmatrix} = \begin{bmatrix} 1 & 0 \\ 0 & 1 \\ 1 & 1 \\ 1 & -1 \end{bmatrix} \begin{bmatrix} x_1 \\ x_2 \end{bmatrix}$$

To design a residual generator for fault detection, the generated residuals must be zero-valued for any values of state variables if there is no fault occurring in the system. The residual generator can be designed according to Equation (2.21) with a linear transformation on the measured vector, which is given as follows:

$$V_0 = \begin{bmatrix} -1.0 & 1.0 & 0.0 & 1.0 \\ -1.0 & -1.0 & 1.0 & 0.0 \end{bmatrix}$$

The two rows of the matrix V_0 are the two left singular vectors corresponding to zero-valued singular values when singular value decomposition is performed on the original system matrix. In this example, the obtained left singular matrix, U, and the singular values matrix, S, are as follows:

$$U = \begin{bmatrix} -1.0 & 0.0 & -1.0 & -1.0 \\ 0.0 & -1.0 & -1.0 & 1.0 \\ -1.0 & -1.0 & 1.0 & 0.0 \\ -1.0 & 1.0 & 0.0 & 1.0 \end{bmatrix} \qquad S = \begin{bmatrix} 1.7321 & 0.0 & 0.0 & 0.0 \\ 0.0 & 1.7321 & 0.0 & 0.0 \\ 0.0 & 0.0 & 0.0 & 0.0 \\ 0.0 & 0.0 & 0.0 & 0.0 \end{bmatrix}$$

It can be easily verified that the generated residual of the ith sensor fault lies in the direction of the ith column of the matrix V_0. For instance, if the first measurement has a bias fault of magnitude m_f and the measurement noise is negligible, then the fault vector is as follows:

$$f = \begin{bmatrix} m_f & 0 & 0 & 0 \end{bmatrix}^T$$

According to Equation (2.22), the residual vector is given by:

$$r(k) = \begin{bmatrix} -1.0 \\ -1.0 \end{bmatrix} m_f$$

Obviously, the generated residual vector is in the direction of the first column of the matrix V_0.

Example 2.: Consider a system with four measured variables $\begin{bmatrix} y_1 & y_2 & y_3 & y_4 \end{bmatrix}^T$ and two state variables $\begin{bmatrix} x_1 & x_2 \end{bmatrix}^T$, which satisfies the following algebraic measurement equation:

$$y_1 = x_1$$
$$y_2 = x_2$$
$$y_3 = x_1^2 + x_1 + x_2^2$$
$$y_4 = x_1^2 - x_2^2$$

In order to design a residual generator for fault detection, the generated residual vector must be zero-valued for any values of state variables $\begin{bmatrix} x_1 & x_2 \end{bmatrix}^T$ if there is no fault occurring in the system. The most obvious nonlinear residual generators can be designed by substituting the two unmeasured state variables, x_1 and x_2, with the two measured variables, y_1 and y_2 in the third and the fourth measurement equations, which is as follows:

$$r = \begin{bmatrix} r_1 \\ r_2 \end{bmatrix} = \begin{bmatrix} y_3 - (y_1^2 + y_1 + y_2^2) \\ y_4 - (y_1^2 - y_2^2) \end{bmatrix}$$

For normal operation conditions, the two residual generators r_1 and r_2 must generate zero residuals. However, it is very challenging to design nonlinear residual generators satisfying this requirement. If data driven modeling techniques such as neural networks and group method of data handling are used, a dataset with a combination of y_1 and y_2 each of which should cover its operational space must be obtained such that the generated data driven models will not produce non-zero residuals in the possible operational state space. It is not arguable that routine operation data do not contain such rich information. If first-principle models are used, the developed models must be accurate enough. If there is significant model uncertainty, the residual generators will cause false alarms even if there are no faults occurring in the system.

Let's further examine the property of the generated residuals. If the first measurement has a bias fault of magnitude m_f and the measurement noise is negligible, then the fault vector is as follows:

$$r = \begin{bmatrix} r_1 \\ r_2 \end{bmatrix} = \begin{bmatrix} -2x_1 m_f - m_f - m_f^2 \\ -2x_1 m_f - m_f^2 \end{bmatrix}$$

It can be observed that the generated residual vector does not have fixed fault direction. The fault direction depends on the operation state x_1 and the fault magnitude

m_f. Therefore, this residual generator design scheme based on prediction error is not appropriate for fault isolation of the considered system.

In general, residual generator design for fault diagnosis should not be simplified as a prediction error problem. In this example, if perfect modeling is available, the following four residual generators based on generalized transformations of the measured variables can be designed for fault isolation:

$$\begin{bmatrix} r_1 \\ r_2 \\ r_3 \\ r_4 \end{bmatrix} = \begin{bmatrix} r_1(y_3, y_4, y_2) \\ r_2(y_3, y_4, y_1) \\ r_3(y_1, y_2, y_4) \\ r_4(y_1, y_2, y_3) \end{bmatrix}$$

The four residual generators r_1, r_2, r_3, and r_4 can now be dedicated to the fault isolation of y_1, y_2, y_3, and y_4, respectively, because only the dedicated residual generators will generate zero-valued residuals and the other three residual generators will generate nonzero residuals if a fault occurs in the system.

However, the assumption of this residual generator design scheme that perfect modeling is achievable may be too much for a real world problem. We believe this design strategy can solve a class of problems for small systems such as heat exchangers, but we are not going to perform further study on this method in this dissertation because such residual generator design will be very much problem dependent.

Comments on the two examples: Because nonlinear residual generator design for fault diagnosis will not always be able to produce directional fault signatures, most of the nonlinear fault diagnosis methods do not have solid theoretical basis. In order to develop a fault diagnosis method with more general application perspectives, linear fault diagnosis methods will be pursued in this dissertation focusing on robust residual generator design to avoid false alarms due to model uncertainty. It is understandable that nonlinear techniques will not be able to deal with model uncertainty.

2.4.2.2 Parity Space Approach for Dynamic Systems

If the number of measurements m is not greater than the number of independent state variables n, the left null space of the matrix C (the null space of C^T) given in Equation (2.20) becomes empty. This means that the measurements do not have adequate redundant information for model based fault diagnosis. Unfortunately, most process systems do have more states than the measurements, which constrains the application of spatial redundancy based parity space approach to fault diagnosis.

The other dimension of redundancy in a technical process is temporal redundancy. The parity space approach to fault diagnosis can significantly extend its application when temporal redundancy is utilized (Patton and Chen, 1991).

With a time window of length $s+1$, the temporal redundancy relationship for a linear dynamic system defined in Equation (2.7) is given by:

$$y_s(k) - H_s u_s(k) = \Gamma_s x(k-s) + M f_s(k) \tag{2.23}$$

where

$$y_s(k) = \begin{bmatrix} y(k-s) \\ y(k-s-1) \\ \cdots \\ y(k) \end{bmatrix} \qquad u_s(k) = \begin{bmatrix} u(k-s) \\ u(k-s+1) \\ \cdots \\ u(s) \end{bmatrix}$$

$$f_s(k) = \begin{bmatrix} f(k-s) \\ f(k-s+1) \\ \cdots \\ f(k) \end{bmatrix} \qquad \Gamma_s = \begin{bmatrix} C \\ CA \\ \cdots \\ CA^s \end{bmatrix}$$

$$H_s = \begin{bmatrix} D & 0 & \dots & 0 \\ CB & D & \dots & 0 \\ \dots & \dots & \dots & \dots \\ CA^{s-1}B & CA^{s-2}B & \dots & D \end{bmatrix} \qquad M = \begin{bmatrix} R_2 & 0 & \dots & 0 \\ CR_1 & R_2 & \dots & 0 \\ \dots & \dots & \dots & \dots \\ CA^{s-1}R_1 & CA^{s-2}R_1 & \dots & R_2 \end{bmatrix}$$

If the number of stacked rows $s+1$ is chosen larger than the number of states n, there always exists a matrix V_0 such that,

$$V_0 \Gamma_s = 0 \tag{2.24}$$

Therefore, the residual vector can then be calculated as follows:

$$r(k) = V_0 (y_s(k) - H_s u_s(k)) \tag{2.25}$$

Correspondingly, the dynamics of the residual vector is given by:

$$r(k) = V_0 M f_s(k) \tag{2.26}$$

The residuals generated by dynamic parity space approach can further be processed to have the properties for fault isolation. The method to generate structured residuals and directional residuals for fault isolation is given in (Gertler, 1997).

2.4.3 Parameter Estimation Approach

The basic idea behind parameter estimation approach is to estimate the model parameters on line and relate the model parameters to physical parameters for fault detection and isolation.

If the model structure of a physical system is known, the empirical model of the system can be derived in the following form:

$$y(t) = \Psi(t)^T \theta \tag{2.27}$$

where

θ = the set of model parameters.

$\Psi^T = [y(t-1),....,y(t-n),u(t-1),...,u(t-m)]$

The least square estimate of θ can be computed as follows:

$$\theta = (\Psi^T \Psi)^{-1} \Psi^T y \tag{2.28}$$

After the model parameters are identified, they may be converted back to the physical parameters for fault isolation. However, because the model parameters are generally related to the physical parameters via a complicated function, it may be extremely difficult to perform this conversion (Doraiswami and Stevenson, 1996). A very interesting example of parameter estimation based approach to fault diagnosis is to identify modal parameters from vibration data for structural damage detection and localization using multivariate autoregressive moving average modeling (Bodeux and Golinval, 2003).

2.5 Residual Evaluation Techniques

In a real process, the measured signals always contain noise. In addition, some unmeasured disturbance may play a part in the system dynamics. If the measurement noise and the unmeasured disturbance are assumed to be white Gaussian, the generated residual consists of two components, which is given by:

$$r(t) = H_y(q)G_f(q)f(t) + H_y(q)G_v(q)v(t) \tag{2.29}$$

where

q = the back shift operator operated on time.

G_ν = the transfer function between the noise/disturbance and the system output.

$\nu(t)$ = the noise/disturbance vector.

In Equation (2.29), the first term is time varying and deterministic, which represents the fault induced contribution, while the second term is stochastic, which represents the noise/disturbance induced contribution.

If structured residual design is used for fault detection and isolation, the residuals generated by each residual generator can be tested against certain threshold. If the threshold is exceeded, the response of this residual generator is determined to be "1" and "0" otherwise. The obtained responses of all the residual generators are then compared with the fault patterns defined by the columns of the designed incidence matrix for fault isolation.

The threshold used for statistical testing can be determined based on the selected false alarm rate. Depending on how the residual generators are designed, the statistical testing can be performed for vector residual, vector time series, or the window average of vector time series (Gertler, 1998).

The m-dimensional vector residual $r(t)$ follows a multivariate normal distribution with zero mean and covariance matrix Φ_r. The statistics $\omega(t) = r(t)^T \Phi_r^{-1} r(t)$ obeys χ^2 distribution with m degrees of freedom. Therefore, the decision rule can be given as follows:

if $\omega \geq \chi^2_{m,\alpha}$, then the residual generator is fired.

if $\omega < \chi^2_{m,\alpha}$, then the residual generator is not fired.

where α is the significance level.

The m-dimensional vector residual $r(t)$ can also be stacked into a vector time series for statistical testing. This vector $R(t)$ is ms dimensional if s time instants are used in the stack. If the vector time series follow a multivariate normal distribution with zero mean and covariance matrix Φ_R. The statistics $\omega(t) = R(t)^T \Phi_R^{-1} R(t)$ obeys χ^2 distribution with ms degrees of freedom. Therefore, the decision rule can be given as follows:

if $\omega \geq \chi^2_{ms,\alpha}$, then the residual generator is fired.
if $\omega < \chi^2_{ms,\alpha}$, then the residual generator is not fired.

where α is the significance level.

2.6 Robust Data Driven Model Based Fault Diagnosis

The success of model based fault diagnosis strongly depends on the fidelity of the mathematical models developed for the monitored system. If the developed mathematical models are not accurate enough to represent the fault free system, the model uncertainty will induce significant residuals resulting in false alarms and the generated residuals may not follow the designed residual patterns resulting in incorrect fault isolation. Evidently, both false alarms and incorrect fault isolation have adverse consequences when real-time fault diagnosis is applied to a safety critical system, such as a nuclear power system. Therefore, it is mandatory to address the robust issues such that the fault diagnosis algorithms are insensitive to model uncertainties and remain highly sensitive to incipient faults.

2.6.1 Motivation

In general, the mathematical models used for model based fault diagnosis can be categorized as follows:

- First-principle models.

- Causal data driven models identified from well-designed experiments.
- Statistical data driven models developed from historical data.

First principle models are usually not appropriate for direct use in model based fault diagnosis for a complex system, such as a nuclear power plant. On the one hand, first principle models always have some inevitable uncertainties because of inherent assumptions made for model development. For an engineering process, distributed parameterization and empirical relationships used will also contribute to uncertainty. The last but not the least source is the uncertainty of parameters used for modeling. On the other hand, because the developed physical models are usually very complicated, it is very difficult to use them directly to design appropriate schemes for fault detection and isolation.

Just like in the case of model based control, data driven models are much more popular than first principle models for fault diagnosis. In practice, there are two fundamentally different data driven modeling approaches. System identification approach identifies empirical models using data obtained from well-designed experiments. Historical data driven modeling approach develops a model from routine operation data saved in a historical database. The data driven models developed from system identification techniques are usually causal models because of the careful control of experiments. On the contrary, historical data driven models are usually not causal models because they can only capture the correlations among the variables contained in the historical data.

The two types of data driven modeling techniques and the corresponding fault diagnosis techniques have very different properties.

Causal data driven models can facilitate fault detection and isolation by testing the consistency of measured variables with the input-output causal relationships. Because the fault effects on the system behavior is explicitly formulated in the developed causal models, fault isolation can be achieved by structured residual design or fixed fault direction residual design. If appropriate causal models are available for a large system, the network structure of cause-effect relationship between the measured variables can

even be explicitly searched for fault isolation (Montmain, 1997), (Montmain, 2000), (Zhao, 2002).

Historical data driven models can only characterize the process variations of the collected data (Ogunnaike and Ray, 1994). Historical data driven model based fault diagnosis performs fault detection by testing the correlation structure of the measured variables against that of the historical data, which are presumed to represent normal operation conditions. In order to avoid false alarms, the historical data must contain all sources of normal variations (Russell, Chiang, and Braatz, 2000). However, this requirement is quite stringent for a technical process such as nuclear energy systems. One of the reasons is that the normal data variation is not repeatable for the same power level because of component degradation and routine operation adjustments. The second reason is that the signal-noise ratio may be low at steady state operation conditions, so the data collected at a single power level may not be able to reveal the correlation among the plant variables.

The comparison between causal data driven modeling and historical data driven modeling clearly shows that model based fault diagnosis needs to use causal data driven models. Unfortunately, causal data driven model based approach to fault diagnosis is not well studied for technical processes because people consider it unrealistic to perform experiments designed in such a manner that all the requirements of system identification are satisfied. Nevertheless, they have ignored the fact that it is indeed pragmatic to identify a model from large-scale simulation software. In nuclear system design, simulation models are actually indispensable to safety analysis and system design. With simulation models at hand, plant tests necessary for system identification can be replaced by simulation runs.

Robust data driven model based approach is developed in this dissertation for fault diagnosis. In this approach, data are generated from the developed first principle models with well-designed simulation calculations. Because data are generated with adequate input-output excitation, the developed data driven models are able to reveal the cause-effect relationships between the input-output data. After the causal models are developed, the model uncertainty is identified on-line from plant measurements. The

characteristics of the identified model uncertainty can then be studied to design robust fault diagnosis schemes using available techniques, which are described in the remainder of the section, to avoid false alarms and incorrect fault diagnosis.

2.6.2 Robust Parity Space Approach to Fault Diagnosis

Many robust fault diagnosis techniques have been developed to deal with model uncertainty based on disturbance decoupling.

Unknown Input Observer (UIO) was systematically studied by Frank's research group (Wuennengerg, 1990). In this method, an UIO observer is designed through appropriately choosing the state feedback gain and the observer matrices such that the state estimation error approaches zeros asymptotically regardless of model uncertainty. Because the residuals are generated as a linear combination of the state estimation error, the residuals are then independent of the disturbances. A unified design method of UIO observers was presented in (Hou and Muller, 1994).

Eigenstructure assignment provides an alternative approach to the decoupling of residuals from model uncertainty (Duan et al., 1998). In this method, the left or right eigenvectors of the observer are assigned to be orthogonal to the directions of model uncertainty. The advantage of this method is that the residuals are decoupled from model uncertainty directly although the state estimation error may not. The disadvantage of the method is that the number of sources of model uncertainty must be smaller than the number of independent measurements in order to achieve the decoupling (Chen and Patton, 1999).

Robust parity space approach is the most commonly accepted robust residual generation technique because of its simplicity in implementation (Chen, 1995). Without loss of generality, the system dynamics with model uncertainty and possible faults are given as follows:

$$\begin{aligned} \dot{x}(t) &= Ax(t) + Bu(t) + E_1 d(t) + R_1 f(t) \\ y(t) &= Cx(t) + Du(t) + E_2 d(t) + R_2 f(t) \end{aligned} \tag{2.30}$$

where

E_1 = the uncertainty distribution matrix related to the state vector.

E_2 = the uncertainty distribution matrix related to the system output.

d = the uncertainty vector.

The model given in Equation (2.30) clearly shows that model uncertainty and possible faults affect the system dynamics in a similar fashion. The only difference is that the uncertainty distribution matrices E_1 and E_2 are different from the fault distribution matrices R_1 and R_2. If the uncertainty distribution matrices are similar to the fault distribution matrices, the distinction between system faults and the disturbances will become impossible no matter how large the fault magnitude is. Therefore, in order to have a sensitive fault detection algorithm for all the possible faults, it is necessary to have an accurate model.

The temporal redundancy relationship for a linear dynamic system defined in Equation (2.30) is given by:

$$y_s(k) - H_s u_s(k) = \Gamma x(k-s) + G_s d_s(k) + M f_s(k) \tag{2.31}$$

where

$$d_s(k) = \begin{bmatrix} d(k-s) \\ d(k-s-1) \\ \dots \\ d(k) \end{bmatrix} \qquad G_s = \begin{bmatrix} E_2 & 0 & \dots & 0 \\ CE_1 & E_2 & \dots & 0 \\ \dots & \dots & \dots & \dots \\ CA^{s-1}E_1 & CA^{s-2}E_1 & \dots & E_2 \end{bmatrix}$$

The robust residuals for fault detection can be generated as follows:

$$r(k) = V_0(y_s(k) - H_s u_s(k)) \tag{2.32}$$

To decouple the residuals from model uncertainty and initial states, the residual generator must satisfy the following two conditions

$$V_0 Z = 0 \qquad (2.33)$$
$$V_0 M \neq 0$$

where

$$Z = \begin{bmatrix} \Gamma_s & G_s \end{bmatrix}$$

2.6.3 Estimation of Model Uncertainty

It is necessary to know the uncertainty distribution matrix for robust fault diagnosis although the magnitude behavior of model uncertainty may be unknown. The application of robust fault diagnosis methods was very limited until uncertainty distribution matrix could be estimated from plant measurements.

Although it is possible to lump parameter uncertainty, system non-linearity, measurement noise, and model reduction together to describe the model uncertainty, this kind of explicit formulation of model uncertainty is usually not adequate to deal with a real world complex system. For a real world complex system, the characteristics of model uncertainty may be completely unknown due to insufficient knowledge about the physical system and the complex interaction between subsystems. Therefore, it is necessary to estimate model uncertainty directly from plant measurements based on a reasonably accurate mathematical model.

The estimation of uncertainty distribution matrix was accomplished by Patton and Chen in 1991 (Patton, 1991b). Their work has received worldwide attention both in the field of fault diagnosis and robust control design. The estimation follows a two-step procedure. The first step is to determine model uncertainty vector and the second step is to derive uncertainty distribution matrix using singular value decomposition.

2.6.3.1 Determination of Model Uncertainty Vector

The discrete formulation of model uncertainties for a linear dynamic system is given as follows:

$$\begin{aligned} x(k+1) &= Ax(k) + Bu(k) + d_1(k) \\ y(k) &= Cx(k) + Du(k) \end{aligned} \tag{2.34}$$

where $d_1(k)$ accounts for all the modeling uncertainties.

The objective is to estimate the uncertainty vector $d_1(t)$ based on the nominal system matrices A, B, C, D, the actual system input $u(k)$, and the actual system output $y(k)$.

If we can assume that the uncertainty vector is slowly time varying, the system model can be rewritten in the state augmentation form given by:

$$\begin{aligned} \begin{bmatrix} x(k+1) \\ d_1(k+1) \end{bmatrix} &= \begin{bmatrix} A & B \\ 0 & \mathrm{I} \end{bmatrix} \begin{bmatrix} x(k) \\ d_1(k) \end{bmatrix} + \begin{bmatrix} B \\ 0 \end{bmatrix} u(k) \\ y(k) &= \begin{bmatrix} C & 0 \end{bmatrix} \begin{bmatrix} x(k) \\ d_1(k) \end{bmatrix} + Du(k) \end{aligned} \tag{2.35}$$

The estimation of the uncertainty vector is then simplified as a deterministic state estimation problem given the system matrices and the measurement. Standard algorithms such as Kalman filtering and de-convolution algorithm (Patton, 1991b) are available to obtain the sequence of uncertainty vectors.

2.6.3.2 Determination of Model Uncertainty Distribution Matrix

The uncertainty decoupling method for robust fault diagnosis only uses the information about uncertainty distribution matrix while the magnitude of model uncertainty is irrelevant. To extract the uncertainty distribution matrix from the

uncertainty vector, the estimated uncertainty vector is organized as a matrix given as follows:

$$\Omega = \left[\hat{d}_1(1) \quad \hat{d}_1(2) \quad ..... \quad \hat{d}_1(M)\right] \tag{2.36}$$

where

M = the number of identified uncertainty sequences.

If the estimated uncertainty vectors do not change directions, the uncertainty distribution matrix is reduced to one column vector, which can be given by:

$$E = \frac{1}{M}\sum_{i=1}^{M}\hat{d}_1(i) \tag{2.37}$$

To extract l most linearly independent directions out of the M uncertainty vectors, singular value decomposition (SVD) can be performed on Ω, which is given by:

$$\Omega = USV^T \tag{2.38}$$

If l most significant singular values are retained, the matrix Ω can be approximated by:

$$\Omega_1 = U\begin{pmatrix} \sigma_1 & ... & 0 & ... & . \\ ... & ... & 0 & ... & 0 \\ ... & ... & \sigma_l & ... & 0 \\ ... & ... & ... & ... & 0 \\ 0 & 0 & 0 & ... & 0 \end{pmatrix}V^T \tag{2.39}$$

The estimated uncertainty distribution matrix can be constructed by the first l columns of the matrix U.

Although the above algorithm is developed to extract the uncertainty distribution matrix, it can also be used to determine the fault distribution matrix from fault data. Because fault distribution matrix is used to characterize the feature of a fault in model based fault diagnosis, this algorithm has not only theoretical but also practical significance in fault diagnosis.

2.7 Summary

A critical review on model based fault diagnosis is presented in this chapter. After the basic theory of observer approach, parity space approach and parameter estimation approach was described, it was emphasized that the performance of model based fault diagnosis is a strong function of the fidelity of the models used for residual generation. This chapter concluded the review with the motivation of robust data driven model based approach to combine the strength of data driven modeling and the theoretical sophistication of residual generation and residual analysis derived from linear system theory for fault diagnosis. In the proposed robust data driven model based approach, data are generated from first principle models with well-designed simulation calculations. Because the data are generated with adequate input-output excitation, the developed data driven models can reveal the cause-effect relationships among variables. After causal models are developed, model uncertainty is identified from plant measurements. The characteristics of the identified model uncertainty can then be studied to design robust fault diagnosis schemes to avoid false alarms and incorrect fault diagnosis.

Chapter 3

Modeling and Simulation of the IRIS Helical Coil Steam Generator System

In order to demonstrate the performance of the procedures and algorithms to be developed, both a steady state model and a dynamic model are developed for the IRIS (International Reactor Innovative and Secure) HCSG systems in this chapter. The steady state simulation study shows that the profile of the primary coolant temperature can be used to indicate the secondary fluid level inside the HCSG tubes. The developed dynamic simulation model is used to generate data such that a linear state space model can be identified using a subspace identification technique and test the robust data driven dynamic model based fault diagnosis algorithm developed in Chapter 6. The developed physics model is also used to study optimal sensor placement design.

3.1 System Description

International Reactor Innovative and Secure (IRIS) is one of the next generation nuclear reactor designs for near term deployment. The IRIS reactor is an integral light-water reactor (LWR), a schematic of which is shown in Figure 3.1 (Carelli et al., 2003). The reactor coolant systems including steam generators, pumps, and pressurizer are all integrated inside the reactor vessel. This integral design eliminates the possibility of large loss of coolant accidents. The reactor has eight Helical Coil Steam Generators (HCSG) connected to four steam lines and four feed water lines. The long lifetime core is achieved by means of 5 percent enriched uranium for the first reactor core and 9 percent enriched uranium for successive reactor cores. The reactor refueling is needed only at the end of the first five years, and afterwards once every eight years. Because of the high burnup, less nuclear waste per unit of reactor power is produced than that in currently operating reactors.

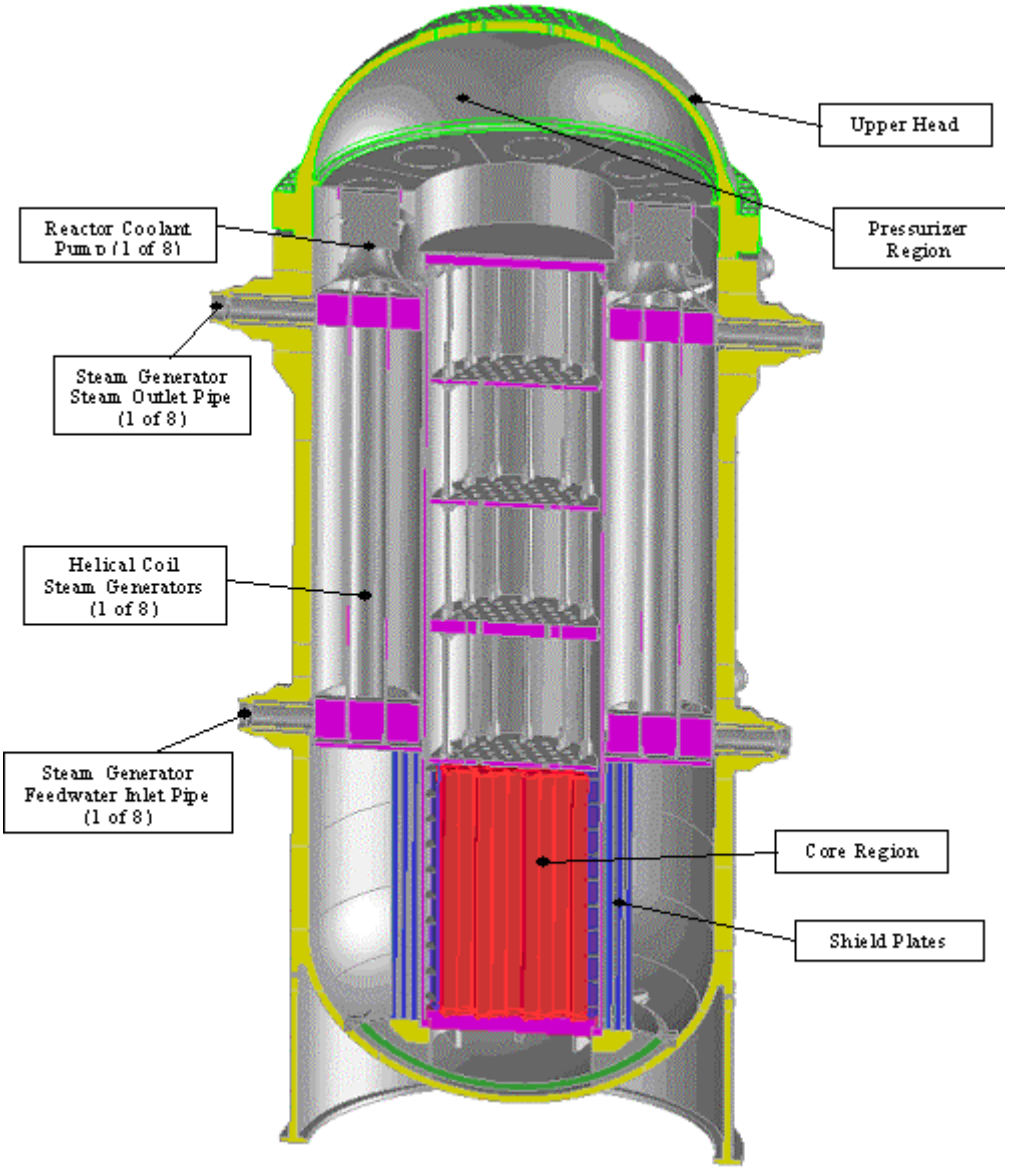

Figure 3.1. IRIS integral design.

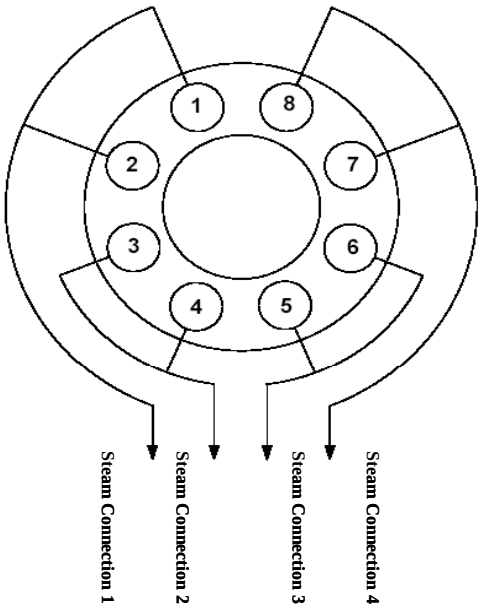

Figure 3.2. IRIS steam generator layout.

The HCSG systems are major contributors to the safety and economy of the IRIS reactor design. The size of steam generators can be reduced through the helical coil design. The heat transfer of the coiled configuration is much more efficient than straight tubes because of the larger heat transfer area per unit volume and the secondary flow induced by the coil geometry. The probability of steam generator tube rupture can be reduced because secondary fluid flows inside SG tubes and thus the tube walls experience compression force from the outside, reducing the likelihood of stress corrosion cracking. In addition, these steam generators produce superheated steam, which avoids the need to install a steam-water separator in the steam generator

In the IRIS reactor design, eight steam generators are installed in four pairs in the annular space between the core barrel and the reactor vessel (RV) wall, which is shown in Figure 3.2 (Carelli et al., 2003). On the primary side, each Reactor Coolant Pump (RCP) is dedicated to discharge primary coolant into one steam generator. Therefore, each RCP+HCSG module constitutes a separate flow path. On the secondary side, a common feed water supply line splits at the vessel and goes to two steam generators. Similarly, the steam discharge lines from two steam generators join to create a common steam line.

This pairing of steam generators reduces the number of feed water and steam lines, and the number of penetrations into and out of the containment, but it has an unfavorable consequence on individual steam generator monitoring in terms of its thermal performance and the secondary flow rate. Figure 3.3 shows a schematic of one pair of steam generators.

In this chapter, the helical coil steam generators are simulated to study the system responses for steady state and transient operation conditions. The simulation model provides an application case for the verification of the developed performance monitoring and fault diagnosis methods. In addition, the steady state analysis has demonstrated the proposed method to monitor the secondary fluid level inside the HCSG tubes through measuring the primary fluid temperature profile.

3.2 Description of HCSG Heat Transfer Mechanism and a Novel Approach to Level Measurement

In the HCSG system, the nominal parameters of which are shown in Figure 3.4, the primary fluid flows downward from the top to the bottom on the shell side. The primary side heat transfer is sub-cooled forced convection along the entire steam generator height and the secondary fluid flows upward inside the coiled tubes from the bottom to the top of the steam generator. The feed water flows into the sub-cooled region of the steam generator. In the sub-cooled region, the heat transfer is mainly due to single-phase turbulent and molecular momentum transfer and the pressure loss is mainly due to wall friction. The saturated region begins when the bulk temperature becomes saturated. The heat transfer in the saturated boiling region is dominated by nucleate boiling, which is much more efficient than single-phase liquid or steam heat transfer. In the saturated boiling region, the generated bubbles do not disappear in the liquid core and the pressure loss is not only due to the wall friction but also due to the interfacial drag between the bubbles and the liquid. The saturated boiling region ends when critical heat flux is reached. After the steam quality becomes greater than 1.0, the liquid evaporation ceases and the steam becomes superheated.

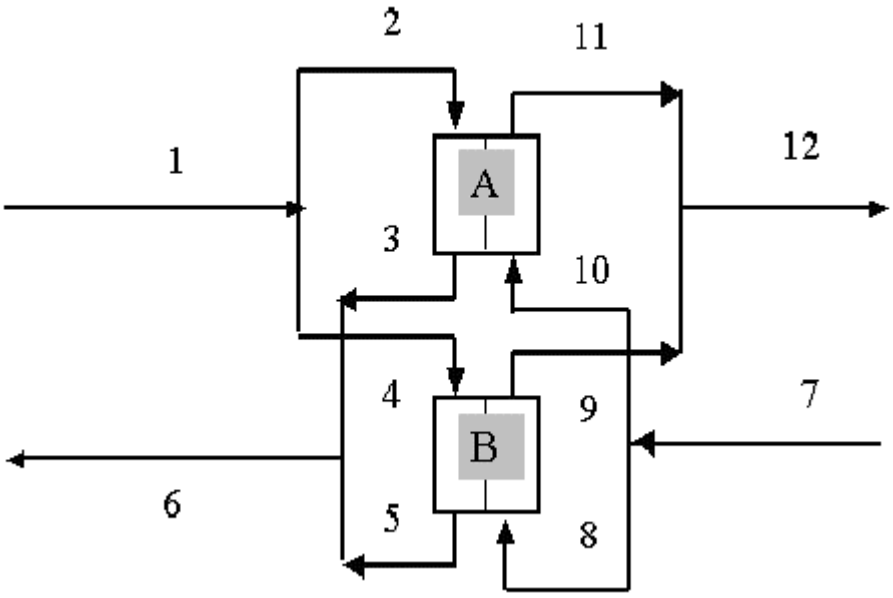

Figure 3.3. A schematic of one pair of steam generators.

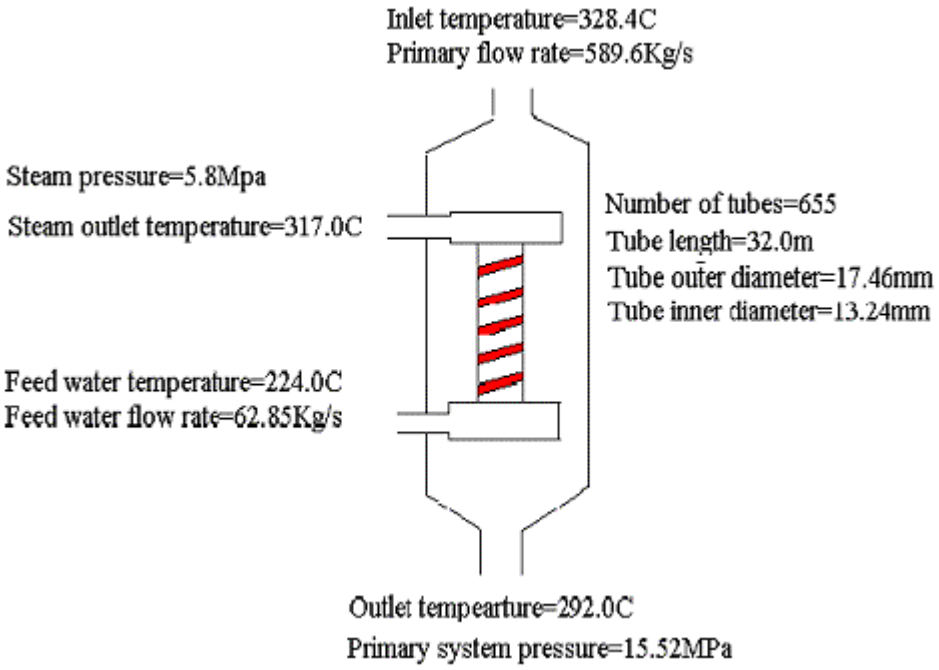

Figure 3.4. HCSG design parameters at full power condition.

The inherent HCSG heat transfer characteristics enable us to use the shell side fluid temperature profile to measure the steam generator level inside the tubes. The secondary fluid flows upward inside the tubes experiencing sub-cooled region, saturated boiling region, and superheated region. Because the heat transfer coefficient in the tubes decreases significantly from the saturated boiling region to the superheated region, a sharp breakpoint of the shell side fluid temperature profile can be observed and used as a practical measure of the water level inside the coiled tubes.

In fact, many types of multiple-point level detectors have been developed based on the principle that the heat transfer coefficient in water is much larger than the heat transfer coefficient in steam (Wang et al., 1998). These designs are common in that a heating rod is embedded into the center of the level detector and a set of thermocouples are installed to measure the temperature profile of the liquid near the inside wall of the level detector. At the level between the steam and the liquid in the measured medium, the measured temperature will show a sharp change.

As is evident, the physical principle of the proposed HCSG level measurement is the same as that of the multiple-point level detector. In the case of HCSG, the heat transfer mechanism is inherent in the system, so it provides an efficient solution to individual steam generator level monitoring.

3.3 Development of HCSG Steady State Model

A detailed steady state model is developed to investigate the feasibility of the proposed tube inside level measurement and prepare the initialization parameters for the dynamic model.

The developed model is based on a straight channel analysis and the helical features are represented implicitly by some correction factors with respect to the friction factor and the heat transfer coefficient. Different empirical correlations associated with the sub-cooled region, saturated region, and superheated region are used to characterize the axially changing pressure losses and heat transfer. In addition, functional steam and water properties are used (Garland and Hoskins, 1988), (Garland and Hoskins, 1989), (Garland and Hoskins, 1992).

3.3.1 Computation Algorithms

The overall computation starts from the bottom of the steam generator and advances upward to the top. For a given cell, the steady state calculation is achieved based on the following iterative algorithm (Lee and Akcasu, 1981):

- Initialize the cell-averaged pressure and enthalpy with the outlet values of the previous cell.
- Iterate over the heat transfer rate and the pressure drop until convergence.
  - Calculate the heat transfer coefficients and the friction factors using the cell averaged thermal properties.
  - Calculate the heat transfer rate from the primary side to the secondary side and the pressure loss within the cell.
  - Calculate the values of the outlet enthalpy and the outlet pressure.
  - Update the cell averaged pressure and enthalpy of the cell.
- End the iteration.

The steady heat balance between the primary coolant and the secondary coolant is governed by:

$$\Delta H^{p} = \frac{\Delta q}{W_p}$$
$$\Delta H^{s} = \frac{\Delta q}{W_s} \qquad (3.1)$$

where

H = the specific enthalpy.

q = the heat transfer rate.

W = the mass flow rate.

s, p = the subscript or superscript denoting the secondary side and the primary side, respectively.

If the acceleration pressure drop due to the change of cross section and density is ignored, the total pressure drop ΔP at steady state conditions is dominated by the frictional pressure drop and gravitational pressure drop, which is given by:

$$\Delta P_s = -\rho_s g \Delta L - \frac{1}{2} f_s (\frac{\Delta L}{D}) \frac{W_s^2}{\rho A_s^2}$$
$$\Delta P_p = \rho_p g \Delta L + \frac{1}{2} f_p (\frac{\Delta L}{D}) \frac{W_p^2}{\rho A_p^2} \quad (3.2)$$

where

ρ = the density.

g = the gravity acceleration.

A = the flow cross section.

f = the friction factor.

ΔL = the flow length.

D =the hydraulic equivalent diameter.

The heat transfer rate from the primary side to the secondary side with tube length ΔL is given by:

$$\Delta q = 2\pi R_o U (T_p - T_s) \Delta L \quad (3.3)$$

where the overall heat transfer coefficient U is given by:

$$U = \frac{1}{\frac{R_o}{R_i h_s} + \frac{R_o}{K_M} \ln \frac{R_o}{R_i} + \frac{1}{h_p}} \quad (3.4)$$

T = the temperature.

R_o = the tube outside radius.

R_i = the tube inside radius.

h = the convection heat transfer coefficient.

K_M = the thermal conductivity of the tube metal.

3.3.2 Heat Transfer Correlations

In the single-phase water and single-phase steam region, the heat transfer coefficient can be calculated using Dittus-Boelter correlation (Kuridan and Beynon, 1997), which is given by:

$$\begin{aligned} Nu &= 0.023\,\mathrm{Re}^{0.8}\,\mathrm{Pr}^{0.4} \quad heating \\ Nu &= 0.023\,\mathrm{Re}^{0.8}\,\mathrm{Pr}^{0.3} \quad cooling \end{aligned} \tag{3.5}$$

where

Nu = the Nusell number.

Pr = the Prantl number.

Re = the Reynolds number.

In the saturated boiling region, the two-phase convection heat transfer coefficient on the secondary side can be calculated using Thom's correlation (Kuridan and Beynon, 1997), which is given by:

$$h_s = (q'')^{0.5}\,\frac{\exp(P/8.69\times10^6)}{0.02253} \tag{3.6}$$

where

q'' = the heating rate.

P = the fluid pressure.

3.3.3 Pressure Drop Correlations

Colebrook equation is employed to compute the single-phase friction factor f_{sp}, which is given by (Smith, 1996):

$$\frac{1}{\sqrt{f_{sp}}} = -2.0\log\left(\frac{\varepsilon/D}{3.7} + \frac{2.51}{\mathrm{Re}_{sp}\sqrt{f_{sp}}}\right) \tag{3.7}$$

where

ε = the average tube roughness.

sp = the subscript denoting single phase.

In order to take into account the effect of coiled geometry, the same ratio of the coil to the straight tube is used for both heat transfer coefficient and friction factor, which is given by (Lee, 1978):

$$\frac{f_{cc}}{f_{ss}} = \left(\mathrm{Re}\left(\frac{R_O}{R_C}\right)^2\right)^{1/20} \tag{3.8}$$

where

f_{cc} =the friction factors for tube coil.

f_{ss} = the friction factor for straight tubes.

R_C = the coil radius.

Modified Chen's correlation is used to calculate the boiling two-phase flow fiction factor in helical coiled tubes given by (Chen 1982):

$$\Phi_{10}^2 = \frac{\Delta P_{tp}}{\Delta P_{sp}} = \psi_1\psi\left(1 + x\left(\frac{\rho_l}{\rho_g} - 1\right)\right) \tag{3.9a}$$

$$\psi = 1 + \frac{x(1-x)((1000/W)-1)(\frac{\rho_l}{\rho_g})}{1+(1-x)((\frac{\rho_l}{\rho_g})-1)} \tag{3.9b}$$

$$\psi_1 = 142.2(\frac{P}{P_{cr}})^{0.62}(\frac{R_I}{R_c})^{1.04} \tag{3.9c}$$

where

Φ_{10}^2 = the two-phase multiplier.

x = the steam quality.

P_{cr} = the critical pressure for water.

ρ_l = the liquid phase density.

ρ_g = the vapor phase density.

3.4 Steady State Results

The developed model was tested with the IRIS HCSG design data. The calculated temperature profiles of the primary fluid and the secondary fluid are shown in Figure 3.5. The calculated lengths of the sub-cooled region, the saturated boiling region and the superheated region are 4.5 m, 21.5 m, and 6.0 m respectively. The calculated steam outlet temperature and the primary inlet fluid temperature are 317.1 C and 327.9 C, respectively, which are 317.0 C and 328.4 C obtained by RELAP (Westinghouse, 2002). The calculated results are within 0.25% error as compared with the results obtained from a more sophisticated code RELAP.

Figure 3.5 clearly shows the break point of primary fluid temperature when the saturated boiling heat transfer transits to the superheated heat transfer at the tube length 26.0 m. This break point can be directly used as an indicator to the steam generator water inventory.

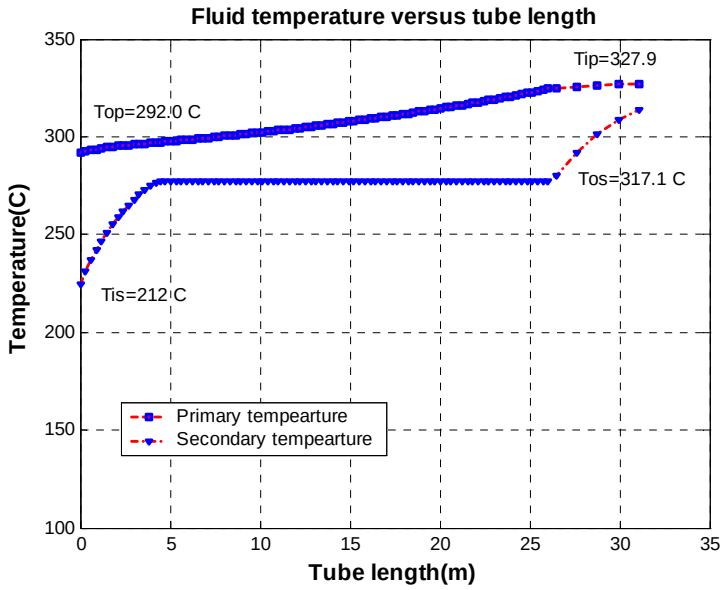

Figure 3.5. Fluid temperature versus tube length at 100% full power.

Figure 3.6 shows the heat transfer coefficients on the primary side and the secondary side. The heat transfer coefficient on the primary side almost maintains at a constant level. The effective heat transfer is dominated by the boiling heat transfer on the secondary side. The average heat transfer coefficient in the boiling region is about four times greater than that in the sub-cooled region and seven times greater than that in the superheated region. The local heat transfer coefficient in the boiling region increases linearly with the axial height. An abrupt increase and an abrupt decrease in heat transfer can be observed from the sub-cooled region to the saturated boiling region and from the saturated region to the superheated steam region respectively.

Figure 3.7 shows the steam quality of the secondary fluid. It is clear that the steam quality can be well approximated as a linear function of the axial coordinates along the tube. Based on this observation, a single node with average thermal properties such as density can be used to describe the behavior in this region if only quasi-steady state transients are to be studied.

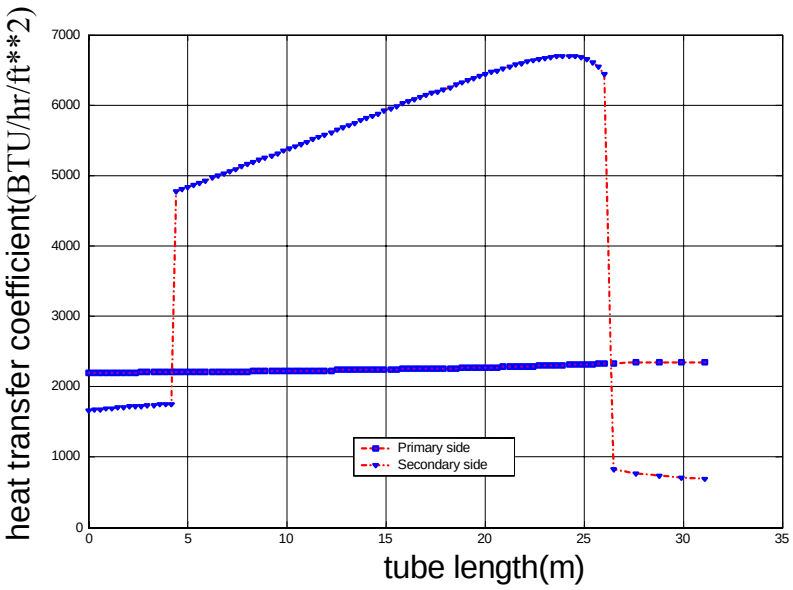

Figure 3.6. Fluid heat transfer coefficients on the primary side and the secondary side at 100% full power.

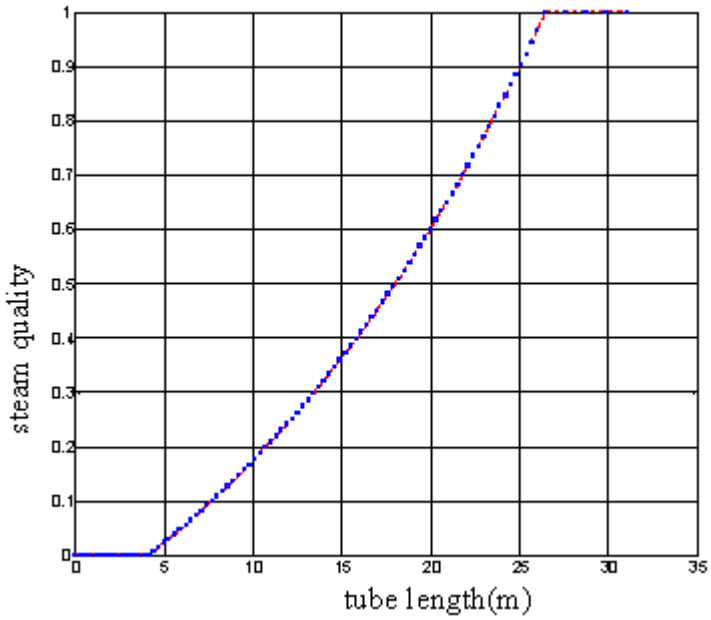

Figure 3.7. Steam quality versus tube length at 100% full power.

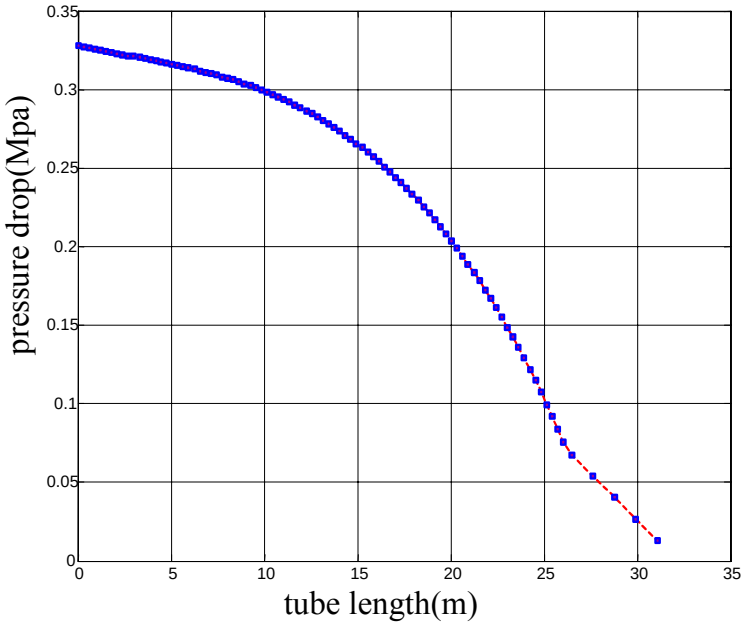

Figure 3.8. Pressure drop versus the tube length on the secondary side at 100% power.

Figure 3.8 shows the pressure drop on the secondary side. The major portion of the pressure drop occurs in the saturated boiling region. The total pressure drop is 0.32 MPa. This result is within 10% error of the result obtained from a more sophisticated code RELAP. The figure also shows that one pressure can be used to characterize the entire superheated region.

In conclusion, a steady state thermal analysis model of HCSG has been successfully developed. The developed model can be used for fault diagnosis under steady state condition and to provide a basis to develop a dynamic process model. The steady state analysis demonstrates that the primary fluid temperature can be used as an indicator to the secondary fluid level inside the HCSG tubes.

3.5 Development of HCSG Dynamic Model

A simplified nodal model is developed to simulate the dynamic behavior of helical coil steam generators under the environment of MATLAB/Simulink. In general, a dynamic process should be modeled as a distributed parameter system characterized by a

set of partial differential equations. However, it may become too complicated to solve such a time dependent system with spatial variations. To simplify the numeric computation, nodal models are sometimes used for an approximate solution. Each node has the same averaged properties, so the spatial dependence can be represented simply by the interaction between adjacent nodes.

3.5.1 Model Assumptions

The overall HCSG model is based on conservation laws of mass, momentum, and energy. As a nodal model, the outlet values of the state variables are used as the nodal representative values. Because the designed FDI system is supposed to work under quasi-steady state conditions, it is assumed in the developed simulation model that the heat transfer coefficients and pressure losses in each heat transfer regime are constant.

In addition to the assumptions implied in a nodal model, the other major assumptions used to build the dynamic model for the helical coil steam generator systems are as follows (Chen, 1976):

- Only one pressure is used to characterize the superheated region.
- The superheated steam satisfies ideal gas law modified by an expansion coefficient.
- The temperature of the second node in the subcooled region is equal to the saturated temperature.
- The pressure drop between the superheated region and the saturated region is constant during any perturbations.
- The pressure drop between the saturated region and the subcooled region is constant during any perturbations.
- The steam quality in the boiling region can be assumed as a linear function of the axial coordinate so the density in the boiling region can be approximated as a function of steam pressure.
- It is assumed that the steam generation rate is equal to the boiling rate.

- It is assumed that the heat transfer coefficients are constant for the superheated region, the saturated region, and the subcooled region.

3.5.2 Nodalization

Figure 3.9 shows the nodalization scheme to simulate the dynamics of HCSG system. In each of the three heat transfer regimes on the secondary side, two nodes with equal length are used to consider the axial temperature changes. Correspondingly, six metal nodes are used to describe the heat transfer from the primary side to the secondary side. For the two nodes of the saturated region on the secondary side, the saturated temperature based on the local pressure is superimposed on the fluid.

3.5.3 Primary Side Heat Balance Equations

The primary coolant temperature can be determined based on the heat balance equations given by:

$$\frac{dT_{pi}}{dt} = a_1 \frac{T_{pi-1} - T_{pi}}{L_i} - a_2 (T_{pi} - T_{wi}) \tag{3.10}$$

where

$$L_i = \begin{cases} L_s & for \quad i = 1,2 \\ L_b & for \quad i = 3,4 \\ L_{sc} & for \quad i = 5,6 \end{cases}$$

$$a_1 = \frac{C_{pp} W_p}{(A_{xs} C_p \rho)_p / 2}$$

$$a_2 = \frac{h_{pw} P_{wp}}{(A_{xs} C_p \rho)_p / 2}$$

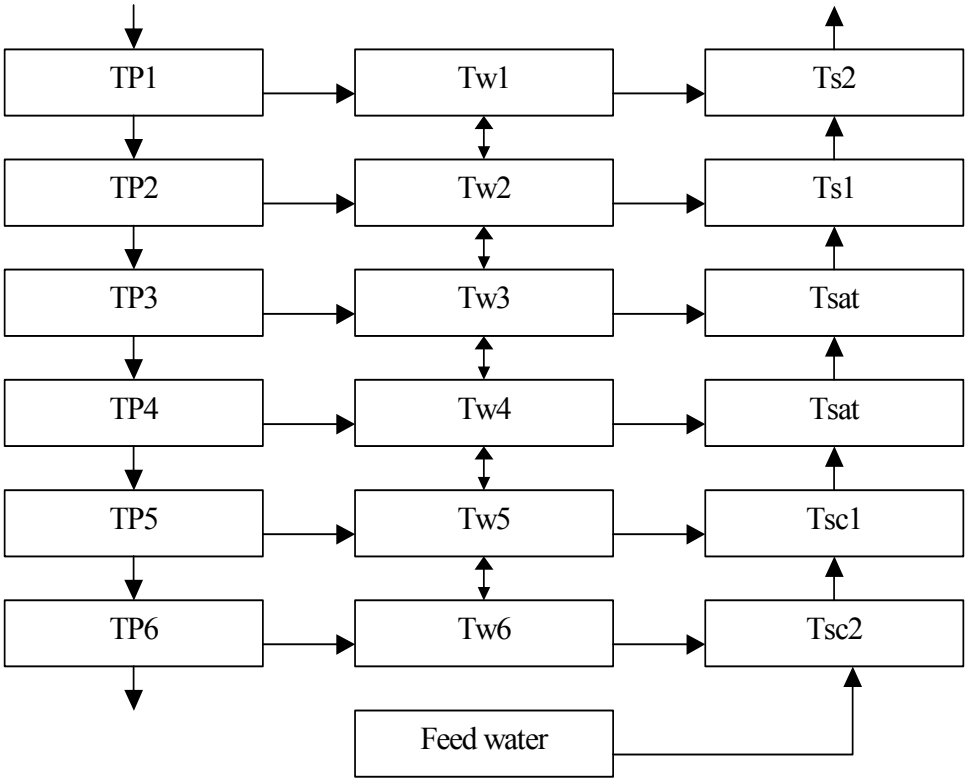

Figure 3.9. Schematic of the nodalization for a helical steam generator.

Tp1,Tp2,Tp3,Tp4,Tp5,Tp6 = Temperature of the primary coolant.
Tw1,Tw2,Tw3,Tw4,Tw5,Tw6 = Temperature of the steam generator tube metal.
Ts1,Ts2,Tsat,Tsat,Tsc1,Tsc2 = Temperature of the secondary fluid for the superheated steam region, the saturated boiling region and the sub-cooled region.

L_s = the superheated length.

L_b = the saturated boiling length.

L_{sc} = the subcooled length.

T_p = the primary side temperature.

T_w = the tube metal temperature.

W_p = the primary coolant flow rate.

C_p = the specific heat.

ρ = the density of the primary coolant.

A_{xs} = the flow area.

h = the heat transfer coefficient.

P_w = the perimeter for heating.

In the above equations, subscript p and w refer to the primary coolant and the tube wall respectively.

3.5.4 Tube Metal Heat Balance Equations

A moving boundary model is used to describe the change of energy distribution in the tube metal due to the heat transfer regime change on the secondary side during a transient. The energy balance equations for the ith node of the tube metal is given by:

$$\frac{d}{dt}((\rho AC_p)_w Z_i T_{w,i}) = (\rho AC_p)_w \dot{Z}_i T_{bw,i+1} - (\rho AC_p)_w \dot{Z}_{i-1} T_{bw,i-1} + Q_{wi} \qquad (3.11)$$

where

Z_i = the length of the ith node of the tube metal.

T_{wi} = the temperature of the ith node of the tube metal.

$(\rho AC_p)_w$ = the heat capacity per unit length.

Q_{wi} = the net income of heat due to the effective heat transfer on the primary side and the secondary side.

$T_{bw,i-1}$, $T_{bw,i+1}$ = the temperature of the metal node below and above the ith node, respectively.

3.5.5 Secondary Side Balance Equations

The state equations of the secondary coolant were derived based on mass and energy balance. Because the pressure waves travel much faster than the fluid velocity, it is assumed that a local pressure disturbance will reach anywhere in the system simultaneously. The exit steam pressure is related to the steam temperature through a further assumption that the superheated steam satisfies the ideal gas law modified by an expansion coefficient.

The mass balance of the steam in the superheated steam nodes, node 1 and node 2, are given by:

$$\dot{M}_{s1} = W_{21} - W_s \tag{3.12a}$$

$$\dot{M}_{s2} = W_b - W_{21} \tag{3.12b}$$

where

M_s = the steam mass in the superheated region.

W_s = the steam flow rate to turbine, which is an external constraint imposed by the controller.

W_{21} = the steam flow rate flowing from the steam node 1 to the steam node 2.

W_b = the steam production rate.

The heat balance equations of the two superheated steam nodes, node 1 and node 2, are given by:

$$\frac{d}{dt}(M_{s1}H_{s1} - P_sV_{s1}) = Q_{s1} + W_{21}H_{s2} - W_sH_{s1} - P_{s1}\dot{V}_{s1} \quad (3.13a)$$

$$\frac{d}{dt}(M_{s2}H_{s2} - P_sV_{s2}) = Q_{s2} + W_bH_g - W_{21}H_{s2} - P_{s2}\dot{V}_{s2} \quad (3.13b)$$

where

M_s = the steam mass in the superheated region.

P_s = the steam pressure in the superheated region.

V_s = the steam volume in the superheated region.

H_s = the specific enthalpy of the steam.

H_g = the specific enthalpy of the saturated steam.

Q_{s1}, Q_{s2} = the heat transfer rate to the two superheated nodes.

$$Q_{s1} = h_{ws}P_{ws}L_s(T_{w1} - T_{s1})/2 \quad (3.14a)$$

$$Q_{s2} = h_{ws}P_{ws}L_s(T_{w2} - T_{s2})/2 \quad (3.14b)$$

where

P_{ws} = the heating perimeter in the superheated steam region.

Assuming the pressure loss in the superheated steam region is small, we have:

$$P_s = P_{s1} = P_{s2} \quad (3.15)$$

Since specific enthalpy is a function of temperature and pressure, then we have:

$$\dot{H}_s = \frac{\partial H_s}{\partial T_s}\dot{T}_s + \frac{\partial H_s}{\partial P_s}\dot{P}_s \quad (3.16)$$

and

$$H_{s2} - H_{s1} = \frac{\partial H_s}{\partial T_s}(T_{s2} - T_{s1}) \quad (3.17)$$

Combining the mass balance equations and the expansion of the specific enthalpy, the energy balance equations (Equations (3.13a) and (3.13b)) can be rewritten as follows:

$$M_{s1}C_{ps}\dot{T}_{s1} + C_{ps}(T_{s1} - T_{s2})\dot{M}_{s1} + (M_{s1}\frac{\partial H_s}{\partial P_s} - V_{s1})\dot{P}_s = Q_{s1} - W_s C_{ps}(T_{s1} - T_{s2}) \quad (3.18)$$

$$M_{s2}C_{ps}\dot{T}_{s2} + (M_{s2}\frac{\partial H_s}{\partial P_s} - V_{s2})\dot{P}_s = Q_{s2} - W_b C_{ps}(T_{s2} - T_{sat}) \quad (3.19)$$

The steam pressure in the superheated region can be described by compressibility adjusted ideal gas law, which is given by:

$$P_s V_s = Z^*_s M_s R(T_{s1} + T_{s2})/(2M_{stm}) \quad (3.20)$$

The time derivative of the steam pressure can then be determined by the following equation:

$$\dot{P}_s = \frac{1}{A_s L_s}[\frac{Z^*_s R}{2M_{stm}}[\dot{M}_s(T_{s1} + T_{s2}) + M_s(\dot{T}_{s1} + \dot{T}_{s2})] - P_s A_s \dot{L}_s] \quad (3.21)$$

where

M_{stm} = the mole mass of steam.

Z^*_s = the steam expansion coefficient.

R = the universal gas constant.

Two-phase averaged density is used in the mass and energy balance equations for the saturated boiling region. It is assumed that the steam quality in this region is a linear function of the axial coordinate, so the two-phase averaged density $\overline{\rho}_b$ is given by:

$$\overline{\rho}_b = \frac{\int_0^1 \rho(x)dx}{\int_0^1 dx} = \frac{1}{(v_f - v_g)}\ln(\frac{v_g}{v_f}) \quad (3.22)$$

where

x = the steam quality.

v_f = the specific capacity of the saturated water.

v_g = the specific capacity of the saturated steam.

Because both v_f and v_g are dependent only on steam pressure, $\overline{\rho}_b$ can then be represented as a function of steam pressure.

The saturated boiling length is determined by the mass balance equations involving the boiling rate, the steam flow rate leaving the saturated boiling region into the superheated region, which is given by:

$$\frac{d}{dt}(\overline{\rho}_b A_s L_b) = W_{db} - W_b \tag{3.23}$$

where

W_{db} = the flow rate leaving the subcooled region for the saturated boiling region.

If we notice

$$\frac{d\overline{\rho}_b}{dt} = \frac{d\overline{\rho}_b}{dP_s}\frac{dP_{sat}}{dt} \tag{3.24}$$

then

$$A_s \overline{\rho}_b \dot{L}_b + A_s L_b K_b \dot{P}_{sat} = W_{db} - W_b \tag{3.25}$$

where

$$K_b = \frac{\partial \overline{\rho}_b}{\partial P}$$

In the operation pressure range, we have the following empirical relationship between the two-phase average density and the steam pressure (Chen, 1976):

$$\overline{\rho}_b(P_s) = 1.61594 + 0.00552445 P_s \tag{3.26}$$

Therefore,

$$\dot{L}_b = \frac{1}{A_s \overline{\rho}_b}[W_{db} - W_b - A_s L_b K_b \dot{P}_{sat}] \tag{3.27}$$

For not a severe pressure transient, it can be assumed that the boiling rate is equal to the steam generation rate W_b, which is given by (Chen, 1976):

$$W_b = \frac{1}{h_{fg}}[h_{wb} U_{wb} (\frac{T_{w3} + T_{w4}}{2} - T_{sat}) L_b] \tag{3.28}$$

where

h_{fg} = the vaporization heat.

In analogy to the saturated boiling region, the mass balance equation for the subcooled region can be given as follows:

$$W_{db} = W_{fw} - \overline{\rho}_{sc} A_{sc} \dot{L}_{sc} - A_s L_{sc} K_{sc} \dot{P}_{sc} \tag{3.29}$$

where

$$K_{sc} = \frac{\partial \overline{\rho}_{sc}}{\partial P_{sc}} = 0.5 \frac{\partial (\rho_{fw} + \rho_f)}{\partial P_{sc}}$$

W_{fw} = the feed water flow rate.

ρ_{fw} = the feed water density.

ρ_f = the density of saturated water.

The heat balance equation for the subcooled region 1 is given by:

$$\frac{d(MC_p T)_{sc1}}{dt} - V_{sc1} \dot{P}_{sc} = h_{wsc} P_{wsc} L_{sc} (T_{w5} - T_{sc1}) + C_{psc} (W_{sc} T_{sc2} - W_{db} T_{sc1}) \tag{3.30}$$

Since the outlet temperature of the subcooled region 1 can be approximated by the saturated temperature (Chen, 1976), then

$$A_s(\rho C_p)_{sc}[T_{sat}\dot{L}_{sc} + K_1 L_{sc}\dot{P}_{sat}] - A_s L_{sc}\dot{P}_{sc} = h_{wsc}P_{wsc}L_{sc}(T_{w5} - T_{sat}) + 2C_{psc}(W_{sc}T_{sc2} - W_{db}T_{sat}) \quad (3.31)$$

where

$$K_1 = \frac{\partial T_{sat}}{\partial P}$$

W_{sc} = the flow rate from the subcooled region 2 to the subcooled region 1.

The temperature of the subcooled region 2 can be determined using the heat balance equation, which is given by:

$$A_s(\rho C_p)_{sc}[T_{sc2}\dot{L}_{sc} + L_{sc}\dot{T}_{sc2}] - A_s L_{sc}\dot{P}_{sc} = h_{wsc}U_{wsc}L_{sc}(T_{w6} - T_{sc2}) + 2C_{psc}(W_{fw}T_{fw} - W_{sc}T_{sc2}) \quad (3.32)$$

If we assume $\dot{M}_{sc1} = \dot{M}_{sc2}$, then we have:

$$W_{sc} = 0.5(W_{fw} + W_{db}) \quad (3.33)$$

Substituting the expression of W_{sc} and W_{db} into the heat balance equation for the subcooled region 1, we have (Chen, 1976):

$$\dot{L}_{sc} = \frac{1}{0.5A_s(\rho C_p)_{sc}(T_{sc2} - T_{sat})}\{0.5 * h_{wsc}P_{wsc}L_{sc}(T_{w5} - T_{sat}) + C_{psc}(W_{fw}T_{sc2} - W_{sc}T_{sat}) - \frac{A_s L_{sc}}{2}[K_{sc}C_{psc}(T_{sc2} - 2T_{sat}) - 1]\dot{P}_{sc}\} - 0.5A_s(\rho C_p)_{sc}K_1 L_{sc}\dot{P}_{sat} \quad (3.34)$$

Noticing the pressure relationship between P_{sc}, P_{sat} and P_s, we have:

$$P_{sc} = P_{sat} + \frac{1}{2}(\Delta P_{tpb} + \Delta P_{spsc}) \quad (3.35)$$

$$P_{sat} = P_{ss} + \frac{1}{2}(\Delta P_{tpb} + \Delta P_{spss}) \tag{3.36}$$

where

P_{sc} = the pressure in the subcooled region.

P_{sat} = the pressure in the saturated region.

ΔP_{tpb} = the two phase pressure loss in the boiling region.

ΔP_{spsc} = the single phase pressure loss in the subcooled region.

ΔP_{spss} = the single phase pressure loss in the superheated region.

3.5.6 HCSG Pressure Controller

The overall control objective of the HCSG system is to supply adequate amount of steam to meet the demand of turbine system. As power demand changes, the turbine throttle valve changes its position to follow the set point changes of turbine header pressure. In the meantime, in order to prevent the carryover of water to the turbine system or dry-out of the steam generator tubes, a feedforward controller is used to suppress a possible large mismatch between the feed water flow rate and the steam flow rate. The combination of the steam pressure feedback control and the feed water flow rate feedforward control is able to effectively control the steam generator pressure. Because the steam pressure is tightly related to the saturated boiling length, the system stability can be ensured through the steam pressure control during power transients. Figure 3.10 shows a schematic of the steam generator pressure control.

Since the steam pressure is maintained by regulating the steam flow rate, the steam flow rate can be determined by the following equation (Guimaraes, 1992):

$$\dot{W}_s = \frac{W_{s0}(1 - C_{st}u) - W_s}{\tau_s} \tag{3.37}$$

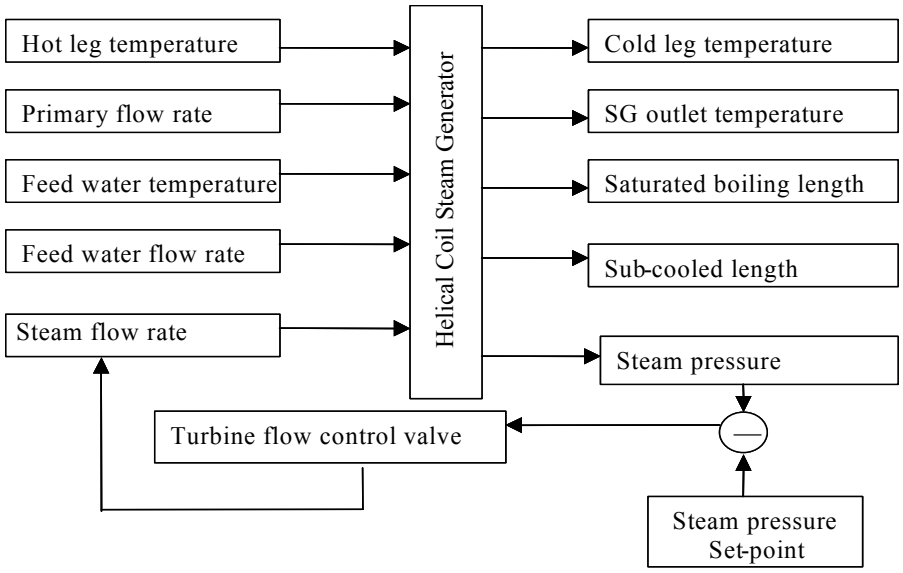

Figure 3.10. Schematic of the helical coil steam generator control system.

where

u = the controller output.

τ_s = the time constant.

W_{s0} = the initial steam flow rate on the secondary side.

C_{st} = the adjustable parameter.

If a PI controller is used, the controller output has both the proportional part $u_1(t)$ and the integral part $u_2(t)$, which is given by (Guimaraes, 1992):

$$u_1(t) = k_1\left(\frac{P_{tb}}{P_0} - \frac{P_{set}}{P_0}\right) \tag{3.38a}$$

$$\frac{du_2(t)}{dt} = k_2\left(\frac{P_{tb}}{P_0} - \frac{P_{set}}{P_0}\right) \tag{3.38b}$$

where

k_1 = the proportional gain.

k_2 = the integral gain.

Table 3.1. Model parameters and steady state performance of dynamic HCSG modeling.

Process Variable	Heat Balance	Model Results
Saturated boiling length (m)	21.5	22.36
Sub-cooled length (m)	4.5	4.42
Cold leg temperature (^{o}C)	292.1	291.98
Steam temperature (^{o}C)	317.1	316.59

P_{tb} = the turbine header pressure.

P_{set} = the turbine header pressure setpoint.

P_0 = the nominal turbine header pressure.

In summary, twenty-one state variables, each of which corresponds to one differential equation, are actually used in the developed simulation model. They include the temperatures of the six nodes on the primary side, the temperatures of the six tube metal nodes, the temperatures of the two superheated steam nodes, the temperatures of the two secondary side sub-cooled nodes, the steam pressure, the saturated boiling length, the sub-cooled length, the steam flow rate, and the controller output. Matlab/Simulink built-in algorithms are available for the solution to these coupled differential-algebraic equations.

3.6 HCSG Transient Results

A steady state analysis is performed using the developed dynamic model for full power operation. A comparison with the heat balance results is shown in Table 3.1. The

calculated lengths of the sub-cooled region, the saturated boiling region and the superheated region are 4.42 m, 22.36 m, and 5.22 m, respectively. The calculated steam outlet temperature is 316.59 ^{o}C and the primary outlet fluid temperature is 291.98 ^{o}C. The calculated results are in good agreement with the heat balance results for all the measured variables.

Figures 3.11 (a) and Figure 3.11 (b) show the open-loop responses of the cold leg temperature and the steam outlet temperature due to the hot leg temperature step increase of 1°C and the feed water flow rate 1% step increase, respectively. During the hot leg temperature transient, the disturbance moves from the top to the bottom. The steam pressure first increases as the steam temperature increases. The increased steam pressure causes the saturated temperature in the saturated boiling region to increase. When the disturbance of the hot leg temperature moves to the saturated boiling region and the sub-cooled region, the saturated boiling length and the sub-cooled length will decrease. As a result, the superheated length becomes longer and the steam temperature continues to increase. The entire transient stops when the steam pressure goes back to its initial level due to the self-regulation of steam pressure when the steam temperature increases and the superheated steam length increases. In the end, the steam outlet temperature increases, the cold leg temperature increases, and the saturated boiling length and the sub-cooled length decrease.

During a feed water flow step increase transient, the disturbance moves from the bottom to the top. When the feed water flow rate increases, the sub-cooled length will increase and the superheated steam length will decrease. This decrease in the superheated steam length explains the initial decrease of the steam temperature. As the disturbance moves to the saturated boiling region, the saturated boiling length will also increase and result in further decrease in the superheated steam length, which will lead to additional decrease in the steam temperature and increase in the steam pressure. The entire transient stops when the steam pressure stabilizes at a higher level to maintain the balance between the steam flow rate and the feed water flow rate. The transient ends up with a deceased steam temperature, a decreased cold leg temperature, an increased saturated boiling length, and an increased sub-cooled length.

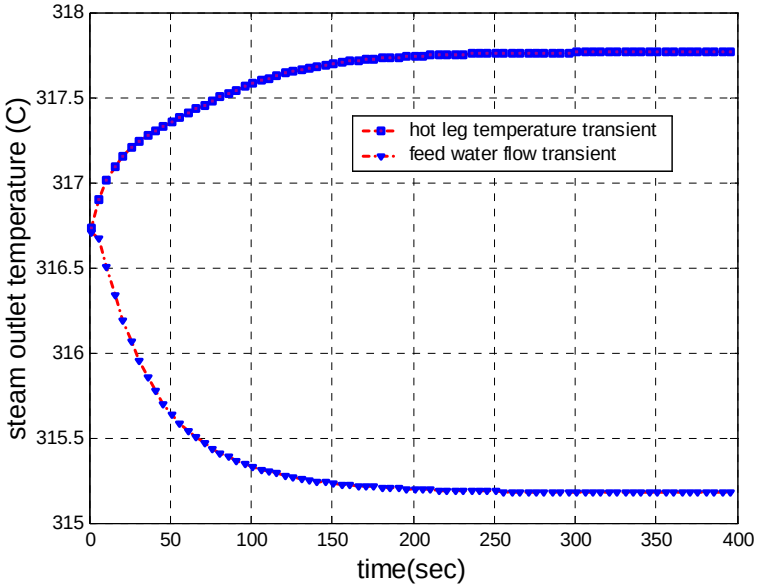

Figure 3.11 (a). Steam temperature open-loop responses due to feed water flow and hot leg temperature transients.

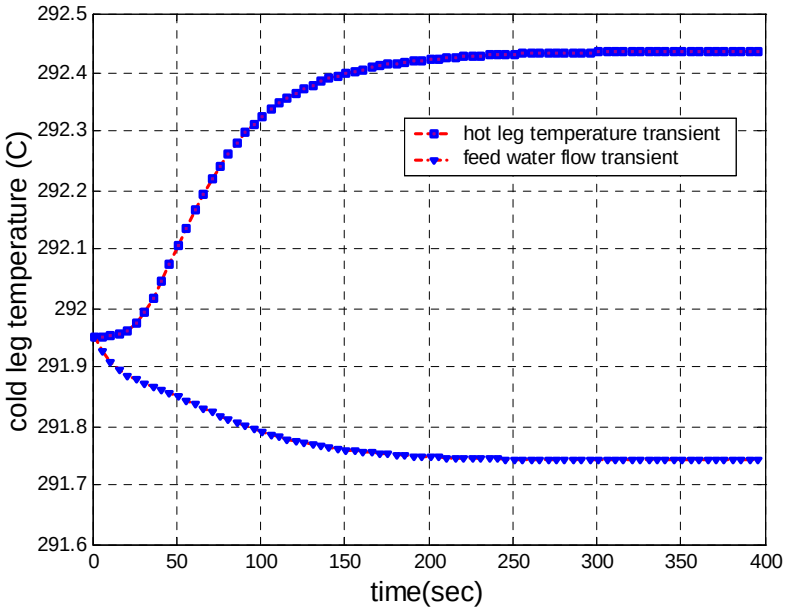

Figure 3.11 (b). Cold leg temperature open loop responses due to feed water flow and hot leg temperature transients.

Figures 3.12 (a) and Figure 3.12 (b) show the closed-loop responses of the cold leg temperature and the steam outlet temperature due to the hot leg temperature step increase of $1^{o}C$ and the feed water flow rate 1% step increase, respectively. As compared with the open loop responses, the response time has been significantly reduced after the steam pressure has been controlled because the HCSG steam pressure is sensitive to the system disturbances.

3.7 Summary

A steady state model has been developed for the IRIS helical coil steam generator to prepare the initialization parameters for the dynamic model and investigate the proposed method of tube inside level detection based on the shell side fluid temperature profile. This model is based on a straight channel analysis with the helical features represented implicitly by some correction factors with respect to friction factors and heat transfer coefficients. Different empirical correlations associated with the sub-cooled region, the saturated region and the superheated region are used to characterize the axially different pressure loss and heat transfer. The calculated primary outlet temperature and the steam outlet temperature are within 0.5% error of the results obtained from a more sophisticated code RELAP. The calculated primary coolant temperature profile has also demonstrated that a clear breakpoint exists when the saturated boiling heat transfer transits to the superheated heat transfer. This breakpoint determined from the primary fluid temperature measurements can be used to indicate the steam generator tube inside water level.

A dynamic model has also been developed to study the dynamic responses of the IRIS helical coil steam generator systems and generate data to study the subspace identification technique in Chapter 6. The developed dynamic model is a nodal model based on conservation laws of mass, momentum, and energy. The steady state performance and the typical results of transient analysis have demonstrated that the developed dynamic model is able to characterize the dynamic behavior of the HCSG system with reasonably good accuracy. The developed dynamic model can be used to study the control and fault diagnosis of IRIS HCSG system.

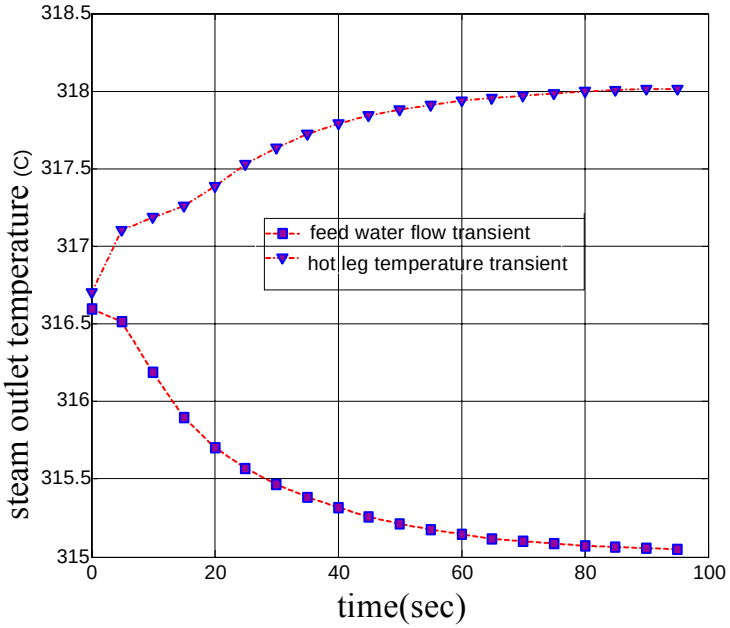

Figure 3.12 (a). Steam temperature closed-loop responses due to feed water flow and hot leg temperature transients.

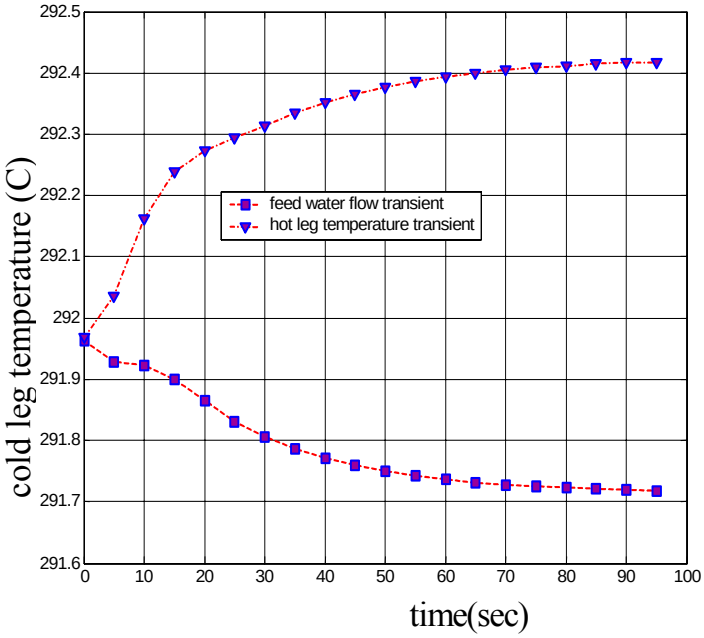

Figure 3.12 (b). Cold leg temperature closed-loop responses due to feed water flow and hot leg temperature transients.

Chapter 4

Sensor Placement Design

In this dissertation, performance monitoring is defined as a task to estimate performance related parameters using available measurements with measurement noise removed for individual components in nuclear power plants. Fault diagnosis is defined as a task to detect and isolate a fault of sensors, actuators, controllers, and equipment.

Sensor placement is an important issue for both control and design of a performance monitoring and fault diagnosis system for nuclear power plants. Without appropriate sensor placement, process performance monitoring and fault diagnosis would become very limited in its correctness and reliability. In order to detect a process fault and locate its root cause, sensors must be placed such that the fault effects can be observed and the observed symptoms should exhibit different patterns for different faults. When process performance is to be monitored, the performance related parameters must be inferable from available measurements. If analytical redundancy is used to monitor critical measurements for better process supervision, sensor placement must ensure that these critical measured variables can be determined with adequate precision from functional relationships.

The role of sensor placement in performance monitoring and fault diagnosis has not been appreciated in nuclear power plant design. Part of the reason is attributed to the lack of communication between research and engineering design. The engineers in industry did not fully understand what analytical redundancy could do for performance monitoring and fault diagnosis. The researchers did not pay enough attention to the full picture of performance monitoring and fault diagnosis to achieve the required engineering objectives. However, to design an efficient performance monitoring and fault diagnosis system for nuclear power systems, sensor placement is indeed an issue that must be addressed in the design phase.

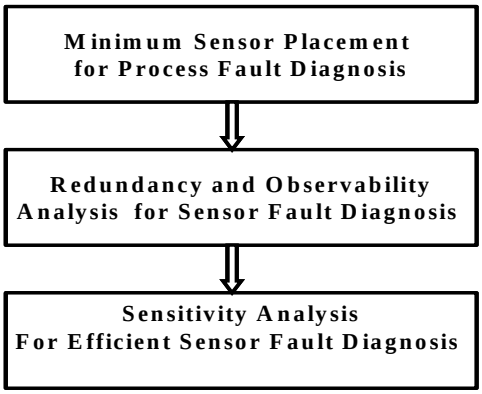

Figure 4.1. Procedure of sensor placement design for fault diagnosis.

A systematic design approach to sensor placement for fault diagnosis is developed in this dissertation. Figure 4.1 shows the procedure of this approach. After the objective of process performance monitoring and fault diagnosis is defined, the cause-effect relationships among the involved variables are first studied using causal graph theory to determine the minimum set of sensors such that the considered process faults, which are represented by some deviation from certain reference values, can be detected and isolated. The reference values are usually calculated by a reliable simulation model using the related reference inputs for a given operation condition.

To determine the deviation from the reference values for reliable process fault diagnosis, it is required that the measured variables should have no instrument faults associated with them. Fortunately, because most process faults do not lead to the violation of mass balance and energy balance equations, these balance equations can actually be used for instrument monitoring without the interference of process faults. If sensor fault diagnosis is based on mass balance and energy balance equations, which is assumed in this dissertation, the second step of sensor placement design is to ensure the estimatability of the measured variables by performing redundancy and observability analysis.

However, even if a variable can be estimated using balance equations, it is still likely that the estimated value may not have enough precision for reliable instrument monitoring as well as performance parameter estimation. It is observed that a measured

variable can be validated efficiently only if the related variable is sensitive in the corresponding balance equations. Therefore, it is necessary to perform a sensitivity study for efficient sensor fault diagnosis, which is the last step of sensor placement design shown in Figure 4.1. In this dissertation, data reconciliation is introduced as a generalized approach to study the sensitivity of a variable in balance equations for sensor placement design.

4.1 Guidelines for Sensor Placement

In instrumentation and control system design, the purpose of sensor placement is to select appropriate variables to achieve the defined operation requirements. Specifically, sensor placement design needs to consider process control, operation performance monitoring, and fault diagnosis. Among the three objectives, only the sensor placement design for control is well studied, and very little research is reported for performance monitoring and fault diagnosis.

4.1.1 Sensor Placement for Control

The sensor placement for process control is to determine the controlled variables and the manipulated variables to achieve the designed control objectives. In most control practices, it is necessary to place sensors to measure the controlled variables and the manipulated variables. However, in some cases, it is also necessary to measure additional process variables for tuning controllers and monitoring control loop performance.

The selection of controlled variables is mainly concerned with the process requirements. The general guideline is that the controlled variables should include: (1) not self-regulating variables, (2) environment and equipment safety critical variables, (3) process performance critical variables, (4) the variables that have strong interactions with other control variables, and (5) the variables with favorable static and dynamic characteristics (Bagajewicz, 2001).

The selection of manipulated variables should ensure that the controlled variables be controlled in a satisfactory manner. The steady state gain between the manipulated variables and the controlled variables should be as large as possible and the dynamic response of the controlled variables should be as timely as possible.

The selection of additional measurements is mainly focused on supervising operation conditions. The plant operation conditions are usually defined by a set of state variables. If possible, a direct measurement of these state variables is desired. If not possible, these states also need to be estimated accurately based on functional relationships. In either case, these measurements must be a sensitive function of the plant operation conditions.

4.1.2 Sensor Placement for Performance Monitoring and Fault Diagnosis

The sensor placement design for performance monitoring is to select appropriate variables such that the operation performance parameters can be determined using functional relationships. If the functional relationships of a system are given, the selection of variables is to search the best set of measurements such that the performance parameters can be inferred most accurately and precisely.

To select variables for fault diagnosis, it is necessary to distinguish between process faults and sensor faults. A process fault is defined as a deviation from the expected normal operation conditions. One type of process faults is related to the deviation of a single process variable from its reference value, one example of which is flow abnormality. For this kind of process faults where mass balance and thermal balance equations will not be violated, the selection of variables to detect and evaluate theses faults is to ensure that the related variables can be accurately estimated based on the given balance equations.

The second type of process faults is related to the deviation of multiple process variables from some reference values. Inappropriate setting of some process variables for a given operation condition is such an example. In this case, fault symptoms are

manifested by abnormal deviation of multiple process variables from the reference values for this operation condition. The selection of variables to detect and distinguish such process faults is to ensure the observability of these process variables through adequate sensor placement.

A sensor fault corresponds to malfunction of an instrument either due to a transducer problem or due to an electrical circuit problem. For sensor faults, mass balance and thermal balance equations will be violated due to the incorrect measurements if the related variables appear in these equations. The selection of variables to detect and rectify sensor faults depends on the functional redundancy and the sensitivity of the measured variables in the balance equations.

It is common that a technical process involves many degrees of redundancy for one variable because process variables are related to each other through balance equations due to the network architecture of components in a large thermal-fluid system. In order to take advantage of this, sensor fault diagnosis should usually be performed using plant-wide balance equations. After the measured variables are validated, process fault diagnosis can then be performed using component based simulation models. The component based simulation models, in general, constrain additional degrees of freedom due to the limitation on operation states as compared with the balance equations where each component is treated as a unit. To detect and distinguish process faults, component based simulation models should be able to determine the reference values of the selected variables for process fault detection and isolation.

Because simulation models always have uncertainty and process parameters are always varying throughout the lifetime of a component, component based simulation models must be tuned on a regular basis such that the models used for process fault diagnosis and performance evaluation can represent the most current operation conditions.

4.2 Sensor Placement Design for Process Fault Diagnosis

Directed Graph (DG) based approach was developed in this dissertation to determine the sensor placement requirements for process fault diagnosis. In this

approach, directed graph is used to describe the propagation of fault effects and cause-effect analysis is performed using graph theory to design sensor placement.

4.2.1 Graph Representation of a Process

Signed Directed Graph (SDG) and Directed graph (DG) are two most popular graph methods to represent the cause effect relationships among plant variables (Kramer and Palowitch, 1987).

4.2.1.1 Sign Directed Graph

In SDG, process variables are represented by individual nodes and the causal relationships between the nodes are represented by signed directed arcs. The states of process variables can take qualitative values such as nominal, high or low. For a measured variable, its values can be determined by a comparison with its reference value obtained from a simulation model. A directed arc can take positive or negative sign, which corresponds to positive or negative influence, respectively. A root node in sign directed graph is connected with at least one effect node but is not connected to any causal nodes. The fault symptoms of a process fault are characterized by a set of nodes that take abnormal values.

Causal analysis may be ambiguous for SDG representation in several situations (Wang and Song, 2002). If multiple paths from node A to node B exist, the product of the arcs along the paths from node A to node B may give different sign products for different paths. For this reason, the directional effects of a change in node A to node B may be ambiguous. If this happens, additional quantitative information is needed to infer the directional effect of a fault at node A on node B.

Another ambiguity may arise for negative feedback control loops (Bhushan and Rengaswamy, 2000). A simple feedback control loop, which is shown in Figure 4.2, consists of a node CV representing the controlled variable, a node M representing the

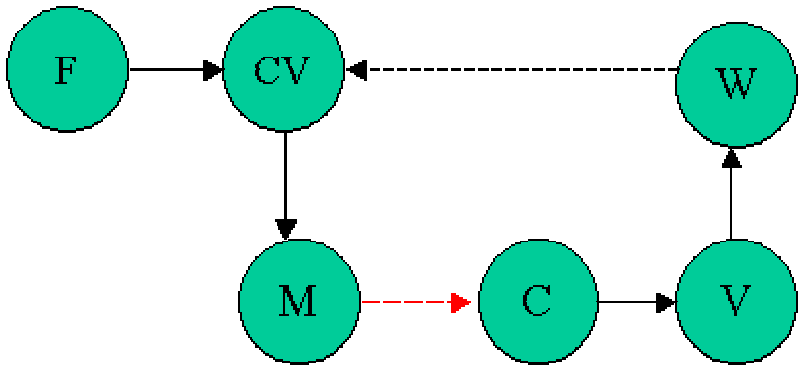

Figure 4.2. SDG graph of a simple feedback control loop.

measured variable, a node C representing the controller, a node V representing the actuation mechanism, and a node W representing the regulated variable. When a disturbance at node F enters the control loop, the disturbance gets into the control loop propagating the disturbance to the node controller (C) via the node M. The resulting change in actuation mechanism (V) regulates the variable W. The node W will have a negative feedback effect on and compensate for the disturbance on the node CV. After a new steady state condition is reached, *the node CV and the node M will become normal*. However, the node C, the node V, and the node W will remain at the values, which are different from the normal, that have caused CV back to the normal value.

This analysis shows that the arc from the node M to the node C is not causal. In other words, even if node C (controller) is abnormal, it does not necessarily indicate that its preceding node M (measurement of controlled variable) is abnormal. Therefore, owing to the noncausal connection, an abnormal node M may or may not cause an abnormal node C.

The U Tube Steam Generator (UTSG) water level control system in PWR is shown as another example to illustrate the ambiguity caused by a feedback control loop. This system has a three-element controller to control the water level in the steam generator as is shown in Figure 4.3. The three elements are steam flow, feed water flow, and steam generator water level. The reference water level is a function of turbine

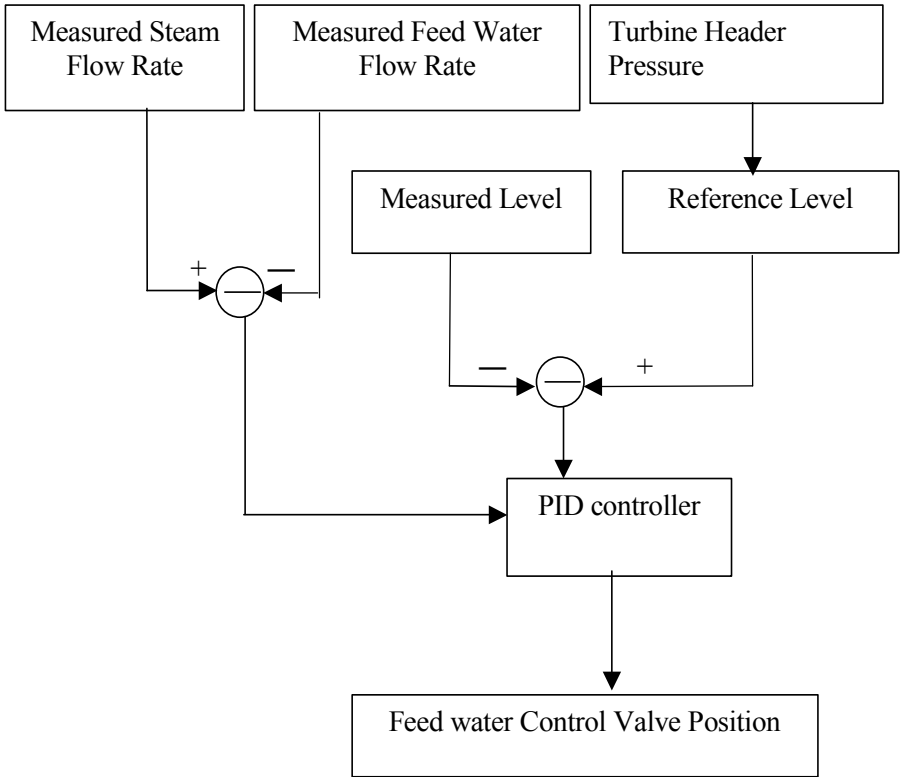

Figure 4.3. UTSG water level control system.

load and steam dump rate through steam dump valves. The SG level error signal is the reference level minus the measured level. The flow mismatch error is the fractional steam flow rate minus the fractional feed water flow rate. The combination of the SG level error and the flow mismatch error is used as the input to the controller. The controller output is used to manipulate the feed water control valve position. Because the main control purpose of the SG level control system is to control the SG water level, the level error has been multiplied by a gain in order to dominate the flow mismatch error signal.

Figure 4.4 shows the SDG for the steam generator system. The node F is a sensor fault that affects the indicated steam generator water level (L_ind). When the node F is abnormal, the disturbance gets into the control loop transmitting the disturbance to the node controller (Ctr). The resulting change in feed water control valve position (FCV) regulates the feed water flow rate Wf. The feed water flow rate change will have a negative feedback effect on the true steam generator water level (L_CV) and will compensate for the disturbance on the indicated steam generator level (L_ind).

Once a new steady state is reached, the steam flow rate and the feed water flow rate must be equal and the indicated steam generator level is equal to the reference steam generator level. If we notice that the steam generator pressure will not have a significant change for an incipient steam generator level sensor fault, the indicated SG level, the controller output Ctr, the feed water control valve position FCV, and the feed water flow rate Wf will all go back to their normal values at steady state conditions. However, the fault effects can be seen in the node L_CV.

From this analysis, it is found that the arc from the node L_CV to the node L_ind is not causal. Although the node L_CV is abnormal, the node L_ind can be normal after a sensor fault of the SG level measurement occurs. In other words, owing to the noncausal connection, an abnormal node L_CV may or may not cause an abnormal node L_ind.

In fact, in order to observe a SG level sensor fault, it is mandatory to place an additional sensor that can observe the change of the true SG level.

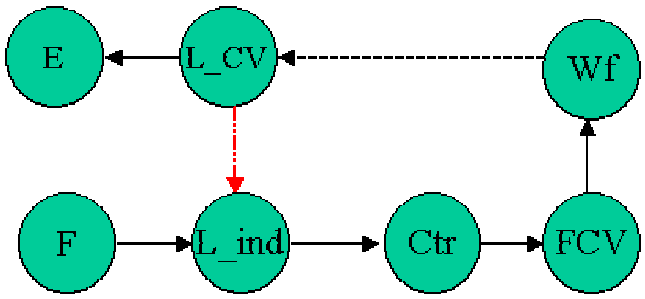

Figure 4.4. SDG graph of nuclear UTSG system.

4.2.1.2 Directed Graph

Although SDG provides more information about the studied process in terms of the cause effect relationships among variables than Directed Graph, Directed Graph is more convenient for sensor placement design. In reality, it is sufficient to know which variable is associated with a process fault and whether the process variable is high or low does not provide significant information for fault diagnosis. Therefore, DG graph approach is investigated in this dissertation for sensor placement design.

The fundamental difference between a SDG graph and a DG graph is that the causal relationships represented by them are different. The arcs in DG graph represent a sufficient cause effect relationship. An arc from node A to node B in a DG graph means that an abnormal node A is a sufficient condition to cause an abnormal node B for all the considered operation conditions. On the other hand, an arc from node A to node B in SDG graph only represents that an abnormal node A may or may not cause an abnormal node B. For example, in the SDG given in Figure 4.4, node L_CV may be abnormal but node L_ind may still be normal if a sensor fault occurs to the node L_ind.

DG graph can be obtained by a simple reduction of the corresponding SDG graph. The SDG graph may consist of noncausal paths and cycles. When it is reduced to DG graph, the noncausal paths and the cycles must be removed and the directional sign of the SDG graph is simply ignored.

4.2.2 Sensor Placement for Process Fault Detection

The sensor placement for process fault detection needs to locate the minimum set of sensors such that all the considered process faults can be observed. This is equivalent to choosing a minimum set of nodes in DG graph such that all of them have connections with the root nodes to represent the process faults. If cyclic nodes are collapsed into supernodes in DG graph, the problem can be simplified as finding the minimum subset of sensors such that there is at least one directed path from all the root nodes.

Although a simple enumeration can be made for a small system, a systematic approach needs to be used for a large system. In this approach, the first step is to build a "bipartite" graph, which consists of a causal set including all the root nodes and an observability set including all the nodes with only input arcs in the DG. In fact, it can be proved that the observability set obtained in this manner contains the key variables that are sufficient to observe all the process faults represented by the root nodes in the DG.After a bipartite graph is obtained from the DG, a subset of the key variables can be chosen from the observability set as the minimum sensor requirements for process fault detection based on the Greedy search algorithm developed by Raghuraj et al., 1999. This algorithm is summarized as follows:

(1) Construct a bipartite graph between the root nodes and the key variables in the observability set.
(2) Select one variable among the unmarked key variables that has the largest number of input arcs.
(3) Mark the selected key variable in step (2) and store it in C.
(4) Find out all the root nodes covered by C (a root node is covered by C if it has at least one arc connections with the elements in C).
(5) If there exist uncovered root nodes,
delete all the arcs from the root nodes determined in Step (4),
go to step (2).
else

output the set C and stop.
(6) end.

If there are no redundant key variables in the observability set, the basic Greedy search algorithm is able to determine the minimum set of sensors for fault detection. However, after a variable has been selected, the subsequently selected variables may also cover the same root nodes that have already been covered by the previously selected variables. In this case, the selected sensors using the basic Greedy search algorithm will contain redundancy for fault observation and thus are not the minimum result. In order to remove the redundant key variables, the location of the minimum set of sensors can be performed using the improved algorithm developed by Raghuraj et al., 1999. The improved algorithm is summarized as follows:
(1) Initiate C and G as empty sets.
(2) Construct a bipartite graph between the root nodes and the key variables in the fault observability set.
(3) Select a variable among the unmarked key variables based on the largest number of incident arcs.
(4) Mark the selected key variable in step (2) and store it in C.
(5) Find out all the root nodes covered by C.
(6) If there exist uncovered root nodes,
delete all the arcs from the root nodes covered by the selected variable to all the previously marked key variables,
store in a buffer set G all the arcs from the root nodes covered by the selected variable to the unmarked key variables .
go to step (3).
else
remove the variables from C that do not have arcs incident on them based on the arcs stored in G.
output the set C and stop.
(7) end.

The number of incident arcs used in Step (3) is defined as the difference between the actual number of arcs incident on a key variable and the number of arcs incident on the same key variable that have been stored in the buffer set G. After the algorithm is completed, the same set of key variables can be obtained in C as is obtained from the Greedy search algorithm. However, the redundant key variables will be stored by tracking the arcs stored in the buffer set G that do not have a connection with the marked key variables. To determine the minimum set of sensors, the redundant key variables must be removed from the obtained key variables stored in C.

Example: Consider a simple example with the bipartite graph shown in Figure 4.5 to illustrate the Greedy search algorithm to determine the minimum set of sensors for process fault detection (Adapted from Raghuraj et al., 1999). In this example, there are six root nodes, R1, R2, R3, R4, R5, and R6 and there are four variables M1, M2, M3, and M4 in the observability set.

Based on the basic Greedy search algorithm, M1 will be selected as the first marked variable for the first iteration because it has the largest number of incident arcs, which is three in this case. For the following three interactions, M2, M3, and M4 will be sequentially selected as the marked variables. In the end, the entire observability set including M1, M2, M3, and M4 will be selected to observe the six root nodes. Obviously, a simple examination of the bipartite graph shows that the minimum set of variables to observe all the root nodes is M2, M3, and M4. The reason why the basic greedy search algorithm fails is that the key variables in the observability set have redundant information.

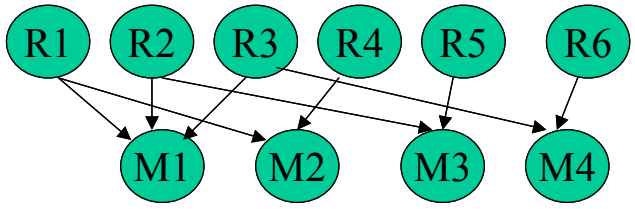

Figure 4.5. An illustration of the improved Greedy search algorithm.

According to the improved Greedy search algorithm, for the first iteration, M1 will also be selected as the first marked variable and stored in set C because it has the largest number of incident arcs, which is three in this case. Meanwhile, the arcs from R1 to M2, R2 to M3, and R3 to M4 will be stored in set G because R1, R2, and R3 are covered by the selected variable M1 and the variables M2, M3, and M4 still have not been marked yet at this stage. After the following four iterations, the entire observability set, including M1, M2, M3, and M4, will be stored in set C and set G will contain the arcs from R1 to M2, R2 to M3, and R3 to M4. As a result, M1 is a marked variable in set C that does not have an arc stored in set G incident on it. Therefore, M1 should be removed from the set G and the minimum set of variables to observe all the root nodes only contain M2, M3, and M4. This result is in agreement with the simple examination of the bipartite graph.

4.2.2 Sensor Placement for Process Fault Isolation

The objective of locating sensors for process fault isolation is to determine a set of variables in the corresponding DG graph that can distinguish the effects of all the process faults. For a set of root nodes, let A_i denote the set of nodes connected to the ith root node. The optimal set of sensors C should be a minimum subset of the set $O = \cup_i A_i$ such that the subset C_i of C that are connected to the ith root node is different from the subset C_j of C that are connected to the jth root node for any one pair of root nodes. In addition, the optimal set should still ensure the fault observability.

A bipartite graph also needs to be built before a graph theory based algorithm can be used for sensor placement design for process fault isolation. The causal set of this bipartite graph includes a set of pseudonodes B_{ij}, each of which denotes a pair of root nodes i and j to be distinguished. The corresponding observability set includes the key variables that can distinguish each pair of the process faults represented by the pseudonodes.

The minimum set of sensors for process fault isolation can also be determined using the algorithm developed by Raghuraj et al., 1999. This algorithm is summarized as follows:

(1) Determine the set of key variables consisting of the different members of A_i and A_j that covers the pseudonode B_{ij}, which denotes the resolution of the root nodes i and the root node j

(2) Construct a bipartite graph between the set of pseudonodes and their observability set.

(3) The individual root nodes are added to the causal set of the constructed bipartite graph.

(4) Apply the algorithm in Section 4.2.1 to determine the minimum set of variables that can cover all the root nodes and the pseudonodes.

The selected variables based on this algorithm can ensure that the specified process faults can be detected and distinguished.

4.3 Redundancy and Observability Analysis

Process fault diagnosis is reliable only if the related measurements do not have instrument faults, so an integrated fault diagnosis system must also address sensor placement design for sensor fault diagnosis.

If sensor faults are diagnosed based on analytical redundancy, no matter what specific diagnostic methods are used, a malfunctioning sensor can be detected, identified, and rectified only if the related variable can be estimated using functional relationships. Therefore, in sensor placement design for sensor fault diagnosis, it is necessary to analyze the redundancy and observability of variables in the functional relationships.

For nuclear power systems, the most commonly used functional relationships are steady state conservation equations, which are considered as the basis for sensor placement design for sensor fault diagnosis in this dissertation. The basic steady state conservation equations include mass balance, energy balance, and momentum balance, which are given as follows:

$$G_{in} - G_{out} = 0$$

$$G_{in} h_{in} - G_{out} h_{out} = \Delta_1 \tag{4.1}$$

$$P_{in} - P_{out} = \Delta_2 + \rho g z + a \frac{\overline{G}^2}{2\rho}$$

where

G_{in} = the inflow mass flow rate.

G_{out} = the outflow mass flow rate.

h_{in} = the specific enthalpy of the inflow fluid.

h_{out} = the the specific enthalpy of the outflow fluid.

P_{in} = the inlet pressure.

P_{out} = the outlet pressure.

Δ_1, Δ_2 = the correction terms for heat loss and additional pressure loss.

a = a factor dependent on geometry and fluid condition.

ρ = the fluid density.

g = the gravity acceleration.

z = the vertical difference between the inlet and the outlet.

In the design phase, the correction terms can be ignored. During plant operation, the correction terms and the coefficient terms can be determined using standard regression methods based on available operation data.

For a nuclear power plant, the sensor configuration becomes a sensor network with the measured variables coupled by functional relationships given in Equation (4.1). Among a given set of sensors, these equations will provide information about whether a sensor is deemed redundant from analytical redundancy point of view and whether an unmeasured variable is observable from the available sensors.

In this section, the redundancy and observability analysis for sensor placement design is presented as a variable classification problem. Although sensor placement

design is method dependent, variable classification gives a theoretical solution to the design.

4.3.1 Variable Classification for Linear Systems

For linear systems, sophisticated methods exist to classify unmeasured variables as observable and unobservable, and classify measured variables as redundant and non-redundant. An easy implementation algorithm is orthogonal transformation based on Q-R decomposition (Sanchez and Romagnoli, 1996).

For steady state conditions, a linear system equation representing functional relationships is given as follows:

$$Ax + Bu = c \tag{4.2}$$

where

x = the set of measured variables.

u = the set of unmeasured variables.

A, B, c= the compatible matrices and vector.

In order to decouple the measured variables x from the unmeasured variables u in Equation (4.2), Q-R decomposition can be performed on the matrix B, which is given by:

$$BE_u = Q_u R_u \tag{4.3}$$

where

E_u = a column permutation matrix on B and $E_u E_u^T = \mathrm{I}$.

$$Q_u = \begin{bmatrix} Q_{u1} & Q_{u2} \end{bmatrix} \tag{4.4}$$

$$R_u = \begin{bmatrix} R_{u1} & R_{u2} \\ 0 & 0 \end{bmatrix} \tag{4.5}$$

where R_{u1} is a square and non-singular upper triangular matrix of the same dimension as the rank of B.

Because the matrix Q_u is orthonormal, if Equation (4.2) is left multiplied by Q_u^T, we have:

$$Q_{u1}^T Ax + \begin{bmatrix} R_{u1} & R_{u2} \end{bmatrix} E_u^T u = Q_{u1}^T c \tag{4.6}$$

$$Q_{u2}^T Ax = Q_{u2}^T c \tag{4.7}$$

Because R_{u1} is a nonsingular matrix with its rank r_u equal to the rank of matrix B, the first r_u unmeasured variables u_{ru} with the row permutation E_u^T acted on the original column vector can be determined by:

$$u_{ru} = R_{u1}^{-1}(Q_{u1}^T c - Q_{u1}^T Ax - R_{u2} u_{n-ru}) \tag{4.8}$$

where

n = the number of unmeasured variables.

Equation (4.8) indicates that the set of unmeasured variables in u_{n-ru} are unobservable. The unmeasured variables are all observable only if $r_u = n$ when the last term disappears in the equation. In addition, if a variable in the set u_{ru} is observable, the corresponding row of matrix $R_{IU} = R_{u1}^{-1} R_{u2}$ must be equal to zero.

Equation (4.7) can be rewritten as follows:

$$Gx = b \tag{4.9}$$

where

$$G = Q_{u2}^T A \tag{4.10}$$

$$b = Q_{u2}^{T} c \tag{4.11}$$

Equation (4.9) implies that a measured variable is not redundant if the corresponding columns of the matrix G are all zeros. This is because such variables will not participate in the derived balance equations.

A simple example is shown here to illustrate how Q-R decomposition is used for variable classification of a linear system. Given a system, shown in Figure 4.6 (adapted from Romagnoli and Sanchez, 2000), three constraint equations of mass balance are defined as follows:

G1+G2-G3=0
G3-G2-G4=0
G4+G5-G6=0

where
G1, G4, G5 = measured flow rates.
G2, G3, G6 = unmeasured mass flow rates.

Step 1: Let us represent the balance equations in two terms corresponding to the measured and the unmeasured variables respectively. For the case problem, the two matrices are as follows:

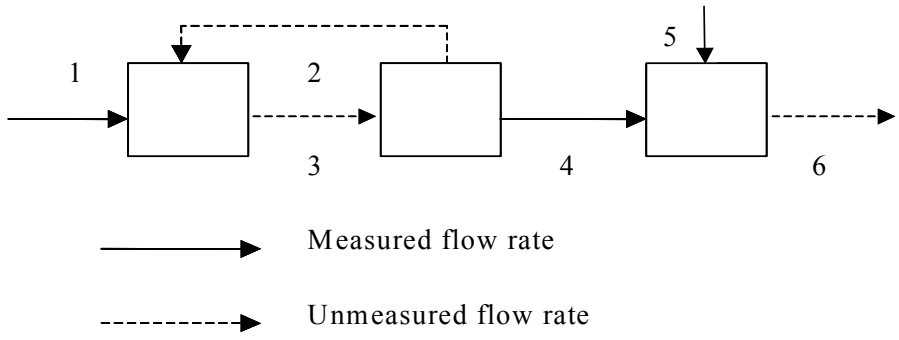

Figure 4.6. Example system for variable classification.

$$A=\begin{pmatrix}1 & 0 & 0\\ 0 & -1 & 0\\ 0 & 1 & 1\end{pmatrix} \qquad B=\begin{pmatrix}1 & -1 & 0\\ -1 & 1 & 0\\ 0 & 0 & -1\end{pmatrix}$$

$$x=\begin{pmatrix}G1\\ G4\\ G5\end{pmatrix} \qquad u=\begin{pmatrix}G2\\ G3\\ G6\end{pmatrix}$$

Step 2: Perform a Q-R decomposition, which gives the related matrices as follows:

$$Q_{u1}=\begin{pmatrix}-0.7071 & 0\\ 0.7071 & 0\\ 0 & 1.0\end{pmatrix} \qquad Q_{u2}=\begin{pmatrix}0.7071\\ 0.7071\\ 0\end{pmatrix}$$

$$R_{u1}=\begin{pmatrix}-1.4142 & 0\\ 0 & -1.0\end{pmatrix} \qquad R_{u2}=\begin{pmatrix}1.4142\\ 0\end{pmatrix}$$

$$E=\begin{pmatrix}1 & 0 & 0\\ 0 & 0 & 1\\ 0 & 1 & 0\end{pmatrix}$$

Then the unmeasured variables can be partitioned into the first subset u_{ru} and the second subset u_{n-ru} based on the following permutation:

$$u_{ru}=\begin{pmatrix}G2\\ G6\end{pmatrix} \qquad u_{n-ru}=\begin{pmatrix}G3\end{pmatrix}$$

Therefore, G3 is definitely unobservable because it cannot be estimated from the available measurements.

Step 3: Determine the redundant relationship among the measured variables, which is as follows:

$$\begin{pmatrix} 0.7071 & -0.7071 & 0 \end{pmatrix} \begin{pmatrix} G1 \\ G4 \\ G5 \end{pmatrix} = 0$$

Therefore, we can conclude that both the measurements G1 and G4 are redundant and G5 is nonredundant based on the coefficient matrix.

Step 4: Determine which unmeasured variables in the subset u_{ru} are observable based on the matrix R_{IU}.

If we calculate $R_{IU} = R_{u1}^{-1} R_{u2}$, the result is as follows:

$$R_{IU} = \begin{pmatrix} -1 \\ 0 \end{pmatrix}$$

Because the second row of R_{IU} is zero while the first row is non-zero, we conclude that $G2$ is unobservable and $G6$ is observable.

In conclusion, the observability analysis shows that G2 and G3 are unobservable and G6 is observable and the redundancy analysis shows that G1 and G4 are redundant and G5 is non-redundant. If Figure 4.6 is examined, the results indeed have meaningful physical interpretation.

4.3.2 Variable Classification for Bilinear Systems

Although nonlinear balance equations can be linearized around some operation points, the variable classification algorithm for linear systems may give incorrect results of observability and redundancy analysis. If we notice that thermal conservation equations are essentially bilinear because the temperature variable and the flow variable appear in terms of products, it is useful to extend the QR algorithm to deal with bilinear systems for variable classification.

In the bilinear variable classification algorithm developed by Sanchez, 1996, the first step is to classify the pair of variables (F, T) into three categories of energy flow

based on which component is measured, where F represents flow rate and T represents temperature.

Category I: both the temperature and the flow rate are measured.
Category II: the temperature is measured but the flow rate is not measured.
Category III: the temperature is not measured.

After the energy flow rate is categorized, the heat balance equations can be rewritten as follows:

$$B_1 f + B_2 V d + B_3 \nu = 0 \tag{4.12}$$

where

f = the enthalpy flow rate of category I.

d = the specific enthalpy of category II enthalpy flow.

ν = the enthalpy flow rate of category III.

V = the unmeasured mass flow rate of category II enthalpy flow.

Since the specific enthalpy of category II enthalpy flow can be calculated from the measured temperature, it can be decomposed into two components as follows:

$$d = \hat{d} + \tilde{d} \tag{4.13}$$

where

$\hat{d}$ = the specific enthalpy consistent with the measured temperature.

$\tilde{d}$ = the correction term of the specific enthalpy, which is to be determined such that the energy balance equations will be satisfied.

Let's introduce a new variable $\theta = V\tilde{d}$, which corresponds to the correction term of enthalpy flow rate, and then we have:

$$B_2 Vd = B_2\theta + B_2 V\hat{d} \tag{4.14}$$

If we separate the mass flow rate into the measured part F_M and the unmeasured part F_U , the heat balance equation given by Equation (4.12) can be further rewritten as follows:

$$\begin{bmatrix} 0 & B_1 & B_2 & B_5 & B_3 \end{bmatrix} \begin{bmatrix} F_M \\ f \\ \theta \\ F_U \\ \nu \end{bmatrix} = 0 \tag{4.15a}$$

where

$$B_5 = B_2\hat{d}$$

At this step, Equation (4.15a) can now be rewritten through adjusting the related matrices to incorporate the mass balance equations and is given by:

$$\begin{bmatrix} O & B_1 & B_2 & B_5 & B_3 \end{bmatrix} \begin{bmatrix} F_M \\ f \\ \theta \\ F_U \\ \nu \end{bmatrix} = 0 \tag{4.15b}$$

where the matrices O and B_5 have been adjusted to include mass balance equations and the matrices B_1, B_2 and B_3 have been modified accordingly by adding appropriate zeros.

For a set of mass flow rate and temperature measurements, i.e., F_M, f, and $\hat{d}$ are known, Equation (4.15b) indicates that the measurements can be adjusted through appropriate correction terms δ_{F_M}, δ_f, and θ such that the specified mass balance and heat balance equations are strictly satisfied. The correction terms satisfy the following equation:

$$\begin{bmatrix} B_{11} & B_5 & B_3 \end{bmatrix} \begin{bmatrix} t \\ F_U \\ \nu \end{bmatrix} = -\begin{bmatrix} O & B_1 \end{bmatrix} \begin{bmatrix} \hat{F}_M \\ \hat{f} \end{bmatrix} = e \tag{4.16}$$

where

$$t = \begin{pmatrix} \delta_{F_M} \\ \delta_f \\ \theta \end{pmatrix} \qquad B_{11} = \begin{pmatrix} O & B_1 & B_2 \end{pmatrix}$$

The second step of bilinear variable classification is to eliminate the unmeasured variables in Equation (4.16). This can be done by a successive QR decomposition on the matrix B_5 and B_3, which results in the following equations:

$$Q_{B3,2}^T B_{11} t + Q_{B3,2}^T B_5 F_U = Q_{B3,2}^T e \tag{4.17}$$

where

$$Q_{B3,2}^T B_3 = 0$$

Let $D = Q_{B3,2}^T B_5$, and a QR decomposition can be further performed for the matrix D, which gives the following equation:

$$Q_{B3,2}^T B_{11} t + \begin{bmatrix} Q_{D,1} & Q_{D,2} \end{bmatrix} \begin{bmatrix} R_{D,1} & R_{D,2} \\ 0 & 0 \end{bmatrix} \begin{bmatrix} F_{U1} \\ F_{U2} \end{bmatrix} = Q_{B3,2}^T e \tag{4.18a}$$

$$Q_{D,2}^{T} Q_{B3,2}^{T} B_{11} t = Q_{D,2}^{T} Q_{B3,2}^{T} e \tag{4.18b}$$

where

$Q_{D,2}^{T} D = 0$

All the unmeasured variables have been eliminated in Equation (4.18b) using two successive QR decompositions. Let $G = Q_{D,2}^{T} Q_{B3,2}^{T} B_{11}$, the zero columns of G correspond to the variables that cannot be estimated from the other measured variables and the nonzero columns of G correspond to the variables that can be estimated from the other measured variables. At this stage, the redundancy analysis of mass flow rate F_M has been completed.

It can also be seen from Equation (4.18a) that the set of unmeasured mass flow rate F_{U2} are not observable and the set of unmeasured mass flow rate F_{U1} are observable if the corresponding rows of $R_{IF} = R_{D,1}^{-1} R_{D,2}$ are all zeros.

The unmeasured mass flow rates F_U have now been partitioned into the observable set F_{Uo} and the unobservable set F_{Ui}. Given this knowledge, Equation (4.16) can be written as follows:

$$B_{11} t + B_{2Uo} F_{Uo} + B_{2Ui} F_{Ui} + \begin{bmatrix} Q_{B3,1} & Q_{B3,2} \end{bmatrix} \begin{bmatrix} R_{B3,1} & R_{B3,2} \\ 0 & 0 \end{bmatrix} \begin{bmatrix} \nu_1 \\ \nu_2 \end{bmatrix} = e \tag{4.19}$$

According to Equation (4.19), it can be stated that the set of unmeasured enthalpy flow ν_2 are not observable. Moreover, the set of unmeasured enthalpy flow ν_1 are observable if the corresponding rows of $R_{IV} = R_{B3,1}^{-1} R_{B3,2}$ are all zeros and if the corresponding rows of $R_{IF2} = R_{B3,1}^{-1} Q_{B3,1}^{T} B_{2Ui}$ are all zeros.

The necessary condition that the temperature variables can be estimated is that the corresponding terms of ν is observable and the corresponding mass flow rates are measured or observable. If a temperature variable can be estimated and is measured, then this temperature variable is redundant. If a temperature variable can be estimated and is not measured, then this unmeasured temperature variable is observable.

4.4 Sensitivity Analysis for Sensor Placement

Sensitivity analysis is discussed in this section for sensor placement design in terms of efficient sensor fault diagnosis. In this dissertation, data reconciliation is proposed as a generalized approach to study the sensitivity of a variable in balance equations. The presentation of this section includes a background description of data reconciliation, a mathematical formulation of data reconciliation, and how data reconciliation can be used for sensitivity analysis.

4.4.1 Data Reconciliation

Data reconciliation was originally developed to adjust process data such that the adjusted values strictly satisfy constraint equations. Aside from other techniques such as neural networks, principal component analysis, and partial least square methods, data reconciliation is one of the major data processing methods for operation monitoring, performance analysis, maintenance planning, and fault diagnosis. This technique was first proposed in the early 1960s, and since then has been successfully applied in chemical and petroleum industries. However, it has hardly received any attentions in the nuclear industry until the 1990s. The current research on the application of data reconciliation to nuclear power plants is carried out mainly in Europe. It is reported by German researchers that *data reconciliation is the best possible quality control mechanism for identifying serious measurement errors in nuclear power plants and a necessary data-preconditioning step for process monitoring, process optimization, and maintenance optimization* (Grauf, Jansky, and Langenstein, 2000), (Svein and Øivind,

2003). Two significant applications of data reconciliation to nuclear plant instrument monitoring are as follows:

(a) Reactor coolant temperature monitoring

Reactor coolant temperature is an important controlled variable in nuclear power systems. Because reactor coolant temperature must not reach the designed maximum value, the incorrect indication of reactor coolant temperature may force the reactor to operate at a lower power level. Therefore, if a reconciled reactor coolant temperature instead is used for plant power control, better operation performance may be achieved.

(b) Feed water flow rate measurement

Feed water mass flow rate is used to calculate reactor thermal power. If the measured feed water flow rate suffers from instrument bias fault, the reactor will be forced to operate at a derated condition. Therefore, if the reconciled feed water flow rate is used, the reactor thermal power output can be estimated based on the reconciled value and significant operation cost due to the feed water flow measurement fault can be saved.

4.4.2 Basic Algorithm of Data Reconciliation

For a given system, the variables involved in the constrained equations can be categorized as the measured variables x with the covariance matrix of presumably Gaussian measurement error Ψ and the unmeasured variables u. The overall task of data reconciliation can be stated as a weighted least-squares estimation problem, which is given by:

$$\min_{(x,u)} (y-x)^T \Psi^{-1} (y-x) \tag{4.20}$$

with the steady state mass balance and heat balance equations as follows:

$$\varphi(x,u)=0 \tag{4.21}$$

It is possible to solve the above minimization problem using nonlinear programming techniques such as sequential quadratic programming and reduced gradient methods. Although these techniques are more general, they need a large amount of computation time and may obscure which variable can be derived from the others. Therefore, a successive linearization algorithm is used in this dissertation to solve the above problem.

Successive linearization is based on the idea that the nonlinear constraints defined in Equation (4.21) can be successively linearized around their approximate operation points until these nonlinear constraints are satisfied with some specified tolerance (Romagnoli and Sanchez, 2002), (Pai and Fisher, 1998). The algorithm can be summarized as follows:

Step 1. Give an initial guess about the estimates (x_0,u_0) based on the measured value of y.

Step 2. Solve for an estimate (x_i^*,u_i^*) by minimizing the objective function defined in Equation (4.20) with the constraint equations linearized around the estimates (x_i,u_i), which is given by:

$$Ax+Bu=c \tag{4.22}$$

where

$$A=\frac{\partial\varphi}{\partial x}\Big|_{(x_i,u_i)}$$

$$B = \frac{\partial \varphi}{\partial u}\Big|_{(x_i, u_i)}$$

$$c = Ax_i + Bu_i - \varphi(x_i, u_i)$$

The solution to the minimization problem with the objective function given in Equation (4.20) and the constraint equations given in Equation (4.22) can be obtained by performing QR decomposition on the matrix B.

$$x_i^* = x_i - \Psi G^T (G\Psi G^T)^{-1}(Gx_i - b) \tag{4.23a}$$

$$u_i^* = R_{u1}^{-1}(Q_{u1}^T c - Q_{u1}^T A x_i^*) \tag{4.23b}$$

where G, b, Q_{u1}, and R_{u1} are the related matrices defined in Equation (4.10), Equation (4.11), Equation (4.4), and Equation (4.5), respectively.

Step 3. Update the estimates (x_{i+1}, u_{i+1}) by minimizing the constraint error. This can be accomplished by searching for a constant t between 0 and 1 such that

$$x_{i+1} = x_i + t(x_i^* - x_i) \tag{4.24}$$

and

$\varphi(x_{i+1}, u_{i+1})$ is minimal.

Step 4. If the estimation is convergent and the nonlinear constraint equations are satisfied, then stop. Otherwise, go to Step 2.

Although the above algorithm is simple, it has provided a general solution to the reconciliation of measured data such that the specified constraint equations, in linear or nonlinear form, are strictly satisfied.

4.4.3 Sensitivity Analysis Procedure

In the design phase, plant-scale balance equations can be developed to reveal the functional relationships among variables. Through investigating the observability and redundancy of variables in the balance equations, the variable classification algorithm presented in section 4.4.2 provides a theoretical solution to sensor placement design for sensor fault diagnosis.

However, sensitivity analysis must also be studied to ensure the diagnostic performance during sensor placement design. Analytical redundancy based fault diagnosis uses equation error for fault detection and isolation. For a given functional relationship, some of the related variables may be more sensitive to generate equation errors than the other variables. An incipient sensor fault can be detected only if the related variable is sensitive in the functional relationships (constraint equations).

In this dissertation, sensitivity analysis is transformed to a precision design problem and is solved using data reconciliation. If a variable is sensitive in the functional relationships, it is expected that data reconciliation algorithm will lead to an estimation with good precision after data reconciliation is performed. Figure 4.7 shows a schematic of the proposed procedure of sensitivity analysis.

At steady state conditions, the constraint equations that the measured variables y should satisfy may be given by:

$$\varphi(y,u) = 0 \tag{4.25}$$

where u is the unmeasured variables.

The nominal values of measured variables y^* can be determined easily from balance equations. In order to study the sensitivities of the involved variables, a perturbation such as a Gaussian noise vector ε is artificially added to the nominal values, which is given by:

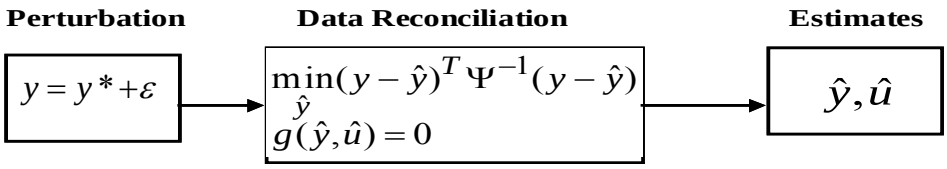

Figure 4.7. Sensitivity analysis using data reconciliation.

$$y = y^* + \varepsilon \tag{4.26a}$$

$$\Psi = \mathrm{cov}(\varepsilon) \tag{4.26b}$$

where y is a perturbed vector, y^* is the nominal values, and Ψ is the covariance matrix of the additive perturbation.

To evaluate the sensitivity of a variable due to the constraint equations, the measured variables are estimated by solving an optimization problem formulated as follows:

$$\min_{(\hat{x},\hat{u})} (y - \hat{y})^T \Psi^{-1} (y - \hat{y}) \tag{4.27}$$

s.t.

$$\varphi(\hat{y}, \hat{u}) = 0$$

where

$\hat{y}$ = the estimated value.

The sensitivity of a variable y_i in the constraint equations can be quantified by a d-factor defined in this dissertation, which is given by:

$$d_i = 1 - \frac{\mathrm{var}(\hat{y}_i - y_i^*)}{\mathrm{var}(y_i - y_i^*)} \tag{4.28}$$

Evidently, a large value of the d-factor given in Equation (4.28) means that the variable is sensitive in the constraint equations. In order to detect a slight fault, the d-

factor must be greater than some critical value. For instance, the d-factor of a variable would become zero if it does not participate in the constraint equations.

The optimization problem defined above is a standard data reconciliation problem. Successive linearization algorithm or standard nonlinear programming techniques may be used to obtain solutions in general cases.

It should be mentioned that the proposed strategy for sensitivity analysis is not dependent on whether the system is linear or nonlinear. For nonlinear system, the calculated d-factor varies at different operation points, a worst case design may be necessary after the d-factor is calculated for all the anticipated operation conditions.

4.5 Gross Error Detection and Identification

To determine performance parameters accurately or perform process fault diagnosis, the measured variables must have sufficiently high precision. Data reconciliation provides a means to improve the precision of measured variables based on analytical redundancy by adjusting the measurements such that the balance equations are strictly satisfied. However, this adjustment is valid only if there is no gross error with respect to the balance equations. If a sensor fault occurs, the faulty sensor must be detected, identified, and reconstructed to avoid the estimated process parameters from misleading the performance monitoring and avoid misdiagnosis of process faults.

4.5.1. Gross Error Detection

The most popular method of gross error detection is to check the validity of the balance equations. In the absence of gross error, the measurement vector x can be written as follows:

$$x = x^* + \varepsilon \tag{4.26}$$

where ε represents a random error vector with zero mean and covariance matrix Ψ.

For a linear system, after the unmeasured variables are eliminated through QR decomposition, the equation residual r can be written as follows:

$$r = Gx - b = G\varepsilon \tag{4.27}$$

where G and b are defined in Equations (4.10) and (4.11), respectively.

Based on the assumption that the measurement error is random, if there is no gross error in the measurements, the residual will satisfy the following properties:

$$E[r] = 0 \tag{4.28a}$$

$$\Phi = E[rr^T] = G\Psi G^T \tag{4.28b}$$

However, when a gross error occurs in the system, a systematic error will appear in the residual. Therefore, gross error detection can be accomplished by testing the following statistics:

$$\tau = r^T \Phi^{-1} r \tag{4.29}$$

If G has a full row rank m, the derived statistics τ in Equation (4.29) will follow a χ^2 distribution with m degrees of freedom. Therefore, a gross error can be detected if the calculated statistics τ is greater than a critical value at the specified error probability.

4.5.2 Fault Identification

For a large-scale system, many sensors may have more than one degree of redundancy for estimation. Even if one sensor is faulty and a gross error has been detected, it is still possible to reconstruct the measured value to estimate performance parameters or perform process fault diagnosis after the source of gross error is identified and eliminated through a systematic procedure.

A serial elimination strategy was developed by Romagnoli to identify the measurements with gross error (Sanchez and Romagnoli, 1994). The basic idea of this strategy is to compare the effect on data reconciliation when individual measurements are eliminated one at a time. If only single faults are considered, a single measured variable is eliminated each time and correspondingly the equation errors are estimated. The variable, whose elimination results in the most significant reduction in the estimate of the equation errors, is considered as a faulty sensor.

If one sensor has gross error, the G matrix in Equation (4.27) can be separated into two parts as follows:

$$G = \begin{bmatrix} G_g & G_c \end{bmatrix} \tag{4.30}$$

where G_g and G_c are the columns of G matrix corresponding to the sensors not suspected of gross error and the sensors suspected of gross error, respectively.

Correspondingly, the covariance matrix of the measurement error can be partitioned into two parts as follows:

$$\Psi = \begin{bmatrix} \Psi_g & 0 \\ 0 & \Psi_c + \Delta\Psi_c \end{bmatrix} \tag{4.31}$$

where $\Delta\Psi_c$ corresponds to the increase in the variance of the measurement due to the suspected gross error.

The covariance matrix of the equation error Φ_n after the effect of gross error is taken into account can be related to the covariance matrix of the measurement error without gross error Φ as follows (Romagnoli and Sanchez, 2000):

$$\Phi_n = \Phi + G_c(\Delta\Psi_c)G_c^T \tag{4.32}$$

where Φ is defined in Equation (4.28b) when there is no gross error in the system.

Because both Φ_n and $\Delta\Psi_c$ are nonsingular, Φ_n^{-1} can be calculated as follows(Romagnoli and Sanchez, 2000):

$$\Phi_n^{-1} = \Phi^{-1} - \Phi^{-1} G_c [(\Delta\Psi_c)^{-1} + G_c (\Delta\Psi_c)^{-1} G_c^T]^{-1} G_c^T \Phi^{-1} \tag{4.33}$$

Now we can compare the contribution of each measured variable to the equation error and identify the source of gross error. The contribution of the ith sensor to the equation error can be measured by the objective function given by:

$$J_i = r^T \Phi_{n(i)}^{-1} r \tag{4.34}$$

where $\Phi_{n(i)}^{-1}$ can be calculated based on Equation (4.33) with the corresponding $\Delta\Psi_{c(i)}$ specified as infinity. Apparently, if $\Delta\Psi_{c(i)}$ corresponding to the ith sensor is specified as infinity, it is equivalent to the elimination of the ith sensor from the total contribution of the equation error.

If only single sensor fault is considered, the objective function given in Equation (4.34) can be calculated for each measured variable when it is eliminated. The measured variable whose elimination results in the smallest value of the objective function will have the largest contribution to the equation error. Therefore, this measured variable is identified as the measurement with a gross error.

4.5.3 Fault Estimation

After a sensor fault is identified based on the algorithm described in section 4.5.2, it is desirable to estimate the fault magnitude and reconstruct the incorrect measurements for use in process fault diagnosis and performance parameter estimation. If this fault reconstruction is reliable, the reconstructed value can still be used even if a gross error has occurred.

For an identified sensor fault, the fault effects on the measurements are given by:

$$x = x^* + \varepsilon + E_r m_b \tag{4.35}$$

where

E_r = the fault distribution matrix, which is one column of the identity matrix for sensor faults.

m_b = the fault magnitude.

The problem of fault magnitude estimation is stated as follows:

$$\min_{\varepsilon} \varepsilon^T \Psi^{-1} \varepsilon \tag{4.36a}$$

s.t.

$$G(x - \varepsilon - E_r m_b) = 0 \tag{4.36b}$$

The solution to the minimization problem defined in Equation (4.36) is given as follows (Romagnoli and Sanchez, 2000):

$$m_b = [P_b (G\Psi G^T)^{-1} P_b]^{-1} P_b^T (G\Psi G^T)^{-1} Gx \tag{4.37}$$

where

$P_b = GE_r$

Therefore, the reconstructed measurement is given by:

$$\hat{x} = x - \Psi G^T (G\Psi G^T)^{-1} Gx - \Psi G^T (G\Psi G^T)^{-1} P_b m_b \tag{4.38}$$

Equation (4.38) shows that the reconstructed value of the measurement with a gross error consists of three terms. The first term is the original measured value, the second term corresponds to the correction on measurement noise due to the constrained minimization, and the third term corresponds to the correction due to the identified gross error.

4.6 Application to HCSG system

In the IRIS reactor design described in Chapter 3, eight steam generators are installed in four pairs in the annular space between the core barrel and the reactor vessel

(RV) wall. A common feed water supply line splits at the vessel and goes to two steam generators. Similarly, the steam discharge lines from two steam generators join to create a common steam line. This pairing of steam generators has reduced the number of feed water and steam lines, and thus the number of penetrations into and out of the containment, but it has caused an unfavorable consequence on individual steam generator monitoring in terms of the thermal performance and the secondary flow rate. A schematic of one pair of IRIS helical coil steam generators is given in Figure 3.3.

According to an engineering analysis, the HCSG fault diagnosis system needs to monitor the following process faults:

(1) Thermal performance degradation of each individual steam generator.
(2) Secondary flow rate abnormality for the pair of steam generators.
(3) Reactor pump flow abnormality.
(4) Feed water temperature abnormality.
(5) Primary side inlet temperature abnormality.
(6) Feed water flow rate abnormality.

Figure 4.8 shows the Directed Graph of one pair of the HCSG systems. In this figure, T and W denote temperature and mass flow rate, respectively. The numeric number appended to T or W denotes the location on the HCSG system configuration. The yellow colored nodes represent the root nodes of the system, each of which corresponds to a process fault. For example, the yellow nodes denoted by W2 and W4 represent the faults associated with the two reactor main pumps pumping the flow into the primary side of SG-A and SG-B, respectively. The DG has clearly illustrated the cause-effect relationships among the involved variables and the propagation pathways from the root node to the other nodes. For instance, if the thermal performance of SG-A has degraded, the node T3 on the primary side and the node T11 on the secondary side will be affected. In other words, SG-A degradation is a sufficient condition to cause abnormal symptoms on the nodes T3 and T11.

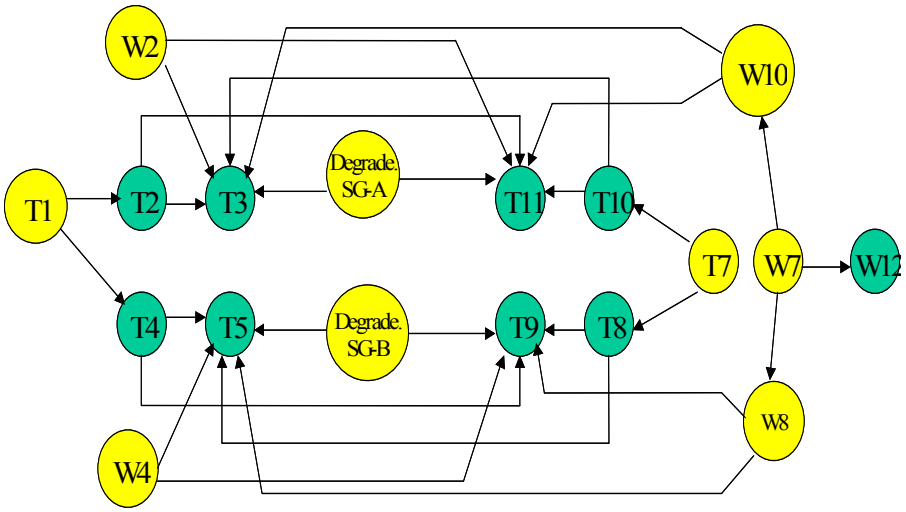

Figure 4.8. The Directed Graph of one pair of HCSG system.

To locate the minimum set of sensors that can observe the considered process faults, the first step is to find out all the nodes that have only input arcs in the DG. A simple examination shows that the nodes having only input arcs are T3, T5, T9, T11, and W12, which should be selected as the members of the fault observability set. Obviously, this observability set is able to detect all the considered process faults.

Figure 4.9 gives the bipartite graph between the root nodes and the observability set {T3, T5, T9, T11, and W12}. The left side of the bipartite graph includes all the considered process faults, which are also the root nodes in the DG graph. The right side of the bipartite graph includes all the process variables in the observability set. The directed arcs in the bipartite graph are determined from the DG graph.

Figure 4.10 (a) shows the bipartite graph when T3 is selected because all the members of the fault observability set cover the same number of root nodes. Figure 4.10 (b) shows the bipartite graph after the arcs from the root nodes that have already been covered by T3 are eliminated. As can be seen, either T5 or T9 is able to cover the remained process faults.

In conclusion, the set of T3 and T5 or the set of T3 and T9 is a minimum set of sensors for process fault detection.

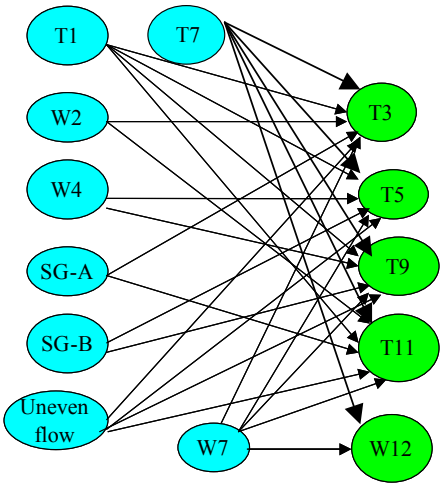

Figure 4.9. Bipartite Graph of one pair of HCSG system.

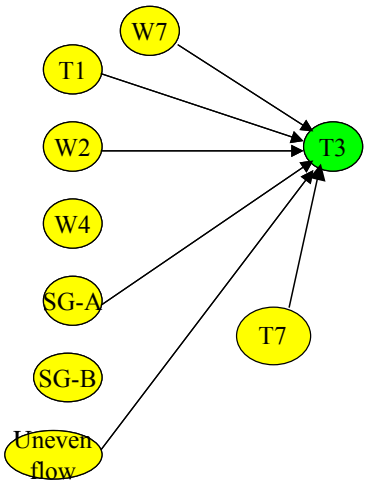

Figure 4.10 (a)

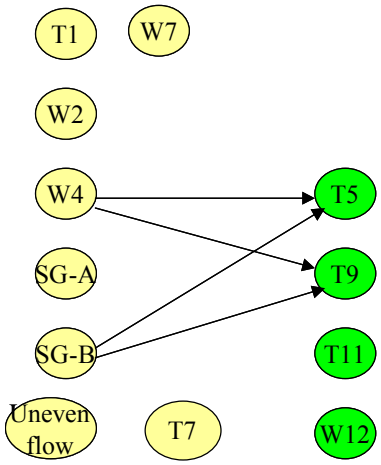

Figure 4.10 (b)

Figure 4.10. Determine the minimum set of sensors for fault detection.

Table 4.1 shows the fault effect matrix for all the root nodes. To determine the minimum set of sensors for fault isolation, it is necessary to determine a subset of the affected nodes such that the fault effects can be distinguished from each other. Table 4-2 shows the bipartite graph, which is presented in matrix form for convienience, to determine the minimum set of sensors for fault isolation. Using the algorithm presented in section 4.2.2, the minimum set of sensors must include T1, T3, T5, T7, T9, T11, W2, W4, and W7 such that the selected faults can be fully isolated.

Efficient process fault diagnosis also depends on a reliable sensor fault diagnosis. However, a sensor fault diagnosis system based on functional relationships can be achieved only if the measured variables and process parameters of interest can be estimated using analytical redundancy through appropriate sensor placement design.

For one pair of IRIS HCSG system shown in Figure 3.3, the mass balance and heat balance equations are given as follows:

W1=W2+W4

W2-W3=0 W4-W5=0

W6-W3-W5=0 W12-W9-W11= 0

W10-W11 = 0 W8-W9=0

W7-W8-W10 = 0

T1=T2=T4

T7=T8=T10

W6h6-W3h3-W5h5=0

W12h12-W9h9-W11h11=0

W2h2+W10h10-W3h3-W11h11=0

W4h4+W8h8-W9h9-W5h5 = 0 (4.39)

In the above equations, the symbols W, h, and T denote mass flow rate, specific enthalpy, and temperature, respectively. It is assumed that the system pressures are constant and the specific enthalpy can be approximated as a function of local fluid temperature. It should be mentioned that these balance equations hold for any operation conditions unless the system configuration changes while data driven models hold only if the collected data are representative enough to cover the entire operation space.

Table 4.1. Fault effect matrix

Process fault	**Observabiltiy Set**
Primary inlet temperature fault (B1)	A1={T1,T2,T3,T4,T5,T9,T11}
SG-A primary side pump flow fault (B2)	A2={W2,T3,T11}
SG-B primary side pump flow fault (B3)	A3={W4,T5,T9}
SG-A heat transfer degradation fault (B4)	A4={T3,T11}
SG-B heat transfer degradation fault (B5)	A5={T5,T9}
Secondary flow distribution abnormally (B6)	A6={T3,T5,T9,T11}
Feed water temperature fault (B7)	A7={T7,T8,T10, T9, T11,T3,T5}
Feed water flow fault (B8)	A8={W7,W8,W10,T3,T5,T9,T11,W12}

Table 4.2. Bipartite matrix to determine the minimum set of sensors for fault isolation.

Pseudonode	Sensor Set for Fault Resolution	Pseudonode	Sensor Set for Fault Resolution
B12	{T1,T2,W2,T4,T5,T9}	B35	{W4}
B13	{T1,T2,T3,W4,T4,T11}	B36	{W4,T3,T11}
B14	{T1,T2,T4,T5,T9}	B37	{W4,T3,T7,T8,T10,T11}
B15	{T1,T2,T3,T4,T11}	B38	{W4,W7,W8,W10,W12,T3,T11}
B16	{T1,T2,T4}	B45	{T3,T5,T9,T11}
B17	{T1,T2,T4,T7,T8,T10}	B46	{T5,T9}
B18	{W7,W8,W10T1,T2,T4,W12}	B47	{T5,T7,T8,T9,T10}
B23	{W2,W4,T3,T5,T9,T11}	B48	{W7,W8,W10,W12,T5,T9}
B24	{W2}	B56	{T3,T11}
B25	{W2,T3,T5,T9,T11}	B57	{T3,T7,T8,T10,T11}
B26	{W2,T5,T9}	B58	{W7,W8,W10,W12,T3,T11}
B27	{W2,T5,T7,T8,T9,T10}	B67	{T7,T8,T10}
B28	{W2,W8,W10,T7,T5,T9,W12}	B68	{W7,W12}
B34	{W4,T3,T5,T9,T11}	B78	{W7,W8,W10,W12,T7,T8,T10}

To analyze the observability and redundancy of variables in the balance equations, the bilinear variable classification algorithm described in section 4.3.2 is used to classify the related variables for the following measurement set:

Case A: {W2, W4, W7, W12, T1, T3, T6, T7, T9, T12}

After the enthalpy flow of category III described in section 4.3.2 is eliminated from the heat balance equations and a Q-R decomposition is performed on the coefficient matrix of the unmeasured flow rate vector, which is given in Equation (4.18), the vector F_{U2} is empty and the vector F_{U1} includes all the unmeasured mass flow rate variables (W1, W6, W8, W9, W10, W11). Meanwhile, the matrix R_{IF} is also empty. Therefore, they are all observable. That W1 and W6 are observable can be easily verified from Figure 3.3. As for W8, W9, W10, W11, they are all observable. The unmeasured mass flow rate W8 and W9 are observable because the heat transferred by each steam generator can be determined from the heat balance equations and T9 is measured. Now that W8 and W9 are observable, W10 and W11 can be determined simply by W7 minus W8.

After the unmeasured mass flow rate variables are partitioned according to Equation (4.19), Q-R decomposition is then performed on the coefficient matrix of the unmeasured enthalpy flow of category III. The enthalpy flow vector ν_1 in Equation (4.19) includes the enthalpy flow variable at location 5 and the enthalpy flow variable at location 11 while the enthalpy flow vector ν_2 is empty. Because the corresponding matrices R_{IV} and R_{IF2} in Equation (4.19) are both empty, the enthalpy flow variables at location 5 and location 11 are observable.

On the other hand, since the mass flow rate variables at locations 5 and 11 are observable, the temperature measurements at the two locations are then observable.

The G matrix obtained from the bilinear variable classification algorithm is tabulated in a table to show the relationships among variables. The zero-valued columns correspond to the enthalpy flow variables that do not participate in redundant relationships. In addition, the columns proportional to each other indicate that the sensor faults of these variables will not be distinguishable in terms of equation residuals. Table

4.3 shows that the temperature sensors T3 and T9 are not redundant. This result can be verified because the heat transferred by SG-A or SG-B could not be determined if either T3 or T9 is eliminated from the set of temperature measurments.

Table 4.4 shows the G matrix obtained from the variable classification algorithm for the linearized functional relationship. From this matrix, we can see that T3 and T9 will not participate in the reduced redundant relationship. Therefore, these two sensors are not redundant. This shows that the linearized variable classification algorithm gives the same results of variable classification as the bilinear variable classification algorithm for the HCSG application.

In order to make the measurements T3 and T9 redundant, T5 and T11 are measured in Case B, which includes the following measurements:

Case B: {W2, W4, W7, W12, T1, T3, T5, T6, T7, T9, T11, T12}

Table 4.5 shows the G matrix obtained from the variable classification algorithm for linearized functional relationship. As compared with Case A, T3 and T9 are redundant in Case B. This result can be easily verified because either T3 or T9 can still be estimated from the other variables even if it is eliminated. In fact, all the variables are redundant and can be obtained from the other measurements based on mass and energy balance equations. The G matrix given in Table 4.5 also has many columns proportional to each other, which means that the sensor faults of these variables will not be distinguishable in terms of equation residuals. These columns correspond to the following three groups:

(1) Group I: {W2, W4, T1, T7};
(2) Group II: {T3, T5};
(3) Group III: {T9, T11}.

Therefore, for the sensor placement of Case B, it is not possible to distinguish the sensor faults within each group of the variables because they will generate the same residual pattern.

Table 4.3. G matrix based on bilinear variable classification
to determine the redundant relationship between the measured variables (Case A)

W2	W4	W7	W12	f2	f4	f7	f12	θ1	θ3	θ6	θ8	θ9	θ10
-.56	-.56	0.22	0.22	0.51	0.51	0.01	0.01	-.52	0.0	-.52	-.11	0.0	-.11
0.11	0.11	-.34	-.34	-.02	-.02	0.19	0.19	-.17	0.0	-.17	-.40	0.0	-.40
0.60	0.60	-.31	-.31	0.15	0.15	0.05	0.05	-0.2	0.0	-0.2	-.27	0.0	-.27
0.07	0.07	-.12	-.12	0.38	0.38	-.24	-.24	-.14	0.0	-.14	0.55	0.0	0.55
0.27	0.27	-.08	-.08	0.14	0.14	-.32	-.32	0.18	0.0	0.18	-.33	0.0	-.33

Table 4.4. G matrix based on linearized variable classification
to determine the redundant relationship between the measured variables (Case A)

W2	T1	T3	W4	T6	W7	T7	T9	W12	T12
0.0075	0.268	0.0	0.0075	-0.22	-0.464	0.0205	0.0	0.394	-0.015
-0.074	-2.64	0.0	-0.074	2.17	-0.381	-0.202	0.0	1.066	0.147

Table 4.5. G matrix based on linearized variable classification
to determine the redundant relationship between the measured variables (Case B)

W2	T1	T3	W4	T6	W7	T7	T9	W12	T12	T11	T5
0.031	1.104	-0.29	0.031	-0.32	-.007	0.084	0.024	-0.28	-0.11	0.024	-.29
0.053	1.907	-0.31	0.053	-0.94	-.110	0.145	-.024	-0.38	-0.06	-0.02	-.31
0.037	1.337	0.69	0.037	-2.47	0.480	0.102	0.004	-0.83	-0.08	0.004	0.69
0.048	1.709	-1.72	0.048	2.04	0.398	0.130	-.004	-0.84	-0.09	-.004	-1.72

Let us examine the above results from the physical point of view. The energy balance equations cannot distinguish a measurement fault in T1 and T7 because they always participate in the same set of energy balance equations. If the measurement T7 is eliminated, it will not be possible to estimate T1 from the remaining measured variable. The result is the same if T1 is eliminated. On the other hand, let's look at the measurement T6 and T12. If T6 is eliminated, the remaining measured variables can still be used to estimate the variable T12. Therefore, the sensor faults of the variables T6 and T12 can be distinguished.

Based on the comparison analysis of the influence of measured variables on the equation error, it can be concluded that physical redundancy is needed to distinguish some of the sensor faults in Case B. Three physically redundant sensors are needed to distinguish the sensor faults of W2, W4, T1, and T7, one redundant sensor is needed to distinguish the sensor faults of T3 and T5, and one redundant sensor is needed to distinguish the sensor faults of T9 and T11. Considering that additional redundant relationships exist if the analysis is extended beyond the pair of HCSG systems, T1 and T7 can be assumed redundant. However, hardware redundancy of T3 or T5 and hardware redundancy of T9 or T11 are necessary to distinguish the sensor faults associated with them. In the analysis, T5 and T9 are chosen to have physically redundant sensors.

In the sensor placement design, an additional issue is to ensure that the sensors of interest can be estimated with enough precision using functional relationships. In other words, the corresponding sensor faults should be detectable with adequate sensitivity. Table 4.6 shows that the d-factors for W2, W4, T7, T9, and T11 are very small after data reconciliation. This indicates that these three variables are not sensitive to the balance equations. Therefore, a sensor fault of these variables may not be detectable if the fault magnitude is small and the fault magnitude may not be accurately reconstructed when a fault is detected.

Let us take W2 as an example to show why W2 is not sensitive to the equation error. The mass flow rate W2 satisfies the following energy balance equation at nominal condition:

Table 4.6. Physical redundant sensor placement based on sensitivity study

	W2	T1	T3	W4	T6	W7	T7	T9	W12	T12	T11	T5
Std [1]	1.82	0.27	0.25	1.85	0.28	0.42	0.20	0.31	0.37	0.28	0.27	0.25
Std [2]	1.82	0.15	0.22	1.85	0.14	0.30	0.20	0.28	0.30	0.16	0.25	0.22
d [3]	0.01	0.43	0.11	0.01	0.52	0.28	0.02	0.06	0.18	0.41	0.07	0.11
d [4]	0.38	0.52	0.11	0.38	0.52	0.32	0.29	0.38	0.38	0.59	0.32	0.36

[1]. Standard deviation of the measured values.
[2] Standard deviation of the reconciled values without physical redundant sensors.
[3]. d-factor without redundant sensors.
[4]. d-factor with redundant sensors for T5, T7, T9, T11, W2, W4.

W2(h2-h3)=W10*(h11-h10) h2= 0.0066*T2-0.6519
h3= 0.0054*T3-0.2826 h11= 0.0034*T11+1.8763
h10= 0.0047*T10-0.0822 W2_nominal=582.5 kg/s
W10_nominal=62.85kg/s h2_nominal=1.5129 E6 J/kg
h11_nominal=2.9541 E6 J/kg h10_nominal=0.9706 E6 J/kg
h3_nominal=1.2942 E6 J/kg (4.40)

If we linearize Equation (4.40) around the nominal operation point, we have:
3.8445*dT2-3.1455dT3+0.2187dW2=0.2135dT11-0.2952dT10+1.9835dW10

Considering that T2 has a measurement error of 1 ^{o}C, the corresponding equation error is equivalent to about 4% measurement error of W2 and 5% measurement error of T10. This analysis indirectly proves that the d-factor indeed is able to represent the sensitivity of the involved variables to the equation error. Based on the results of sensitivity analysis given in Table 4.5, W2, W4, T7, T9, and T11 need to have physically redundant measurements such that a sensor fault can be detected with enough sensitivity.

Combining the sensitivity analysis and fault isolation capability, the sensor placement is chosen to be as follows:
Case C: {W2, W4, W7, W12, T1, T3, T5, T6, T7, T9, T11, W2-2, W-4, T5-2, T7-2, T9-2, T11-2}.
where W-2, W-4, T5-2, T7-2, T9-2, T11-2 indicate physical redundant sensors for W2, W4, T5, T7, T9, and T11, respectively.

Figure 4.11 (a) shows the gross error detection statistics defined in Equation (4.29) as a comparison with the detection limit based on χ^2 distribution to detect a sensor fault of W2 with a bias fault magnitude of 2% nominal value when redundant measurement for W2 exists. It is clear the fault can be detected immediately when the fault at the 150th sample. On the contrary, if there is no physically redundant measurement of W2, Figure 4.11 (b) shows that the fault cannot be effectively detected.

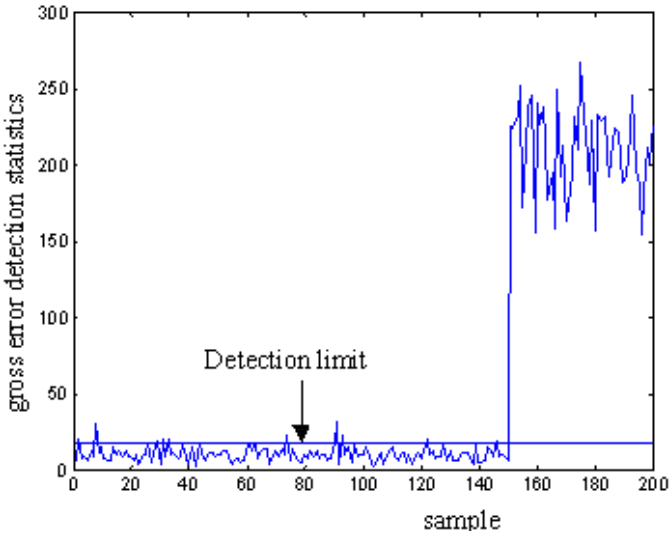

Figure 4.11 (a). Fault detection of W2 measurement error with redundant measurement.

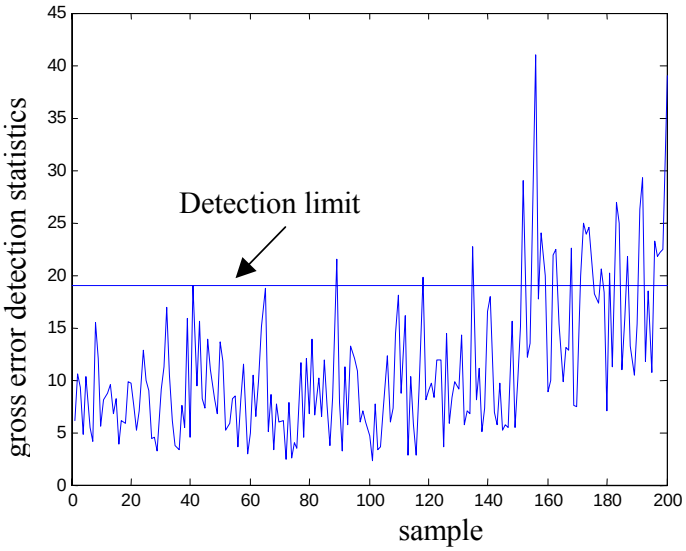

Figure 4.11 (b). Fault detection of W2 measurement error without redundant measurement.

Figure 4.12 (a) and Figure 4.12 (b) show a comparison of fault reconstruction of W2 measurement fault without and with the physically redundant measurement of W2. Because W2 is not constrained tightly by the energy balance equations as is shown by the sensitivity analysis, a measurement fault can be reconstructed only if physical redundancy exists. For the W2 measurement fault, the faulty measurement W2 is 594.6 kg/s with the true value being 582.52 kg/s. If there is no physical redundant measurement for W2, the reconstructed value is 593.64 kg/s based on the fault reconstruction algorithm introduced in section 4.5.3. It is clear that the fault cannot be reconstructed correctly. However, if a physical redundant measurement for W2 is placed, the reconstructed value is 582.50 kg/s. The fault effects can be identified correctly based on the algorithm introduced in section 4.6.2, and completely compensated using the fault reconstruction algorithm.

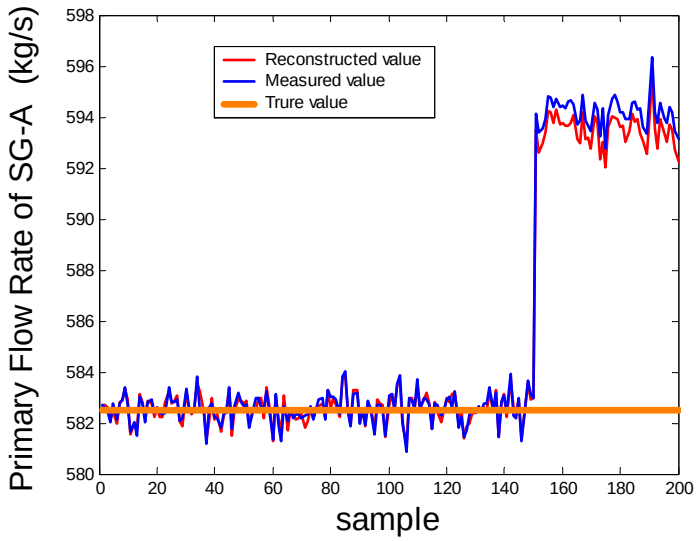

Figure 4.12 (a). Fault reconstruction of W2 measurement error without redundant measurement

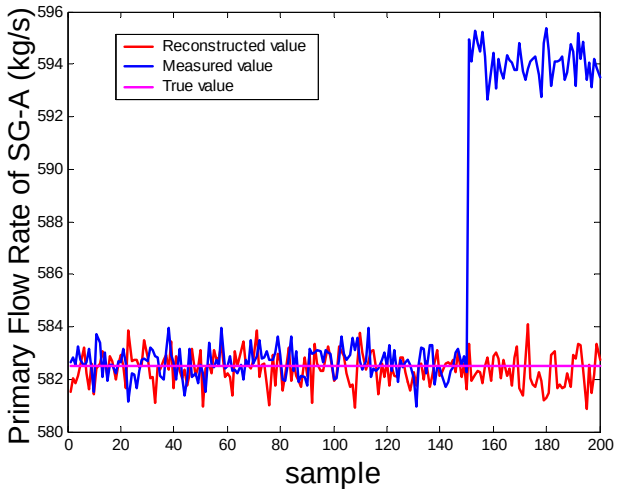

Figure 4.12 (b). Fault reconstruction of W2 measurement error with redundant measurement.

Figure 4.13 shows the secondary side mass flow rate using bilinear data reconciliation algorithm for Case A sensor placement. In the Figure, the secondary mass flow rate of SG-A begins to decrease and the secondary mass flow rate of SG-B begins to increase at the 100th sample. The bilinear data reconciliation algorithm is able to track the change of secondary mass flow rate with very good precision. It demonstrates that parameter estimation is an efficient approach to monitor process faults when the measurements have been reconciled using data reconciliation algorithms.

Figure 4.14 shows the estimated heat transfer rate using bilinear data reconciliation algorithm for Case A sensor placement. The brute force estimate of the heat transfer rate of SG-A is calculated directly from the measured primary flow rate and primary side inlet and outlet temperature while the brute force estimate of the heat transfer rate of SG-B is calculated by the total heat transfer rate minus the heat transfer rate of SG-A. Because of the mass flow rate has been added with 1% measurement noise and the temperature has been added with 0.025% measurement noise, the calculated total heat transfer rate has a significant variance for SG-B. However, if data reconciliation is performed on the measured data, the precision of the estimated heat transfer rate can be significantly improved.

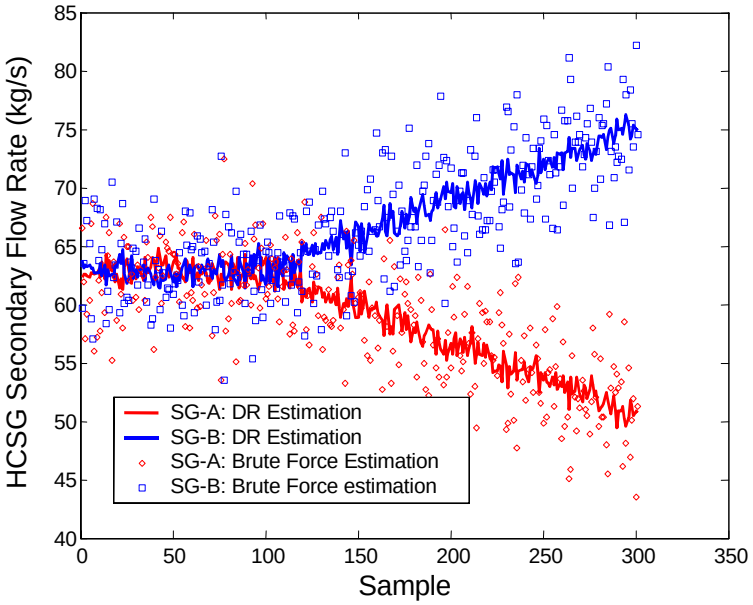

Figure 4.13. Bilinear data reconciliation result of HCSG secondary flow rate.

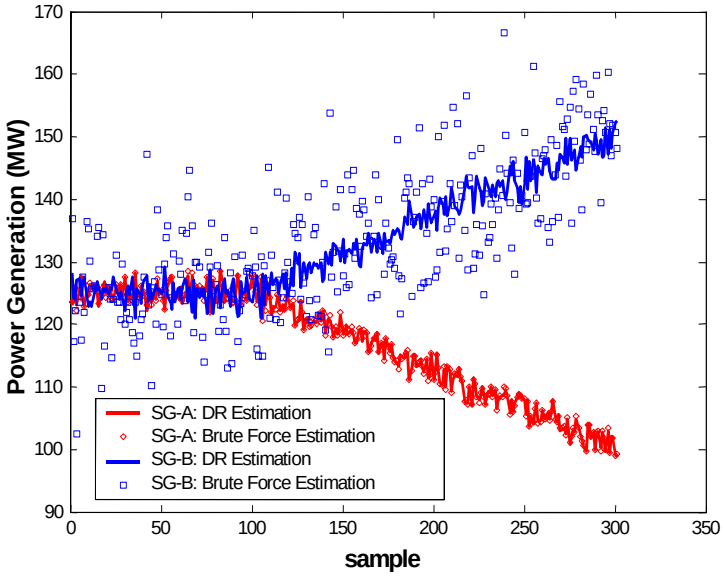

Figure 4.14. Bilinear data reconciliation result of heat transfer rate.

4.7 Summary

Sensor placement design has been studied for performance monitoring and fault diagnosis in this Chapter. The sensor placement design for process fault diagnosis is solved by studying the cause-effect relationships among process variables using causal graph theory. If mass balance and energy balance are used to determine performance parameters and for sensor fault diagnosis, then orthogonal projection algorithm would be implemented to perform redundancy and observability analysis for sensor placement design. Finally, it is observed that a sensor fault can be detected and reconstructed efficiently only if it is sensitive in the corresponding balance equations, and data reconciliation provides a generalized approach to sensitivity analysis in sensor placement design for efficient sensor fault diagnosis.

Chapter 5

Fault Diagnosis during Steady State Conditions

5.1 Introduction

Steady state fault diagnosis is an essential part of the integrated approach to performance monitoring and fault diagnosis for condition-based maintanance of nuclear power systems. Although many techniques, mainly data driven model based as reviewed in Chapter 1, have been developed, none of them is sophisticated enough for the application to nuclear power systems. To address the stringent requirements in nuclear power systems, the most recent progress in data driven model based fault diagnosis with an emphasis on how the FDI capability is dependent on data is presented. Robust PCA model based approach and hybrid PCA approach are developed as two new techniques with improved performance for steady state fault diagnosis in this chapter.

Reconstruction PCA model based approach is proposed as the baseline algorithm for steady state fault diagnosis because of its explicit representation of fault detectability and identifability. In this approach, the fault effects are characterized by the subspace spanned by the fault measurements so that both process faults and sensor faults can be dealt with in a unified manner. The number of principal components is chosen to achieve the best reconstruction of all the measured variables. This method of choosing the number of principal components is also unique in that it can determine which measured variables have a low correlation with the other variables and thus should be eliminated for model development. The reconstruction PCA model based approach to fault isolation is performed by comparing the reconstruction errors when each candidate fault is assumed. The fault along the direction for which the reconstruction error reaches the minimum is considered as the true fault. Because this fault isolation logic follows the philosophy of assumption-based methods, it can give more conclusive results of fault isolation than other approaches.

A hybrid PCA approach is developed in this dissertation for steady state fault diagnosis. In this approach, certain prior knowledge is explicitly incorporated into the developed PCA model. The prior knowledge may include the information about the source of major variation contained in the collected data and the partially available material and energy balance equations. The developed hybrid PCA approach is more sensitive in detecting minor faults after some large variations are removed through appropriate decomposition of the variation contained in the data.

Robust PCA model based approach is developed for steady state fault diagnosis in this dissertation. In this approach, PCA models are developed from the data generated from reliable simulation models, therefore, the assumption that the collected data must cover the entire possible operation modes can be easily satisfied with well designed simulation calculations. Meanwhile, model uncertainties are identified from plant measurements and explicitly formulated in the fault diagnosis algorithm. Therefore, false alarms and misdiagnosis of traditional model based approach to fault diagnosis due to model uncertainty can be avoided.

5.2 Principal Component Analysis for Fault Diagnosis

The basic idea of fault diagnosis using multivariate statistical methods such as PCA is to project the collected data onto a low-dimensional space where the regions of normal operation and abnormal operation can be characterized by fewer state variables.

Because PCA model represents the variation of normal operation data in a reduced dimensional space, it has better performance of generalization than when the entire measurement space is used. PCA modeling separates the entire measurement space into a model subspace capturing the variation of state variables and a residual subspace containing random variations. The separate characterization of the two subspaces can provide further insights in terms of the changes in operation conditions. In addition, the linear model extracted by PCA enables us to determine which variables are most affected by a fault and which variables are most responsible for the fault.

5.2.1 Motivation of Statistical Modeling

A formal analysis was performed by Qin, 2003, to investigate the theorectical basis to extract process models from measurement data using statistical methods. This analysis is important to understand the requirement of data quality in developing statistical models for fault diagnosis.

For an engineering process, the steady state constraints imposed by balance equations are given by:

$$B_1 x^* + B_2 d = 0 \tag{5.1}$$

$$x = x^* + \varepsilon \tag{5.2}$$

where

x^* = the true values of the measured vector.

x = the m dimensional measurement vector.

d = the unmeasured state vector.

ε = the measurement noise vector.

B_1, B_2 = the related matrices.

If we premultiply Equation (5.1) by $B_2^{\perp}$, the orthogonal complement of B_2, then we have:

$$(B_2^{\perp})^T B_1 x^* = C x^* = 0 \tag{5.3}$$

The above equation indicates that x^* must live in the null space of C. If the rank of C is q, x^* can be represented by a linear combination of $m - q$ independent factors given by:

$$x^* = Gs \tag{5.4}$$

where the $m-q$ columns of G spans the null space of C.

Correspondingly,

$$x = Gs + \varepsilon \tag{5.5}$$

Equation (5.5) shows that the measured data can be projected onto a lower dimensional space without loss of information. The variation of the measured data can be totally explained by the variation of the independent factors if all of them are incorporated. From the physical point of view, the number of independent factors is equal to the number of independent measured disturbances, independent unmeasured disturbances, and the setpoint changes, which exist in a system. In order to have an efficient model capable of characterizing all the possible normal operation conditions, it is necessary to fully excite the process system with all the modes of independent factors being excited. If the collected normal data do not contain all the modes, the developed model will not be able to distinguish the difference between a new operation mode and an actual fault in the system.

The above formal analysis has motivated the development of statistical methods to extract process models from measurement data and pinpointed the requirement of data quality for model development.

Example: For the system given in Figure 4.5, the matrices B_1 and B_2, related to the mass balance equations, are given as follows:

$$B_1 = \begin{pmatrix} 1 & 0 & 0 \\ 0 & -1 & 0 \\ 0 & 1 & 1 \end{pmatrix} \qquad B_2 = \begin{pmatrix} 1 & -1 & 0 \\ -1 & 1 & 0 \\ 0 & 0 & -1 \end{pmatrix}$$

$$x = \begin{pmatrix} G1 \\ G4 \\ G5 \end{pmatrix} \qquad u = \begin{pmatrix} G2 \\ G3 \\ G6 \end{pmatrix}$$

The orthogonal complement of B_2 and the C matrix are as follows:

$$B_2^{\perp} = \begin{pmatrix} 0.7071 \\ 0.7071 \\ 0 \end{pmatrix} \qquad C = \begin{pmatrix} 0.7071 & -0.7071 & 0 \end{pmatrix}$$

where the rank of C is 1. If we choose the matrix G such that each column of G is the basis of the null space of C, then matrix G has the form:

$$G = \begin{pmatrix} 0.7071 & 0 \\ 0.7071 & 0 \\ 0 & 1 \end{pmatrix}$$

Therefore, it can be concluded from Equation (5.5) that there are only two independent factors in the system and any measurement vector can be represented by a linear combination of these two independent factors, which is given by:

$$\begin{pmatrix} G1 \\ G4 \\ G5 \end{pmatrix} = \begin{pmatrix} 0.7071 & 0 \\ 0.7071 & 0 \\ 0 & 1 \end{pmatrix} \begin{pmatrix} s1 \\ s2 \end{pmatrix}$$

Obviously, this result can be verified by examining the flowchart given in Figure 4.5.

5.2.2 PCA Algorithm

Principal Component Analysis (PCA) was originally developed by Pearson, 1901, as a statistical method of dimensional reduction while preserving the variation of data. The PCA algorithm will be derived in the context of process monitoring in this section.

For a measurement vector $x \in R^m$, in general, it can be represented in m dimensional space as follows:

$$x = \sum_{i=1}^{m} t_i p_i \tag{5.6}$$

where

p_i = the basis vectors of the m dimensional space, which are orthonormal.

t_i = the component of the vector x when projected onto the basis vector p_i.

Apparently, since the basis vectors are orthonormal, t_i can be given by:

$$t_i = x^T p_i \tag{5.7}$$

If the true dimensionality of the measurement vector is l, where $l < m$, then the projection can be separated into two parts, which is given by:

$$x = \sum_{i=1}^{l} t_i p_i + \sum_{j=l+1}^{m} \tilde{t}_i \tilde{p}_i \tag{5.8}$$

where the second term represents the random vectors obtained by projecting the vector x onto the remaining ($m - l$) dimensional space.

The objective of PCA algorithm is then to determine the true number of components directly from the measured data such that the second part of Equation (5.8) behaves purely random. This is equivalent to determining l principal components such that the mean squared error of the approximation, given by Equation (5.9) is minimized.

$$\varepsilon^2 = E[\varepsilon^T \varepsilon] \tag{5.9}$$

The PCA algorithms can be developed either by the NIPALS procedure (Wold, Esbebsen, and Geladi, 1987) or by eigenvalue decomposition procedure (Russell, Chiang, and Braatz, 2000). The eigenvalue decomposition procedure is presented here for its simplicity.

Given a data matrix *X* associated with *n* observations and *m* measured variables when the mean values are removed, the first principal component is obtained by finding out a basis vector p_1 such that the score vector t_1 of the original data along this direction has maximized variance, which is given by:

$$\max_{p_1}\{E[\text{var}(t_1)]) = \max_{p_1} \frac{p_1^T \Sigma p_1}{p_1^T p_1} \tag{5.10}$$

with the constraints

$$p_1^T p_1 = \text{I}$$

where

$$\Sigma = X^T X$$

The solution of Equation (5.10) is actually the eigenvector of Σ corresponding to its maximum eigenvalue, that is:

$$\Sigma(p_1) = \lambda_1 p_1 \tag{5.11}$$

where

λ_1 = the largest eigenvalue of the covariance matrix.

Correspondingly, the variance of the original data along the first principal component is then given by:

$$E[\text{var}(t_1)] = \lambda_1 \tag{5.12}$$

In order to obtain the jth principal component, the following constraints must be satisfied (Jackson, 1991):

$$\max_{p_k}\{E[t_k]\} = \max_{p_k} \frac{p_k^T \Sigma p_k}{p_k^T p_k} \tag{5.13}$$

such that

$$p_k^T p_k = \text{I}$$

p_k is orthogonal to p_j for $j = 1,2....k-1$

and

the score vector of t_k is orthogonal to the score vector of t_j for $j = 1,2....k-1$

The solution of Equation (5.13) can also be obtained by solving the eigenvalue problem of the scatter matrix Σ, which is given by:

$$\Sigma(p_k) = \lambda_k p_k \tag{5.14a}$$

$$E\{\text{var}(t_k)\} = \lambda_k \tag{5.14b}$$

Obviously, the above PCA algorithm has chosen the eigenvectors of the covariance matrix of the measured data as the basis vectors for projection. The far-reaching implication of the projection in this manner is that the variation of the measured data can be separated into the variation in the principal component subspace and the variation remained in the residual space. The PCA decomposition of the original measurement data is given by:

$$X = TP^T + \widetilde{T}\widetilde{P}^T \tag{5.15}$$

where

P = the loading matrix whose columns span the principal component space (PCS) and consist of the eigenvectors corresponding to the largest l eigenvalues of the matrix Σ.

$\widetilde{P}$ = the loading matrix whose columns spans the residual space (RS) and consist of the eigenvectors corresponding to the smallest $m - l$ igenvalues of the matrix Σ.

For a measurement vector x, the PCA algorithm estimates the true value by a projection onto the PCS and filter out the random component, which is given by:

$$\hat{x} = PP^T x \tag{5.16}$$

The estimation error of the approximation is given by:

$$\varepsilon = x - \hat{x} = \widetilde{P}\widetilde{P}^T x \tag{5.17}$$

The expectation of the mean squared error is given by:

$$\varepsilon^2 = E[\varepsilon^T \varepsilon] = E[x^T \tilde{P}\tilde{P}^T \tilde{P}\tilde{P}^T x] = E[\tilde{T}^T \tilde{T}] = \sum_{k=l+1}^{m} \lambda_k \tag{5.18}$$

The above equation shows that the mean squared error is equal to the sum of the least significant eigenvalues of the covariance matrix. This also indicates that the choice of the number of principal components is to abandon the eigenvectors as the basis vectors for expansion that correspond to the least significant eigenvalues of the covariance matrix of the original measured data.

5.2.3 Selection of the Number of Principal Components

Many approaches have been proposed to determine the number of principal components for different applications. An excellent survey paper by Valle, Li, and Qin, 1999, summarized these methods and proposed the variance of reconstruction error criterion for process monitoring.

Information criteria such as Akaike Information Criterion (AIC) (Akaike, 1974), Minimum Description Length (MDL) (Rissanen, 1978), and Imbedded Error Function (IEF) (Malinowski, 1977) were used in signal processing literature to determine the number of independent sources by selecting the number of principal components. These criteria have solid statistical foundation with the assumption that the independent measurement noise components have equal variance corresponding to the smallest $m-l$ eigenvalues of the covariance matrix of the original signal. This assumption is valid for covariance matrix based PCA when all the signals have equal variance of measurement errors. However, for correlation matrix based PCA, which is most commonly used in process monitoring, the measurement errors usually do not have the same variance and the eigenvalues corresponding to the smallest $m-l$ eigenvalues are usually quite different.

In the field of chemometrics, the most commonly used criteria are Cumulative Percent Variance, Scree Plot, Average Eigenvalue, and Cross Validation. Cumulative percent variance method selects the number of principal components by setting a subjective threshold of cumulative percent variance. Scree plot method is based on the

plot of the fraction of variance explained by each principal component. The plot orders the principal components from the one that explains the largest amount of variation to the one that explains the least amount of variation. This method considers the beginning point of the Scree as the most reasonable number of principal components. Average eigenvalue method assumes that all the components whose corresponding eigenvalues are less than the average value should be discarded. When cross validation method is used to determine the number of principal components, the original data are randomly divided into N blocks, the cross validation error is computed as the residual sum of squares (RSS) for one block of data with the PCA model built using the other blocks of data. The number of principal components is chosen to be the one beyond which the RSS begins to increase (Wold, 1978).

The cross validation method is the best available method to determine the number of principal components when large amount of data are available and when the objective of modeling is for prediction.

Qin and Dunia originally developed an algorithm to determine the number of principal components specifically for process monitoring (Qin and Dunia, 1998). This algorithm determines the number of principal components such that the best reconstruction of measurement error can be achieved.

Considering that the measured data are corrupted with additive sensor faults, the measurement vectors are given by:

$$x = x^* + f\xi_i \tag{5.19}$$

where

ξ_i = the fault direction of the ith sensor fault.

x^* = the noise containing measurement vector at normal operation condition.

The reconstructed value x_i of a given measured vector x , which is an estimate of x^*, along the fault direction ξ_i is given by:

$$x_i = x - f_i \xi_i \tag{5.20}$$

The best reconstruction needs to find the fault magnitude f_i such that the reconstruction error is minimized. The reconstruction error is defined as the distance between x_i and the projection onto the model space, which is given by (Dunia and Qin, 1998):

$$SPE_i = \| x_i - x^* \|^2 = \| \tilde{x}_i \|^2 = \| \tilde{x} - f_i \tilde{\xi}_i \|^2 \tag{5.21}$$

where the symbol ~ represents a projection onto the residual space which is induced by the pre-multiplication operator of $\tilde{P}\tilde{P}^T$.

To minimize the reconstruction error, the derivative of SPE_i with respect to f_i should be zero. That is:

$$\frac{d(SPE_i)}{df_i} = 2\tilde{\xi}_i^T (\tilde{x} - f_i \tilde{\xi}_i) = 0 \tag{5.22}$$

Therefore, the fault magnitude can be determined as follows:

$$f_i = \frac{\tilde{\xi}_i^T \tilde{x}}{\tilde{\xi}_i^T \tilde{\xi}_i} = \frac{\tilde{\xi}_i^T x}{\tilde{\xi}_i^T \tilde{\xi}_i} \tag{5.23}$$

The reconstructed value of the measurements along the fault direction ξ_i can now be obtained by:

$$x_i = x - f_i \xi_i = (\mathrm{I} - \xi_i \frac{\tilde{\xi}_i^T}{\tilde{\xi}_i^T \tilde{\xi}_i}) x \tag{5.24}$$

Because the measured data contain noise, there always exists a portion of unreconstructable error. The variance of the unreconstructed variation along the fault direction ξ_i is then given by:

$$u_i = \mathrm{var}[\xi_i^T (x^* - x_i)] = \mathrm{var}[\xi_i^T \xi_i f_i] = \mathrm{var}[\frac{\widetilde{\xi}_i^T x^*}{\widetilde{\xi}_i^T \widetilde{\xi}_i}] = \frac{\widetilde{\xi}_i^T \mathrm{cov}(x^*)\widetilde{\xi}_i}{(\widetilde{\xi}_i^T \widetilde{\xi}_i)^2} \tag{5.25}$$

Equation (5.25) is obtained by noticing that the fault magnitude f in Equation (5.19) is zero for normal operation data and thus $x = x^*$ in Equation (5.24).

The optimal number of principal components needs to ensure that a reliable reconstruction can be achieved for normal operation data independent of the direction chosen for fault reconstruction. In other words, the criterion to determine the number of principal components can be formulated to minimize the normalized variance of reconstruction error (VRE) in terms of the number of principal components k, which is given by:

$$VRE(k) = \sum_{i=1}^{m} \frac{u_i}{\mathrm{var}(\xi_i^T x)} \tag{5.26}$$

Dunia and Qin proved that the normalized VRE could always achieve a minimum (Dunia and Qin, 1998b). Intuitively, the VRE in the residual space will monotonically decrease with respect to k because the eigenvalues of the covariance matrix decreases. Meanwhile, the variance of the reconstruction error in model space will go to infinity when k approaches m, because $\widetilde{\xi}_i$ in the denominator of Equation (5.25) tends to be zero. In combination, the VRE can reach a global minimum.

Dunia and Qin have also revealed the relationship between the method of the VRE approach and the cross validation approach to determine the number of principal components (Valle, Li, and Qin, 1999). The VRE approach is equivalent to cross

validation approach when the noise variances are not too much different and the variance of the signal is larger than the variance of the noise.

One of the uniqueness of VRE approach is that it is able to optimally choose the number of principal components in order to have the best fault reconstruction. In addition, this approach can determine which measured variables have a low correlation with the other variables. If the VRE is greater than the variance of the original data, the model prediction will be worse than the simple average of the raw measured data. Therefore, these variables should not be included in the PCA model for process monitoring.

5.2.4 Fault Detection

Fault detection can be performed by monitoring the change of the correlation structure of the measured data. Because the variation of data is separated in the principal component space and the residual space, two statistics, T^2 statistics and Q statistic are defined to measure the variation in the two spaces, respectively. If a new observation exceeds the effective region in the PC space defined by the normal operation data, a change in operation regime can be detected. If a significant residual is observed in the residual space, a special event, either due to disturbance changes or due to changes in the relationship between variables, can be detected.

5.2.4.1 T^2 Statistics

The T^2 statistics measures the variation in the PC space, which is given by:

$$T^2 = t^T \Sigma^{-1} t \tag{5.27}$$

where

Σ = the sample variance matrix of the training data.

t = the score vector.

If the measured data at normal operation conditions follow a multivariate normal distribution, T^2 statistics is related to an F distribution, which is given by:

$$T_{\alpha}^{\ 2} = \frac{m(N-1)}{N-m} F_{m,N-m;\alpha} \tag{5.28}$$

where

m = the number of variables.

N = the number of observations.

α = the significance level.

During normal operation conditions, the T^2 criterion is given as follows:

$$T^2 < T_{\alpha}^{\ 2} \tag{5.29}$$

T^2 statistics may be oversensitive when some of the eigenvalues of the correlation matrix are close to zeros.

Another limitation of T^2 statistics arises from the assumption that the raw data follows multivariate normal distribution. The assumption is true only when the normal operation data are collected at one operation condition. However, the normal operation data are usually collected under different operation conditions for an engineering process where many operation modes are possible. Therefore, it should be cautious when T^2 statistics is used for process monitoring.

5.2.4.2 Q Statistics

The Q statistics measures the variation in the residual space, which is defined as the sum squared error (SSE) given by:

$$Q = \varepsilon^T \varepsilon \tag{5.30}$$

where

$$\varepsilon = \widetilde{P}\widetilde{P}^T x$$

A fault is detected if the Q statistics exceeds a threshold given by:

$$Q \geq Q_\alpha \tag{5.31}$$

If the residual vector follows multivariate normal distribution, the threshold of Q statistics is given by (Jackson and Mudholkar, 1979):

$$Q_\alpha = a(b + c\alpha)^d \tag{5.32}$$

where

α = the critical value for standard normal distribution at a given significance level.

$$a = \sum_{i=k+1}^{p} \lambda_i$$
$$b = 1 + [\theta_2 h_0 (h_0 - 1)] / a^2$$
$$c = (\sqrt{2\theta_2} h_0) / a$$
$$d = 1 / h_0$$
$$\theta_2 = \sum_{i=k+1}^{p} \lambda_i^{\,2}$$
$$\theta_3 = \sum_{i=k+1}^{p} \lambda_i^{\,3}$$
$$h_0 = (1 - 2a\theta_3) / (3\theta_2^{\,2})$$

Because the assumption that the residual vector follows multivariate normal distribution is much more relaxed than multivariate normal distribution of the original measured data, Q statistic is more appropriate than T^2 statistics for process monitoring.

5.2.4.3 Conditions for Fault Detectability

In general, the fault effects on measurements are multi-dimensional. One-dimensional fault is a simple fault whose effect shows only in one measured variable

while a multi-dimensional fault shows its effects in multiple measurements. A sensor fault outside any control loops is one-dimensional. Most process faults such as fouling of heat exchangers and pipe leakage are multi-dimensional. In the presence of feedback and feedforward control, even a sensor fault may become multi-dimensional because the fault effects may be propagated to many other variables (Yoon and MacGregor, 2001).

The fault effects of a multi-dimensional fault can be uniformly represented as follows:

$$x = x^* + Ef \tag{5.33}$$

where

E = the fault distribution matrix.

f = the fault magnitude vector.

If a fault occurs, the SSE will be as follows:

$$SSE = \| \tilde{x}^* + \tilde{E}f \|^2 \tag{5.34}$$

where

$$\tilde{E} = \tilde{P}\tilde{P}^T E$$

The necessary condition for fault detectability is that $\tilde{E}f \neq 0$. In other words, a fault can be detected only if the projection of fault distribution matrix onto the residual space, $\tilde{E}$, is not empty, and the fault magnitude vector f is not orthogonal to the space spanned by $\tilde{E}$. This result is understandable because a detectable fault must have significant effects on residuals that are used as fault signatures for fault detection.

The sufficient condition for fault detection has also been derived by Dunia and Qin, 1998b, which is written as follows:

$$\| \tilde{E}f \| > 2\delta_\alpha \tag{5.35}$$

where

$$\delta_\alpha = \sqrt{Q_\alpha}$$

The above condition cannot be used directly in real practice. We are here to derive a more specific condition for practical use.

Since $\| \widetilde{E} f \| \geq \sigma_{\min}(\widetilde{E}) \| f \|$, a more restrictive condition for fault detectability can then be given by:

$$\| f \| > 2 \frac{\delta_\alpha}{\sigma_{\min}(\widetilde{E})} \tag{5.36}$$

where $\sigma_{\min}$ denotes the minimum singular value.

The above derivation assumes that the measured data have been standardized with zero mean and unit variance. In order to guarantee the detectability of a sensor fault, the minimum fault magnitude of the measured value is given by:

$$\| f_m \| \geq \frac{2\delta_\alpha}{\sigma_{\min}(\widetilde{E})} \sigma_m \tag{5.37}$$

where σ_m is the standard deviation of the normal operation data and $\| f_m \|$ is the minimum fault magnitude.

Three implications can be drawn from Equation (5.37). The first implication is that it is more difficult to detect a fault whose normal operation data has a larger variation. The second implication is that the minimal detectable fault magnitude increases when the dimension of the residual space increases. The third implication is that the minimal detectable fault magnitude increases when the signal-to-noise ratio decreases since the Q statistic limit is a sensitive function of the signal-to-noise ratio.

5.2.5 Fault Isolation

Fault isolation is important to locate the root causes after a fault is detected. If there is a large amount of historical data, fault isolation can be simplified as a

classification problem (Russell, Chiang, and Braatz, 2000). However, because the same fault may have different fault magnitudes and the fault effects on the measured variables may vary with the operation conditions, the classification method may become unrealistic although it is easy for implementation. The most popular approach to fault isolation is to investigate the contribution of individual measurements to the model residuals. As compared with the classification approach, the advantage is that there is no need to prepare fault data. However, contribution based approach may give inconclusive results for fault isolation if two faults are quite similar. If fault effects are known in terms of fault distribution matrix, reconstruction based approach is able to lead to conclusive results for fault isolation.

5.2.5.1 Classification Based Approach

The fundamental assumption of pattern classification is that the objects from the same class share some common statistical relationship and this commonality can be quantitatively measured. In the context of fault isolation, distance and direction can both be candidates to measure the commonality. However, because possible fault magnitude is unpredictable before fault diagnosis is performed, fault direction should be a better measure to characterize different faults.

Standard pattern classification involves two steps. The first step is feature extraction, which transforms measured variables from a high dimensional space to a lower dimensional space such that the objects in the same class will cluster and the objects in different classes will have separation. PCA itself is a commonly used method for feature extraction. The second step is to develop a classifier that is able to assign an object in the feature space to a specific class such that the total classification error is minimum.

One of the popular algorithms of distance-based classification is the Bayesian classifier. In this classifier, an object is assigned to the ith class if the ith discriminant function reaches the maximum value, which is given by:

$$g_i(x) > g_j(x) \qquad \text{for } j \neq i \tag{5.38}$$

where

$g_i(x) = P(\omega_i \mid x)$

$P(\omega_i \mid x)$ = a posteriori probability, which is the probability that a sample vector x is assigned to class ω_i.

If the objects follow multivariate normal distribution with mean vector μ_i and covariance matrix Σ_i for the ith class, the discriminant function for the ith class is given by (Russell, Chiang, and Braatz, 2000):

$$g_i(x) = -\frac{1}{2}(x-\mu_i)^T \Sigma_i^{-1}(x-\mu_i) - \frac{1}{2}\ln(\det(\Sigma_i) + \ln P(\omega_i) \tag{5.39}$$

where

$P(\omega_i)$ = the prior probability for class ω_i.

The Bayesian classifier can be performed either for the score vectors or for the residual vectors depending on which space contains the vital discriminant information (Raich and Cinar, 1997).

Direction-based classifier compares the similarity of principal components between different classes. Considering two classes of data, the two classes of data will produce two PCA models, $P1$ and $P2$. The angles α_k between the two sets of PCA model directions can be related to the eigenvalues of s_k, and is given by:

$$P1^T P2 P2^T P_1 = L^T S L \tag{5.40a}$$

$$\cos(\alpha_k) = s_k^{1/2} \tag{5.40b}$$

where L consists of the consensus coordinates and s_k is the kth largest eigenvalues of S, which corresponds to the smallest angle between the kth dimensional coordinate subspaces (Krzanowski, 1979).

A generalized similarity measure in terms of the PCA model directions can be defined as the sum of the cosines of angles between PCA model axes as follows (Raich and Cinar, 1995):

$$f = \frac{1}{p}\sum_{k=1}^{p} s_k \tag{5.41}$$

where

p = the dimensionality in the consensus coordinate systems.

f = the similarity factor.

The directional-based classification is most useful to analyze the residual structure for fault isolation. If there is a process fault such as heat exchanger fouling, the generated residuals will have certain directional features, the direction-based classification can be used to compare the similarity between the new residuals and the predefined residual structure.

A sensitive fault detection algorithm has also been developed by monitoring the differences between the reference principal components and the principal components representing the current operation conditions. If the correlation structure is changed, the cosine angle between the first reference PC and the first PC at the current condition can be directly used for fault detection. However, if the variances of the first few major principal components are similar, the directions of principal components may change drastically although the correlation structure indeed does not change. In this case, it is better to monitor the changes of subspace spanned by the principal components with similar variance for robust fault detection. The dissimilarity of the subspace $P1$ defined by the reference PCA model to the subspace $P2$ defined by the current PCA model can be measured by the following index A_m (Kano, Hasebe, Hashimoto, and Ohno, 2001):

$$A_m = \sqrt{1-|\lambda_m|} \tag{5.42}$$

where

λ_m = the smallest eigenvalue of the matrix $P2^T P1P1^T P2$.

5.2.5.2 Contribution Based Approach

The contribution-based approach quantifies the contribution of each process variable to T^2 statistics and Q statistic to determine the root causes after a fault happens.

The Q statistic-based contribution approach decomposes the SSE into individual components contributed by each measured variable as follows:

$$SSE = \sum_{i=1}^{m} SSE_i$$

where

$SSE_i = (x_i - \hat{x}_i)^2$

$\hat{x}_i$ = the ith component of the matrix $PP^T x$.

The contribution of the ith process variable to the Q statistic is then given by:

$$CONT_i = \frac{SSE_i}{SSE} \tag{5.43}$$

The T^2 statistics based contribution approach first determines which score components are out of control. A score component t_j is considered as abnormal if the standardized score is greater than the average T_α^2 assigned to each degree of freedom, that is:

$$(\frac{t_j}{\sigma_j})^2 > \frac{T_\alpha^2}{m_p} \tag{5.44}$$

where

m_p = the number of principal components.

The contribution of each variable x_i to the out-of-control score t_j, denoted by $CONT_{j\leftarrow i}$, is then given by:

$$CONT_{j\leftarrow i} = P_{ij}(x_i - \hat{x}_i)$$

where P_{ij} is the ith row of the jth principal component vector.

The total contribution of the process variable x_i to the out-of-control T^2 statistics is given by (Kourti and MacGregor, 1996):

$$CONT_i = \sum_{j=1}^{n_t} \frac{t_j}{\sigma_j}[P_{ij}(x_i - \hat{x}_i)] \qquad (5.45)$$

where n_i is the number of score components out of control.

Contribution based approach does not give immediate results of fault isolation because these contributions are derived from correlation based models (Yoon and MacGregor, 2000). However, contribution plots do indicate which group of variables are highly correlated with a detected fault. Fortunately, contribution plots work quite well for sensor and actuator fault isolation in real practice.

5.2.5.3 Reconstruction Based Approach

Reconstruction based approach to fault isolation belongs to the philosophy of assumption based fault diagnosis (Kavuri and Venkatasubramanian, 1992). A set of candidate fault directions are chosen based on prior knowledge or inferred from historical data. Fault identification is performed by comparing the reconstruction error when each

candidate fault is assumed. The fault along whose direction the reconstruction error reaches the minimum is considered as the true fault.

Given an abnormal measurement vector x with the true fault magnitude f_i along the fault direction E_i, if the candidate fault direction is assumed to be E_j, in analogy to Equation (5.24), the reconstruction error along this direction is given by (Qin, 2003):

$$\tilde{x}_j = \tilde{x} - \tilde{E}_j f_j = (\mathrm{I} - \tilde{E}_j \tilde{E}_j^+)\tilde{x} = (\mathrm{I} - \tilde{E}_j \tilde{E}_j^+)\tilde{x}^* + (\mathrm{I} - \tilde{E}_j \tilde{E}_j^+)\tilde{E}_i f_i \tag{5.46}$$

where $\tilde{E}_j^+$ denotes the pseudoinverse of E_j which satisfies that $\tilde{E}_j \tilde{E}_j^+ \tilde{E}_j = \tilde{E}_j$.

If the assumed fault is the true fault, i.e. $E_j = E_i$, using Equation (5.46), the SSE is then given by:

$$SSE_i = \| (I - \tilde{E}_i \tilde{E}_i^+)\tilde{x}^* \|^2 \tag{5.47}$$

It is easy to show that the sum square of the reconstructed error is minimal only if the assumed fault is the true fault. This provides the technical basis to determine the true fault out of candidate faults with a conclusive result. Moreover, the sum square of the reconstructed error along the true fault direction can always be brought back within the Q statistic limit.

However, it is also possible that the sum square of the reconstructed error will be smaller than the Q statistic limit even if the reconstruction is not performed along the true fault direction. A sufficient condition to avoid this from happening is as follows (Qin, 2003):

$$| \tilde{f} | > \frac{2\delta_i}{\sin(\alpha_{ij})} \tag{5.48}$$

where

α_{ij} = the angle between $\widetilde{E}_i$ and $\widetilde{E}_j$.

δ_i = the confidence limit of the Q statistic of the reconstruction error along the ith fault direction.

Equation (5.48) is a very conservative condition for fault identification. For this reason, we do not suggest to relate fault isolation to the Q statistics. Instead, fault isolation is only based on comparing the reconstruction error.

In addition, Equation (5.48) holds only when the fault is one-dimensional. In general, in order to ensure that $\| SSE_j \|^2 > Q_\alpha$ if $j \neq i$, a sufficient condition is given by:

$$\| f \| > \frac{2\delta_i}{\sigma_{\min}\{(\mathrm{I} - \widetilde{E}_j \widetilde{E}_j^{+})\widetilde{E}_i\}} \tag{5.49}$$

5.3 Application to the IRIS HCSG Systems

The application of reconstruction based PCA approach to IRIS HCSG systems is presented in this section.

5.3.1 Data Generation and Model Development

The data were generated for one pair of the steam generators, SG-A and SG-B, to simulate the measurements in actual nuclear power plants, where most measurements are highly correlated with other measurements. For this pair of steam generators, it is assumed that the available measured variables include:

- W1: the flow rate into the primary side of SG-A and SG-B.
- T1: the primary side inlet temperature.
- T3: the primary side outlet temperature of SG-A.
- T5: the primary side outlet temperature of SG-B.

- T6: the primary side outlet temperature of SG-A and SG-B
- W6: the flow rate leaving the primary side of SG-A and SG-B.
- W7: the feed water flow rate into the secondary side of SG-A and SG-B.
- T7: the feed water temperature.
- W12: the steam flow rate leaving the secondary side of SG-A and SG-B.
- T12: the steam temperature leaving the secondary side of SG-A and SG-B.
- T9: the steam temperature leaving the secondary side of SG-A.
- T11: the steam temperature leaving the secondary side of SG-B.

The normal operation data was generated by perturbing the feed water flow rate W7 ranging from 80% nominal value to 100% nominal value to simulate reactor power change using the simulation model developed in Chapter 3. In the simulation, it is also assumed that the two steam generators are at operation in perfect symmetry and the primary flow rate and the primary inlet temperature are constant.

Because the secondary fluid flows inside the helical coil tubes, it is unrealistic to install instruments to directly measure the mass flow rate of each steam generator. However, it is a realistic postulation that the mass flow rate into the secondary side of the steam generator pair may be uneven due to flow path blockage. This anticipated operation condition is selected as a process fault in the analysis. The fault data were generated by linearly increasing the secondary mass flow rate into SG-A from 100% nominal value to 120% nominal value while reducing the secondary mass flow rate into SG-B from 100% nominal value to 80% nominal value.

After the data were generated, the temperature data were added with white Gaussian noise with three standard deviation of 0.25% nominal value and the mass flow rate data was added with white Gaussian noise with three standard deviation of 1% nominal value.

Table 5.1 summarizes the cross correlation coefficients of the simulated measured data. As is expected, the variables W1, W6, T1, and T7 do not have meaningful correlations with the other variables.

Table 5.1. Cross correlation coefficients of the generated data

Variables	W1	T1	T3	T5	W6	T6	W7	T7	W12	T12	T11	T9
W1	1.0000	-0.0059	0.0320	0.0382	-0.0162	0.0242	-0.0299	0.0448	-0.0280	0.0220	0.0217	0.0231
T1	-0.0059	1.0000	0.0206	0.0164	-0.0032	0.0139	-0.0177	0.0334	-0.0177	0.0095	0.0096	0.0084
T3	0.0320	0.0206	1.0000	0.9836	-0.0068	0.9834	-0.9895	-0.0232	-0.9897	0.9505	0.9500	0.9498
T5	0.0382	0.0164	0.9836	1.0000	-0.0064	0.9838	-0.9900	-0.0234	-0.9901	0.9519	0.9528	0.9521
W6	0.0162	-0.0032	-0.0068	-0.0064	1.0000	-0.0075	0.0083	0.0023	0.0065	-0.0052	-0.0077	-0.0126
T6	0.0242	0.0139	0.9834	0.9838	-0.0075	1.0000	-0.9900	-0.0285	-0.9904	0.9522	0.9520	0.9522
W7	-0.0299	-0.0177	-0.9895	-0.9900	0.0083	-0.9900	1.0000	0.0227	0.9967	-0.9629	-0.9630	-0.9623
T7	0.0448	0.0334	-0.0232	-0.0234	0.0023	-0.0285	0.0227	1.0000	0.0280	-0.0239	-0.0249	-0.0270
W12	-0.0280	-0.0177	-0.9897	-0.9901	0.0065	-0.9904	0.9967	0.0280	1.0000	-0.9633	-0.9633	-0.9627
T12	0.0220	0.0095	0.9505	0.9519	-0.0052	0.9522	-0.9629	-0.0239	-0.9633	1.0000	0.9871	0.9875
T11	0.0217	0.0096	0.9500	0.9528	-0.0077	0.9520	-0.9630	-0.0249	-0.9633	0.9871	1.0000	0.9877
T9	0.0231	0.0084	0.9498	0.9521	-0.0126	0.9522	-0.9623	-0.0270	-0.9627	0.987	0.9877	1.0000

In order to give all the measurements the same weights, a PCA model is developed using the correlation matrix. Table 5.2 tabulates the AIC criteria, the variance of reconstruction error, and the eigenvalues of the correlation matrix as a function of the number of principal components. The AIC criteria do not give a solution to the number of principal components. This is not because the selected penalty factor in the formula of AIC criterion is not appropriate. Instead, none of information criteria based methods can ensure the calculated number of principal components is appropriate because the assumption made to derive the likelihood function for use in AIC does not hold.

When PCA is performed for correlation matrix, the eigenvalues corresponding to the several small eigenvalues of the correlation matrix are usually quite different. This contradicts the assumption made to determine the likelihood of the unknown parameters for PCA model development. The variance of reconstruction error has a global minimum when the number of principal components is chosen to be three. Therefore, according to the minimum VRE, three principal components should be chosen for PCA modeling.

According to the eigenvalues of the correlation matrix given in Table 5.2, the number of principal components is estimated as seven. However, it can be seen from Table 5.1 that four independent variables have very low correlation coefficients with the other variables and thus they should be discarded. This indirectly shows that the number of principal components determined based on the minimum VRE is correct.

Figure 5.1 shows the ratio of the VRE to the variance of the raw data. The ratios are greater than 1.0 for W1, T1, W6, and T7. This indicates that the developed model cannot give model predictions better than simple averages of the raw data for these variables. If the cross correlation coefficients are examined, they indeed do not have physically meaningful correlation with the other variables. Therefore, it is demonstrated that VRE method is able to automatically exclude variables that do not consist of significant information for use in the model development.

Table 5.2. Determination of the number of Principal Components

Number of PCs	1	2	3	4	5	6	7	8	9	10	11	12
AIC(1.0E5)	1.08	0.98	0.85	0.63	0.20	0.041	0.036	0.029	0.024	0.014	0.0022	**0.0012**
VRE(1.0E4)	1.0	0.0003	**0.0002**	0.0003	0.077	0.031	0.033	0.034	0.053	0.098	0.53	∞
Eigenvalues	35.9	13.3	12.9	12.7	12.3	4.7	1.7	1.73	1.3	1.4	1.1	0.7

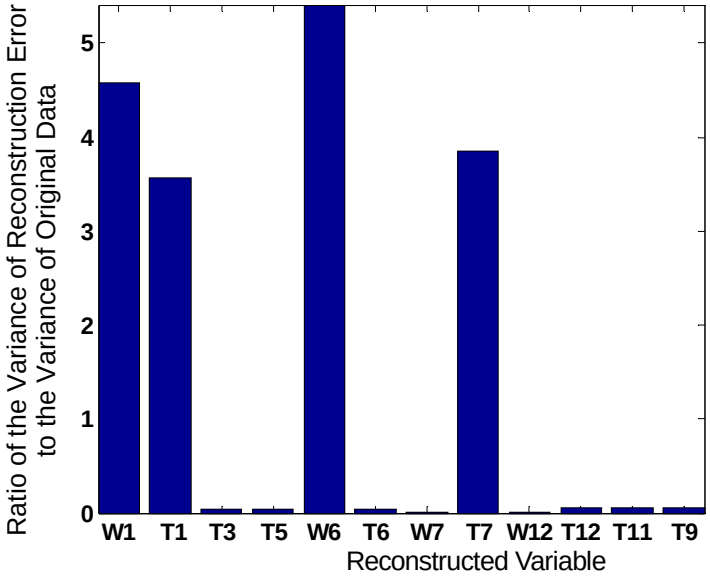

Figure 5.1. The ratio of the variance of reconstructed error to the variance of the original data.

5.3.2 Results of Single Fault Detection and Isolation

Table 5.3 shows the minimum fault magnitudes that can be detected for the eight sensor faults. The minimum fault magnitudes are 1.7 ^{o}C for the primary outlet temperature sensors, 5.7 kg/s for the secondary flow meters, and 2.2 ^{o}C for the secondary steam temperature sensors. Figure 5.2 plots the comparison between the sum prediction error and its threshold for T3 sensor fault with the minimum detectable fault magnitude.

Figure 5.3 shows that the Q statistic can be used to track the progression of the uneven secondary flow distribution of the HCSG pair. The fault can be detected at the 10th sample when the secondary flow rate of one steam generator has 102% nominal value and the secondary flow rate of the other steam generator is 98% nominal flow rate.

Table 5.3. Minimum detectable fault magnitudes for sensor fault detection.

Variable	T3 (C)	T5 (C)	T6 (C)	W7 (kg/s)	W12 (kg/s)	T12 (C)	T11 (C)	T9 (C)
Detection Limit[1]	1.7	1.7	1.7	5.7	5.7	2.2	2.2	2.2
Percent [2]	0.6	0.6	0.6	4.5	4.5	0.7	0.7	0.7

[1] Detection Limit=Minimum detectable fault magnitude.
[2] Percent=Percent of nominal value of the minimum detectable fault magnitude.

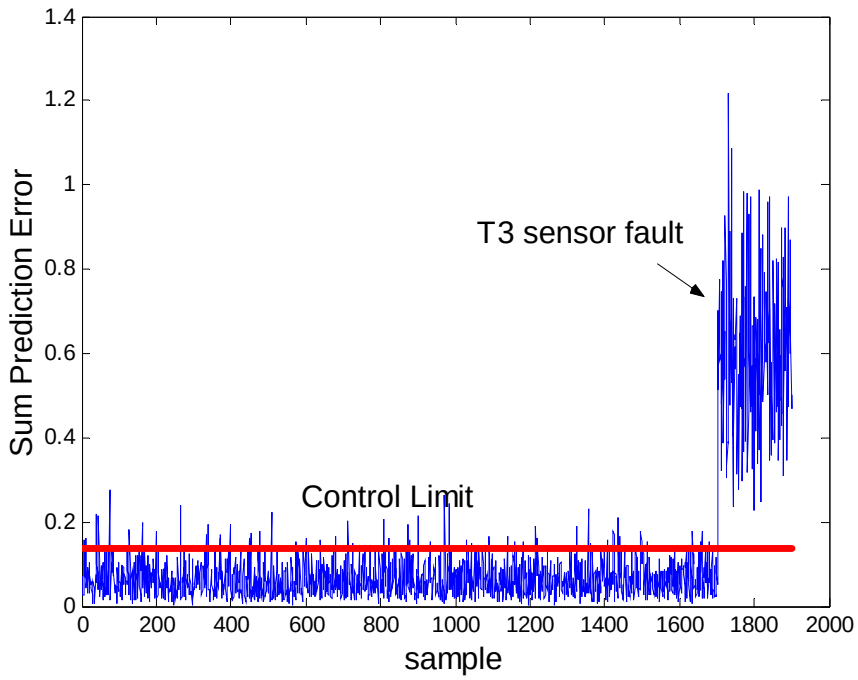

Figure 5.2. Detection of a fault with the minimum detectable fault magnitude.

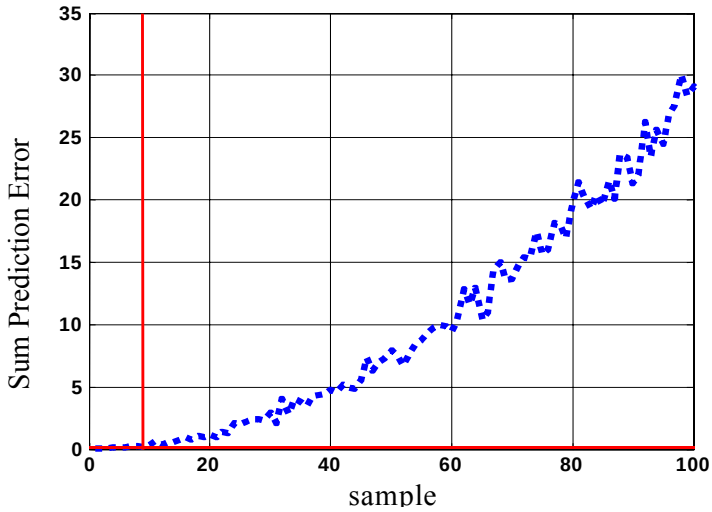

Figure 5.3. Tracking the progression of the uneven flow distribution fault.

Figure 5.4 shows the results of isolating the uneven HCSG flow distribution fault. The upper subplot gives the fault direction characterizing the fault effects on the eight measured variables. In this case, the fault effects can be characterized as a one-dimensional vector. After the fault occurs, the most significant symptom is that one of the steam generator will have a primary side outlet temperature lower than the nominal value and the other steam generator will have a primary side outlet temperature higher than the nominal value. The lower subplot shows the ratios of the reconstruction errors to the thresholds for six snapshots with different severity of uneven flow distribution. All the six snapshots have exactly the same signatures, which is necessary for robust fault isolation. If the reconstruction is performed along the other candidate faults (eight sensor faults) except the uneven flow distribution fault, the reconstruction errors are all much greater than 1.0. Only when the reconstruction is performed along the direction of uneven flow distribution fault can it be brought back within the predetermined threshold. Therefore, the uneven flow distribution fault can be correctly isolated.

Table 5.4 tabulates the cosine angle between a pair of fault directions projected onto the residual space for all the faults. If two fault directions projected onto the residual space are very similar, it will be unrealistic to distinguish their fault effects. In this example, the uneven flow distribution fault is more similar to a T3 sensor fault and a T5 sensor fault than the other sensor faults because of a larger value of cosine.

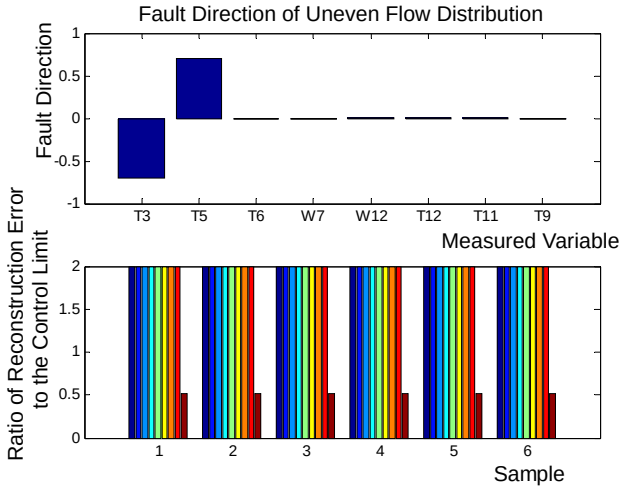

Figure 5.4. Isolation of the uneven flow distribution fault.

Table 5.4. Cosine of the angle between the fault directions projected onto the residual space

Variable	T3	T5	T6	W7	W12	T12	T11	T9	Process Fault
T3	1.0	-0.28	-0.28	0.24	0.24	0.02	0.02	0.02	-0.79
T5	-0.28	1.0	-0.27	0.24	0.24	0.02	0.02	0.02	0.81
T6	-0.28	-0.27	1.0	0.24	0.24	0.02	0.01	0.01	-0.01
W7	0.24	0.24	0.24	1.0	-0.22	0.03	0.03	0.03	0.01
W12	0.24	0.24	0.24	-0.22	1.0	0.03	0.03	0.03	0.01
T12	0.02	0.02	0.02	0.03	0.03	1.0	-0.49	-0.50	-0.01
T11	0.02	0.01	0.01	0.03	0.03	-0.49	1.0	-0.49	-0.01
T9	0.02	0.01	0.01	0.02	0.03	-0.50	-0.49	1.0	-0.01
Process Fault	-0.79	0.81	-0.01	0.01	0.01	-0.01	-0.01	-0.01	1.0

5.3.3 Results of Dual Fault Detection and Isolation

The reconstruction error based approach can be easily extended to detect and isolate multi-dimensional faults such as simultaneous multiple faults because of the unified representation of the fault effects. The application to one pair of HCSG systems is presented in this section. For simplicity without loss of the generality, it is assumed here that the possible simultaneous faults are limited to dual faults for all the sensors in the system.

Table 5.5 lists the reconstruction results of simultaneous T3 sensor fault with a 1% bias and W7 sensor fault with a 3% bias. The true values of the T3 and W7 are 299.41 ^{o}C and 100.56 kg/s, respectively. The measured values with sensor faults are 302.33 ^{o}C and 104.33 kg/s, respectively. The rectified values using reconstruction-based approach are 299.32 ^{o}C and 100.96 kg/s. The rectified values using traditional PCA approach are 299.78 ^{o}C and 99.58 kg/s. The reconstruction-based PCA approach does give better fault reconstruction than traditional PCA approach.

Table 5.5. Reconstruction of simultaneous sensor faults T3 and W7

Variable	T3 (C)	T5 (C)	T6 (C)	W7 (kg/s)	W12 (kg/s)	T12 (C)	T11 (C)	T9 (C)
True value	299.41	299.41	299.41	100.56	100.56	325.27	325.27	325.27
Measured Value	302.33	299.23	299.29	104.33	100.50	325.30	325.13	325.41
Reconstruction PCA	299.32	299.23	299.29	100.96	100.50	325.30	325.13	325.41
Traditional PCA	299.78	299.75	299.81	99.58	99.55	325.24	325.19	325.19

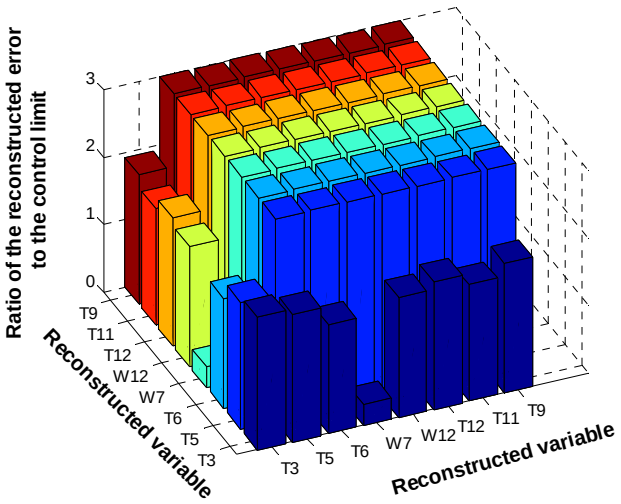

Figure 5.5. Identification of simultaneous dual faults (W7 and T3 sensor faults).

Figure 5.5 shows the ratio of the reconstruction error to the threshold of the sum prediction error. It can be seen that the ratio is greater than 1.0 when the reconstruction is performed using any candidate fault distribution matrices other than a dual fault of T3 sensor fault and W7 sensor fault. In other words, neither a single T3 sensor fault nor a single W7 sensor fault nor the other dual faults are able to fully explain the fault effects. The true fault can be correctly identified by the fact that the reconstruction is able to bring the reconstruction error back to below the threshold only if the fault distribution matrix corresponds to simultaneous T3 sensor fault and W7 sensor fault.

5.4 Hybrid PCA Model Based Fault Diagnosis

5.4.1 Motivation

Historical PCA model based fault diagnosis depends on how data are collected. There are two options to collect data and build correlation-based PCA models for nuclear power systems. One option is to collect data around certain operation points and the other option is to collect data during operation condition changes such as reactor startup. Because signal-to-noise ratio may be too small, the former approach may fail to capture

the correlations between measured variables. In practice, the latter approach is more realistic in building statistical models.

When operation condition changes, many measured variables will have significant amount of variation due to the manipulation of a few variables for operation condition changes. However, the large variation due to operation condition changes may conceal the correlations between some variables. The immediate consequence is that the developed statistical model will not be sensitive to detect a fault for such variables.

A simple example is designed to illustrate this problem encountered for fault diagnosis. In this example, two independent white Gaussian signals, u1 and u2, are used to excite a hypothetical system consisting of two signals, y1 and y2.

For Case A, the four signals were generated as follows:

$$u1 = N(0,1)$$
$$u2 = N(0,1)$$
$$y1 = 5u1 + 2u2$$
$$y2 = 4u1 + 3u2$$

The correlation coefficient of the generated data matrix [u1, u2, y1, y2] for Case A is given as follows:

1.0000	-0.0157	0.9181	0.7753
-0.0157	1.0000	0.3819	0.6193
0.9181	0.3819	1.0000	0.9622
0.7753	0.6193	0.9622	1.0000

For Case B, the data were generated with a larger variation of $u2$ in the following manner:

$$u1 = N(0,1)$$
$$u2 = 10 * N(0,1)$$

$$y1 = 5u1 + 2u2$$
$$y2 = 4u1 + 3u2$$

The correlation matrix of the generated data [u1, u2, y1, y2] for Case B is given as follows:

1.0000	0.0083	0.2556	0.1434
0.0083	1.0000	0.9689	0.9908
0.2556	0.9689	1.0000	0.9934
0.1434	0.9908	0.9934	1.0000

If we compare the correlation matrices for Case A and Case B, it is clear that a large variation of the signal u2 has annihilated the correlation between the signal u1 and y1 and y2.

Assuming all the data were added with 0.1% random Gaussian noise, based on the algorithm presented in section 5.2, the minimum detectable fault magnitudes were calculated for u1, u2, y1, and y2 sensor faults, respectively, which are given as follows:

0.006986, 0.011685, 0.033654, and 0.031368 for Case A.
0.029867, 0.064126, 0.129584, and 0.191066 for case B.

This result illustrates that a PCA model built from data with a large amount of variation for Case B will lead to a worse fault detection capability of the signal u1. If we examine Equation (5.36) carefully, the minimum detectable fault magnitude is proportional to the inverse of the minimum singular value of $\widetilde{E}$. However, if a variable has very low correlation with the other variables, the resulting residual component vectors will have small loadings on this variable and lead to a small minimum singular value of $\widetilde{E}$. Therefore, the corresponding minimum detectable fault magnitude would then be large.

To avoid the difficulties in detecting a slight fault using data collected during operation condition changes, one possible solution is to decompose the variation contained in the collected data into different components and to perform an individual analysis for each components. For instance, for the above example, if the variation of u2 is totally removed, the resulting PCA model is able to detect u1, y1, y2 sensor faults with a fault magnitude of 0.006242, 0.031206, and 0.024967, respectively, which are much smaller than those for Case B.

A hybrid PCA model based approach is proposed for fault detection and isolation with better performance in this dissertation. The hybrid PCA modeling integrates the available knowledge about the system into the developed PCA models. When data are collected during operation condition changes, some of the variation caused by independent manipulated variables, or caused by mass balance and energy balance are usually known. Therefore, it is desired to decompose the variation according to their sources and remove the variation caused by the known sources.

5.4.2 Constrained PCA Algorithm

Constrained PCA (CPCA) algorithm (Takane and Hunter, 2001) provides the mathematical basis to implement hybrid PCA modeling for fault diagnosis. In CPCA, the prior system knowledge is explicitly formulated in the PCA analysis. CPCA first decomposes the data matrix according to the given external information, and then applies the traditional PCA algorithm to the decomposed matrices.

The first step of CPCA involves projecting the original data matrix onto the spaces spanned by the matrices of the external information.

In general, two types of external information exist. The first one is that some constraints are imposed on the columns of the data matrix and the second one is that some external information is provided for the rows of the data matrix. When CPCA is applied to fault diagnosis, the row constraints may be the known redundant measurements, or mass balance and energy balance equations. The column constraints

may be related to the variables contributing to the large variation that may affect the sensitivity of fault detection.

The potential advantages of incorporating the external information for fault diagnosis include:

(a) Decompose the variation of measured variables so that the fault detection algorithm is more sensitive;

(b) Provide an integrated approach to combining correlation based statistical modeling and first-principle based modeling.

Given a data matrix X, the row constraint matrix G, the column constraint matrix H, the decomposition of the matrix X takes the following form (Takane and Hunter, 2001):

$$X = GMH' + BH' + GC + E \tag{5.50}$$

where the first term is related to the information that can be explained by both G and H, the second term is related to the information that can be explained by H but not by G, the third term is related to the information that can be explained by G but not by H, and the last term is the residual corresponding to what cannot be explained either by G or by H.

The decomposition of matrix X defined in Equation (5.50) does not have unique solution unless the following orthogonal conditions are satisfied:

$$G'B = 0 \tag{5.51a}$$
$$H'C = 0 \tag{5.51b}$$

The least square estimates of M, B, and C are given by:

$$\hat{M} = (G'G)^{-1} G'XH(H'H)^{-1} \tag{5.52a}$$

$$\hat{B} = (\mathrm{I} - P_G)^{-1} XH(H'H)^{-1} \tag{5.52b}$$

$$\hat{C} = (G'G)^{-1}G'X(\mathrm{I} - P_H)' \tag{5.52c}$$

where P_G and P_H are orthogonal projection operators onto the space spanned by the column vectors of G and H, respectively. These two projection matrices are defined as follows:

$$P_G = G(G'G)^{-1}G' \tag{5.53a}$$

$$P_H = H(H'H)^{-1}H' \tag{5.53b}$$

The matrix P_G is the projector onto the column space of G along the null space of G' and the matrix Q_G is the projector onto the null space of G' along the column space of G. The matrices P_G and Q_G have the following properties (Takane and Hunter, 2001):

$$P_G^2 = P_G \text{ and } Q_G^2 = Q_G \tag{5.54a}$$
$$P_G'P_G = P_G \text{ and } Q_G'Q_G = Q_G \tag{5.54b}$$
$$P_GQ_G = Q_GP_G = 0 \tag{5.54c}$$
$$P_GG = G \text{ and } G'P_G = G' \tag{5.54d}$$
$$G'Q_G = 0 \tag{5.54e}$$

Similarly, the matrices P_H and Q_H have the same properties.

If we substitute the least square estimates of M, B, and C into Equation (5.50), the following decomposition can be obtained:

$$X = P_GXP_H' + Q_GXP_H' + P_GXQ_H' + Q_GXQ_H' \tag{5.55}$$

Because the column spaces of the four terms are mutually orthogonal, the trace of the original data matrix can be uniquely decomposed into the sum of the traces of the four individual components.

Prior Knowledge in Terms of Columns

The G matrix is known in this case. If $H = \mathrm{I}$, then $P_H = \mathrm{I}$ and $Q_H = 0$. Therefore, we have:

$$X = P_G X + Q_G X \tag{5.56}$$

In order to show the incorporation of column information into PCA modeling, an illustrating example is designed using the following Matlab code:

```
x1=randn(2000,1);
x2= randn(2000,1);
u1=x1;
u2=20*x1+2*x2;
ndata=length(u1);
y1=5*u1+2*u2;
y2=4*u1+3*u2;
Data0=[u1,u2,y1,y2];
[ndata,m]=size(Data0);
Data=[];
noi=[0.1,0.1,0.1,0.1];
for idata=1:1:ndata
temp=Data0(idata,:)+noi.* Data0(idata,:).*ndn(1,4);
Data=[Data;temp];
end;
```

The minimum detectable fault magnitudes are 0.519547, 10.392210, 23.356498, and 33.239751, for u1, u2, y1, and y2, respectively, based on the developed PCA model.

If it is known that most of the variation of the collected data set arises from the variation of x1, we can choose G consisting of a column vector of u1. Based on the algorithm defined in Equation (5.56), the original data matrix can be decomposed into

two components. The first component explains the variation caused by x1 and the second components explains the remaining variation.

After the decomposition, the mean value of the first component is -0.0313, -0.6212, -1.3976, and -1.9876, and the standard deviation is 0.9828, 19.5311, 43.9392, and 62.4907, for u1, u2, y1, and y2, respectively. On the other hand, the mean value of the second component is -0.0056, 0.0012, -0.0118, and -0.6212, and the standard deviation is 2.8624, 6.0906, and 8.8678, for u2, y1, and y2, respectively. It is clear that the first component has contributed to significant portion of the total variation for u2, y1, and y2.

Figure 5.6 shows a comparison of fault detection between traditional PCA and CPCA using column information for a sensor fault of u2 with a bias of 0.75 injected at the 1200th sample. The upper subplot shows the results for CPCA and the lower subplot shows the results for traditional PCA. It is clear that the fault of the given fault magnitude can be detected using CPCA while it cannot be detected using traditional PCA.

Figure 5.7 shows the FDI results of a sensor fault of y1 with a bias of 1.5 injected at the 1200th sample based on the constrained PCA using column information. The upper subplot shows that the fault can be detected immediately and the lower subplot shows that the prediction error can still be used for correct fault isolation.

Prior Knowledge in Terms of Rows

The column constraint matrix H is known in this case. If $G = \mathrm{I}$, then $P_G = \mathrm{I}$ and $Q_G = 0$. Therefore, we have:

$$X = XP_H + XQ_H \tag{5.57}$$

For the same example as used when prior knowledge is known in terms of columns, if the constraint equation is known for the signal y2, the constraint equation can be embedded into the developed constrained PCA model with the matrix H given as $H = \begin{bmatrix} 4 & 3 & 0 & -1 \end{bmatrix}$

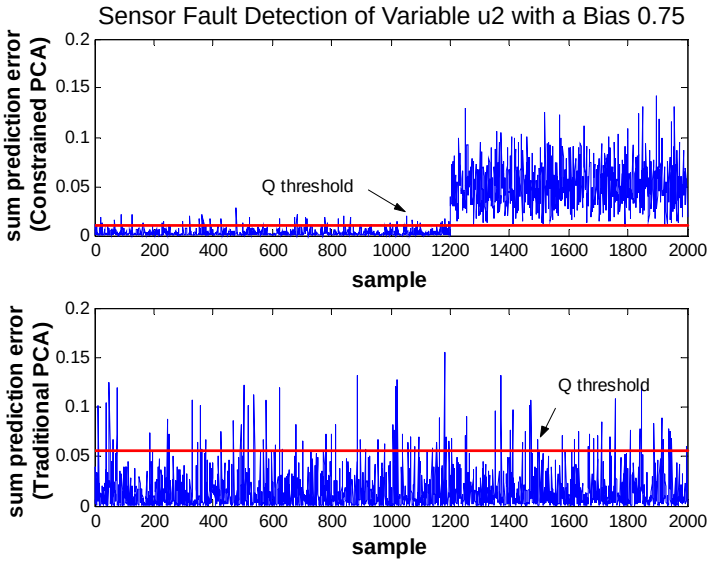

Figure 5.6. Comparison of fault detection between traditional PCA and constrained PCA using column information.

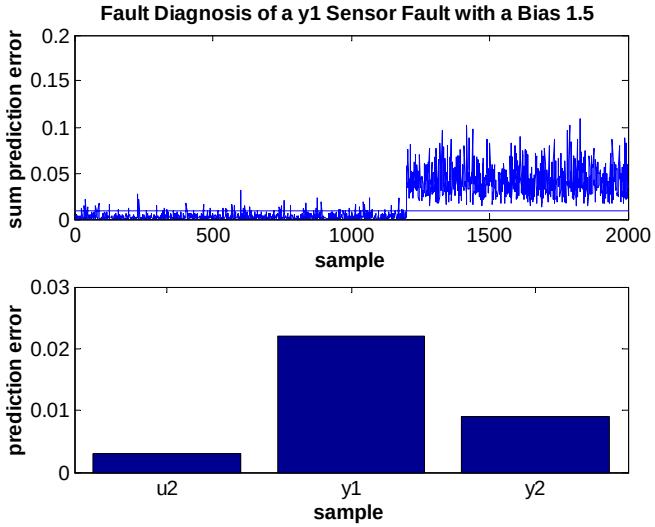

Figure 5.7. Fault detection and isolation of y1 sensor fault based on constrained PCA using column information.

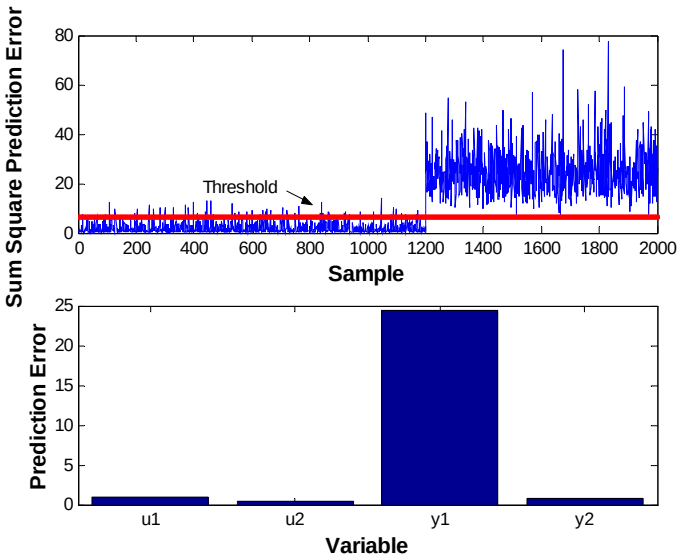

Figure 5.8. Fault diagnosis of y2 sensor fault with a bias of 1.5 based on constrained PCA using row information.

Let's define $G = XH'$, the data matrix can then be decomposed into two components. The first component explains the variation defined by the constrained equation given by H and the second component explains the remaining variation. If the second component is examined, we can find that most of the variation contained in the original data has been removed by the first decomposed component. Therefore, we can expect that a fault of smaller magnitude can be detected by performing a standard PCA on the second decomposed component.

Figure 5.8 shows a comparison of the fault diagnosis with constrained PCA using row information for y1 sensor fault with a bias of 1.5. The upper subplot shows that the fault can be successfully detected. If we recall that the minimum detectable fault magnitudes are 0.519547, 10.392210, 23.356498, and 33.239751, for u1, u2, y1, and y2, respectively, for traditional PCA approach, the detectable fault magnitude based on the constrained PCA approach is indeed much smaller. The lower subplot shows the prediction error based on the PCA analysis on the second decomposed component. It is clear that the sensor fault can be correctly identified.

5.4.3 Application to the HCSG System

The hybrid PCA model based fault diagnosis algorithm is applied to the same data set generated for HCSG system and compared with the results presented in section 5.3.

According to a simple analysis, most of the variation contained in the operation data is caused by the variation of the feed water flow rate. Therefore, a constrained PCA model can be developed with the G matrix defined by the column of feed water flow rate.

A standard PCA is performed for the second component of the decomposed data matrix. Figure 5.9 plots the original data and the first decomposed component for T3 and T6 as a function of W7. As we can see, the decomposed first component is indeed able to explain the variation caused by the feed water flow rate. Figure 5.10 shows the results of fault diagnosis of a T5 sensor fault with 0.25% bias based on the constrained PCA algorithm using the prior information that feed water flow rate is predominant on the variation of the collected data. Compared with the minimum detectable fault magnitude given in Table 5.3, the sensitivity of the fault detection has improved significantly through incorporating prior knowledge into the constrained PCA algorithm.

By imposing a constraint on the feed water flow rate and the steam flow rate, a constrained PCA was performed with the following constraints:

$$H = \begin{bmatrix} 0 & 0 & 0 & 1 & -1 & 0 & 0 & 0 \end{bmatrix}$$

A standard PCA is performed over the second component of the decomposed data matrix. Figure 5.11 plots the original data and the first decomposed component for W12 as a function of W7. As we can see, the decomposed first component satisfied the specified constraint equation that the steam flow rate is equal to the feed water flow rate. Figure 5.12 shows the results of fault diagnosis of a T3 sensor fault with 0.25% bias based on CPCA using the constraints W7=W12. Compared with the minimum detectable fault magnitude given in Table 5.3, the sensitivity of the fault detection can also be improved significantly through incorporating prior knowledge into the constrained PCA algorithm.

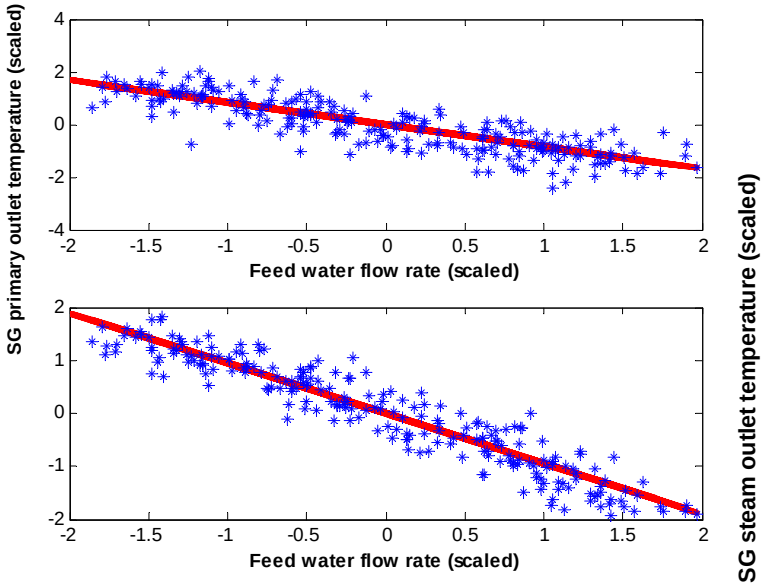

Figure 5.9. Component decomposition of constrained PCA analysis using column information.

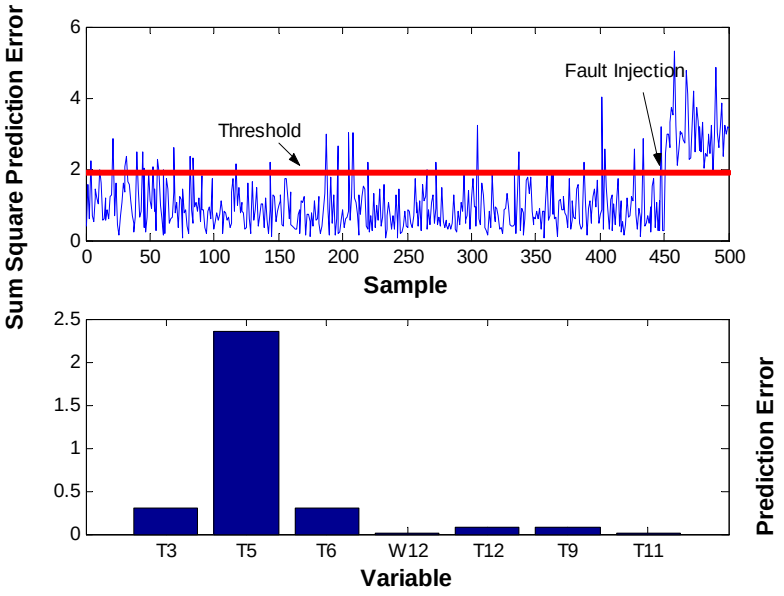

Figure 5.10. Fault diagnosis of a T5 sensor fault with 0.25% bias based on constrained PCA using column information.

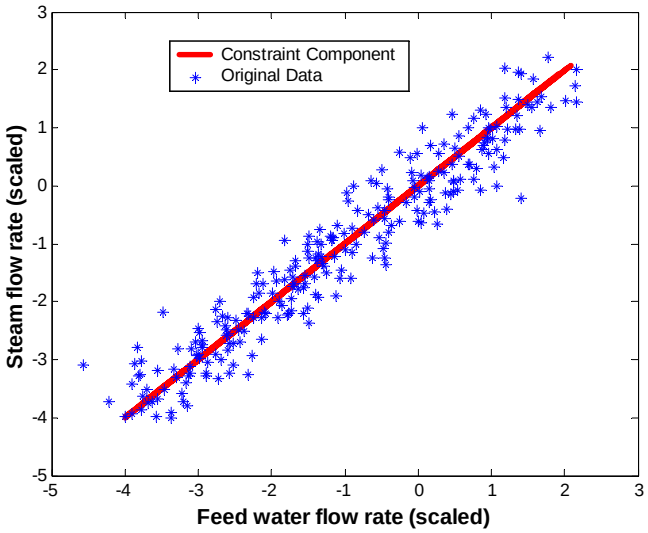

Figure 5.11. Component decomposition of constrained PCA analysis using row information.

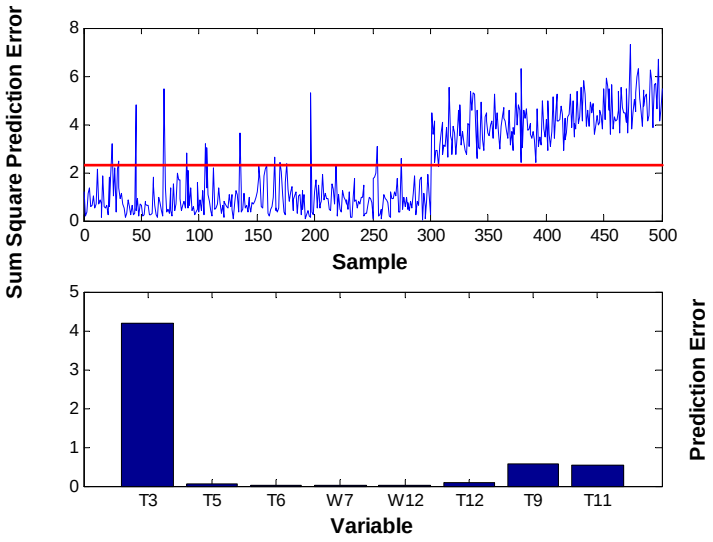

Figure 5.12. Fault diagnosis of a T3 sensor fault with 0.25% bias using constrained PCA with the constraint W7=W12.

5.5 Robust PCA Model Based Approach to Fault Diagnosis

Robust PCA model based approach to steady state fault diagnosis is developed in this dissertation. In this approach, a PCA model is built using data generated from a simulation model. After the uncertainty of the developed PCA model is identified, robust residual generators are then designed such that the model mismatch can be decoupled. In this section, the algorithm of robust PCA model based steady state fault diagnosis is derived first and then applied to a pair of IRIS helical coil steam generators. The robust PCA model based fault diagnosis approach can relax the stringent requirements of data collection for traditional historical data based fault diagnosis methods and will increase the potential of using model based approach to fault diagnosis to solve engineering problems. The developed algorithm can be applied to any subsystems in nuclear power plants.

5.5.1 Identification of Model Uncertainty

The developed PCA model from simulation data always has a certain degree of uncertainty when used to describe the relationships among measured variables in a real process. The model uncertainty can be ascribed to the simplification used in the simulation model, the parameter uncertainty for simulation, and the model reduction error. For a complex system such as a nuclear power plant, it might be too difficult to know the characteristics of model uncertainty due to incomplete understanding about the physical system. For this reason, the model uncertainty needs to be estimated from plant measurements.

If model uncertainty is considered as an additive unknown disturbance term, the system model can be described as follows (Chen and Patton, 1999):

$$y = y^* + E_d d + \varepsilon \tag{5.58}$$

where

y = the plant measured values.

y^* = the estimated value from the developed PCA model.

ε = the measurement noise.

d = the magnitude of model uncertainty vector.

E_d = the distribution matrix of model uncertainty.

The estimated value from the PCA model, y^*, can be calculated as follows:

$$y^* = P_M t_M \tag{5.59}$$

where P_M is the loading matrix of the developed PCA model and t_M is the corresponding score matrix.

The uncertainty distribution matrix E_d can be estimated by studying the structured properties of the difference between the measured values and the predicted values. Given that the plant measurement data matrix is Y, the difference between the plant measurements and the model predictions, Ω_1, is as follows:

$$\Omega_1 = Y - P_M P_M^T Y \tag{5.60}$$

If the columns of Ω_1 change only due to the measurement noise, it is safe to state that the uncertainty distribution matrix E_d is a vector and the magnitude of model uncertainty is a scalar function. In this case, the matrix E_d can be approximated as a simple average of the columns of Ω_1.

In general, the columns of Ω_1 have varying directions and the model uncertainty vector lives in a multi-dimensional space. To extract the dominant directions, the

singular value decomposition (SVD) procedure can be performed on Ω_1. This is given by:

$$\Omega_1 = U_1 S_1 V_1^T \tag{5.61}$$

If the diagonal matrix S_1 has n_d dominant singular values, the number of dominant directions is then n_d and the matrix Ω_1 can be approximated by:

$$\Omega_1 \approx U \Lambda V^T \tag{5.62}$$

where Λ is a diagonal matrix whose diagonal elements are the n_d most dominant singular values, U contains the corresponding n_d left singular vectors and V contains the corresponding n_d right singular vectors.

The orthonormal matrix U obtained from the SVD procedure can be directly used as the estimated uncertainty distribution matrix E_d. If the developed PCA model is able to characterize the major relationships, the column dimension of E_d should be much smaller than the number of the measurements.

5.5.2 Robust PCA Based Fault Detection

Different process faults and sensor faults have different effects on the plant measurements. For a simple sensor fault, only one measurement is affected and the fault effects can be characterized by a one-dimensional vector. However, a process fault usually affects multiple measurements. In the presence of feedback, a sensor fault may also affect multiple measurements because of fault propagation within and across control loops.

In general, in order to deal with process faults and sensor faults in a consistent manner, a multi-dimensional fault distribution matrix should be used to characterize the

fault effects on measurements (Dunia and Qin, 1998a). The measurement vector y with both model uncertainty and fault effects can be described as follows:

$$y = P_M t_M + E_d d + E_f f + \varepsilon \tag{5.63}$$

where E_f is the fault distribution matrix and f is the fault magnitude vector.

To design a residual generator for fault detection, r_0, for the system given in Equation (5.63), a linear transformation B needs to be performed on the measured variables, which is written as follows:

$$r_0 = By \tag{5.64}$$

Because the generated residuals for fault detection should be decoupled from both model uncertainty and operation states, the transformation matrix B must satisfy the following condition:

$$B\begin{bmatrix} P_M & E_d \end{bmatrix} = 0 \tag{5.65}$$

Therefore, the residual r_0 generated by the transformation matrix B given in Equation (5.65) will be dependent only on the fault magnitude, which is given as follows:

$$r_0 = BE_f f + B\varepsilon \tag{5.66}$$

If the measurement noise ε follows certain distribution with covariance matrix Ψ, the residual vector r_0 for fault free conditions will follow the same distribution with zero-valued expected value and covariance matrix Φ, which is given by:

$$\Phi = \mathrm{cov}(r_0) = B\Psi B^T \tag{5.67}$$

If the covariance matrix of measurement noise Ψ is unknown, the covariance matrix Φ can be learned directly from fault free data.

Because the components of r_0 are usually correlated, it is not convenient to define a statistical test on the generated residual for change detection. For this reason, the SVD procedure can be performed on Φ, which is given by:

$$\Phi \approx U \Lambda U^T \tag{5.68}$$

where U contains n_0 left singular vectors and Λ consists of n_0 non-zero singular values.

The SVD of the covariance matrix Φ allows us to construct a linear transformation $W_0 = U\Lambda^{-1/2}$ such that a new residual vector R_0 will become uncorrelated, which is given by:

$$R_0 = W_0^T r_0 = W_0^T B y \tag{5.69}$$

If the measurement noise ε follows normal distribution, the transformed residual vector R_0 for fault free conditions follows n_0 dimensional multivariate normal distribution with zero mean and unit variance (Romagnoli and Sanchez, 2000). Correspondingly, the 2-norm of this residual, $|| R_0 ||_2^2$, follows a χ^2 distribution with n_0 degrees of freedom. Therefore, for a specified critical value α, a threshold δ_0^2 can be determined for fault detection in terms of $|| R_0 ||_2^2$, which is given by:

$$|| R_0 ||_2^2 \leq \delta_0^2 = \chi_{n_0,\alpha}^2 \tag{5.70}$$

Based on the transformed 2-norm residual $|| R_0 ||_2^2$ and its threshold δ_0^2, a robust fault detection index ϖ_0 can be calculated for fault detection, which is given as follows:

$$\varpi_0 = \frac{\| R_0 \|_2^2}{\delta_0^2} \tag{5.71}$$

If the robust fault detection index ϖ_0 is smaller than 1.0, the system is considered as operating at normal operation conditions. Otherwise, a fault will be detected.

The robust fault detection index can ensure that no false alarms will be caused by model uncertainty if it can be characterized by the specified uncertainty distribution matrix E_d. However, in order to detect a fault, the fault direction and the fault magnitude must satisfy the following condition:

$$\| R_0 \|_2^2 = \| W_0^T (BE_f f + B\varepsilon) \|_2^2 \geq \delta_0^2 \tag{5.72}$$

It can be observed from Equation (5.72) that a fault is not detectable if the column space of the fault distribution matrix E_f lives in the null space of the matrix $W_0^T B$. A trivial case is that a fault will not be detectable if E_f lives in the joint column space of P_M and E_d because the fault effects are the same as the effects resulted from the model uncertainty and the normal operation changes.

Even if a fault is detectable, the fault magnitude must be large enough to distinguish the fault effects from measurement noise. A sufficient condition for absolute fault detectability is given by:

$$\| W_0^T BE_f f \|_2 \geq 2\delta_0 \tag{5.73}$$

If the measurement data were standardized with a standard deviation of σ_m, this sufficient condition can be further simplified as follows:

$$\| f \|_2 \geq 2\delta_0 (\sigma_{\min}(W_0^T BE_f))^{-1} \tag{5.74}$$

where $\sigma_{\min}$ denotes the minimum singular value.

5.5.3 Robust PCA Model Based Fault Isolation

Reconstruction PCA model based approach developed by Dunia and Qin, 1998b, is extended for robust fault isolation in this dissertation. In reconstruction PCA approach, a multi-dimensional fault is described by a subspace in which the fault effects are characterized. Fault isolation is achieved by reconstructing the fault measurements in different candidate fault subspaces until the fault effects can be fully explained. For a given set of candidate faults, if the reconstruction error can be brought back to the normal region for one candidate fault, a decision can then be made that this candidate fault is the true fault of the system. Because this method is assumption based, the fault isolation result is more conclusive than contribution-based approach and classification based approach (Russell, Chiang, and Braatz, 2000). In this dissertation, the fault reconstruction algorithm will be extended to when there is model uncertainty.

For a system with the true fault characterized by the fault distribution matrix E_i, the fault measurement y can be described as follows:

$$y = y^* + E_d d + E_i f + \varepsilon \tag{5.75}$$

Considering a candidate fault E_j, the reconstructed value of the measurement vector, y_j, in the fault subspace E_j is given by:

$$y_j = y - E_j f_j \tag{5.76}$$

Because y_j is the expected value after the fault effects are eliminated, the best estimate of the fault magnitude vector f_j can be determined by minimizing the distance between y_j and the joint column space of P_M and E_d (Qin, 2003). The minimization problem is mathematically written as follows:

$$\min_{f_j} \| By_j \|_2^2 = \min_{f_j} \| By - BE_j f_j \|_2^2 \tag{5.77}$$

If the matrix BE_j has full column rank of n_e, the SVD on the matrix BE_j will not have zero singular values, which takes the following form:

$$BE_j = E_j^0 \Lambda_j V_j^T \tag{5.78}$$

where E_j^0 and V_j are the left and right singular vectors corresponding to the n_e nonzero singular values.

After the SVD procedure is performed, the minimum 2-norm solution to Equation (5.77) is given by:

$$f_j = V_j \Lambda_j^{-1} (E_j^0)^T (By) \tag{5.79}$$

According to Equation (5.79), the fault can be completely reconstructed along all the n_e directions if the matrix BE_j has full column rank. However, if the matrix BE_j does not have full column rank, n_e, the SVD on the matrix BE_j will result in only n_p nonzero singular values, where $n_p < n_e$. In this case, the fault can still be reconstructed according to Equation (5.79), but the fault can only be partially reconstructed along n_p fault directions that correspond to the non-vanishing left singular vectors (Dunia and Qin, 1998b).

The reconstructed error of the measured vector in the candidate fault subspace E_j^0, $r_{i|j}$, can now be calculated as follows:

$$r_{i|j} = By_j = (\mathrm{I} - E_j^0 (E_j^0)^T) By = (\mathrm{I} - E_j^0 (E_j^0)^T)(B\varepsilon + BE_i^0 \tilde{f}) \tag{5.80a}$$

where

$$\tilde{f} = \Lambda_i V_i^T f \tag{5.80b}$$

If the fault measurement is reconstructed in the true fault subspace, the substitution of $j = i$ into Equation (5.80a) shows that the reconstructed error $r_{i|j}$ will be independent of fault magnitude vector f. Therefore, the reconstructed error $r_{i|j}$ will be reduced to within the normal region when there is no fault, which is given by:

$$r_{i|i} = (\mathrm{I} - E_i^0 (E_i^0)^T) B\varepsilon \tag{5.81}$$

In order to define a convenient statistics, similar to robust fault detection, a linear transformation W_i can be performed on the reconstruction error $r_{i|j}$ to generate the transformed residual $R_{i|j}$, which is given by:

$$R_{i|j} = W_i^T (\mathrm{I} - E_j^0 (E_j^0)^T) By \tag{5.82}$$

The transformed residual $R_{i|i}$ when the fault measurement is reconstructed in the fault subspace E_i can be computed as follows:

$$R_{i|i} = W_i^T (\mathrm{I} - E_i^0 (E_i^0)^T) B\varepsilon \tag{5.83}$$

Given that n_i singular values are retained to calculate the transformation W_i, the transformed residual vector $R_{i|i}$ follows a multi-dimensional normal distribution with zero mean and unit variance if the measurement noise has normal distribution. Correspondingly, the norm of the transformed residual $\| R_{i|i} \|_2^2$ will follow a $\chi^2_{ni,\alpha}$ distribution with n_i degrees of freedom. Therefore, a threshold of $\| R_{i|i} \|_2^2$ can be derived to determine whether the fault measurement is reconstructed in the true fault subspace E_i, which is given as follows:

$$|| R_{i|i} ||_2^2 \leq \delta_i^2 = \chi_{ni,\alpha}^2 \tag{5.84}$$

A robust fault isolation index can also be derived for fault isolation, which is given as follows:

$$\varpi_i = \frac{|| R_{i|j} ||_2^2}{\chi_{ni,\alpha}^2} \tag{5.85}$$

If the fault isolation index ϖ_i is less than 1.0, the fault measurement can then be fully reconstructed in the assumed fault subspace. Otherwise, the assumed fault E_j is not the true fault E_i that has occurred in the system. Based on this logic, the fault isolation can be successfully achieved if the set of candidate faults is complete. Once a fault is isolated, the fault magnitude vector can be estimated using Equation (5.79).

However, in order to avoid that a fault E_j would not be isolated as a fault E_i, the following condition must be satisfied:

$$|| R_{i|j} ||_2^2 = || W_i^T (\mathrm{I} - E_j^0 (E_j^0)^T)(B\varepsilon + BE_i^0 \tilde{f}) ||_2^2 > \delta_i^2 \text{ for all } j \neq i \tag{5.86}$$

Because the matrix $\mathrm{I} - E_j^0 (E_j^0)^T$ has eigenvalues of either zero or one, the following inequality holds (Dunia and Qin, 1997):

$$|| W_i^T (\mathrm{I} - E_j^0 (E_j^0)^T) B\varepsilon || \leq || W_i^T B\varepsilon || \tag{5.87}$$

For the same reason, if we denote the statistical threshold of $|| W_i^T B\varepsilon ||$ as δ_{i0}, we have $\delta_{i0} \geq \delta_i$. Therefore, one sufficient condition to avoid a fault E_i from being identified as fault E_j can be given as follows:

$$\| W_i^T (\mathrm{I} - E_j^0 (E_j^0)^T) B E_i^0 \tilde{f} \| > 2\delta_{i0} \text{ for all } j \neq i \tag{5.88}$$

This sufficient condition can be further simplified as follows:

$$\| \tilde{f} \| > 2\delta_{i0} \{\sigma_{\min}[W_i^T [\mathrm{I} - (E_j^0)(E_j^0)^T](BE_i^0)]\}^{-1} \tag{5.89}$$

5.5.4 Identification of Fault Distribution Matrix

The robust fault detection and isolation algorithm presented here involves the determination of fault distribution matrix E_f. For a simple fault such as sensor faults affecting only one variable that is not used for control, the fault distribution matrix E_f is nothing but the corresponding column vector of the identity matrix. However, for a complex fault, the fault distribution matrix E_f must be identified either from simulation data or from plant measurements.

If fault data is generated from simulation, the fault distribution matrix E_f can be identified directly from simulation data using the same methods as used to identify the model uncertainty distribution matrix E_d.

If fault data is obtained from plant measurements, the fault distribution matrix E_f cannot be identified directly by performing SVD on the difference between the fault data and the predicted data because the fault data has included the effects of model uncertainty. Fortunately, as can be seen from Equation (5.82), it is not necessary to know E_f if the matrix E_f^0 can be determined as far as fault isolation is concerned.

If we combine Equation (5.65) and Equation (5.75), the fault measurements that contain model uncertainty satisfy the following equation:

$$By = B\varepsilon + BE_f f \tag{5.90}$$

Given that the matrix Y is constructed by N observations of fault measurements, where N is much larger than the number of measurements, and if the noise effects are ignorable, Equation (5.90) can be written in matrix form as follows:

$$Z = BY = BE_f F = E_f^0 \widetilde{F} \tag{5.91}$$

where

$$F = \begin{bmatrix} f(1) & f(2) & \dots & f(N) \end{bmatrix}$$

$$\widetilde{F} = \begin{bmatrix} \widetilde{f}(1) & \widetilde{f}(2) & \dots & \widetilde{f}(N) \end{bmatrix}$$

Because the column rank of E_f and the row rank of F are assumed equal, the matrix $\widetilde{F}$ should have a row rank that is equal to the column rank of E_f^0. Therefore, the column space of E_f^0 can be extracted by performing the SVD procedure on the matrix Z, which is given as follows:

$$Z = U_1 S_1 V_1^T \tag{5.92}$$

where the matrix S_1 is diagonal with only non-zero singular values retained, U_1 is the corresponding left singular matrix, and V_1 is the corresponding right singular matrix.

If the noise effects are considered, the insignificant singular values should be discarded in Equation (5.92) although they are not exactly zeros.

Because the fault distribution matrix E_f^0 and the matrix U_1 contain the basis vectors of the same column space, E_f^0 and U_1 are equivalent within a similarity transformation. This implies that we can simply choose E_f^0 to be U_1, which will not affect the results of fault isolation based on Equation (5.82).

5.5.5 Application to the HCSG System

In order to have a realistic simulation with most measurements correlated with each other, one pair of steam generators is analyzed here. It is presumed that the available measurements include: (1) T3: the primary side outlet temperature of SG-A; (2) T5: the primary side outlet temperature of SG-B; (3) T6: the primary side outlet temperature of SG-A and SG-B; (4) W7: the feed water flow rate into the secondary side of SG-A and SG-B; (5) W12: the steam flow rate leaving the secondary side of SG-A and SG-B; (6) T9: the steam temperature leaving the secondary side of SG-A; and (7) T11: the steam temperature leaving the secondary side of SG-B.

Both sensor faults and process faults were considered in the HCSG fault diagnosis. The seven considered sensor faults were of the bias type. Because the generated residuals in the developed robust fault diagnosis algorithm were dependent only on fault magnitude, the same algorithm can be used to detect a fault of sensor drift. The secondary side tube blockage is a process fault considered for the HCSG system. When this process fault occurs, the flow rate into the secondary side of each steam generator will be different. However, because the secondary fluid flows inside the helical coil tubes, it is unrealistic to directly measure the flow rate into each steam generator and the fault effects cannot be directly observed based on the flow rates. For this reason, the fault needs to be monitored from the other measured variables such as the primary outlet temperature and the steam outlet temperature.

The fault distribution matrix is identified from the simulation data for the tube blockage fault in the system. The fault data is generated by linearly increasing the feed water flow rate into SG-A from 100% nominal value to 110% nominal value while reducing the feed water flow rate into SG-B from 100% nominal value to 90% nominal value. The SVD procedure is performed on the difference between the simulated fault data and the PCA model prediction to extract the fault distribution matrix. One left singular vector is retained to characterize the fault direction, which is shown in Figure 5.13. As can be seen, T3 and T11 have negative components while T5 and T9 have positive components. The extracted fault direction has clear physical explanation.

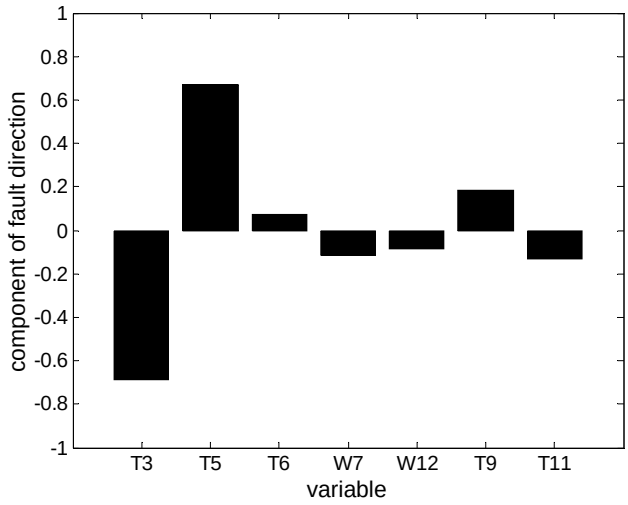

Figure 5.13. Fault direction of tube blockage fault.

The thermal degradations of SG-A and SG-B are considered to simulate model uncertainty. During nuclear power plant operations, the gradual thermal degradation of steam generators is inevitable. Any engineering applicable fault diagnosis algorithm must be able to distinguish such inevitable disturbances from sensor and process faults. In this demonstration study, the steam generator degradation was simulated by reducing the effective heat transfer coefficient from the primary side to the secondary side such that the steam temperature will decrease by 5 ^{o}C during 1000 samples at 100% nominal value of the feed water flow rate. After the data were generated, the temperature data were mixed with white Gaussian noise with three standard deviations of 0.25% nominal value and the flow rate data were mixed with white Gaussian noise with three standard deviations of 1% nominal value. Figure 5.14 shows the direction of the model uncertainty when the thermal degradation was considered as a disturbance. As can be seen, the model uncertainty is characterized by the increase of primary outlet temperature T3, T5, and T6, and the decrease of steam outlet temperature T9 and T11, which is in agreement with the physical effects of steam generator thermal degradation.

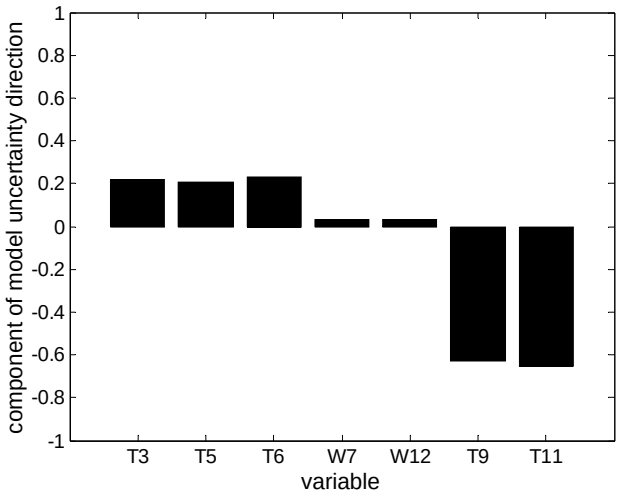

Figure 5.14. Direction of model uncertainty due to thermal degradation.

In order to test the developed robust PCA model based fault diagnosis algorithm, the tube blockage fault data and the thermal degradation data to simulate model uncertainty were generated at 90% nominal value of the feed water flow rate. Figure 5.15 shows a comparison of the fault detection with and without model uncertainty decoupling. The upper subplot shows the calculated fault detection index without model uncertainty decoupling as the thermal degradation progresses and the lower subplot shows the calculated results with model uncertainty decoupling. If the model uncertainty is not decoupled, the fault detection index will be greater than the detection limit, 1.0, as the severity of thermal degradation increases. This means that the model uncertainty due to HCSG thermal degradation will cause false alarms. However, if the model uncertainty is decoupled, the robust fault detection index is consistently smaller than the detection limit, 1.0, even if the thermal degradation becomes significant. It is also interesting to notice that the robust fault detection algorithm is robust to the changes in operation conditions. Although the model uncertainty distribution matrix is identified at 100% nominal value of the feed water flow rate, the robust fault detection algorithm will still not cause false alarms when the tube blockage occurs at 90% nominal value of the feed water flow rate.

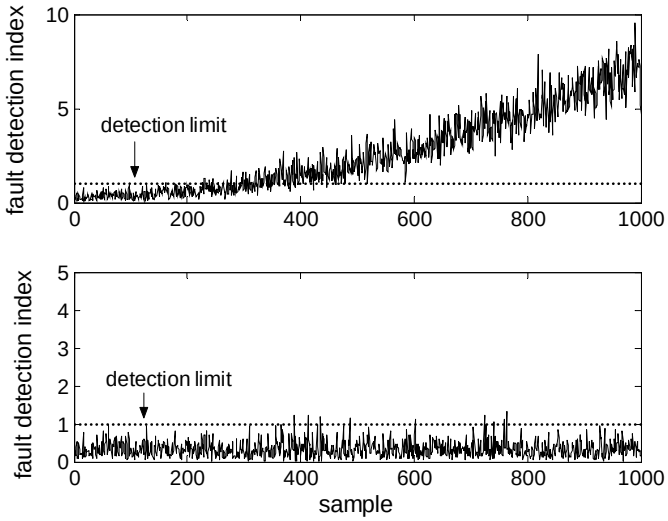

Figure 5.15. Comparison of robust detection algorithm with traditional method.

Figure 5.16 shows the fault isolation index for HCSG tube blockage fault after the fault effects are reconstructed in the eight candidate fault subspaces corresponding to seven sensor faults and one process fault. In the Figure, the tube blockage process fault is injected after the 200th sample. It can be seen that the fault isolation index can be reduced to be less than 1.0 only if the fault reconstruction is performed in the subspace of the tube blockage fault. Therefore, this fault can be correctly isolated as a tube blockage fault.

Figure 5.17 shows the results of fault estimation for a T3 sensor fault with a bias of 1.7 ^{o}C when the fault is injected after the 200th sample. Before the fault is injected, the HCSG system is operating at 90% nominal value of the feed water flow rate, so the initial temperature of T3 is 295.5 ^{o}C instead of 292.0 ^{o}C at 100% full opera operation condition. The HCSG has the thermal degradation progressing for the plotted 1000 samples to simulate model uncertainty. It can be seen that the fault estimation algorithm described in section 5.5.3 is still able to reconstruct the injected sensor faults successfully although there is model uncertainty. In addition, it can be observed that the variance of the measured value can also be reduced through the fault reconstruction algorithm before the fault is injected.

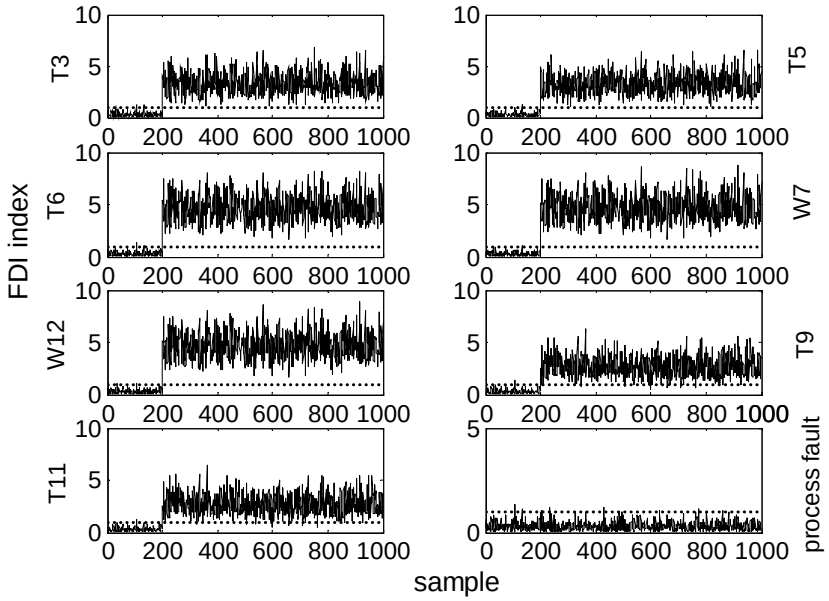

Figure 5.16. Isolation of HCSG tube blockage process fault

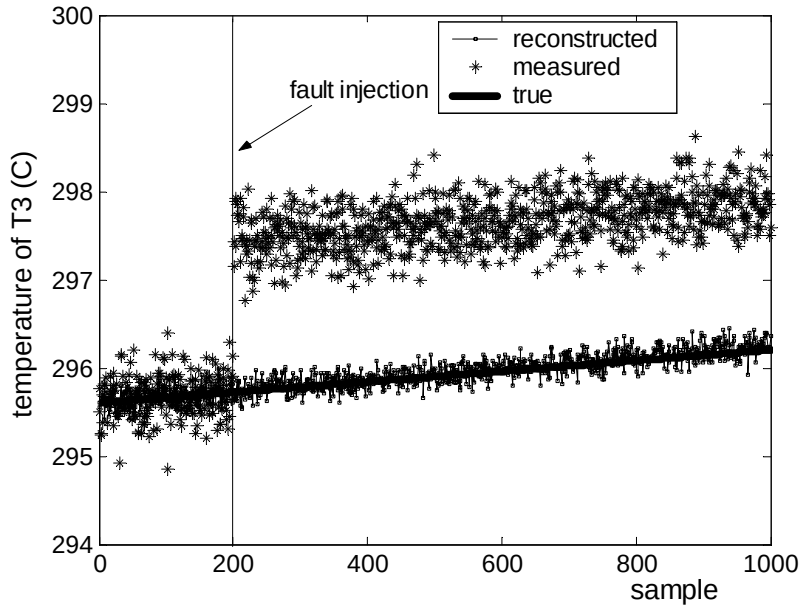

Figure 5.17. Fault reconstruction of a T3 sensor bias fault with a magnitude of 1.7 C.

An integrated framework of robust PCA model based fault diagnosis is developed developed in this section. The identification of model uncertainty is achieved by performing SVD on the difference between plant measurements and model prediction. Robust fault detection algorithm calculates a fault detection index that is larger than 1.0 only if a fault occurs even if the PCA model has model uncertainty. Robust fault isolation is based on determining a fault isolation index that measures how well the fault measurements can be reconstructed when reconstructed in different candidate fault subspaces. Because the fault isolation algorithm is assumption based, a candidate fault is confirmed to be the true fault only if the fault effects can be fully explained by the fault assumption. The developed robust fault isolation algorithm is unique in that the fault reconstruction will not be affected by model uncertainty. In addition, two situations are separated for identifying the fault distribution matrix. It is pointed out that it is not possible to identify the fault distribution matrix directly from fault measurements if there is model uncertainty. However, it is realistic and sufficient to identify the components of the fault distribution matrix living in the null space of model uncertainty for the developed FDI method.

The developed robust PCA model based fault diagnosis algorithm has been demonstrated through the application to the IRIS HCSG system. The steam generator thermal degradation is considered as model uncertainty. Both sensor faults of the involved seven variables and the process fault of tube blockage can be correctly detected and isolated based on the calculated fault detection index and fault isolation index when model uncertainty is considered. The FDI results also demonstrate that the developed methods are robust to operation changes and model uncertainty.

5.6 Summary

Fault diagnosis techniques during steady state conditions are studied in this chapter. Reconstruction based PCA was proposed as a baseline approach for steady state fault diagnosis of nuclear power systems. This approach is appropriate when significant amount of historical data is available to cover the entire space of anticipated operation

conditions. Because reconstruction model based PCA is an assumption-based approach, it can provide more conclusive results of fault isolation than other approaches. Hybrid PCA approach was developed to incorporate prior knowledge into PCA modeling for steady state fault diagnosis. In some cases, it can detect small faults after large variations are removed from raw data. Robust data driven model based approach was derived for steady state fault diagnosis. In this approach, data driven models are developed from simulation data and model uncertainties are identified from plant measurements and explicitly represented in the robust fault diagnosis algorithm. This approach is able to avoid false alarms caused by the model uncertainty when physical model based methods are used or caused by inadequate amount of data when historical data based methods are used.

Chapter 6

Fault Diagnosis during Transient Conditions

6.1 Introduction

Dynamic model based fault diagnosis is expected to have better robustness than steady state fault diagnosis. For Generation-IV nuclear power plants with load following capability, it becomes mandatory to utilize dynamic models for fault diagnosis. Besides, for the purpose of fault tolerant control, reliable and immediate diagnostic information during dynamic conditions can only be provided by dynamic model based fault diagnosis. As will be explained later, dynamic model-based fault diagnosis also utilizes temporal redundancy in addition to spatial redundancy and thus requires fewer sensors for fault isolation than steady state fault diagnosis.

Traditional approach to robust dynamic fault diagnosis consists of three steps. The first step is to develop a dynamic model from experimental data or system physics. The second step is to identify model uncertainty from real time plant measured data. The last step is to apply robust parity space theory to design dynamic residual generators that are robust to model uncertainty for fault detection and isolation.

Robust data driven dynamic fault diagnosis approach is proposed in this dissertation. In this approach, a low order state-space model was developed using subspace identification method from simulation tools used in nuclear system design. A new robust dynamic residual generator design algorithm was developed to combine the identification of model uncertainty with robust residual generation into one step. The robust residual generator design was implemented by solving a generalized eigenvalue problem.

The theory of subspace identification is presented first in this chapter. The one-step robust dynamic residual generator design algorithm is then described. Finally, the

developed algorithm is demonstrated through the application to IRIS HCSG system for dynamic fault diagnosis.

6.2 Theory of Subspace Identification

Subspace identification is the most important contribution in the field of system identification in the 1990s. The initial concepts and ideas of subspace identification were originated by De Moor, 1988, and the theory and implementation became mature in 1995 (Van Overschee and De Moor, 1995).

Subspace identification combines the theory in linear system, statistics, optimization, and numerical linear algebra for dynamic system identification. Subspace identification *extracts model information from the column space of certain matrices obtained from input-output data and Kalman state information from the row space of these matrices without knowing the system matrices* (Van Overschee and De Moor, 1995). The major advantage of subspace identification is that no explicit model parameterization is needed and only numerical linear algebra such as singular value decomposition and QR decomposition is needed for implementation. Therefore, subspace identification can provide a numerically stable algorithm to develop dynamic models from input-output data.

A linear state space model structure is assumed in subspace identification. Although many industrial processes have nonlinearity, this nonlinearity can be handled either by recursive updating of a linear model or by using model uncertainty decoupling techniques for robust control and fault diagnosis design. Most importantly, linear state space model is the only class of systems tractable with rigorous theory. The mathematical representation of a linear state space model is as follows:

$$\begin{aligned} x_{k+1} &= Ax_k + Bu_k + w_k \\ y_k &= Cx_k + Du_k + v_k \end{aligned} \tag{6.1}$$

where u_k is the input vector, y_k is the output vector, x_k is the state vector, and w_k and v_k are zero mean white Gaussian noise vectors with the following constant covariance structure:

$$E[\begin{bmatrix} w_i \\ v_j \end{bmatrix}(w_i^T, v_j^T))] = \begin{pmatrix} \Sigma^w & \Sigma^{wv} \\ \Sigma^{vw} & \Sigma^v \end{pmatrix}\delta_{ij} \tag{6.2}$$

On the condition that the input and output data are available, subspace identification aims at determining (Van Overschee and De Moor, 1995):

(1) The order of the unknown system.

(2) The system matrices A, B, C, D within a similarity transformation.

(3) The noise characteristic matrices Σ^w, Σ^v, and Σ^{vw}.

6.2.1 Block Data Equations

In subspace identification, block Hankel data matrices are used to extract the model information and the Kalman state information from data using geometric projection. A block Hankel matrix of a signal has its column vector stacked in rows and the stacked column vectors in time sequences arranged in columns. For instance, the block Hankel matrix of the input signal is constructed as follows:

$$U_k^s = \begin{pmatrix} u_k & u_{k+1} & \cdots & u_{k+N-1} \\ u_{k+1} & u_{k+2} & \cdots & u_{k+N} \\ \cdots & \cdots & \cdots & \cdots \\ u_{k+s-1} & u_{k+s} & \cdots & u_{k+s+N-1} \end{pmatrix} \tag{6.3}$$

where k denotes the discretized time instant of the first row and first column element, s denotes the number of row blocks and N denotes the number of columns used to construct the block Hankel matrix. The block Hankel matrix Y_k^s, W_k^s, V_k^s can be constructed similarly for the signal y, w, and v, respectively.

The extended observability matrix Γ_s relating the state vector to the stacked output vector is defined as follows:

$$\Gamma_s = \begin{bmatrix} C \\ CA \\ \dots \\ CA^s \end{bmatrix} \tag{6.4}$$

The Toeplitz block matrices H_s and G_s are further defined as follows:

$$H_s = \begin{bmatrix} D & 0 & \dots & 0 \\ CB & D & \dots & 0 \\ \dots & \dots & \dots & \dots \\ CA^{s-1}B & CA^{s-2}B & \dots & D \end{bmatrix} \tag{6.5}$$

$$G_s = \begin{bmatrix} 0 & 0 & \dots & 0 \\ C & 0 & \dots & 0 \\ \dots & \dots & \dots & \dots \\ CA^{s-1} & CA^{s-2} & \dots & 0 \end{bmatrix} \tag{6.6}$$

The concept of Kalman state sequences in system dynamics is emphasized in subspace identification. The key of subspace identification is to identify the Kalman state sequences directly from the input-output data without knowing the system matrices. A Kalman state sequence involved in block data equation is defined as follows:

$$X_k = \begin{bmatrix} x_k & x_{k+1} & \cdots & x_{k+N-1} \end{bmatrix} \tag{6.7}$$

Based on the above matrices, the block data equation can be obtained as follows:

$$Y_k^s = \Gamma_s X_0 + H_s U_k^s + G_s W_k^s + V_k^s \tag{6.8}$$

In order to identify the Kalman state sequences from the input-output data using geometric projection, it is also necessary to build block Hankel matrix of the input and output signals for the past block data and the future block data separately.

Given that the past block matrix and the future block matrix have the same number of row blocks $s+1$, the past block matrix and the future block matrix of the input signal are defined as follows:

$$U_p = U_k^s \tag{6.9a}$$

$$U_f = U_{k+s+1}^s \tag{6.9b}$$

The past block matrix and the future block matrix of the output signal can be defined similarly.

6.2.2 Recovery of System Matrices from State Sequence

Subspace identification technique is deeply rooted in the fact that the Kalman state sequence can be identified from input-output data. If the state sequence has been determined from the input-output data without knowing the system matrices, the identification problem can be transformed to a least squares estimation problem with respect to the system matrices and the process and measurement noise covariance matrices.

Given that two adjacent state sequences $\hat{X}_{k+1}$ and $\hat{X}_k$ have been determined, they are related to the system matrices A, B, C, and D in the following manner (Gauss-Markov model):

$$\begin{pmatrix} \hat{X}_{k+1} \\ Y_k^s \end{pmatrix} = \begin{pmatrix} A & B \\ C & D \end{pmatrix} \begin{pmatrix} \hat{X}_k \\ U_k^s \end{pmatrix} + \begin{pmatrix} W_k \\ V_k \end{pmatrix} \tag{6.10}$$

The system matrices can then be recovered by solving a least-squares problem such that the Frobenius norm of the difference of two sides of Equation (6.10), which is

defined as the square root of the sum of the absolute squares of the matrix elements, is minimized (Van Overschee and De Moor, 1995).

Three major subspace identification algorithms N4SID (Numerical algorithms for Subspace State Space System Identification), MOESP (Multiple Output-Error State Space), and CVA (Canonical Variate Analysis) exist. These algorithms differ only in how the Kalman state sequences are extracted from input-output data and how the system matrices are recovered. Because N4SID has been implemented in the Matlab system identification toolbox, the following discussion is based on N4SID algorithm.

6.2.3 Extractability of Kalman State Sequence from Input-output Data

It will be proved that Kalman state sequence can indeed be extracted from input-output data in this section. In the next two sections, two techniques are described showing how to obtain Kalman state sequence from input-output data.

6.2.3.1 System Decomposition

For an operating system, the state variables and the system output variables are excited both by deterministic inputs and by stochastic noises. In other words, the state vector and the measurement vector can be decomposed into two components as follows:

$$\begin{aligned} x_{k+1} &= x_k^d + x_k^s \\ y_k &= y_k^d + y_k^s \end{aligned} \tag{6.11}$$

where the superscripts d and s correspond to the deterministic component and the stochastic component, respectively.

Because the involved system is linear, the system defined in Equation (6.1) is equivalent to the supposition of one deterministic system and one stochastic system. The deterministic subsystem is given by:

$$x_{k+1}^{d} = Ax_k^{d} + Bu_k^{d}$$
$$y_k^{d} = Cx_k^{d} + Du_k \tag{6.12}$$

The stochastic subsystem is given by:

$$x_{k+1}^{s} = Ax_k^{s} + w_k^{s}$$
$$y_k^{s} = Cx_k^{s} + v_k \tag{6.13}$$

To show the equivalency between the original system and the decomposed two subsystems, we can prove that for a given deterministic input $u(s)$ and stochastic input $w(s)$, the responses of the dynamic system Equation (6.1) and the dynamic system Equation (6.11) are the same. This is given in the Laplace domain as:

$$y(s) = C(s\mathrm{I} - A)^{-1}Bu(s) + Du(s) + C(s\mathrm{I} - A)^{-1}w(s) + v(s) \tag{6.14}$$

6.2.3.2 Extraction of Kalman State Vector

Kalman filter theory invented by R. Kalman in 1960 enables us to estimate the state vector sequences x_k for the dynamic system given by Equation (6.1) from the input-output data (Kalman, 1960). In subspace identification, we need to design a bank of Kalman filters to estimate a Kalman state sequence simply by working on the block Hankel matrix of past inputs and past outputs. In other words, the state estimate of Kalman state vector, $\hat{x}_{k+1}$, needs to be derived from the information up to time instant k only. Because this is the theoretical foundation of subspace identification, we have proved that this is indeed true in this dissertation following the procedure to prove the Kalman filter equation presented by Becerra, 2004.

It is obvious from Equation (6.1) that the estimated mean of the state vector $\bar{x}_k$ propagates in the following manner:

$$\begin{aligned} \bar{x}_{k+1} &= A\bar{x}_k + Bu_k \\ \bar{x}_0 &= x_0 \end{aligned} \tag{6.15}$$

where

$\bar{x}_0$ = the initial state estimate of the process.

Apparently, the estimated mean of the state vector $\bar{x}_k$ follows exactly the deterministic part of the dynamics defined in Equation (6.1). However, $\bar{x}_k$ is different from x_k^d since the initial state estimate is still a random variable.

The covariance matrix of the estimation error of the state vector P_x propagates as follows:

$$\begin{aligned} P_{x,k+1} &= E[(x_{k+1} - \bar{x}_{k+1})(x_{k+1} - \bar{x}_{k+1})^T] \\ &= AP_{x,k}A^T + \Sigma^w \end{aligned} \tag{6.16}$$

since

$$x_{k+1} = Ax_k + Bu_k + w_k$$

The estimated mean value of the output vector $\bar{y}_k$ is as follows:

$$\bar{y}_k = C\bar{x}_k + Du_k \tag{6.17}$$

The covariance matrix of the estimation error of the output vector P_y propagates as follows:

$$P_{y,k} = E[(y_k - \bar{y}_k)(y_k - \bar{y}_k)^T] = CP_{x,k}C^T + \Sigma^v \tag{6.18}$$

since

$$y_k = Cx_k + Du_k + v_k$$

The covariance matrix between the state estimate and the output is given by:

$$P_{xy,k} = E[(x_k - \bar{x}_k)(y_k - \bar{y}_k)^T] = P_{x,k}C^T \tag{6.19}$$

In subspace identification, the state estimate of Kalman state vector $\hat{x}_{k+1}$ is determined using only the information up to the time instant k. This is a one-step predictor and is different from the classical Kalman filtering setting where the full input-output information including the current information is used. In classical Kalman filtering, the information up to the time instant $k+1$ is used to estimate the state $\hat{x}_{k+1}$.

For this reason, it is assumed that the estimate of the state vector $\hat{x}_{k+1}$ is a linear function of the available system output y_k, which is given by:

$$\hat{x}_{k+1} = Ky_k + g \tag{6.20}$$

where K is a matrix and g is a vector to be determined.

The optimal state estimate can be obtained by minimizing the objective function given by:

$$J = E[(x_{k+1} - \hat{x}_{k+1})^T (x_{k+1} - \hat{x}_{k+1})] \tag{6.21}$$

The above minimization problem is equivalent to minimizing the following objective function:

$$
\begin{aligned}
J &= tr\{E[(x_{k+1} - (Ky_k + g))(x_{k+1} - (Ky_k + g))^T]\} \\
&= tr\{E[(x_{k+1} - \hat{x}(k+1|k) - (Ky_k + g - \hat{x}(k+1|k))) \\
&\qquad (x_{k+1} - \hat{x}(k+1|k) - (Ky_k + g - \hat{x}(k+1|k)))^T]\}
\end{aligned}
\tag{6.22a}
$$

If we notice $\hat{x}(k+1|k) = A\bar{x}_k + Bu_k$ and substitute $y_k = y_k - \bar{y}_k + \bar{y}_k$ into Equation (6.22a), the objective function can be further simplified as follows (Becerra, 2004):

$$
\begin{aligned}
J = tr\{E[&P(k+1|k) + K(P_{y,k} + y_k \bar{y}_k^T)K^T) + (g - \hat{x}(k+1|k)(g - \hat{x}(k+1|k))^T \\
&+ 2F\bar{y}_k (g - x(k+1|k))^T - 2FP_{yx,k}]\}
\end{aligned}
\tag{6.22b}
$$

where

$$P(k+1|k) = E[(x_{k+1} - \hat{x}(k+1|k))(x_{k+1} - \hat{x}(k+1|k)^T]\}$$

$$P_{yx,k} = E[(y_k - \bar{y}_k)(x_{k+1} - \hat{x}(k+1|k)^T]\}$$

If we recall the following two formula of matrix derivatives:

$$\frac{d}{dK}(tr[KHK^T]) = 2HK$$

and

$$\frac{d}{dg}(tr[DgH]) = D^T H^T,$$

the minimal value is reached when the following conditions are satisfied:

$$\frac{\partial J}{\partial g} = 2(g - \hat{x}(k+1|k)) + 2K\bar{y}(k) = 0 \tag{6.23a}$$

$$\frac{\partial J}{\partial K} = 2K(P_{y,k} + \bar{y}_k \bar{y}_k{}^T) - 2E[(x_{k+1} - \hat{x}(k+1|k))(y_k - \bar{y}_k))^T] + 2(g - \hat{x}(k+1|k))\bar{y}_k^T = 0 \tag{6.23b}$$

The solution is then given by:

$$g = \hat{x}(k+1|k) - K\bar{y}_k \tag{6.24a}$$

$$K = E[(x_{k+1} - \hat{x}(k+1|k))(y_k - \bar{y}_k)^T]P_{y,k}^{-1} \tag{6.24b}$$

After cumbersome algebra, the non-steady state Kalman state estimate $\hat{x}_{k+1}$ can be obtained by the following recursive formula:

$$\hat{x}_{k+1} = A\hat{x}_k + Bu_k + K_k[y_k - C\hat{x}_k - Du_k] \tag{6.25a}$$

$$K_k = E[(x_{k+1} - \hat{x}(k+1|k))(y_k - \bar{y}_k)^T]P_{y,k}^{-1} = AP_{x,k}C^T + \Sigma^w \tag{6.25b}$$

$$P_{y,k} = E[(y_k - \bar{y}_k)(y_k - \bar{y}_k)^T] = CP_{x,k}C^T + \Sigma^v \tag{6.25c}$$

The covariance of the state estimation error is given by:

$$\begin{aligned} P_{x,k+1} &= E[(x_{k+1} - \hat{x}_{k+1})(x_{k+1} - \hat{x}_{k+1})^T] \\ &= E[(Ax_k + w - A\hat{x}_k - K_k(y_k - \bar{y}_k))(Ax_k + w - A\hat{x}_k - K_k(y_k - \bar{y}_k))^T] \\ &= AP_{x,k}A^T + \Sigma^w + (AP_{x,k}C^T + \Sigma^w)(CP_{x,k}C^T + \Sigma^v)^{-1}(AP_{x,k}C^T + \Sigma^w)^T \end{aligned} \tag{6.26}$$

The results obtained here are the same as the results of the combined non-steady state Kalman filter given in Van Overschee and De Moor, 1996.

If the recursive form of Kalman state estimate given in Equation (6.25) is written explicitly, the non-steady state Kalman state estimate is as follows:

$$\hat{x}_k = \begin{pmatrix} L_1 & L_2 & L_3 \end{pmatrix} \begin{pmatrix} \hat{x}_0 \\ u_0 \\ \cdots \\ u_{k-1} \\ y_0 \\ \cdots \\ y_{k-1} \end{pmatrix} \tag{6.27}$$

where L_1, L_2, and L_3 are three linear operators acting on the initial state, the past input vectors, and the past output vectors, respectively.

Although the derivation of the Kalman state estimate is a natural extension of the classical Kalman filter, the theoretical foundation of subspace identification has been established, which ensures that the Kalman state estimate $\hat{x}_k$ can be obtained by expressing itself as a linear function of the past $k-1$ inputs and outputs as well as the initial state estimate.

6.2.3.3 Extraction of Kalman State Sequence

Based on Equation (6.27), the kth block row of the process state, which is X_k based on the notation of Equation (6.7), can be written in matrix form as follows:

$$\begin{aligned} \hat{X}_k &= \begin{pmatrix} \hat{x}_k & \hat{x}_{k+1} & \cdots & \hat{x}_{k+N-1} \end{pmatrix} \\ &= \begin{pmatrix} L_0 & L_P \end{pmatrix} \begin{pmatrix} \hat{X}_0 \\ -- \\ W_p \end{pmatrix} \end{aligned} \tag{6.28}$$

where

$\hat{X}_0$ = the estimate of the initial state sequence.

$$W_p = \begin{pmatrix} U_p \\ Y_p \end{pmatrix}$$

Equation (6.28) indicates that the Kalman state sequence can be generated by a bank of non-steady state Kalman filters working in parallel on each of the columns of the block Hankel data matrix of the past inputs and past outputs. If the estimate of the initial state vector $\hat{x}_0$ and the covariance matrix of the initial state estimate error $P_{x,0}$ are known, the estimate of the state vector $\hat{x}_k$ can be obtained by an iteration of a Kalman filter over k time steps. The Kalman state sequence $\hat{X}_k$ can be obtained by running N parallel non-steady state Kalman filters simultaneously in the same manner if the estimate of the initial state sequence $\hat{X}_0$ is known.

The last but not the least point of subspace identification is that the estimated Kalman state sequence is not unique, which depends on the choice of the initial state estimate and the covariance matrix of initial state estimation error. In other words, the recovered system matrices based on subspace identification may not be able to reproduce the true system states. However, through appropriate choice of the initial state sequence, the input-output responses of the identified system will be the same as the real system.

6.2.4 Orthogonal Projection Methods

The objective of subspace identification is to recover Kalman states from input-output data without the knowledge of system matrices. Subspace identification technique achieves Kalman state estimate by exploring the relationship among the spaces of the input, output, and state sequences through geometric projection. In orthogonal projection methods, we constrain the row space of the identified Kalman state sequence to be in the combined row space of W_P and U_f.

Starting from Equation (6.28), it can be easily proved that an estimate of the future output block matrix Y_f, denoted by Z_f, is a linear combination of the past information block matrix W_p and the future input block matrix U_f, which is given by (Van Overschee and De Moor, 1996):

$$Z_f = (L_p, L_u)\begin{pmatrix} W_p \\ U_f \end{pmatrix} \tag{6.29}$$

where

L_p = a linear operator acting on W_p.

L_u = a linear operator acting on U_f.

The prediction error of future output can be represented by the Frobenius norm given by:

$$\| Y_f - (L_p, L_u)\begin{pmatrix} W_p \\ U_f \end{pmatrix} \|_F \tag{6.30}$$

To make the prediction error minimized with the constraint that the rows of Z_f lie in the joint row space of W_P and U_f, it can be proved that the optimal solution to the minimization problem with the specified constraint is to perform an orthogonal projection of the row space of the matrix Y_f onto the joint row space of matrix W_p and U_f (Favoreel, De Moor, and Van Overschee, 1998).

The orthogonal projection of the row space of matrix A onto the row space of matrix B is computed in the following manner:

$$C = A/B = AB^T (BB^T)^{-1} B$$

Theorem 6.1: *If the deterministic input u_k is uncorrelated with the process noise w_k and the measurement noise v_k; the input u_k is persistently excited of order 2k; the number of measurements goes to infinity $N \to \infty$; and the process noise w_k and the measurement noise v_k are not identically zero, then we have (Van Overschee and De Moor, 1996):*

$$Z_k = Y_f / \begin{pmatrix} W_p \\ U_f \end{pmatrix} = \Gamma_s \hat{X}_k + H_s U_f \tag{6.31}$$

Theorem 6.1 shows one way to predict the future output based on the past inputs and outputs as well as the current inputs without the information about the system matrices. More importantly, Theorem 6.1 gives the relationship between the Kalman state estimate and the input and output in a direct manner assuming that the row space of $\hat{X}_k$ lies in the joint row space of matrix W_p and U_f.

6.2.5 Oblique Projection Methods

Although Theorem 6.1 gives the relationship between the Kalman state estimate and the optimal prediction of the future output through an orthogonal projection, it is not convenient in implementation to recover the Kalman state directly because the future input term U_f is involved. To overcome this difficulty arising from the term U_f, an oblique projection method can be used to relate the Kalman state estimate to the oblique projection matrix with the constraint that the row space of Kalman state sequence lies in the row space of matrix W_p such that the future block Hankel matrix U_f will have no effects on the obtained projection matrix.

Starting from the orthogonal projection theory, it is quite intuitive to obtain the oblique projection, which is as follows:

$$Y_f /_{U_f} W_p = \Gamma_s \tilde{X}_k$$

where $\tilde{X}_k$ is the initial Kalman filter state estimate involved in the oblique projection.

The oblique projection of the row space of matrix A along the row space of matrix B onto the row space of matrix C is computed in the following manner:

$$A/_B C = [A/B^{\perp}][C/B^{\perp})^{+}C$$

where $A/B^{\perp}$ represents the orthogonal projection of the row space of A onto the orthogonal complement of the row space of B. Obviously, $B/_B C = 0$.

Theorem 6.2: *If the deterministic input u_k is uncorrelated with the process noise w_k and the measurement noise v_k; the input u_k is persistently excited of order 2k; the number of measurements goes to infinity $N \to \infty$; and the process noise w_k and the measurement noise v_k are not identically zero*.

Let O_k be defined as the oblique projection as follows:

$$O_k = Y_f /_{U_f} W_p \tag{6.32}$$

If singular value decomposition is performed on the oblique projection matrix, then we have

$$O_k = \begin{pmatrix} U_1 & U_2 \end{pmatrix} \begin{pmatrix} S_1 & 0 \\ 0 & 0 \end{pmatrix} \begin{pmatrix} V_1^T \\ V_2^T \end{pmatrix} = U_1 S_1 V_1^T \tag{6.33}$$

The following claims can be stated (Van Overschee and De Moor, 1996):

(1) The matrix O_k is equal to the product of the extended observability matrix Γ_S and the estimated Kalman filter state sequence $\hat{X}_k$, that is:

$$O_k = \Gamma_S \hat{X}_k \tag{6.34}$$

(2) The order of the system is equal to the number of singular values of O_k that are not zero.

(3) The extended observability matrix Γ_S can be obtained as follows:

$$\Gamma_S = U_1 S_1^{1/2} T \tag{6.35}$$

where T is a similarity transformation matrix.

(4) The part of the state sequences $\hat{X}_k$ can be computed as follows:

$$\hat{X}_k = T^{-1} S_1^{1/2} V_1^T$$

(5) The state sequences $\hat{X}_k$ is related to the matrix O_k as follows:

$$\hat{X}_k = \Gamma_S^+ O_k \tag{6.36}$$

Theorem 6.2 provides an optimal solution to the linear combination of the past inputs and outputs, that is, $O_k = L_p W_p$, so that the prediction error of the future output is minimized with respect to the Frobenius norm. The row space of this optimal solution O_k is the projection of the row space of Y_f along the row space of U_f onto the row space of W_p.

For a system with l outputs and n true states, the oblique projection matrix O_k has $k \cdot l$ rows and N columns, whose rows span a subspace of $k \cdot l$ dimensional row space in the N dimensional ambient space. However, only n states are sufficient to predict the future output from the past information. Therefore, it is necessary for subspace identification to determine the true number of states from the oblique projection matrix. In mathematics, this problem can be formulated as follows (Favoreel, De Moor, and Van Overschee, 1998):

$$\min_{R \in R^{li \times q}} || O_k - R ||_F^2 \tag{6.37}$$

with the constraint that the rank of R is n.

The best solution to the minimization problem given in Equation (6.37) is as follows:

$$R \approx O_k = \Gamma_k \hat{X}_k = U_1 S_1 V_1^T \tag{6.38}$$

The columns of Γ_k spans n-dimensional space because the original system is observable and the rows of $\hat{X}_k$ are n-dimensional since the system has n states. Because the oblique projection matrix O_k is a product of $\hat{X}_k$ and Γ_k, the rank of O_k is indeed equal to n

Moreover, the column space of O_k is the same as the column space of Γ_k since each column of O_k is nothing but a linear combination of the columns of Γ_k as is shown in Equation (6.38). For the same reason, the row space of O_k is the same as the row space of $\hat{X}_k$ since each row of O_k is nothing but a linear combination of the rows of $\hat{X}_k$ as is also shown in Equation (6.38). Therefore, after a singular decomposition of O_k, there are theoretically only n nonzero singular values. However, for a real world problem where N is not infinite and there may be nonlinearity, the singular value decomposition of O_k does not produce zero singular values. In this situation, the predominant singular values are used to determine the order of system dynamics.

Because the column space of O_k is the same as the column space of Γ_k and the row space of O_k is the same as the row space of $\hat{X}_k$, Equation (6.38) can then be split into two parts as follows:

$$\begin{aligned} \Gamma_k &= U_1 S_1^{1/2} T \\ \hat{X}_k &= T^{-1} S_1^{1/2} V_1^T \end{aligned} \tag{6.39}$$

Therefore, we have the results (6.35) and (6.36), which can be used to estimate the extended observability matrix Γ_k and the Kalman state sequence $\hat{X}_k$ directly from the input and output data without the knowledge of system matrices.

At this point, Kalman state sequence has been identified from the input-output data without the knowledge of system matrices, the dynamic system identification is then transformed to a least squares estimation problem, which is described in section 6.2.2.

Example 1: An illustrating example is designed here to help understand why the extended observability matrix and the Kalman state sequence can be extracted from projection matrix based on singular value decomposition, as shown in Equation (6.39).

Given two matrices A and B and a matrix $C = AB$ as follows:

$$A = \begin{bmatrix} 1.0 & 1.0 \\ 2.0 & 7.0 \\ 1.0 & -1.0 \\ 2.0 & 2.0 \\ 3.0 & 0.0 \end{bmatrix} \quad B = \begin{bmatrix} 1.0 & 2.0 & 3.0 \\ 2.0 & 1.0 & 1.0 \end{bmatrix} \quad C = \begin{bmatrix} 3.0 & 3.0 & 2.0 \\ 16.0 & 11.0 & -1.0 \\ -1.0 & 1.0 & 4.0 \\ 6.0 & 6.0 & 4.0 \\ 3.0 & 6.0 & 9.0 \end{bmatrix}$$

The matrix A has 2-dimensional column space and the matrix B has 2-dimenisonal row space. It can be verified that the rank of C is also 2. If a singular value decomposition is performed on C, we have:

$$C = U_1 S_1 V_1^T = \begin{bmatrix} -0.1993 & -0.114 \\ -0.8275 & 0.4611 \\ -0.0277 & -0.3896 \\ -0.3986 & -0.2280 \\ -0.3405 & -0.7554 \end{bmatrix} \bullet \begin{bmatrix} 22.7163 & 0 \\ 0 & 10.7688 \end{bmatrix} \bullet \begin{bmatrix} -0.7582 & -0.6234 & -0.1448 \\ 0.3521 & -0.1448 & -0.9247 \end{bmatrix}$$

Obviously, the matrix C has two non-zero singular values. Because U_1 is orthonormal, it is always possible to find a transformation matrix $T = S_1^{-0.5} U_1^T A$ such that $A = U_1 S_1^{0.5} T$ and $B = T^{-1} S_1^{0.5} V_1^T$. The matrix T is a full rank square matrix and thus invertible because the matrix A has full column rank, the same as the rank of S_1. For the example problem, the transformation matrix T is given by:

$$T = \begin{bmatrix} -0.7764 & -1.4186 \\ -0.7019 & 0.9287 \end{bmatrix}$$

This simple example clearly shows the reasoning behind Equation (6.39). It should be emphasized that subspace identification is based on the major result of Equation (6.34) with three significant implications:

(1) The projection matrix can be obtained directly from input-output data;

(2) The column space of Γ_k has the same dimension as the number of states.

(3) The row space of $\hat{X}_k$ has the same dimension as the number of states.

In fact, subspace identification theory is established by revealing the equivalence between the column space of a projection matrix and the column space of the extended observability matrix and the equivalence between the row space of the projection matrix and the row space of the Kalman state sequence. It is because of the importance of subspace that this identification technique was given the name of subspace identification.

6.3 Robust Dynamic Fault Diagnosis Algorithm

After system dynamics is identified either from data generated by simulation calculations or from on-line experimental data using subspace identification technique, the developed model will always have certain degrees of uncertainty either because the simulation model does not truly represent the physical system or because a model reduction is implicitly performed in subspace identification.

In general, the uncertainty of a dynamic model can be represented as follows (Chen and Patton, 1999):

$$\begin{aligned} x(k+1) &= Ax(k) + Bu^*(k) + w(k) + d(k) \\ y^*(k) &= Cx(k) + Du^*(k) \end{aligned} \tag{6.40}$$

where $d(k)$ is a vector representing the deterministic model uncertainty, $w(k)$ is a vector representing stochastic process noise, $u^*(k)$ is the true input vector, and $y^*(k)$ is the true output vector.

In Equation (6.40), the model uncertainty term plays the same role on the system dynamics as the process disturbance defined in Equation (6.1) except that model uncertainty is deterministic. In fact, the model uncertainty term is an extension of process disturbance from modeling point of view, which may arise from unmeasured inputs, non-linear terms in system dynamics, terms related to time-varying dynamics, linearization and model reduction, parameter variation, and simulation model uncertainty, etc.

Given that the measured inputs and outputs are corrupted with some measurement noise v_u and v_y, respectively, and some additive sensor faults, the observed input vector $u(k)$ and the observed output vector $y(k)$ are then as follows (Li and Shah, 2002):

$$u(k) = u^*(k) + v_u(k) + E_u f_u(k) \tag{6.41a}$$
$$y(k) = y^*(k) + v_y(k) + E_y f_y(k) \tag{6.41b}$$

where $f_u(k)$ and $f_y(k)$ are the fault magnitude vectors and E_u and E_y are the fault distribution matrices for the inputs and the outputs, respectively.

The objective of robust fault detection is to generate a residual that is statistically significant **if and only if** the fault magnitude vectors are not zero, i.e., the residual $r(t)$ satisfies the following property:

$$r(t) \neq 0 \quad \text{iff} \quad f_u(t) \neq 0 \text{ or } f_y(t) \neq 0 \tag{6.42}$$

If different residual patterns are predefined to signify different faults, the task of fault isolation is then to design some residual generators such that each fault must generate the predefined residual pattern regardless of its fault magnitude. Such a formulation of fault isolation problem can avoid the use of fault information for fault

isolation, which may depend on fault magnitude and is difficult to obtain in nuclear power systems.

6.3.1 Robust Dynamic Fault Detection Algorithm

Considering a time window of length S, the dynamic redundancy relation in stacked vector form can be derived for the given system defined in Equation (6.40) as follows:

$$y_s^*(k) = \Gamma_s x(k-s) + H_s u_s^*(k) + G_s d_s(k) + G_s w_s(k) \tag{6.43}$$

where $y_s^*(k)$, $u_s^*(k)$, $w_s(k)$, and $d_s(k)$ are the stacked column vectors of $y^*(k)$, $u^*(k)$, $w(k)$, and $d(k)$ at a sequence of s time instants, respectively. The matrices H_s and G_s are Toeplitz block matrices that relate the system inputs and the model uncertainty to the system outputs, respectively.

The stacked output error vector within the given time window can be written as follows:

$$e_s(k) = y_s(k) - H_s u_s(k) = \widetilde{H}_s \widetilde{z}_s(k) \tag{6.44}$$

where

$$\widetilde{H}_s = \begin{pmatrix} \mathrm{I} & -H_s \end{pmatrix}$$

$$\widetilde{z}_s(k) = \begin{pmatrix} y_s^T(k) & u_s^T(k) \end{pmatrix}^T$$

From Equation (6.43) and Equation (6.44), the stacked output error vector can be rewritten in its physical form as follows (Li and Shah, 2002):

$$e_s(k) = \Gamma_s x(k-s) + G_s d_s(k) + G_s w_s(k) + \widetilde{H}_s \begin{pmatrix} v_{ys}(k) \\ v_{us}(k) \end{pmatrix} + \widetilde{H}_s E_z f_{sz}(k) \tag{6.45}$$

where

$$E_z = \begin{pmatrix} \mathrm{I}_{s+1} \otimes E_y & 0 \\ 0 & \mathrm{I}_{s+1} \otimes E_u \end{pmatrix}$$

and I_{s+1} is a s dimensional identity matrix, $\otimes$ represents the Kronecker product, and $f_{sz}(k)$ is the stacked fault magnitude vector combining both the output faults and the input faults.

Equation (6.44) and Equation (6.45) represent the computational form of the output error and its internal form from system physics, respectively. In order to construct a residual signal insensitive to the initial states and the model uncertainty, a linear transformation is performed on the original stacked output error vector. That is, a residual vector, $r_s(k)$, can be designed for robust fault detection through a transformation matrix V_0 with the following constraints:

$$r_s(k) = V_0(y_s(k) - H_s u_s(k)) \tag{6.46a}$$

$$V_0 \Gamma_s x(k-s) = 0 \tag{6.46b}$$

$$V_0 G_s d_s(k) = 0 \tag{6.46c}$$

Accordingly, the internal form of the residual vector takes the following simplified form:

$$r_s(k) = V_0 \tilde{H}_s \begin{pmatrix} v_{ys}(k) \\ v_{us}(k) \end{pmatrix} + V_0 G_s w_s(k) + V_0 \tilde{H}_s E_z f_{sz}(k) \tag{6.47}$$

If there is no measurement and process noise, the internal form of the residual vector defined in Equation (6.47) is only a function of the fault magnitude. Therefore, such a residual generator has the desired property for robust fault detection.

The residual vector generated from Equation (6.47) follows a multi-dimensional Gaussian distribution that is zero-mean with a covariance matrix that can be determined from the data obtained for fault free conditions. If a sensor fault occurs in the system, Equation (6.47) indicates that the fault condition residual vector will also follow a multi-

dimensional Gaussian distribution with the same covariance matrix but with a non-zero mean value. Therefore, fault detection can be achieved by detecting the change of the mean value of the generated residual vectors. In order to avoid false alarms and missing detection rates due to noise, an Exponentially Weighted Moving Average (EWMA) filter (Lowry et al., 1992) can be applied to the residual vector (Qin and Li, 2001), which is given by:

$$\bar{r}_s(k) = \gamma \cdot \bar{r}_s(k-1) + (1-\gamma) r_s(k) \tag{6.48}$$

where $\bar{r}_s(k)$ is the EWMA filtered residual vector and γ is the forgetting factor for filtering. The filtered residual vector for fault free condition also follows zero mean Gaussian distribution with the covariance matrix $\bar{R}_{s0}(k)$ given by (Del Castillo, 2002), (Qin and Li, 2001):

$$\bar{R}_{s0}(k) = \frac{1-\gamma}{1+\gamma}\left(R_{s0}(k) + 2\sum_{j=1}^{s}\gamma^j E\{r_s(k) r_s(k-j)^T\}\right) \tag{6.49a}$$

where $R_{s0}(k)$ is the covariance matrix of the unfiltered residual vector.

To simplify the computation, asymptotic covariance matrix can be used, which is given by (Rigdon, 1995):

$$\lim_{s\to\infty} \bar{R}_{s0}(k) = \frac{\gamma}{2-\gamma} R_{s0}(k) \tag{6.49b}$$

The filtered square weighted residual can be used as a fault signal for fault detection with better performance than a simple weighted residual, which is given by:

$$\bar{\beta}_s(k) = \bar{r}_s^T(k)(\bar{R}_{s0})^{-1}\bar{r}_s(k) \tag{6.50}$$

During fault free condition, the filtered square weighted residual $\bar{\beta}_s(k)$ follows a central χ^2 distribution. If $\bar{\beta}_s(k)$ does not follow a central χ^2 distribution at a specified

significance level α, the decision can then be made that a fault has occurred to the system at this significance level. That is, a fault is detected if the fault detection index $\omega_s(k)$ is greater than 1.0, which is defined as follows:

$$\varpi_s(k) = \frac{\overline{\beta}_s(k)}{\chi_\alpha^2} \tag{6.51}$$

6.3.2 One-Step Robust Dynamic Residual Generator Design

As described in section 6.3.1, the key of robust fault detection is to design a linear transformation matrix such that the generated residuals are independent of the initial states and insensitive to the model uncertainties, which is written in Equation (6.46). The traditional method of dealing with model uncertainty in robust residual generator design has two steps. The first step is to determine the model uncertainty vector using Kalman filter technique and the second step is to determine the uncertainty distribution matrix using SVD algorithm. This approach is presented in Chapter 2.

A new approach was been developed for robust dynamic residual generator design in this dissertation. Inspired by subspace identification algorithm, this approach utilizes block data matrix equation to determine the relationship between the subspace spanned by the projection matrix of measured data and the subspace spanned by the projection matrix of model uncertainty. The advantage of this approach is that robust residual generator design does not need to identify the model uncertainty vector and the distribution matrix.

Let's recall the block data matrix Y_k , U_k , P_k , W_k , $V_{u,k}$, $V_{y,k}$ and Z_k defined for the output, input, model uncertainty, process disturbance, input noise, output noise, and past information, which are written as follows:

$$Y_k = \begin{bmatrix} y_s(k) & y_s(k+1) & \cdots & y_s(k+N-1) \end{bmatrix} \tag{6.52a}$$

$$U_k = \begin{bmatrix} u_s(k) & u_s(k+1) & \cdots & u_s(k+N-1) \end{bmatrix} \tag{6.52b}$$

$$P_k = \begin{bmatrix} d_s(k) & d_s(k+1) & \cdots & d_s(k+N-1) \end{bmatrix} \tag{6.52c}$$

$$W_k = \begin{bmatrix} w_s(k) & w_s(k+1) & \cdots & w_s(k+N-1) \end{bmatrix} \tag{6.52d}$$

$$V_{u,k} = \begin{bmatrix} v_{us}(k) & v_{us}(k+1) & \cdots & v_{us}(k+N-1) \end{bmatrix} \tag{6.52e}$$

$$V_{y,k} = \begin{bmatrix} v_{ys}(k) & v_{ys}(k+1) & \cdots & v_{ys}(k+N-1) \end{bmatrix} \tag{6.52f}$$

$$Z_k = \begin{pmatrix} Y_k \\ U_k \end{pmatrix} \tag{6.52g}$$

The block data matrix equation can be derived as follows:

$$Y_{k+1} = \Gamma_s X_{k+1} + H_s U_{k+1} - H_s V_{u,k+1} + G_s P_{k+1} + G_s W_{k+1} + V_{y,k+1} \tag{6.53}$$

If we postmultiply the Equation (6.53) by Z_k^T, then we have:

$$Y_{k+1} Z_k^T = \Gamma_s X_{k+1} Z_k^T + H_s U_{k+1} Z_k^T - H_s V_{u,k+1} Z_k^T + G_s P_{k+1} Z_k^T + G_s W_{k+1} Z_k^T + V_{y,k+1} Z_k^T \tag{6.54}$$

Considering that the model uncertainty is a deterministic variable, and the input measurement noise, the output noise, and the process noise are all uncorrelated white Gaussian, if the size of data is sufficiently big, then we have:

$$\Omega_{YZ} = \Gamma_s \Omega_{XZ} + H_s \Omega_{UZ} + G_s \Omega_{PZ} \tag{6.55}$$

where Ω denotes the corresponding product term in Equation (6.54).

If Equation (6.55) is then premultiplied by the complement matrix of Γ_s, denoted by $\Gamma_s^{\perp}$, then we have:

$$\Gamma_s^{\perp} (\Omega_{YZ} - H_s \Omega_{UZ}) = \Gamma_s^{\perp} G_s \Omega_{PZ} \tag{6.56}$$

The left hand side of Equation (6.67) can be determined from the measured data and the right hand side of the equation is related to the space spanned by the model uncertainty vectors. Therefore, a singular value decomposition can be performed on the

related matrix on the left hand side of the equation to determine the null space spanned by the model uncertainty vectors.

Redefine the matrix on the left hand side of Equation (6.56) as Θ, that is:

$$\Theta = \Gamma_s^{\perp}(\Omega_{YZ} - H_s\Omega_{UZ}) \tag{6.57}$$

If a singular value decomposition is performed on Θ, we have:

$$\Theta = \begin{bmatrix} U_\Theta & U_\Theta^{\perp} \end{bmatrix} \begin{bmatrix} S_\Theta & 0 \\ 0 & 0 \end{bmatrix} \begin{bmatrix} V_\Theta \\ V_\Theta^{\perp} \end{bmatrix} \tag{6.58}$$

Obviously, the obtained matrix U_Θ satisfies the following equation:

$$(U_\Theta^{\perp})^T(\Gamma_s^{\perp}G_sP_{k+1})Z_k^T = 0 \tag{6.59}$$

If there is at least one columns of Z_k^T which do not lie in the null space of $(U_\Theta^{\perp})^T(\Gamma_s^{\perp}G_sP_{k+1})$, then we have:

$$(U_\Theta^{\perp})^T(\Gamma_s^{\perp}G_sP_{k+1}) = 0 \tag{6.60}$$

If it is further assumed that the model uncertainty is piecewise constant, a linear transformation matrix V_0 satisfying the desired property of robust residual generator defined in Equation (6.46), can be chosen as follows:

$$V_0 = (U_\Theta^{\perp})^T(\Gamma_s^{\perp}) \tag{6.61}$$

Based on the above algorithm, robust residual generator can be designed without knowing the model uncertainty vector. Compared with the classical approach developed by Chen and Patton, 1999, this algorithm is much easier for implementation.

Example 2.: An illustrating example is designed here to demonstrate that the developed one-step algorithm is able to design dynamic residual generators for robust fault detection without the need to identify model uncertainty explicitly.

Considering a linear dynamic system with four inputs and four outputs, the system matrices are identified as follows:

$$A = \begin{bmatrix} 0.5 & 0.5 \\ -0.5 & 0.5 \end{bmatrix} \qquad B = \begin{bmatrix} -0.4 & 0.1 & -1.1 & 1.2 \\ 1.7 & 0.3 & 1.2 & -0.1 \end{bmatrix}$$

$$C = \begin{bmatrix} 0.3 & -0.6 \\ 0.2 & 2.2 \\ 0.2 & -0.2 \\ 0.7 & 0.2 \end{bmatrix} \qquad D = \begin{bmatrix} 0 & 0 & 0 & 0 \\ 0 & 0 & 0 & 0 \\ 0 & 0 & 0 & 0 \\ 0 & 0 & 0 & 0 \end{bmatrix}$$

The normal operation data are generated with measurement noise of 1% signal-to-noise ratio for all the four input signals and the four output signals, and process noise of 3% signal-to-noise ratio, and model uncertainty of constant direction. The distribution matrix and the magnitude vector of model uncertainty are given as follows:

$$E_d = \begin{bmatrix} 0.25 & 0.5 \\ 0.5 & 0.25 \end{bmatrix} \qquad d = \begin{bmatrix} 10.0 \\ 10.0 \end{bmatrix}$$

Because the number of state variables is 2 in this example, the block data matrix of Y_k , U_k, and Z_k can be constructed with s equal to 2 and N equal to 2000 according to Equation (6.52), where the system is excited with input signal $u = \sum_{i=1}^{10} \cos(i\pi t)$ and the initial state vector $x(0) = \begin{bmatrix} 0 & 0 \end{bmatrix}^T$.

After the extended observability matrix Γ_s is constructed from the system matrices, the dimension of the matrix is 12 by 2. If a singular value decomposition is performed on Θ defined in Equation (6.57), which has a dimension of 10 by 24, we have

the following singular values from large to small in order, 3.2281e+006, 4.5777e+003, 121.3397, 59.2458, 1.5377, 0.9983, 0.1805, 0.0910, 0.0230, and 0.0164. Because a sharp drop occurs at the second singular value, the last nine left singular vectors can be retained to design robust residual generator for fault detection. In fact, if we remove the measurement noise and process noise, the last 9 singular values of Θ would be exactly zeros.

Figure 6.1 shows a comparison between the residual norms without the model uncertainty decoupled and with the model uncertainty decoupled. The new test data of 2000 samples are generated by exciting the system with input signal $u = \sum_{i=1}^{10} \sin(i\pi t)$ with the initial state vector $x(0) = [1.0 \quad 1.0]^T$ and introducing the model uncertainty at the 1000th sample. The upper subplot shows the results when the model uncertainty is not decoupled. As can be seen, the residuals are small before the 1000th sample although the system is excited by a different input signal at a different initial state vector. However, false alarms will be produced after the 1000th sample. The lower subplot shows the results when the model uncertainty is decoupled using the developed algorithm in this section. It can be seen that the generated robust residuals will not produce false alarms after the 1000th sample when model uncertainty was introduced.

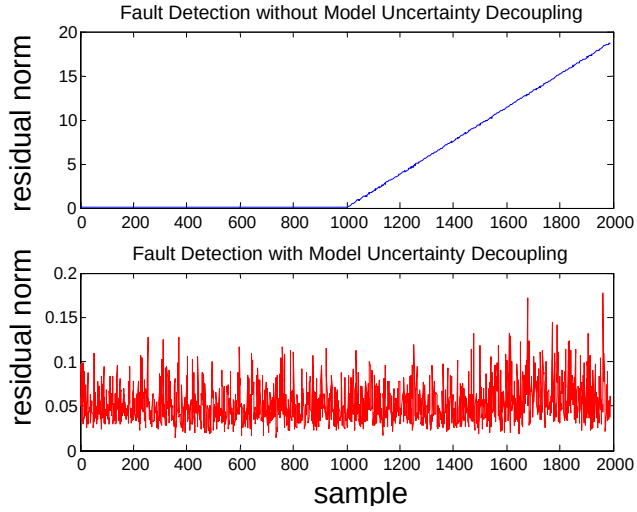

Figure 6.1. Robust fault detection for the example case during normal operation condition.

The simple example has demonstrated that the newly developed robust residual generation algorithm is able to decouple model uncertainty without the need to identify model uncertainty vector explicitly.

6.3.3 Robust Fault Isolation Algorithm

Structured residuals generated by multiple residual generators provide a simple and systematic approach to fault isolation. If residual generators are designed such that each one is only sensitive to a subset of the considered faults, a fault isolation scheme can then be achieved since each fault corresponds to a different residual pattern.

Although it is possible to design numerous residual structures for fault isolation with different isolation capability, a generalized residual set is a simple design scheme for single fault isolation (Qin and Li, 2001). In this scheme, each residual set is sensitive to all faults but one. In particular, the residual structure dedicated to the isolation of the ith fault is given as follows:

$r_i(t) = 0$ for the ith fault. (6.62a)

$r_i(t) \neq 0$ for other faults. (6.62b)

The fault direction matrix E_u and E_y are decomposed into the first part $E_{ui,1}$ and $E_{yi,1}$ corresponding to the faults to be desensitized, and the second part $E_{ui,2}$ and $E_{yi,2}$ corresponding to the faults to be sensitized, that is:

$$E_{ui} = \begin{pmatrix} E_{ui,1} & E_{ui,2} \end{pmatrix} \quad (6.63a)$$

$$E_{yi} = \begin{pmatrix} E_{yi,1} & E_{yi,2} \end{pmatrix} \quad (6.63b)$$

The primary residual vector for robust fault detection defined in Equation (6.47) can then be rewritten as follows:

$$r_s(k) = V_0 \widetilde{H}_s \begin{pmatrix} v_{ys}(k) \\ v_{us}(k) \end{pmatrix} + V_0 G_s w_s(k) + V_0 \widetilde{H}_s E_{z1} f_{sz1}(k) + V_0 \widetilde{H}_s E_{z2} f_{sz2}(k) \tag{6.64}$$

where E_{z1} and E_{z2} are constructed from $E_{ui,1}$, $E_{yi,1}$ and $E_{ui,2}$, $E_{yi,2}$, respectively, in the same manner as E_z is constructed from E_u and E_y.

The residual generator V_i dedicated to the isolation of the ith fault is designed as follows:

$$V_i \cdot V_0 \widetilde{H}_s E_{z1} = 0 \tag{6.65}$$

In order to make the residual generator given in Equation (6.65) still sensitive to the other faults, the transformation matrix V_i can be obtained by solving an optimization problem such that its row vectors v can minimize the objective function J defined as follows:

$$J = \frac{(vM_1)(vM_1)^T}{(vM_2)(vM_2)^T} \tag{6.66}$$

where

$$M_1 = V_0 \widetilde{H}_s E_{z1}$$
$$M_2 = V_0 \widetilde{H}_s E_{z2}$$

A complicated algorithm based on Cholesky decomposition and standard eigenproblem was developed to solve the above optimization problem in (Li and Shah, 2002). In this dissertation, the optimization is formulated as a generalized eigenproblem defined as follows:

$$M_1 M_1^T v^T = \lambda M_2 M_2^T v^T \tag{6.67}$$

Similarly, in order to remove the noise effects on decision-making, an EWMA filter can also be applied to each of the generated residual vectors and an FDI index is used to check its significance of change. The FDI index is defined as follows:

$$\varpi(k) = \frac{\overline{\beta}_s(k)}{\chi_\alpha^2} \tag{6.68}$$

6.4 Application to the HCSG System

The developed algorithm was applied to the sensor fault diagnosis using the dynamic model identified from the data generated by the HCSG simulation model in Chapter 3. The considered sensor faults include both the input and the output faults related to the system model.

In the HCSG system, the steam pressure is controlled and the steam pressure sensor fault will propagate within the control loop. The feed water flow rate is regulated when reactor power changes, so it is important to have a correct indication of the feed water flow rate for this power transient. The detailed results are therefore presented for these two sensor faults. To demonstrate the systematic solution to sensor FDI of the developed approach, the FDI results of all the other sensor faults are also summarized.

6.4.1 Data Generation and Subspace Identification

A linear state space model is identified for the HCSG system at full power operation condition using subspace identification technique. The data characterizing the system dynamics are generated by exciting the developed simulation model in Chapter 3 with white Gaussian noise inputs of standard deviation 1% power. The perturbed inputs include the hot leg temperature, the primary flow rate, the feed water flow rate, the feed water temperature, and the steam flow rate. The appropriate choice of the excitation inputs plays a significant role in the quality of the identified model. If too much power is included in the input signals, some nonlinear modes of the system will be excited. On the

contrary, if the included power is too small, the identified model cannot capture enough system dynamics.

Figure 6.2 shows the singular values of the oblique projection matrix for different number of state variables ranging from 1 to 50. The number of states is chosen as five since a significant breakpoint can be observed at this point. If too many state variables are chosen, the resulting model will lose the capability of generalization because some of the degrees of freedom will be used to model the system noise. If too few state variables are used, the resulting model may not be able to explain some significant dynamics of the system. In general, the number of state variables should be chosen such that no significant information can be included if it is further increased. As can be seen from the figure, a reduced order model can indeed be developed through a systematic approach of subspace identification. The original 19th order physical model has been reduced to a 5th order empirical model that can still capture the dominant dynamics of the system.

In order to test the generalization capability of the identified model, a test data set is generated with the reactor power at 90% full power and the input excitation power corresponding to a standard deviation of 0.5% nominal values. Figure 6.3 shows the comparison of results between the cold leg temperature obtained from the simulation model and the corresponding predicted values based on the identified model. The prediction errors are indeed very small.

The prediction error index γ can be used to quantify the prediction performance of the identified model, which is given by (Favoreel, De Moor, and Van Overschee, 1998):

$$\gamma = \frac{1}{N}\sqrt{\sum_{k=1}^{N}(y_k - \hat{y}_k)^2 / \sum_{k=1}^{N} y_k^2} \tag{6.69}$$

where N is the number of test data points, y_k is the actual value of the kth data point, and $\hat{y}_k$ is the predicted value of the kth data point.

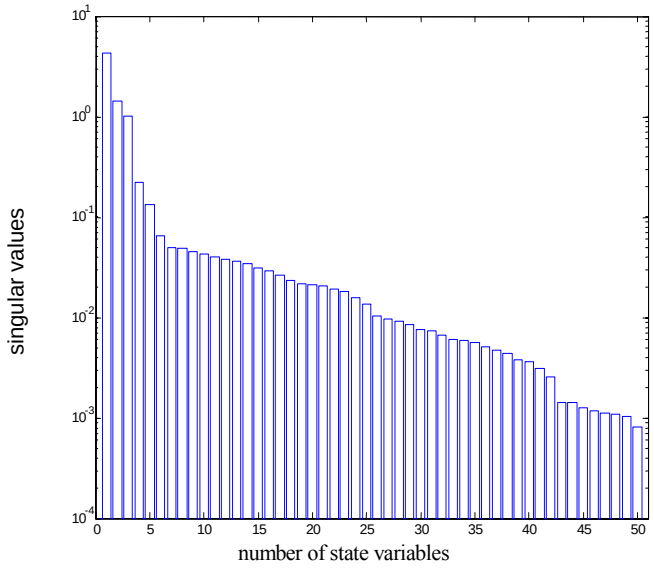

Figure 6.2. The singular values of the projection matrix.

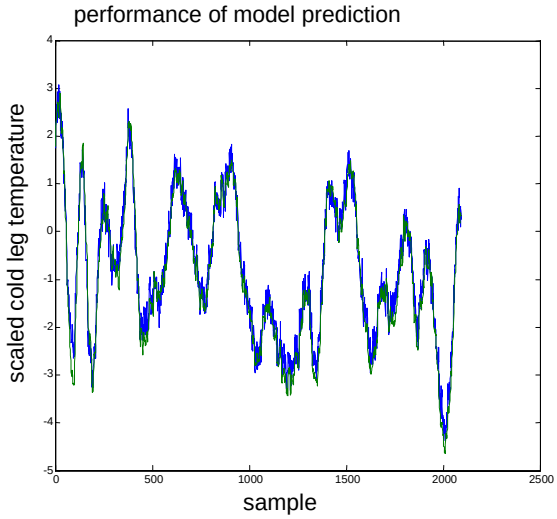

Figure 6.3. Model prediction of cold leg temperature.

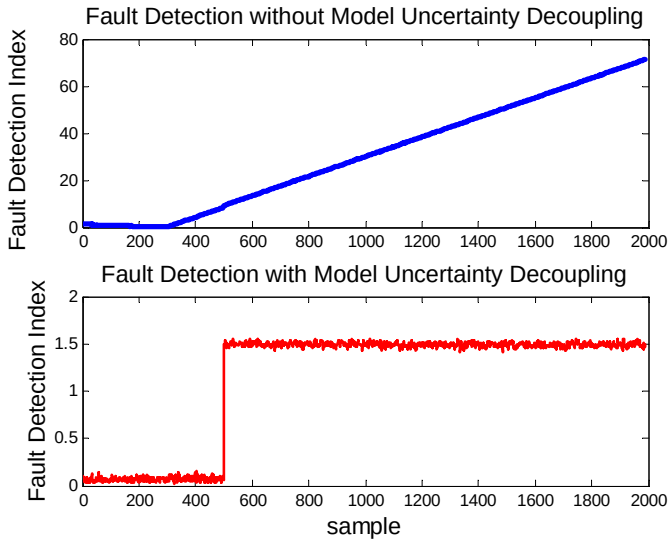

Figure 6.4. Robust fault detection for cold leg temperature sensor fault.

The prediction error indices are 11.2%, 8.3%, 8.8%, 10.6%, 10.2% and 8.3% for the cold leg temperature, the steam pressure, the steam outlet temperature, the sub-cooled length and the saturated boiling length, respectively. These small indices show that the identified model is able to give a good prediction for all the outputs even if the reactor is operating at a different power level with different magnitude of perturbations.

6.4.2 Robust Fault Detection Design

To show the performance of the developed robust fault detection algorithm, the identified linear state space model was used to generate data with model uncertainty. The model uncertainty was introduced by adding an additive term to the state vector after the 300th sample. The model uncertainty term has a fixed direction but the magnitude of the model uncertainty varies linearly with time.

Figure 6.4 shows the performance of the developed robust fault detection algorithm to sensor faults. Model uncertainty is introduced after the 300th sample and a cold leg temperature sensor fault with a bias of 1 ^{o}C is injected after the 500th sample. The upper plot shows that if model uncertainty is not decoupled the fault detection index will not be able to distinguish a sensor fault and model uncertainty. However, the lower

plot shows that the developed robust fault detection algorithm results in a fault detection index greater than 1.0 only after a fault has occurred in the system. Therefore, it can be concluded that the developed robust fault diagnosis algorithm is able to decouple model uncertainty without loss of the capability of fault detection.

Figure 6.5 shows the performance of the fault detection index for a feed water flow meter bias fault with a magnitude of 2% at 1500 second during the transient when the reactor power is reduced from 100% to 95% at a rate of 0.0012 Full Power/min. The fault detection residual generator responds to the fault with no time delay and generates a significant fault signal as significant as 10.0 compared with the fault detection index of less than 1.0 for fault free condition. It can also be seen that the generated fault detection index has the desirable property that it returns to an insignificant level when the fault is recovered during the transient at 2500 seconds.

After the reactor reaches 95% power level, the fault detection index remains less than 1.0, which can demonstrate that the identified model has learned the system dynamics appropriately because the model still retains its good prediction capability at 95% power level, an unknown operation condition, although the model is built from the data collected at 100% power level.

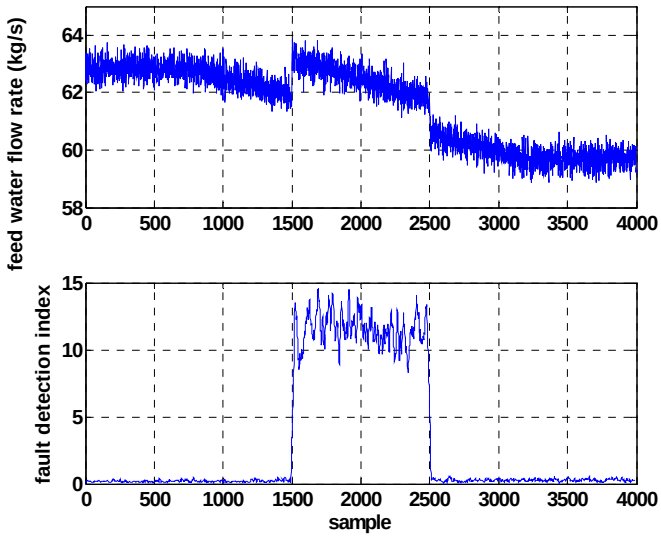

Figure 6.5. Fault detection of feed water flow meter sensor fault during a reactor power transient.

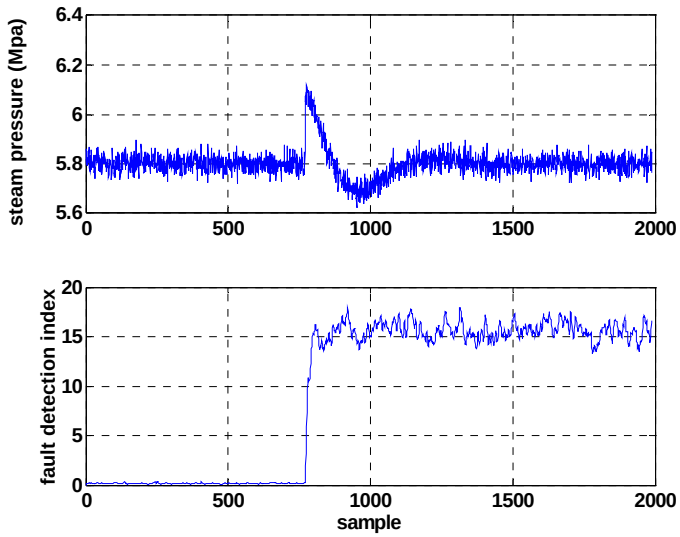

Figure 6.6. Fault detection of steam pressure sensor fault.

From the viewpoint of FDI robustness, it can be concluded that a dynamic model is superior to a static model in which case model prediction is simply an interpolation among the data used to train it without revealing the causal relationship among the measured variables and thus without the capability of generalization outside the training space.

Figure 6.6 shows the performance of fault detection for a steam pressure sensor bias fault of 2% magnitude at the 800th sample when the reactor is initially operating at 90% full power. Because the steam pressure is controlled in the HCSG system, the steam pressure will experience a fault-induced transient. The fault detection index responds immediately when the sensor fault occurs at the 800th sample. It is interesting to notice that the fault detection index is almost constant after the fault occurs. On the one hand, this indicates that the identified model is able to represent the system dynamics initiated by the fault. On the other hand, the fault detection index does not return to an insignificant level even though the measured steam pressure has been brought back to the original level. This is because some other process variables such as the saturated boiling length and the sub-cooled length cannot be brought back to their original values due to the sensor fault.

6.4.3 Robust Fault Isolation Design

Ten residual generators were designed for fault isolation. Each of the ten residual generators corresponds to ten linear transformations on the original estimation error vector such that it is sensitive to all faults but the one to which the residual generator is dedicated for fault isolation. The ten residual generators are dedicated to the isolation of the following sensor faults:

Variable 1: the cold leg temperature.
Variable 2: the steam pressure.
Variable 3: the steam temperature.
Variable 4: the saturated boiling length.
Variable 5: the sub-cooled length.
Variable 6: the hot leg temperature.
Variable 7: the steam flow rate.
Variable 8: the feed water temperature.
Variable 9: the feed water flow rate.
Variable 10: the primary flow rate.

Figure 6.7 shows the FDI indices of the ten residual generators responding to the feed water flow meter bias fault with a magnitude of 2% at 1500 second during the transient when the reactor power is reduced from 100% to 95% at a rate of 0.0012 Full Power/min. As can be seen, the residual generator dedicated to the isolation of the ninth variable produces an insignificant FDI index of less than 1.0 while all the other residual generators do not. Therefore, the feed water flow meter sensor fault can be correctly isolated when the fault is detected between 1500 second and 2500 second (See Figure 6.5) during the reactor power transient.

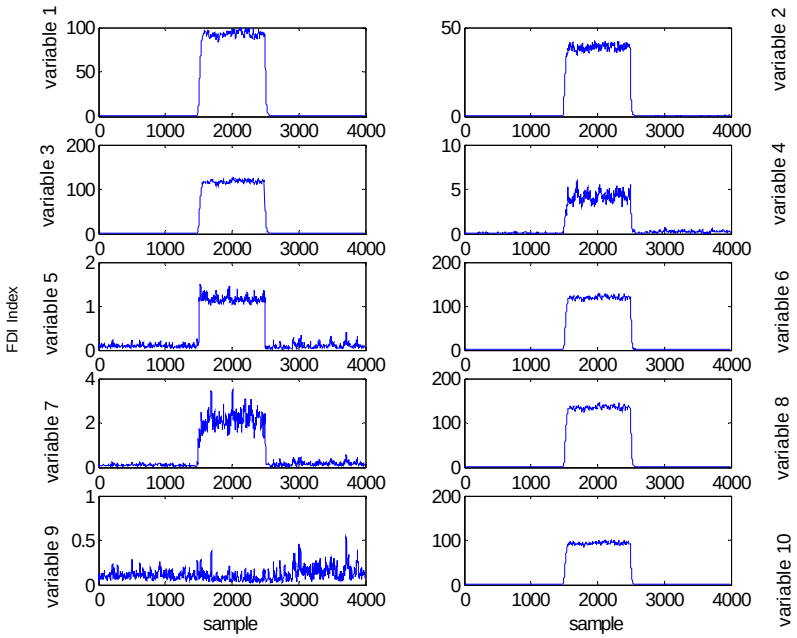

Figure 6.7. Fault isolation of feed water flow meter sensor fault during a reactor power transient.

The FDI indices for the fifth variable and the seventh variable are approximately 1.2 and 2.0, respectively, while the FDI indices for the other variables are significantly greater than 1.0. It can be seen from this that the fault isolation of feed water flow meter fault has less confidence level when it is to be isolated from a sub-cooled length measurement fault or a steam flow meter fault than the other faults. This result is also in agreement with the statement obtained in Chapter 2 that an input fault may be not isolatable. In addition, an insight we can obtain here is that FDI performance testing at design phase with a reliable simulation model should still be emphasized.

Figure 6.7 has also demonstrated the success of the developed FDI method in that a predetermined logic of fault isolation is achieved through studying the identified model. This is a significant difference from many recently published literatures where FDI is inappropriately paraphrased as a pattern recognition problem. Pattern recognition needs to determine the fault features through the collection of faulty data, which is unrealistic in process engineering application.

The fault isolation residual generators have shown the robustness of the developed method to measurement noises. Although all the measured variables are added with 0.2% white Gaussian noise, the residual generators can successfully eliminate their effects on the residuals after EWMA filters are applied to the residuals.

Figure 6.8 shows the FDI indices of the designed ten residual generators for the fault isolation of a steam pressure sensor fault. In the figure, the FDI indices of all the variables, except the second variable, are greater than 1.0; therefore, the steam pressure sensor fault can be isolated correctly throughout the fault induced transient. As compared with static model based FDI approaches, the developed approach is able to isolate a controlled variable related sensor fault at the initial stage when it occurs. In the meantime, fault misdiagnosis can be avoided during the fault-induced transient. Moreover, fault isolation is based on the identified model rather than fault information through appropriate design of residual generators such that the generated residuals follow the predetermined logic.

Table 6.1 summarizes the FDI results for the five other sensor faults of the HCSG system that occur at 95% full power. The five faults are listed as follows:

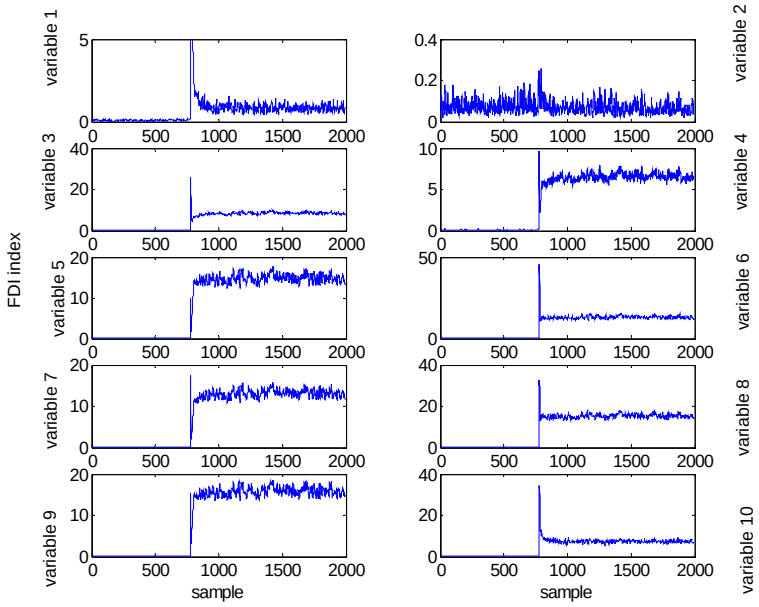

Figure 6.8. Fault isolation of steam pressure sensor fault.

Table 6.1. The FDI indices of bias type sensor faults

Faults / FDI index	Fault free	Fault 1	Fault 2	Fault 3	Fault 4	Fault 5
Fault detection	0.22	40.3	18.3	9.42	5.04	25.7
Cold leg temperature	0.15	**0.22**	1.7	2.25	3.45	6.3
Steam pressure	0.16	1.47	2.4	2.10	2.39	1.2
Steam temperature	0.16	2.43	**0.23**	**0.45**	4.31	22.0
Saturated boiling length	0.18	6.99	2.59	2.65	1.43	15.7
Sub-cooled length	0.18	12.7	9.2	6.30	2.06	1.3
Hot leg temperature	0.19	14.7	3.33	**0.31**	4.94	24.9
Steam flow rate	0.20	29.9	14.94	8.18	**0.22**	14.9
Feed water temperature	0.20	38.3	18.75	8.72	3.74	**0.24**
Feed water flow rate	0.19	28.8	14.64	7.31	4.55	7.43
Primary flow rate	0.16	16.1	4.51	1.65	5.76	23.7

Fault 1: cold leg temperature sensor fault with a bias of 1.0 ^{o}C,

Fault 2: steam temperature sensor fault with a bias of 1.0 ^{o}C,

Fault 3: hot leg temperature sensor fault with a bias of 1.0 ^{o}C,

Fault 4: steam flow meter fault with a bias of 1% nominal flow rate,

Fault 5: feed water temperature sensor fault with a bias of 1.0 ^{o}C.

During fault free conditions, the fault detection index is 0.22, which is less than 1.0 and will not trigger a false alarm. The FDI indices produced from all the designed residual generators for fault isolation are also less than 1.0 for fault free condition. This indirectly proves that the EWMA filtered residual vector does indeed follow a multi-dimensional Gaussian distribution with zero mean and a constant covariance matrix.

The fault detection indices are all significantly greater than 1.0 after the five faults occur. When the FDI indices of the ten residual generators designed for fault isolation are examined, they follow the predetermined logic of fault isolation for all the faults but hot leg temperature sensor fault. For the hot leg temperature sensor fault, both the

residual generator dedicated to the isolation of the steam temperature sensor fault and the residual generator dedicated to the isolation of the hot leg temperature sensor fault generate an insignificant residual, which indicates an unknown fault according to the residual design scheme for isolation.

The reason why the hot leg temperature sensor fault was diagnosed as an unkown fault is that there is a maximum sensitivity of the designed residual generator to an input fault, which is determined by the system model itself. However, because the designed residual generator can maintain the capability of being insensitive to the fault that it is designed to isolate regardless of the fault magnitude, the predetermined logic for fault isolation can always be followed if the fault magnitude is big enough. It is found that the hot leg temperature sensor fault can be unambiguously isolated if its fault magnitude is increased to 3 ^{o}C. This example also demonstrates the importance of FDI design in reactor design phase and the necessity of testing its performance based on a realistic simulation.

6.5 Summary

A robust dynamic fault diagnosis algorithm is presented in this chapter for dynamic fault diagnosis of nuclear power systems. The theory of subspace identification was first described to extract low order state-space model from data generated by simulation calculations. Robust parity space approach was then combined with subspace identification to design residual generators. A new one-step algorithm was derived without the need of explicitly identifying model uncertainty for uncertainty decoupling. The implementation of robust residual generator design was formulated as a generalized eigenvalue problem. Finally, the developed robust dynamic fault diagnosis algorithm was applied to the IRIS HCSG systems for transient fault detection and isolation. It was shown that the developed algorithm was able to deal with model uncertainty for dynamic fault diagnosis without causing false alarms and can be used for fault tolerant control.

Chapter 7

Summary, Conclusions, and Recommendations for Future Research

7.1 Summary and Conclusions

The preceding chapters have presented an integrated approach to the performance monitoring and fault diagnosis of nuclear power systems using robust data driven model based methods for both steady state and dynamic operation conditions. The developed methods were demonstrated through the application to IRIS helical coil steam generator systems.

A steady state model was developed for the IRIS helical coil steam generator to prepare for the initialization parameters of dynamic simulation and find out a unique method to monitor the tube inside water inventory. The calculated primary outlet temperature and the steam outlet temperature based on the developed model are within 0.5% error of the results obtained from a more sophisticated simulation. The calculated primary coolant temperature profile also demonstrated that a clear breakpoint exists when the saturated boiling heat transfer transits to the superheated heat transfer. It was proposed that the breakpoint determined from the primary fluid temperature measurements could be used to indicate the HCSG tube inside water inventory.

A dynamic model was also developed to study the dynamic responses of the IRIS helical coil steam generator systems for control and fault diagnosis design. The developed dynamic model is a nodal model, which has two nodes each, to represent the axial changes in the superheated, saturated, and sub-cooled region of the primary side and the secondary side. The steady state results and the typical transient results showed that the developed dynamic model was able to characterize the HCSG behavior with reasonably good accuracy to study the control and fault diagnosis of IRIS HCSG system.

Sensor placement was considered as a crucial design element of performance monitoring and fault diagnosis of nuclear power systems. A systematic approach was

developed in this dissertation to accomplish sensor placement design in reactor design phase. In this approach, the minimum set of sensors for process diagnosis was determined based on cause effect analysis using graph theory. If steady state balance equations were used for sensor fault diagnosis, the minimum set of sensors were determined based on observability and redundancy analysis using orthogonal projection algorithm. Finally, to ensure reliable sensor fault diagnosis and accurate performance parameter estimation, data reconciliation was used to study the sensitivities.

Steady state fault diagnosis is useful for condition-based maintenance in nuclear power plants. Reconstruction based PCA was proposed as a baseline approach, which is able to deal with both sensor faults and process faults through characterizing the fault effects in a unified manner. When reconstruction based PCA approach was used, the conditions of fault detectablity and fault identifiablity could be quantitatively evaluated, which is very important for applications to nuclear power systems. In addition, reconstruction based PCA approach can usually give more conclusive results in terms of fault isolation since a decision is made only if the fault effects can be fully explained through the reconstruction procedure.

Hybrid PCA model based approach was developed in this dissertation to improve the performance of steady state fault diagnosis through incorporating prior knowledge. When historical data were collected during reactor power changes, many measured variables would have significant amount of variation due to the manipulation of a few variables. Hybrid PCA model based approach allowed us to decompose the variation of the collected data based on this prior knowledge. The demonstration example showed that the developed algorithm could lead to more sensitive fault diagnosis after some large variations were removed.

An integrated framework of robust PCA model based fault diagnosis was developed to deal with the situation when no qualified historical data were available for fault diagnosis. In this approach, PCA models were developed from data generated by well-designed simulation calculations. Robust fault detection was achieved by calculating a fault detection index, which was robust to model uncertainty, that was larger than 1.0 only if a fault occurred. Robust fault isolation was based on determining a fault

isolation index, which was also robust to model uncertainty, that measured how well the fault measurements could be reconstructed in different candidate fault subspaces with model uncertainty. The developed algorithm was demonstrated through applying to the IRIS HCSG system with the thermal degradation considered as model uncertainty. Both sensor faults and process faults could be correctly detected and isolated based on the calculated fault detection index and fault isolation index when model uncertainty was considered.

The importance of dynamic fault diagnosis to nuclear power systems was emphasized in order to enhance the robustness to plant disturbance and meet the needs of fault tolerant control and transient fault diagnosis. The goal of dynamic fault diagnosis algorithm, which was proposed in this dissertation, was to use subspace identification technique to identify a low order state-space model from plant data and then apply parity space approach for model based fault diagnosis. Because data with persistent excitation were usually not available in nuclear power systems, robust subspace model based dynamic fault diagnosis algorithm was developed in this dissertation, and was able to deal with dynamic model uncertainty. The uniqueness of the developed algorithm was that a separate procedure of identifying model uncertainty was not necessary. Instead, after a subspace model was identified from simulation data, the robust residual generator design for fault diagnosis was achieved by combining the identification of model uncertainty and the robust residual generator design into one step. The demonstration example through applying to the IRIS HCSG systems showed that the developed algorithm could avoid false alarms due to dynamic model uncertainty for transient fault diagnosis.

7.2 Recommendations for Future Research

To the author's knowledge, this dissertation is the only work focused on developing fault diagnosis methods including sensor placement design, steady state fault diagnosis, and dynamic fault diagnosis for application to nuclear power systems. Although the proof-of-principle was demonstrated for the developed algorithms using IRIS HCSG systems, these algorithms still need to be implemented on a laboratory

system and tested using real nuclear power plant data before they can be integrated into the Generation-IV I&C systems.

Sensor placement design based on graph theory was presented to determine the minimum set of sensors for process fault detection and isolation and was applied to IRIS Helical Coil Steam Generator systems. In this application, the DG graph was developed by hand from engineering models. To facilitate computer aided design, this process can be automated by developing a general purpose software, which allows an automatic transformation of engineering models into DG and the determination of minimum requirements of sensor placement for a specified objective of fault diagnosis.

The developed robust data driven model based fault diagnosis methods in this dissertation were based on linear data driven models in order to deal with model uncertainty. Further study need to be performed to deal with the nonlinearity inherent in nuclear power systems. One foreseeable solution is to use multiple locally linear models built from data generated by a high fidelity nonlinear simulation model through perturbing the system inputs at different operating conditions. For a known operation condition, the measured data would be compared with the available model prediction using classification algorithms to determine which linear model would be able to best fit the current data sequence. It is this best linear data driven model that would be used for robust fault diagnosis.

Although this dissertation has only dealt with process performance monitoring and fault diagnosis, equipment diagnostics is also very important in the integrated fault diagnosis system to improve the operational safety and economics of nuclear power systems. In fact, the developed fault diagnosis algorithms are also relevant to equipment diagnostics. For instance, the proposed steady state fault diagnosis algorithm can be directly used to diagnose the malfunctioning of steam turbines using the measurements of temperature, steam pressure, and steam flow rate at inlet and outlet points. The proposed subspace identification algorithm can be combined with first principle-based models to detect and localize structural damages. Some initial efforts on on-board vibration monitoring using subspace based covariance driven modal identification for nonstationary excitation have been made by Basseville, Abdelghani, and Benveniste,

1999. It is worthwhile to demonstrate its performance for structural monitoring of major components in nuclear power plants.

References

Akaike H., “Information Theory and an extension of the Maximum Likelihood Principle,” Procesedings 2nd International Symposium on Information Theory, Petrov and Caski, Eds, 267-281, 1974.

Bagajewicz M. J., Process Plant Instrumentation: Design and Upgrade, Technomic Publishing Company, Inc., 2001.

Bakshi B. R. and Stephanopoulos G., “ Wavenet: a Multi-resolution, Hierarchical Neural Network with Localized Learning,” AIChE Journal, 39, 1, 57-81, 1993.

Bartlett F. E. and Uhrig R. E., “Nuclear Power Plant Status Diagnosis using an Artificial Neural Network,” Nuclear Technology, 97, 272-181, 1992.

Basseville M., “Detecting Changes in Signals and Systems: A Survey,” Automatica, 24, 3, 309-326, 1988.

Basseville M., Abdelghani M, and Benvenise A., “Subspace based fault detection algorithms for vibration monitoring,” Automatica, 36, 101-109, 1999.

Beard R. V., Failure Accommodation in Linear Systems Through Self-Reorganization, PhD Thesis, MIT, USA, 1971.

Becerra V. M., Advanced System Identification, 2004.
http://www.personal.rdg.ac.uk/~shs99vmb/notes/asi/Lecture7.pdf

Berec L., “A multi-model Method to Fault Detection and diagnosis: Bayesian Solution, an Introductory Treaties,” International J. of Adaptive Control and Signal Processing, 12 , 1, 81-92, 1998.

Bhushan M. and Rengaswamy R., “Design of Sensor Network based on the Signed Directed Graph of the Process for Efficient Fault Diagnosis,” Industrial and Eng. Chem. Research, 39, 999-1019, 2000.

Bodeux J. B. and Golinval J. C., “Modal Identification and Damage Detection Using the Data-Driven Stochastic Subspace and ARMAV Methods,” Mechanical Systems and Signal Processing, 27, 1, 83-89, 2003.

Carelli M. D., Conway L., Oriani L., Pertovic B., Todreas N. E., et al., “The Design and Safety Features of the IRIS Reactor,” ICONE 11, Tokyo, Japan, April 20-23, 2003.

Chen A. T., Digital Simulation for Nuclear Once-Through Steam Generators, Ph.D. Dissertation, The University of Tennessee, 1976.

Chen B. H., Wang X. Z. and McGreavy C., "On-line operational support system for faults diagnosis in process plants," Computers & Chemical Engineering, 22, Supplement 1, S973-S976, 1998.

Chen J. and Patton R. J., "A Re-examination of Fault Detectability and isolability in Linear Dynamic Systems," 567-573, IFAC Fault Detection, Supervision and Safety for Technical Process, Espoo, Finland, 1994.

Chen J., Robust Residual Generation for Model Based Fault Diagnosis of Dynamic Systems, PhD dissertation, University of York, York, UK, 1995.

Chen J. and Patton R. J., Robust Model-based Fault Diagnosis for Dynamic Systems, Kluwer Academic Publishers, 1999.

Chen L., " Steam-water Two Phase Flow Frictional Pressure Drop in Straight Tubes," Selected Papers of Multiphase Flow and Heat Transfer, Xian Jiaotong University Press, 7.1-7.6, 1982.

Choi S. S., Chung S. H., and Lee D. H., "Automating Strategies of Emergency Operation for Optimal Shutdown in Pressurized Water Reactors," IEEE Transactions on Nuclear Science, 45, pp. 17-29, 1998.

Chow E. Y., and Willsky A. S., "Analytical Redundancy and the Design of Robust Detection System," IEEE Trans. Automat. Contr. AC-29, 7, 603-614, 1984.

Clark R. N., "Instrument Fault Detection," IEEE Trans. Aero. & Electron. Syst. AES-14, 456-465, 1978.

Dash S. and Venkatasubramanian V., "Challenges in the Industrial Applications of Fault Diagnosis Systems," Computers in Chem. Eng. , 24, 785-791, 2000.

Daly K. C., Gai E., and Harrison V., "Generalized Likelihood Test for FDI in Redundant Sensor Configuration," Journal of Guidance & Control, 2, 1, 9-17, 1979.

De Moor B., Mathematical Concepts and Techniques for Modeling Static and Dynamic Systems, PhD Dissertation, Department of Electrical Engineering, Katholieke Universiteit Leuven, Belgium, 1988.

Del Castillo E., Statistical Process Adjustment for Quality Control, John Wiley & Sons, Inc., 2002.

Dong D. and McAvoy T. J., "Batch Tracking via Nonlinear Principal Component Analysis," AIChE Journal, 42, 8, 2199-2208, 1996.

Doraiswami R. and Stevenson M., " A Robust Influence Matrix Approach to Fault Diagnosis," IEEE Trans. Contr. Sys. Techno., 4, 1, 29-39, 1996.

Duan G. R., Patton R. J., Chen J., and Chen Z., " A Parametric Approach for Robust Fault Detection in Linear Systems with Unknown Disturbances," IFAC Symposium on Fault Detection, Supervision and Safety for Technical Processes, SAFEPROCESS'97, 307-312, 1998.

Dunia R., and Qin S. J., "Subspace Approach to Multi-dimensional Fault Identification and Reconstruction," AIChE Journal, 44, 8, 1813-1831, 1998b.

Dunia R., Qin S. J., Edgar T. F., and McAvoy T. J., "Identification of faulty sensors using principal component analysis,". AIChE Journal, 42, 10, 2797-2811, 1996a.

Dunia R., Qin S. J., Edgar T. F., and McAvoy T. J., "Use of principal component analysis for sensor fault identification," Comp. and Chem. Eng., 20, S713-S718, 1996b.

Dunia R. and Qin S. J., "Joint Diagnosis of Process and Sensor Faults using Principal Component Analysis," Control Engineering Practice, 6, 457-469, 1998.

Dunia and Qin S. J., "A Unified Geometric Approach to Process and Sensor Fault Identification," Computers Chem. Engng, 22, 7-8, 927-943, 1998b.

Erbay A.S. and Upadhyaya B. R., "A Personal Computer-Based On-Line Signal Validation System for Nuclear Power Plants," Nuclear Technology, 119, 63-75, 1997.

Favoreel W., De Moor B., and Van Overschee P., "Subspace State Space System Identification for Industrial Processes," Proc. Of the 5th IFAC Symposium on Dynamic and Control of Process Systems, pp. 322-330, 1998.

Frank P. M., "Fault Diagnosis in Dynamic Systems using Analytical and Knowledge Based Redundancy: A Survey and Some New Results," Automatica, 26, 3, 459-474, 1990.

Frank P. M., Ding S. X., and Marcu T., "Model Based Fault Diagnosis in Technical Process," Transactions of the Institute of Measurement and Control, 22, 1, 57-101, 2000.

Gallagher J. M., Jr., Leider J. P., and Crunk S., "Disturbance Analysis and Surveillance System Scoping and Feasibility Study: Final Report," EPRI NP-2240, Westinghouse Electric Corporation, NTIS, 1982.

Gan C. and Danai K., "Model-Based Recurrent Neural Network for Modeling Nonlinear Dynamic Systems," IEEE Trans. on Systems, Man, and Cybernetics- part B: Cybernetics, 30, 2, 344-351, 1999.

Gertler J. J., Fault Detection and Diagnosis in Engineering Systems, Marcel Dekker Inc., 1998.

Garland W. J. and Hoskins J. D., "Approximate Functions for the Fast Calculation of Light-Water Properties at Saturation," International Journal of Multiphase Flow, 14, 3, 333-348, 1988.

Garland W. J. and Hoskins J. D., "Simple Functions for the Fast Approximation of Light-Water Thermodynamic Properties," Nuclear Engineering and Design, 113, 21-34, 1989.

Garland W. J., Wilson R. J., Bartak J., Cizek J., Stastny M., and Zentrich I., "Extensions to the Approximation Functions for the Fast Calculation of Saturated Water Properties," Nuclear Engineering and Design, 136, 381-388, 1992.

Grauf E., Jansky J., Langenstein M., "Reconciliation of process data in Nuclear Power Plants (NPPs)," Proceedings of ICONE 8 International Conference on Nuclear Engineering, April 2-6, Baltimore, USA, 2000.

Gribok V. A., Attieh I., Hines J. W., and Uhrig R. E., "Regularization of Feed Water Flow Rate Evaluation for Venturi Meter Fouling Problems in Nuclear Power Plants," Ninth International Meeting on Nuclear Reactor Thermal Hydraulics (NURETH-9), San Francisco, CA, Oct 3-8, 1999.

Guimaraes L., Non-linear dynamics of a once-through steam generator, PhD Dissertation, The University of Tennessee, Knoxville, 1992.

Hashemian H. M., Thie J. A., Upadhyaya B. R., and Holbert K. E., "Sensor Response Time Monitoring using Noise Analysis," SMORN-V Progress in Nuclear Energy, 21, 605-611, 1988.

Hashemian H. M., "Optimized Maintenance and Management of Aging of Critical Equipment in Nuclear Power Plants," Power Plant Surveillance and Diagnosis, Springer, 2002.

Hashemian H. M., "Advanced Instrumentation and Maintenance Technologies for Nuclear Power Plants," U.S. Nuclear Regulatory Commission, NUREG/CR-5501, 1998.

Himmelblau D. M., Fault Detection and Diagnosis in Chemical and Petrochemical Processes. Elsevier, New York, 1978.

Hines J. W., A Hybrid, Approach to Fault Detection and Isolation Merging Analytical Redundancy and Neural Network Techniques, Ph.D. dissertation, Department of Nuclear Engineering, The Ohio State University, 1994.

Hines J. W. and Wrest D. J., “Signal Validation using Adaptive Neural Fuzzy Inference Ssytems,” Nuclear Technology, 181-193, 1997.

Holbert K. E. and Upadhyaya B. R., “An Integrated Signal Validation System for Nuclear Power Plants,” Nuclear Technology, 92, 3, 411-427, 1990.

Holbert K. E. and Upadhyaya B. R., “Empirical Process Modeling Technique for Signal Validation,” Annals of Nuclear Energy, 21, 7, 387-403, 1994.

Hou M. and Muller P. C., “Disturbance Decoupled Observer Design: A Unified Viewpoint,” IEEE Trans. Automat. Contr., 39, 6, 1338-1341, 1994.

Isermann R., and Freyermuth B., “Process Fault Diagnosis Based on Process Model Knowledge: Part I: Principles for Fault Diagnosis with Parameter Estimation,” J. Dyn. Sys. Meas. & Contr.-Trans. Of the ASME 113, 4, 620-626, 1991a.

Isermann R., and Freyermuth B., “Process Fault Diagnosis Based on Process Model Knowledge: Part II: Case Study Experiments,” J. Dyn. Sys. Meas. & Contr.-Trans. Of the ASME 113, 4, 627-633, 1991b.

Isermann R. and Ballé P., “Trends in the Application of Model-based Fault Detection and Diagnosis of Technical Processes**,”** Control Engineering Practice 5, 5, 709-719, 1997.

Jackson J. E., and Mudholkar G., “Control Procedures for Residuals Associated with Principal Component Analysis,” Technometrics, 21, 341-449, 1979.

Jackson J. E., A user guide to principal components. John Wiley & Sons, New York, 1991.

Jae M. and Moon J. H., “Use of a Fuzzy Decision-Making Method in Evaluating Severe Accident Management Strategies,” Annals of Nuclear Energy, 29, pp. 1597-1606, 2002.

Jones H. L., Failure Detection in Linear Systems, PhD Thesis, MIT, USA, 1973.

Kalman R., “A New Approach to Linear Filtering and Prediction Problems,” J. Basic Eng., 82, 35-50, 1960.

Kano M., Hasebe S., Hashimoto I., and Ohno H., “A new Multivariate Statistical Process Monitoring Method using Principal Component Analysis,” Computers and Chemical Engineering, 25, 1103-1113, 2001.

Kavuri S. N. and Venkatasubramanian V., “Combining Pattern Classification and Assumption-based Techniques for Process Fault Diagnosis,” Computers Chem. Engng. 16, 4, 299-312, 1992.

Kavaklioglu K. and Upadhyaya B. R., "Monitoring Feedwater Flow Rate and Component Thermal Performance of Pressurized Water Reactors by Means of Artificial Neural Networks," Nuclear Technology, 107, 112-123, 1994

Kim K., Kwon K., Hwang I., Lee D., Park W., Kim J., and Lee S., "Development of advanced I&C in Nuclear Power Plants: ADIOS and ASICS," Nuclear Engineering and Design, 207, pp. 105-119, 2001.

Kim K. and Bartlett E. B., "Error Prediction for Nuclear Power Plant Fault Diagnosis Advisor using Neural Networks," Nuclear Technology, 108, 283-297, 1994.

Krzanowski W. J., "Between-group Comparison of Principal Components," Journal of the American Statistical Association, 74, 703-707, 1979.

Kresta J. V., Marlin T. E., MacGregor J. F., "Development of Inferential Process Models using PLS," Computers Chem. Engng., 18, 597-611, 1994.

Kourti T. and MacGregor J. F., "Process Analysis, Monitoring and Diagnosis Using Multivariate Projection Methods - A Tutorial," Chemometrics and Intelligent Laboratory Systems, 28, 3-21, 1995.

Kourti T. and MacGregor J. F., "Multivariate SPC Methods for Process and product Monitoring," Journal of Quality Technology, 28, 409, 1996.

Kramer M. A. and Palowitch B. L., Jr., "A rule based approach to fault diagnosis using the signed directed graph," AIChE Journal, 33, 1067-1078, 1987.

Kuridan R. M. and Beynon T. D., "Analysis of the Steam Generator for the Safe Integral Reactor Concept," Progress in Nuclear Energy, 31, 3, 273-287, 1997.

Lee J. C. and Akcasu A. Z., Simplified Models for Transient Analysis of Nuclear Steam Generator, EPRI NP-1772, 1981.

Lee M., Nonlinear Dynamic Modeling of a Once-Through Steam Generator, Ph.D. Dissertation, The University of Tennessee, 1978.

Li W. and Shah S., "Structured Residual Vector-Based Approach to Sensor Fault Detection and Isolation," Journal of Process Control, Vol. 12, pp. 429-443, 2002.

Ljung L., System Identification: Theory for the User, Prentice Hall, Englwood Cliffs, N. J., 1999.

Lowry C. A., Woodall W. H., Champ C. W., Rigdon S. E., "A multivariate exponentially weighted moving average control chart," Technometrics, 34, 46–53, 1992.

Malinowski E. R., "Determination of the Number of Factors and the Experimental Error in a Data Matrix," Anal. Chem, 49, 4, 612-617, 1977.

Mera R. K., and Peschon J., "An Innovations Approach to Fault Detection and Diagnosis in Dynamic Systems," Automatica,, 7 637-640, 1971.

MacGregor J. F., Jackle C., Kiparissides C., Koutondi M., " Process Monitoring and Diagnosis by Multinlock PLS Methods," Kourti," AIChE Journal, 40, 5, 826-838, 1994.

Mosterman P. J. and Biswas G., "Monitoring, prediction and fault isolation in dynamic physical systems," Proceeding AAAI 1997, pp. 100-105, 1997.

Montmain P. J. and Gentil S., "Dynamic causal model diagnostic reasoning for online technical process supervision," Automatica, 36, 1137-1152, 2000.

Nuclear Regulatory Commission, Office of Nuclear Reactor Regulations, TMI-2 Lessons Learned Task Force, Final Report, NRC Report NUREG-0585, NTIS, October 1979.

Nomikos P. and MacGregor J. F., "Monitoring Batch Processes using Multiway Principal Component Analysis," AIChE Journal, 40, 8, 1361-1375, 1994.

O'Hara, J. M., "I&C&HMI Workshop White Paper for the Human-System Interaction Working Shop," Brookhaven National Laboratory, 2002.

Ogunnaike B. A. and Ray W. H., Process Dynamics, Modeling, and Control, Oxford University Press, New York, 1994.

Ohga Y. and Seki H., "Abnormal Event Identification in Nuclear Power Plants using a Neural Network and Knowledge Processing," Nuclear Technology, 101, 159-163, 1993.

Pai D. C. and Fisher G. D., "Application of Broyden's method to reconciliation of nonlinearly constrained data," *AIChE J.* 34, 873-876, 1988.

Park J. H. and Rizzoni G., "A new Interpretation of the Fault Detection Filter. 1: Closed Form Algorithm," International Journal of Control, 60, 5, 767-787, 1994a.

Park J. H., Halevi Y., Rizzoni G., "A new Interpretation of the Fault Detection Filter. 2: The Optimal Detection Filter," International Journal of Control, 60, 6, 1339-1351, 1994b.

Park J. H. and Seong P. H., "An Intelligent Knowledge Base Development Tool for Knowledge Acquisition and Verification for NPP Dynamic Alarm Processing Systems," Annals of Nuclear Energy, 29, pp. 447-463, 2002.

Patton R. J. and Chen J., "A Review of parity Space Approaches to Fault Diagnosis," 65-81, IFAC Fault Detection, Supervision and Safety for Technical Processes, Baden-Baden, Germany, 1991.

Patton R. J. and Chen J., "Optimal Selection of Unknown Input Distribution Matrix in the Design of Robust Observers for Fault Diagnosis," Automatica, 29, 4, 837-841, 1991b.

Patton R. J. and Chen J., "Observer Based Fault Detection and isolation: Robustness and Application," Contr. Engr. Practice, 5, 5, 671-682, 1997.

Patton R. J. and Chen J., "A Review of parity Space Approaches to Fault Diagnosis for aerospace Systems," J. of Guidance, Contr. & Dynamics, 17, 2, 278-285, 1994.

Pearson K., On Lines and Planes of Closest Fit to Systems of Points in Space, Philosophical Magazine Series B, 2, 559-572, 1901.

Qin S. J. and McAvoy T. J., "Nonlinear PLS Modeling using Neural Network," Computers Chem. Engng., 16,4, 379-391, 1992.

Qin S. J. and Dunia R., "Determining the Number of Principal Components for Best Reconstruction," IFAC DYCOPS'98, Greece, 1998.

Qin S. J. and Li W., "Detection and identification of faulty sensors in dynamic process," AIChe Journal, 47, 7, pp. 1581-1593, 2001.

Qin S. J. "Process chemometrics: basics and beyond," 3rd International Chemometrics Research Meeting, 2002.

Qin S. J., "Statistical Process Monitoring: Basics and Beyond," Journal of Chemometrics, 17, 480-502, 2003.

Raich A. C. and Cinar A., "Statistical Process Monitoring and Disturbance Diagnosis in Multivariable Continuous Processes," AIChE Journal, 42, 4, 995-1009, 1996.

Raich A. C. and Cinar A., "Multivariate Statistical Methods for Monitoring Continuous Processes, Assessment of Discrimination Power of disturbance Models and Diagnosis of Multiple Disturbances," Chemometrics and Intelligent Lab. Systems, 30, 37-48, 1995.

Raich A. C., and Cinar A., "Diagnosis of Process Disturbances by Statistical Distance and Angle Measures," Computers Chem. Engng, 21, 6, 661-673, 1997.

Raghuraj R., Bhushan M., and Rengaswamy R., "Locating Sensors in Complex Chemical Plants Based on Fault Diagnostic Observability Criteria," AIChE Journal, 45, 2, 310-322, 1999.

Ranaweera D. K., "Comparison of neural network models for fault diagnosis of power systems," Electric Power Systems Research, 29, 2, 99-104, 1994.

Rengaswamy R., Mylaraswamy D., Årzén K. E., and Venkatasubramanian V., "A comparison of model-based and neural network-based diagnosis methods," Engineering Applications of Artificial Intelligence, 14, 6, 805-818, 2001.

Rigdon S. E., "A double-integral equation for the in-control average run length of a multivariate exponentially weighted moving average control chart," Statistics and Probability Letters, 24, 365–73, 1995.

Rissanen J., "Modeling by Shortest Data Description," Automatica, 14, 465-471, 1978.

Romagnoli J. M. and Sanchez M. C., Data Reconciliation and Reconciliation for Chemical Process Operations, Academic Press, San Diego, 2000.

Russell E., Chiang L. H., and Braatz R. D., Data Driven Methods for Fault Detection and Diagnosis in Chemical Processes, Springer, 2000.

Sanchez M. and Romagnoli J. M., "Comparative Analysis of Identification/Bias Estimation Techniques," AADECA'94, 14th National Symposium Automatic Control, 1994.

Sanchez M. and Romagnoli J. M., "Use of Orthogonal Transformations in Data Classification and Reconciliation," Computers Chem. Engng, 20, 5, 483-493, 1996.

Savage C., "Session on Generation IV Nuclear Energy Systems: Roadmap and Concepts", ANS Transactions, Milwaukee, WI, June 2001.

Simani S. and Fantuzzi C., "Fault diagnosis in power plant using neural networks," Information Sciences, 127, 3-4, 125-136, 2000.

Smith E. M., Thermal Design of Heat Exchangers, John Wiley, New York, 1996.

Sweeney F. J., Upadhyaya B. R., and Shieh D. J., "In-Core Coolant Flow Monitoring of Pressurized Water Reactors Using Temperature and Neutron Noise," Nuclear Engineering and Design, 89, 101-106, 1985.

Shieh D. J., Upadhyaya B. R., and Sweeney F. J., "Application of Noise Analysis Technique for Monitoring the Moderator Temperature Coefficient of Reactivity in Pressurized Water Reactors," Nuclear Engineering and Design, 95, 1, 14-21, 1988.

Singer R. M., Gross K. C., Herzog J. P., King R. W., and Wegerich S. W., "Model Based Nuclear Power Plant Monitoring and Fault Detection: Theoretical Foundations," Proc. 9th Intl. Conf. On Intelligent Systems Applications to Power Systems, Seoul, Korea, 1996.

Svein S. and Øivind Berg, "Data reconciliation and fault detection by means of plant-wide mass and energy balances," Progress in Nuclear Technology, 43, 97-104, 2003.

Takane Y. and Hunter A. A., "Constrained Principal Component Analysis: A Compreshensive Theory," Applied Algebra in Engineering, Communication, and Computing, 12, 391-419, 2001.

Upadhyaya B. R., Kitamura M., and Kerlin T. W., "Multivariate Signal Analysis Algorithms for Process Monitoring and Parameter Estimation in Nuclear Power Reactors," Annals of Nuclear Energy, 7, 1-11, 1980.

Upadhyaya B. R. and Kitamura M., "Stability Monitoring of Boiling Water Reactors by Time Series Analysis of Neutron Noise," Nuclear Science and Engineering, 77, 4, 480-492, 1981.

Upadhyaya B. R. and Skorska M., "Sensor Fault Analysis Using Decision Theory and Data Driven Modeling of Pressurized Water Reactor Systems," Nuclear Technology, 64, 70-77, 1984.

Upadhyaya B. R., "Sensor Fault Detection and Estimation," Nuclear Safety, 26 (1), 32-43, 1985.

Upadhyaya, B. R., Wolvaardt F., and Glockler O., An Integrated Approach for Sensor Failure Detection in Dynamic Processes, Research Report prepared for the Measurement and Control Engineering Center, University of Tennessee, Report No. NE-MCEC-BRU-87-01, March 1987.

Upadhyaya B. R. et al., Development and Testing of an Integrated Signal Validation System for Nuclear Power Plants, Volumes 1, 2, 3, Final Report prepared for the U.S. Department of Energy by The University of Tennessee, DOE/NE/37959-034,35,36, September 1989.

Upadhyaya B. R. and Eryurek E., "Application of Neural Networks for Sensor Validation and Plant Monitoring," Nuclear Technology, 97, 2, 170-176, 1992.

Upadhyaya B. R. and Ferreira P. B. "On-Line Fault Monitoring and Isolation of Field Devices Using Group Method of Data Handling," Proc. MARCON 99, Vol. 2, pp. 79.01-79.15, May 1999.

Upadhyaya B. R. and Kaistha K., "Incipient Fault Detection and Isolation of Field Devices in Nuclear Power Systems using Principal Component Analysis," Nuclear Technology, 136, 2, 221-230, 2001.

Upadhyaya B. R., Zhao K., and Lu B., "Fault Monitoring of Nuclear Power Plant Sensors and Field Devices," Progress in Nuclear Technology, 43, 1-4, 337-342, 2003.

Upadhyaya B. R. and Lu B., "Data Mining for Monitoring Plant Devices Using GMDH and Pattern Classification," Chapter in Statistical Data Mining and Knowledge Discovery, (Ed) H. Bozdogan, 269-279, Chapman & Hall/CRC, Boca Raton, 2004.

Valle S., Li W., and Qin S. J., "Selection of the Number of Principal Components: The Variance of the Reconstruction Error Criterion with a Comparison to Other Methods," Ind. Eng. Chem. Res., 38, 4389-4401, 1999.

Van Overschee P. and De Moor B., "A Unifying Theorem for Three Subspace System Identification Algorithms," Automatica, Special Issue on Trends in System Identification, 31, 12, 1853-1864, 1995.

Van Overschee P. and De Moor B., Subspace Identification for Linear Systems: Theory, Implementation, and Applications, Kluwer Academic Publishers, 1996.

Venkatasubramanian V. and Chan K., "A Neural Network Methodology for Process Fault Diagnosis," AIChE Journal, 35, 12, 1993-2002, 1989.

Venkatasubramanian V., and Cvaidyanathan R., and Yamamoto Y., "Process Fault Detection and Diagnosis using Neural Networks I: Steady State Processes," Computers and Chemical Engineering, 14, 7, 699-712, 1990.

Venkatasubramanian V., Rengaswamy R., Yin K., and Kavuri S. N., "A Review of Process Fault Detection and Diagnosis Part I: Quantitative Model Based Methods," Computers and Chemical Engineering, 27, 293-311,2003a.

Venkatasubramanian V., Rengaswamy R., Kavuri S. N., "A Review of Process Fault Detection and Diagnosis Part II: Qualitative models and search strategies," Computers and Chemical Engineering, 27, 313-326,2003b.

Venkatasubramanian V., Rengaswamy R., Kavuri S. N., and Yin K. "A Review of Process Fault Detection and Diagnosis Part III: Process History Based Methods," Computers and Chemical Engineering, 27, 327-346,2003c.

Wang H. and Song Z., "Statistical Process Monitoring using Improved PCA with Optimized Sensor Locations," Journal of Process Control, 12, 735-744, 2002.

Wang W., Jiang Y., Lu L., and Wei Y., "A Novel Encoding Water Level Monitor System During and After LOCAs in a Nuclear Heating Reactor," Nuclear Engineering and Design, 179, 275-280, 1998.

Watanabe K., Matsura I., Abe M., Kubota M., Himmelblau D. M., "Incipient Fault Diagnosis of Chemical Processes via Artificial Neural Networks," AIChE Journal, 35, 11, 1803-1812, 1989.

Westinghouse, IRIS Base Input Deck and Steady State Qualification for RELAP 5 MOD3.3, 2002.

Willsky A. S. and Jones H. L., "A Generalized Likelihood Ratio Approach to the Detection and Estimation of Jumps in Linear Systems," IEEE Trans. Automat. Contr. AC-21, 108-121, 1976.

Wold S., "Cross validation estimation of the number of components in factor and principal component analysis," Technometrics, 20 , 397-406,1978.

Wold S., Ruhe A., Wold H., and Dunn W., "The collinearity Problem in Linear Regression: The Partial Least Squares Approach to Generalized Inverses," SIAM Journal of Science Statistical Computer, 5, 735-743, 1984.

Wold S., Esbebsen K., and Geladi P., "Principal Component Analysis," Chemometrics Intelligent Lab. Systems, 2, 37-52, 1987.

Wuennengerg J., Observer based Fault Detection in Dynamic System, Ph.D. Dissertation, University of Duisburg, Germany, 1990.

Yoon S. and MacGregor J. F., "Fault Diagnosis with Multivariate Statistical Models Part I: using Steady State Fault Signatures," Journal of Process Control, 11, 387-400, 2001.

Zhao K., Development of a Data Driven Multiple Observers and Digraph Approach for Fault Detection and Isolation of Nuclear Power Plant Sensors and Field Devices, M.S. Thesis, The University of Tennessee, Knoxville, 2002.

Appendices

Appendix 1 Matlab Code for HCSG Steady State Simulation

```
clear all;
close all;
Tmax = 300;
%Number of tubes=655;
N =655; N0=8;
% Tube inner diameter=13.24mm
Ri_thermal=13.24/2*1.0E-3;
% Tube outside diameter=17.46mm
Ro_thermal=17.46/2*1.0E-3;
%Tube inside flow area;
Ri_hydraulic=Ri_thermal;
%Internal shell external diameter Di=0.61 m;
Di=0.61;
%External shell internal diameter Dt=1.62m
Do=1.62;
%Radial pitch=25mm;
t=25*1.0E-3;
%Total shell side projected area
shadow=1.0;
Ap_total=1/4*pi*(Do^2-Di^2)*(1-Ro_thermal*2/t)*shadow;
Ap=Ap_total/N;
%Shell side hydraulic radius=2*flow area/wetting perimeter
%Wetting area
Peri_wet=N*2*pi*Ro_thermal;
Ro_hydraulic=2*Ap_total/Peri_wet;
%Tube side hydraulic dimater
Ri_hydraulic=Ri_thermal;
%Flow area on the secondary side;
As=pi*(Ri_hydraulic^2);
%Cross section for the tube;
Aw=pi*(Ro_thermal^2-Ri_thermal^2);
%Tube length
Lt=32;
%Flow rate on the primary side=4707/8kg/s;
Wp=4707/N/N0;
%Flow rate on the secondary side=502.8kg/s;
Ws=502.8/N/N0*1.00;
% Inlet temperature on the primary side
Tpin=328.4+273;
%Primary system outlet temperature
Tpout=292+273;
%Feed water temperature;
Tfw=224+273;
%Steam outlet temperature;
Tsout=317+273;
%Geometric tube radius
Ri=Ri_thermal;
Ro=Ro_thermal;
T100=[];
T200=[];
P100=[];
P200=[];
H100=[];
H200=[];
Hall=[];
Ltube=[];
XX=[];
Kw=16.0;  %W/m/K
%Pressure on the secondary side
Ps0=5.8*1.01325;
%Ps0=6.0*1.01325;
deltaPs=0.296;
Ps=Ps0+deltaPs;
%Pressure on the primary side
Pa0=15.52;
```

```
deltaPa=0.072;
Pa=Pa0+deltaPa;
scwater(Pa,Ps);
load data1;
HH1=dxxx(:,1);
TT1=dxxx(:,2);
load data2;
HH2=dyyy(:,1);
TT2=dyyy(:,2);
%%%%%%%%%%%%%%%%%%%%To determine the subcooled boiling length%%%%%%%%%%%%%%%%%%%%%%%%%%
P1in=Pa;
P2in=Ps;
T2in=Tfw;
T1in=Tpout;
[P1sat,H1in,Cp1in,rho1in]=hsub(P1in,T1in);
[P2sat,H2in,Cp2in,rho2in]=hsub(P2in,T2in);
%%%%%%%%%%iterate till saturated temperature is reached%%%%%%%%%%%%%%%%%%%%%%%%%%%%%%%%%%%%
i=1;
deltaz=0.03;
Lsub=0.0;
T1sub(1)=T1in;
T2sub(1)=T2in;
P1sub(1)=P1in;
P2sub(1)=P2in;
Xsub(1)=0.0;
[Tsat,dum1,dum2,dum3,dum4,dum5,dum6,dum7,dum8]=hsat(P2in);
while abs(T2sub(i)-Tsat)/Tsat >0.001
[T1out,T2out,T1avg,T2avg,P1out,P2out,P1avg,P2avg,h1,h2,Unew,H1out,H2out]=itersub0_new(T1in,T2in,H1in,H2in,P1in,P2in,Wp,
Ws,deltaz,...
Kw,Ri_thermal,Ro_thermal,Ri_hydraulic,Ro_hydraulic,Ap,As);
T1sub(i+1)=T1out;
T2sub(i+1)=T2out;
P1sub(i+1)=P1out;
P2sub(i+1)=P2out;
P1asub(i+1)=P1avg;
P2asub(i+1)=P2avg;
h1sub(i+1)=h1;
h2sub(i+1)=h2;
Usub(i+1)=Unew;
Xsub(i+1)=0.0;
LLsub(i+1)=Lsub;
T1in=T1out;
T2in=T2out;
P1in=P1out;
P2in=P2out;
H1in=H1out;
H2in=H2out;
i=i+1;
Lsub=deltaz+Lsub;
end;
fprintf('Subcooled heat transfer coefficient on the primary side===%f(BTU/hr/ft**2)\n',h1*0.1761);
fprintf('Subcooled heat transfer coefficient on the seconday side===%f(BTU/hr/ft**2)\n',h2*0.1761);
fprintf('Temperature on the primary side===%f(C)\n',T1out-273);
fprintf('Temperature on the secondary side===%f(C)\n',T2out-273);
fprintf('Subcooled boiling length===%f(m)\n',Lsub);
Ltube=[Ltube,LLsub(2:end)];
T100=[T100,T1sub(2:end)];
T200=[T200,T2sub(2:end)];
P100=[P100,P1sub(2:end)];
P200=[P200,P2sub(2:end)];
H100=[H100,h1sub(2:end)];
H200=[H200,h2sub(2:end)];
Hall=[Hall,Usub(2:end)];
XX=[XX,Xsub(2:end)];

%%%%%%%%%%%%%%%%%%Prepare initial data for satuarated region calculation%%%%%%%%%%%%
[Tsat,h2f,h2g,k2f,k2g,mu2f,mu2g,Prf,Prg]=hsat(P2in);
Tp0=T1sub(end);
```

```
Ts0=Tsat;
hp0=h1sub(end);
Usub_end=Usub(end);
%%%%%%%%%%%%%%%%%%%To determine the saturated boiling length%%%%%%%%%%%%%%%%%%%%%%%%%
hp=hp0;
Tpsat=Tp0;
hsold=h2sub(end);
U0old=8888;
U0new=9999;
hsnew=hsold*1.25;
while abs((U0new-U0old)/U0old > 0.01) | abs((hsnew-hsold)/hsold > 0.01)
a=Ro/Kw*log(Ro/Ri)+1/hp0;
b=Ro/Ri;
A=(exp(Ps*1.0E6/8.69E6)/0.02253);
c=-(A^2)*Ro/Ri*(Tpsat-Tsat);
hsold=(-b+(b^2-4*a*c)^0.5)/(2*a);
a1=Ro/(Ri*hsold);
b1=Ro/Kw*log(Ro/Ri);
c1=1/hp;
U0old=1/(a1+b1+c1);
%Compute Hfg
[dum,Hsf,Hsg]=hsat(Ps);
Hfg=Hsg-Hsf;
[dum1,dum2,Cpp,rhop]=hsub(Pa,Tpsat);
B=Ws*Hfg/(Wp*Cpp);
deltaT=Tpsat-Tsat;
G=Ws/(As);
De=2*Ri;
R=0.15*Hfg*(De^(-0.1))*G^0.51;
CHF=(Ro/Ri*U0old*(deltaT+B))/(1+Ro*B/(Ri*R)*U0old);
xi=1-CHF/R;
Tpdryout=Tpsat+Ws/(Wp*Cpp)*xi*Hfg;
a=Ro/Kw*log(Ro/Ri)+1/hp0;
b=Ro/Ri;
A=(exp(Ps*1.0E6/8.69E6)/0.02253);
c=-(A^2)*Ro/Ri*(Tpsat-Tsat);
hsnew=(-b+(b^2-4*a*c)^0.5)/(2*a);
a1=Ro/(Ri*hsnew);
b1=Ro/Kw*log(Ro/Ri);
c1=1/hp;
U0new=1/(a1+b1+c1);
end;
fprintf('Saturated heat transfer coefficient on the seconday side===%f(BTU/hr/ft**2)\n'...
,hsnew*0.1761);
fprintf('Dryout temperature on the primary side===%f(C)\n', Tpdryout-273);
fprintf('Dryout quality on the secondary side===%f\n', xi);
U0avg=(U0new+Usub_end)/2;
Lbavg=Wp*Cpp/(2*pi*Ro*U0avg)*log((Tpdryout-Tsat)/(Tp0-Tsat));
fprintf('Average boiling length===%f(m)\n', Lbavg);
%%%%%%%%%%%%%%%%%%%
```

```
P2sat(1)=P2in;
h1sat(1)=H100(end);
h2sat(2)=H200(end);
Xsat(1)=0.0;
X(1)=0.0;
Xin=0.0;
while (X(i) < xi)

[T1out,X2out,T1avg,T2avg,P1out,P2out,P1avg,P2avg,h1,h2,Unew,H1out,H2out]=...
itersat0_new(T1in,H1in,H2in,Xin,P1in,P2in,Wp,Ws,deltaz,Kw,Ri_thermal,Ro_thermal,Ri_hydraulic,Ro_hydraulic,Ap,As);

T1sat(i+1)=T1out;
T2sat(i+1)=Tsat;
Xsat(i+1)=X2out;
X(i+1)=X2out;
Xin=X2out;
P11sat(i+1)=P1out;
P22sat(i+1)=P2out;
h1sat(i+1)=h1;
h2sat(i+1)=h2;
Usat(i+1)=Unew;
LLsat(i+1)=Lsat;
HH1(i+1)=H1out;
HH2(i+1)=H2out;
T1in=T1out;
T2in=T2out;
P1in=P1out;
P2in=P2out;
H1in=H1out;
H2in=H2out;
i=i+1;
Lsat=deltaz+Lsat;
end;
fprintf('X2out==%f,Lsat==%f T1out=%f h2=%f P2out=%f\n',X2out,Lsat,T1out,h2,P2out);
Ltube1=Ltube(end);
Ltube2=LLsat+Ltube1;
Ltube=[Ltube,Ltube2];
T100=[T100,T1sat];
T200=[T200,T2sat];
P200=[P200,P22sat];
H100=[H100,h1sat];
H200=[H200,h2sat];
Hall=[Hall,Usat];
XX=[XX,Xsat];
%%%%%%%%%%%%%%%To compute the temperature profile in the superheated region%%%%%%%%%%%%%
P1in=Pa;
P2in=P22sat(end);
T1in=T100(end);
T2in=T200(end);
nss=50;
Lss=Lt-Ltube(end);
deltaz=Lss/nss;
%%%%%%%%%iterate till saturated temperature is reached%%%%%%%%%
i=1;
T1ss(1)=T1in;
T2ss(1)=T2in;
P1ss(1)=P1in;
P2ss(1)=P2in;
H11sg(1)=H100(end);
H22sg(1)=H200(end);
Xss=1.0;
Length=0.0;
[P1sat,H1in,Cp1in,rho1in]=hsub(P1in,T1in);
[dum,H2in,Cp2in,vsin]=hsh(P2in,T2in);
%H1in=HH1(end);
%H2in=HH2(end);
while Length<Lss
```

```
[T1out,T2out,T1avg,T2avg,P1out,P2out,P1avg,P2avg,h1,h2,Unew,H1out,H2out]=iterss0_new(T1in,T2in,H1in,H2in,P1in,P2in,Wp,W
s,deltaz,...
Kw,Ri_thermal,Ro_thermal,Ri_hydraulic,Ro_hydraulic,Ap,As);
T1ss(i+1)=T1out;
T2ss(i+1)=T2out;
P1ss(i+1)=P1out;
P2ss(i+1)=P2out;
Xss(i+1)=1.0;
H1in=H1out;
H2in=H2out;
P1ssavg(i+1)=P1avg;
P2ssavg(i+1)=P2avg;
T1in=T1out;
T2in=T2out;
P1in=P1out;
P2in=P2out;
Lssg(i+1)=deltaz;
H11sg(i+1)=h1;
H22sg(i+1)=h2;
Uass(i+1)=Unew;
i=i+1;
Length=deltaz+Length;
end;
fprintf('Length==%f T1out=%f T2out=%f P2out=%f\n',Length,T1out,T2out,P2out);
Ltube1=Ltube(end);
Ltube2=cumsum(Lssg)+Ltube1;
Ltube=[Ltube,Ltube2];
T100=[T100,T1ss];
T200=[T200,T2ss];
P200=[P200,P2ss];
H100=[H100,H11sg];
H200=[H200,H22sg];
Hall=[Hall,Uass];
XX=[XX,Xss];
fprintf('Superheated heat transfer coefficient on the primary side===%f(BTU/hr/ft**2)\n',H11sg(i)*0.1761);
fprintf('Superheated heat transfer coefficient on the seconday side===%f(BTU/hr/ft**2)\n',H22sg(i)*0.1761);
fprintf('Temperature on the primary side===%f(C)\n',T1ss(i)-273);
fprintf('Temperature on the secondary side===%f(C)\n',T2ss(i)-273);
fprintf('Superheated boiling length===%f(m)\n',Lss);

figure;
T11=T100-273;
T22=T200-273;
x1=plot(Ltube(1:10:end),T11(1:10:end),'marker','s','markersize',4,...
        'markeredgecolor','b','markerfacecolor',[.6 0 .6],...
        'linestyle','--','color','r','linewidth',2);
hold on;
x2=plot(Ltube(1:10:end),T22(1:10:end),'marker','v','markersize',4,...
        'markeredgecolor','b','markerfacecolor',[.6 0 .6],...
        'linestyle','-.','color','r','linewidth',2);
xlabel('Tube length(m)');
ylabel('Temperature(C)');
grid on;
title('Fluid temperature versus tube length');
hold off;
legend([x1,x2],'Primary tempearture','Secondary tempearture');
figure(2);
x1=plot(Ltube(1:10:end),H100(1:10:end)*0.1761,'marker','s','markersize',4,...
        'markeredgecolor','b','markerfacecolor',[.6 0 .6],...
        'linestyle','--','color','r','linewidth',2);
hold on;
x2=plot(Ltube(1:10:end),H200(1:10:end)*0.1761,'marker','v','markersize',4,...
        'markeredgecolor','b','markerfacecolor',[.6 0 .6],...
        'linestyle','-.','color','r','linewidth',2);
xlabel('Tube length(m)');
ylabel('Heat Transfer Coefficient(BTU/Hr/ft**2)');
grid on;
title('Heat transfer coefficient versus tube length');
```

```
hold off;
legend([x1,x2],'Primary side','Secondary side');
grid on;

figure(3);
x1=plot(Ltube(1:10:end),P200(1:10:end)-P200(end),'marker','s','markersize',4,...
            'markeredgecolor','b','markerfacecolor',[.6 0 .6],...
            'linestyle','--','color','r','linewidth',2);
xlabel('Tube length(m)');
ylabel('Pressure Drop(Mpa)');
grid on;
title('Pressure drop versus tube length on the seconsary side');
grid on;

figure(4);
x1=plot(Ltube(1:10:end),XX(1:10:end),'marker','s','markersize',4,...
            'markeredgecolor','b','markerfacecolor',[.6 0 .6],...
            'linestyle','--','color','r','linewidth',2);
xlabel('Tube length(m)');
ylabel('Steam Quality');
grid on;
title('Steam quality versus tube length');
grid on;
```

Appendix 2 Matlab Code for HCSG Transient Simulation

```
close all;
clear all;
Tmax = 300;
JJ=778.16; %BTU/ft/lbf;
Fudge1=1.0;
Fudge2=1.0;
%from mm to ft;
c1=0.1*0.3937/12;
%conversion from kg to lbm;
c2=1/0.4536;
%Number of tubes=820;
N =655;
% Tube inner diameter=13.24mm
Ri_thermal=13.24/2*c1;
% Tube outside diameter=17.46mm
Ro_thermal=17.46/2*c1;
% Inlet temperature on the primary side
Tpin=1.8*328.4+32;

%Tube inside flow area;
Ri_hydraulic=Ri_thermal;
As=pi*Ri_hydraulic^2;

%Internal shell external diameter Di=0.61 m;
Di=0.61*1000*c1;
%External shell internal diameter Dt=1.62m
Do=1.62*1000*c1;
%Radial pitch=25mm;
t=25*c1;
%Total shell side projected area
Ap_total=1/4*pi*(Do^2-Di^2)*(1-Ro_thermal*2/t);
%Shell side hydraulic radius=2*flow area/wetting perimeter
%Wetting area
Peri_wet=N*2*pi*Ro_thermal;
Ro_hydraulic=2*Ap_total/Peri_wet;
Ap=pi*Ro_hydraulic^2;

%Tube side hydraulic dimater
Ri_hydraulic=Ri_thermal;
%Flow area on the secondary side;
As=pi*(Ri_hydraulic^2);
%Cross section for the tube;
Aw=pi*(Ro_thermal^2-Ri_thermal^2);

%Specific heat capacity;
Cpp=1.3355;
Cpw=0.109;
%Cps=1.0185;
Cpfw=1.122;
```

```
Cpsc=1.122;

%Density lbm/ft**3
rhop=44.75;
rhow=526.0;
%rhos=1.876;
rhoavg=8.86; %for entire boiling region;
rhofw=51.71;
rhof=46.91; %for boiling water
rhosc=(rhofw+rhof)/2;


Ps=5.8;
Ps=Ps; Ts=(280+318)/2+273;
[dum,dum,Cps,vss]=hsh(Ps,Ts);
Cps=Cps*9.4783E-4/(2.2046*1.8);
rhos=1/vss*0.06243;

%Initial heat transfer coefficient

Rii=Ri_thermal;
Roo=Ro_thermal;
ccc=0.1761;

Kw=(10.1924/3600)*1.0;
hp=21000*ccc/3600.0;
hs=8500*ccc/3600.0;
hsc=16000*ccc/3600.0;
hb=55000*ccc/3600.0;

hpw=Kw*hp/(Kw+hp*Roo*(0.5+log(Roo/Rii)/(1-(Roo/Rii)^2)));
hws=Kw*hs/(Kw+hs*Rii*(log(Rii/Roo)/(((Rii/Roo)^2)-1)-0.5));
hwsc=Kw*hsc/(Kw+hsc*Rii*(log(Rii/Roo)/(((Rii/Roo)^2)-1)-0.5));
hwb=Kw*hb/(Kw+hb*Rii*(log(Rii/Roo)/(((Rii/Roo)^2)-1)-0.5));


%Feed water temperature=224C;
Tfw=1.8*224+32;

%Tube length
Lt=32*3.2808; %total bundle length
Lb=21.5*3.2808;  %this value is fixed to determine accurate heat transfer coefficient in this region.
Lsc=4.5*3.2808; %this value is malipulated given that hwsc is known.
Ls=Lt-Lb-Lsc;
%%%%%Heating circumference%%%%%
Ri=Ri_thermal;
Ro=Ro_thermal;
Uwb=2*pi*Ri;
Uws=2*pi*Ri;
Uwsc=2*pi*Ri;

Ptable=5.0:0.1:6.0;
```

```
Tsavg=(280+318)/2+273;
Ttable=[];
HfgTable=[];
hsTable=[];
for PPP=5.0:0.1:6.0
[Tsat,hf,hg,kf,kg,muf,mug,Prf,Prg]=hsat(PPP);
[dum,hss,dum,dum]=hsh(PPP,Tsavg);
Ttable=[Ttable,Tsat];
hsTable=[hsTable,hss];
HfgTable=[HfgTable,hg-hf];
end;
c3=1000/6.895;
Ptable=Ptable*c3; %Pressure;
Ttable=(Ttable-273)*1.8+32; %Saturated temperature;
cc1=9.4783E-4/2.2046;
HfgTable=HfgTable*cc1;
hsTable=hsTable*cc1;
a=POLYFIT(Ptable,Ttable,1);
X5=a(2);K5=a(1);
b=POLYFIT(Ptable,HfgTable,1);
X4=b(2); K4=b(1);
c=POLYFIT(Ptable,hsTable,1);
dHsdPs=c(1);

N0=8;
%Flow rate on the primary side=560.46kg/s;
Wp=4707*c2/N/N0*Fudge1;
Wp0=Wp;
Wp1=Wp;
Wp2=Wp;
Wp3=Wp;
Wp4=Wp;
Wp5=Wp;

Fraction=1.0;
%Flow rate on the secondary side=62.85kg/s;
AdjustFactor=1.0;
Wsec=502.8*c2/N0/N*Fraction*AdjustFactor;
Ws=Wsec;
Wb=Wsec;
Wfw=Wsec;
Wsg=Wsec;
Ws0=Wsec;
Ri=Ri_thermal;
Ro=Ro_thermal;


%Preparing data matrix;
a1=Ap*Cpp*rhop/2;   %primary side;
a2=Aw*Cpw*rhow/2;   %metal;
a3=As*Cps*rhos/2;   %secondary side;
a4=hpw*pi*Ro/a1;
```

```
a51=Cpp*Wp0/a1;
a52=Cpp*Wp1/a1;
a53=Cpp*Wp2/a1;
a54=Cpp*Wp3/a1;
a55=Cpp*Wp4/a1;
a56=Cpp*Wp5/a1;

a6=hpw*pi*Ro/a2;
a7=hwb*pi*Ri/a2;
a8=hws*pi*Ri/a2;
a9=hws*pi*Ri/a3;

a11=As*Cpsc*rhosc/2; %
a12=hwsc*pi*Ri/a2; %
a13=hwsc*pi*Ri/a11; %
a14=144/(JJ*Cpp*rhop);
%dHsdPs=(1245.9-1251.8)/50.0;
a15=144/(JJ*Cps*rhos)-dHsdPs/Cps;
dHscdPsc=(430.47-430.19)/500;
a16=144/(JJ*Cpsc*rhosc)-dHscdPsc/rhosc;

%Saturated temperature for 7Mpa
c3=1000/6.895;
Ps=5.8*c3;
deltaP=0.2;
Psat=(5.8+deltaP)*c3;
%X5=402.94; K5=0.14;  %Tsat~Psat
Tsat=X5+K5*Psat;
%Tsat=546.6;  %Exit temperature=317C and Degree of superheat is 43.4;
Hfg=X4+K4*Psat;
sim('htsgss');

a99=hws*pi*Ri/Cps;
a88=2*Wfw/As/rhosc;
a77=2/As/rhosc;
Ksc=(1/0.02152-1/0.02145)/20;
Kb=0.00552445;
dTsatdP=K5;

Z=0.76634; % 570K, 60atm;
R=4.55465*3.5314455E-5*14.696006/(5/9*2.2046223E-3); %cm^3atm/deg*g
Ct=Ws/Ps;
Ktb=1.5428e-004;

Pset=5.8*c3;

%%%%%%%%%%%%%%%%%%%%%%%%%%%%%Generate Fault Free Data%  %%%%%%%%%%%%%%%%%%%%%%
NormData=[];
PsBias=0.0;
WsBias=0.0;
WfwBias=0.0;
```

```
TclBiasPer=0.0;
Cs0=Ws/Ps;
CsInc=1.0;
Pcor=1.0;
tout=[];
htsgdata=[];
TpinInc=1.0;
TfwInc=0.0;
WfwInc=0.0;
WsInc=0.0;
WsPer=0.0;

sim('HCSG_Transient');
NormData=htsgdata;
figure(1);
mg=20;
mmm1=find(tout>500);
mmm=mmm1(1);
aaa.time=tout(mmm+1:mg:end)-tout(mmm);
aaa.Tstm=(NormData(mmm+1:mg:end,6)-32)/1.8;
aaa.Tcold=(NormData(mmm+1:mg:end,3)-32)/1.8;
aaa.Prs=NormData(mmm+1:mg:end,4)/145.038;
aaa.Lb=NormData(mmm+1:mg:end,7)*0.3048;
aaa.Lsc=NormData(mmm+1:mg:end,12)*0.3048;

NormData=[];
PsBias=0.0;
WsBias=0.0;
WfwBias=0.0;
TclBiasPer=0.0;
Pcor=1.0;
tout=[];
htsgdata=[];
TpinInc=0.0;
TfwInc=0.0;
WfwPer=0.01;
WfwInc=WfwPer*Wfw;
Cs0=Ws/Ps;
CsInc=1.0;
WsPer=0.0;
sim('HCSG_Transient');
NormData=htsgdata;
mmm1=find(tout>500);
mmm=mmm1(1);
bbb.time=tout(mmm+1:mg:end)-tout(mmm);
bbb.Tstm=(NormData(mmm+1:mg:end,6)-32)/1.8;
bbb.Tcold=(NormData(mmm+1:mg:end,3)-32)/1.8;
bbb.Prs=NormData(mmm+1:mg:end,4)/145.038;
bbb.Lb=NormData(mmm+1:mg:end,7)*0.3048;
bbb.Lsc=NormData(mmm+1:mg:end,12)*0.3048;

figure(1);
```

```
x1=plot(aaa.time,aaa.Tcold,'marker','s','markersize',3,...
            'markeredgecolor','b','markerfacecolor',[.6 0 .6],...
            'linestyle','--','color','r','linewidth',2);
hold on;
x2=plot(bbb.time,bbb.Tcold,'marker','v','markersize',3,...
            'markeredgecolor','b','markerfacecolor',[.6 0 .6],...
            'linestyle','-.','color','r','linewidth',2);
xlabel('time(sec)');
ylabel('cold leg temperature (C)');
grid on;
hold off;
legend([x1,x2],'hot leg temperature transient','feed water flow transient');

figure(2);
x1=plot(aaa.time,aaa.Tstm,'marker','s','markersize',3,...
            'markeredgecolor','b','markerfacecolor',[.6 0 .6],...
            'linestyle','--','color','r','linewidth',2);
hold on;
x2=plot(bbb.time,bbb.Tstm,'marker','v','markersize',3,...
            'markeredgecolor','b','markerfacecolor',[.6 0 .6],...
            'linestyle','-.','color','r','linewidth',2);
xlabel('time(sec)');
ylabel('steam outlet temperature (C)');
grid on;
hold off;
legend([x1,x2],'hot leg temperature transient','feed water flow transient');



figure(3);
x1=plot(aaa.time,aaa.Prs,'marker','s','markersize',3,...
            'markeredgecolor','b','markerfacecolor',[.6 0 .6],...
            'linestyle','--','color','r','linewidth',2);
hold on;
x2=plot(bbb.time,bbb.Prs,'marker','v','markersize',3,...
            'markeredgecolor','b','markerfacecolor',[.6 0 .6],...
            'linestyle','-.','color','r','linewidth',2);
xlabel('time(sec)');
ylabel('steam pressure (Mpa)');
grid on;
hold off;
legend([x1,x2],'hot leg temperature transient','feed water flow transient');
```

Appendix 3 Matlab Code for HCSG Bilinear Data Reconcilation

```
close all;
%%%
```

```
TTT7=[];
for Ttemp=T7_nominal-10:1:T7_nominal+10
 [mid,Htemp,mid,mid]=hsub(P7_nominal,Ttemp);
 HHH7=[HHH7,Htemp/1.0E6];
 TTT7=[TTT7,Ttemp];
end;
[Ch7,mid] = POLYFIT(TTT7,HHH7,1);

HHH1=[];
TTT1=[];
for Ttemp=T1_nominal-10:1:T1_nominal+10
 [mid,Htemp,mid,mid]=hsub(P1_nominal,Ttemp);
 HHH1=[HHH1,Htemp/1.0E6];
 TTT1=[TTT1,Ttemp];
end;
[Ch1,mid] = POLYFIT(TTT1,HHH1,1);

HHH6=[];
TTT6=[];
for Ttemp=T6_nominal-30:0.1:T6_nominal+30
 [mid,Htemp,mid,mid]=hsub(P1_nominal,Ttemp);
 HHH6=[HHH6,Htemp/1.0E6];
 TTT6=[TTT6,Ttemp];
end;
[Ch6,mid] = POLYFIT(TTT6,HHH6,1);

%%%
```

```
%theta={1,3,9}
%FU={W1,W3,W5,W6,W8,W10,W9,W11} Unmeasured flow
%V={2,4,5,6,8,10,11} enthalpy flow with temperature unmeasured


%Index    1   2   3   4
    xFM=[2   4   7  12];
    nFM=length(xFM);
%Index    1   2
    xf= [7  12];
    nxf=length(xf);
%Index    1   2   3
 xTheta= [1   3   9];
    nxTheta=length(xTheta);
%Index    1   2   3   4   5   6    7    8
   xFu= [1   3   5   6   8   9   10   11];
   nxFu=length(xFu);
%Index    1   2   3   4   5  6   7
    xv= [2   4   5   6   8  10  11];
   nxv=length(xv);
%%%neq1=number of enthaply balance equations
neq1=6;
O1=zeros(neq1,nFM);
B1=zeros(neq1,nxf);
B2=zeros(neq1,nxTheta);
B5=zeros(neq1,nxFu);
B3=zeros(neq1,nxv);
%%%neq2=number of mass balance equations
neq2=8;
E4=zeros(neq2,nFM);
E1=zeros(neq2,nxf);
E2=zeros(neq2,nxTheta);
E8=zeros(neq2,nxFu);
E3=zeros(neq2,nxv);


%Index    1   2   3   4
%    xFM=[2   4   7  12];
%    nFM=length(xFM);
%Index    1   2
%    xf= [7  12];
%    nxf=length(xf);


W11_Pred=[];
W9_Pred=[];
W11_brute=[];
W9_brute=[];
Q1_brute=[];
Q2_brute=[];
Q11=[];
Q22=[];
```

```
Est_Flow=[];
Est_Temp=[];
noise_Flow=0.01/3;
noise_temp=0.0025/3;
load iris_ss XmNormal XmFault X_nominal WsecInd1 WsecInd2;
ndata=150;
NormData=[];
for i=1:1:ndata
   temp=XmNormal(i,:);
   NormData=[NormData;temp];
end;
XmData=[NormData;XmFault];
Wsec1Data=[NormData(:,7)/2;WsecInd1];
Wsec2Data=[NormData(:,7)/2;WsecInd2];


%Index    1   2   3   4   5   6   7   8    9   10   11  12   13  14  15  16   17    18
%XmFault=[W1  T1  T3  T5  W6  T6  W7  T7  W12  T12  T11  T9  tT3 tT9 tT1  tT7 tT11 tT12];

%XmFault=XmData;
[ndata,mdata]=size(XmData);
ndata_n=ndata-50;
mmp=1;
XmData(ndata_n+1:ndata,mmp)=XmData(ndata_n+1:ndata,mmp)+ones(ndata-ndata_n,1).*X_nominal(mmp).*0.01;


DataRecon=[];
DataRecon1=[];

DataRaw=[];
%Index    1   2   3   4
%    xFM=[2   4   7  12];
%    nFM=length(xFM);


for itt=1:1:ndata
FlowData = XmData(itt,[1 5 7 9])';
FlowData([1,2])=FlowData([1,2])/2;
FlowData0= X_nominal([1 5 7 9])';
FlowData0([1,2])=FlowData0([1,2])/2;
FM=FlowData+noise_Flow*randn(4,1).*FlowData0;
TempData0=X_nominal([2,6,8,10]);

T1=XmData(itt,2)+noise_temp*randn(1).*TempData0(1);
T6=XmData(itt,6)+noise_temp*randn(1).*TempData0(2);
T7=XmData(itt,8)+noise_temp*randn(1).*TempData0(3);
T12=XmData(itt,10)+noise_temp*randn(1).*TempData0(4);

[mid,H10,Cpp,mid]=Hsub(P6_nominal,T1);
[mid,H60,Cpp,mid]=Hsub(P6_nominal,T6);
[mid,H70,Cpp,mid]=Hsub(P7_nominal,T7);
[mid,H120,mid,mid]=hsh(P12_nominal,T12);
```

```
H10=H10/1.0E6;
H60=H60/1.0E6;
H70=H70/1.0E6;
H120=H120/1.0E6;

%Index    1   2
%     xf= [7  12];
%     nxf=length(xf);

aa=  FM([3,4])'.*[H70 H120];
f=aa';


TempData0=X_nominal([3,12])
TT3=XmData(itt,3)+noise_temp*randn(1).*TempData0(1);
TT9=XmData(itt,12)+noise_temp*randn(1).*TempData0(2);;
[mid,H30,Cpp,mid]=Hsub(P6_nominal,TT3);
[mid,H90,mid,mid]=hsh(P12_nominal,TT9);
H30=H30/1.0E6;
H90=H90/1.0E6;


Qptot=aa(2)-aa(1);
Qp1=FM(1)*(H10-H30);
Qp2=Qptot-Qp1;
Flow9=Qp2/(H90-H70);
Flow11=FM(4)-Flow9;
W11_brute=[W11_brute;Flow11];
W9_brute=[W9_brute;Flow9];
Q1_brute=[Q1_brute;Qp1];
Q2_brute=[Q2_brute;Qp2];

H20=H10; H40=H10; H80=H70; H100=H70;  H50=H60;  H110=H120;


%Index    1   2   3   4
%     xFM=[2   4   7  12];
%Index    1   2
%     xf= [7  12];
%xTheta= [1   3   9];
%Index    1   2   3   4   5   6    7    8
   %Fu= [1   3   5   6   8   9   10   11];
%Index    1   2   3   4   5  6   7
   %xv= [2   4   5   6   8  10  11];
%%%neq1=number of enthaply balance equations


Hd=[H10 H30 H90];
%%%%%%%%%%%%%%%%%%%%%%%%%%%%%%%%%%%%%%%%%%%%Energy Balance Equations%%%%%%%%%%%%%%%%%%%%%%%%%%%%
%%%    [O B1 B2 B5 B3][FM f Theta Fu v]'=0.
%%   Constraint 1: W1dh1+h10*W1-v2-v4=0
          B2(1,1)=1;     B5(1,1)=H10;       B3(1,1)=-1; B3(1,2)=-1;
```

```
%%  Constraint 2: W3dh3+h30W3+v5-v6=0
        B2(2,2)=1;    B5(2,2)=H30;      B3(2,3)=1; B3(2,4)=-1;
%%  Constraint 3: f7- v8-v10=0
B1(3,1)=1;                          B3(3,5)=-1;B3(3,6)=-1;
%%  Constraint 4: f12-W9dh9-h90W9- v11=0
B1(4,2)=1;  B2(4,3)=-1;    B5(4,6)=-H90;    B3(4,7)=-1;
%%  Constraint 5: -W3dh3 -h30W3  +v2+v10-v11=0
        B2(5,2)=-1;     B5(5,2)=-H30;    B3(5,1)=1;B3(5,6)=1;B3(5,7)=-1;
%%  Constraint 6: -W9dh9 -h90W9  +v4+v8-v5=0
        B2(6,3)=-1;     B5(6,6)=-H90;    B3(6,2)=1;B3(6,5)=1;B3(6,3)=-1;

%%%%%%%%%%%%%%%%%%%%Mass Balance Equations%%%%%%%%%%%%%%%%%%%%
%%%   [E4 E1 E2 E8 E3][FM f Theta Fu v]'=0.
%Index   1   2   3   4
%    xFM=[2   4   7  12];
%Index   1   2   3   4   5   6    7    8
  %Fu= [1   3   5   6   8   9   10   11];

%%  Constraint 1: W1-W2-W4=0;
E4(1,1)=-1;  E4(1,2)=-1; E8(1,1)=1;
%%  Constraint 2: W2-W3=0;
E4(2,1)=1;              E8(2,2)=-1;
%%  Constraint 3: W4-W5=0;
E4(3,2)=1;              E8(3,3)=-1;

%%  Constraint 4: W6-W3-W5=0;
                E8(4,4)=1;  E8(4,2)=-1;  E8(4,3)=-1;

%%  Constraint 5: W12-W9-W11=0;
E4(5,4)=1;              E8(5,6)=-1; E8(5,8)=-1;
%%  Constraint 6: W10-W11=0;
                E8(6,7)=1;  E8(6,8)=-1;
%%  Constraint 7: W8-W9=0;
                E8(7,5)=1;  E8(7,6)=-1;
%%  Constraint 8: W7-W8-W10=0;
E4(8,3)=1;              E8(8,5)=-1;  E8(8,7)=-1;


%%%%%%%%%%%%%%%%%%%
```

```
[QB,RB,Ev]=qr(B33);
QB1=QB(:,1:rv);
RB1=RB(1:rv,1:rv);
RB2=RB(1:rv,rv+1:end);
QB2=QB(:,rv+1:end);
%%%  Define a new matrix D
D=QB2'*B22;
%%% QR decomposition of matrix D
rf=rank(D,1.0E-10);
[n,m]=size(D);
[QD,RD,EFu]=qr(D);
QD1=QD(:,1:rf);
RD1=RD(1:rf,1:rf);
RD2=RD(1:rf,rf+1:end);
QD2=QD(:,rf+1:end);
%%%  The process constraint equation is reduced to be as follows:
%%%  QD2'*QB2'*B11*t=QD2'*QB2'*e;
%%%
```

```
fprintf('The unmeasured flow is unobservable\n');
disp(uuu2);
RIF=inv(RD1)*RD2;
GGRIF=(abs(RIF)>1.0E-10);
ccc=any(GGRIF,2);
ind_obs=find(ccc==0);
ind_unobs=find(ccc~=0);

%%% fe=the number of determinable unmeasured flow rates.
fe=length(ind_obs);

fprintf('The observable umeasured flow is as follows\n');
uuu1=uuu(1:rf);
disp(uuu1(ind_obs));

if ~isempty(ind_obs);
FLow_Estimate=inv(RD1)*QD1'*QB2'*e-inv(RD1)*QD1'*QB2'*B11*t_estimate;
if norm(FLow_Estimate(ind_obs)-FLowE_old)<1.0E-10*norm(FLow_Estimate(ind_obs)) break; end;

  for i=1:1:length(xTheta)
    for j=1:1:length(ind_obs)
       if  xTheta(i)==uuu1(ind_obs(j))
      init_V(i)=FLow_Estimate(ind_obs(j));
       end;
    end;
  end;
 FLowE_old=FLow_Estimate(ind_obs);
else
break;
end;

end;



%      xFM=[2   4   7  12];
%xTheta= [1   3   9];

fprintf('The reconciled measured flow is\n');
FM_pred=FM+t_estimate(1:nFM);
f_pred=f+t_estimate(nFM+1:nxf+nFM);
Theta_pred=t_estimate(nFM+nxf+1:end);
Ind_Theta=uuu1(ind_obs);

ijk=0;
for inum=1:1:nxTheta
    icol=find(xTheta(inum)==Ind_Theta);
    if ~isempty(icol)
    ijk=ijk+1;
    Flow_Theta(ijk)=FLow_Estimate(icol);
    end;
end;
```

```
for iii=1:1:nFM
fprintf('iii=%d FM=%f\n',[xFM(iii),FM_pred(iii)]);
end;
fprintf('\n');



T_pred(1)= interp1(HHH7,TTT7,f_pred(1)/FM_pred(1));
T_pred(2)= interp1(HHH12,TTT12,f_pred(2)/FM_pred(2));

for jjj=1:1:nxf
fprintf('jjj=%d enthalpy=%f  temperature=%f\n',[xf(jjj),f_pred(jjj),T_pred(jjj)]);
end;

fprintf('The estimated flow is\n');
for iii=1:1:fe
fprintf('iii=%d flow=%f\n',[uuu1(ind_obs(iii)),FLow_Estimate(iii)]);
end;

fprintf('The reconciled temperature is as follows\n');
delta_d=Theta_pred./Flow_Theta';
Hd_pred=Hd'+delta_d;
Fd_pred=Flow_Theta';

%xTheta= [1   3   9];

Te_pred(1)=interp1(HHH1,TTT1,Hd_pred(1));
Te_pred(2)=interp1(HHH6,TTT6,Hd_pred(2));
Te_pred(3)=interp1(HHH12,TTT12,Hd_pred(3));
for iii=1:1:nxTheta
fprintf('iii=%d specific enthalpy=%f  temperature=%f\n',[xTheta(iii),Hd_pred(iii),Te_pred(iii)]);
end;

%%% Estimation of vector v.
%%%Reordering the observable and the unobservable mass flow rates.
Fud=FLow_Estimate;
xFud=uuu1(ind_obs);
xFui=[uuu1(ind_unobs);uuu2];
fe1=length(xFud);
fe2=length(xFui);
for inum=1:1:fe1
   icol=find(xFud(inum)==xFu);
   B2d(:,inum)=B22(:,icol);
end;

B2i=[];
for inum=1:1:fe2
   icol=find(xFui(inum)==xFu);
   B2i(:,inum)=B22(:,icol);
end;
```

```
vvv=Ev'*xv';
vvv1=vvv(1:1:rv);
vvv2=vvv(rv+1:end);

fprintf(' The undeterminable variables v include\n');
disp(vvv2);

RIV=inv(RB1)*RB2;
RIFi=inv(RB1)*QB1'*B2i;
vf=inv(RB1)*QB1'*e-inv(RB1)*QB1'*B11*t_estimate-inv(RB1)*QB1'*B2d*Fud;

if isempty(RIV)
   ccc1=zeros(length(vvv1),1);
else
GGRIV=(abs(RIV)>1.0E-10);
ccc1=any(GGRIV,2);
end;
if isempty(RIFi)
   ccc2=zeros(length(vvv1),1);
else
GGRIFi=(abs(RIFi)>1.0E-10);
ccc2=any(GGRIFi,2);
end;

indv_obs=find(ccc1==0 & ccc2==0 );
indv_unobs=find(ccc1~=0 | ccc2~=0);
fprintf(' The determinable variables v are as follows\n');


Hv_pred(1)=vf(1)/FLow_Estimate(7);
Hv_pred(2)=vf(2)/FLow_Estimate(6);
Fv_pred=[FLow_Estimate(7);FLow_Estimate(6)];

Tv_pred(1)=interp1(HHH6,TTT6,Hv_pred(1));
Tv_pred(2)=interp1(HHH12,TTT12,Hv_pred(2));


% xTheta= [2   3   4   8   9  10];

%aaa=(Hd_pred(1)*Fd_pred(1)-Hd_pred(2)*Fd_pred(2))/(Hv_pred(2)*Fv_pred(2)-Hd_pred(6)*Fd_pred(6));
%bbb=(Hd_pred(3)*Fd_pred(3)-Hv_pred(1)*Fv_pred(1))/(Hd_pred(5)*Fd_pred(5)-Hd_pred(4)*Fd_pred(4));
aaa=(Hd_pred(1)*Fd_pred(1)-Hd_pred(2)*Fd_pred(2));
bbb=(Hd_pred(3)*Fd_pred(3)-Hv_pred(1)*Fv_pred(1));

Q11=[Q11,aaa];
Q22=[Q22,bbb];


for ill=1:1:length(indv_obs)
fprintf(' inum=%d enthalpy=%f specific enthalpy=%f temperature=%f\n',[vvv1(ill),vf(ill),Hv_pred(ill),Tv_pred(ill)]);
end;
fprintf(' The undeterminable variables v include\n');
```

```
disp(vvv1(indv_unobs));

rr(1)=f(1)-Hd_pred(1)*Fd_pred(1)-Hd_pred(3)*Fd_pred(3);
rr(2)=f(2)-Hd_pred(2)*Fd_pred(2)-vf(1);
rr(3)=f(4)-Hd_pred(5)*Fd_pred(5)-vf(2);
rr(4)=f(3)-Hd_pred(4)*Fd_pred(4)-Hd_pred(6)*Fd_pred(6);
rr(5)=(Hd_pred(1)*Fd_pred(1)-Hd_pred(2)*Fd_pred(2))-(Hv_pred(2)*Fv_pred(2)-Hd_pred(6)*Fd_pred(6));
rr(6)=(Hd_pred(3)*Fd_pred(3)-Hv_pred(1)*Fv_pred(1))-(Hd_pred(5)*Fd_pred(5)-Hd_pred(4)*Fd_pred(4));
fprintf(' The constrained residual for the energy equations\n');
fprintf(' %f  %f  %f  %f  %f  %f\n',rr);


%%%  Unmeasured tempeartures are determinable only if the mass flow is
%%%  measured or determinable and the enthalpy is determinable.
aaaa=FLow_Estimate(6);
bbbb=FLow_Estimate(1);
W11_Pred=[W11_Pred;aaaa];
W9_Pred=[W9_Pred;bbbb];
afl=[FM_pred',FLow_Estimate']
atemp=[T_pred,Te_pred,Tv_pred];
Est_Flow=[Est_Flow;afl];
Est_Temp=[Est_Temp;atemp];


tempd=[FM_pred',T_pred,Te_pred([2,5])];
DataRecon=[DataRecon;tempd];
tempd=[FM_pred',T_pred,Te_pred,aaa,bbb];
DataRecon1=[DataRecon1;tempd];

DataRaw=[DataRaw;[FM',T1,T6,T7,T12,TT3,TT9]];
end;


figure (1);
plot(W11_Pred(1:2:end),'r-');
hold on;
plot(W9_Pred(1:2:end),'b-');
hold on;
plot(W11_brute(1:2:end),'ro');
hold on;
plot(W9_brute(1:2:end),'bo');

figure (2);
plot(Q11,'r-')
hold on;
plot(Q1_brute,'ro')

hold on;
plot(Q22,'b-')
hold on;
plot(Q2_brute,'bo')
```

```
fprintf(' %d  %d %d   %d   %d %d %d   %d %d %d %d   %d\n',[xFM,uuu1(ind_obs)']);
for i=1:1:ndata
   fprintf(' %f  %f  %f   %f   %f  %f  %f   %f  %f  %f  %f   %f\n',Est_Flow(i,:));
end;

fprintf(' %d  %d %d   %d   %d %d %d   %d %d %d %d   %d\n',[xf,xTheta,vvv1']);

for i=1:1:ndata
   fprintf(' %f  %f  %f   %f   %f  %f  %f   %f  %f  %f  %f   %f\n',Est_Temp(i,:));
end;
```

Appendix 4 Matlab Code for HCSG linear Data Reconcilation

```
close all;
%%%%%%%%%            Data Generation for Simulation          %%%%%
%%Primary inlet pressure: 15.5Mpa
%%Primary inlet temperature:  328.5 C
%%Primary inlet flow rate:  563.0 kg/s
%%Primary outlet pressure: 15.5+0.072 Mpa
%%Primary outlet temperature:  292.2 C
%%Primary outlet flow rate: 563.0 kg/s
%%Secondary inlet feed water pressure: 5.8+0.296 Mpa
%%Secondary inlet feed water temperature: 224.0 C
%%Secondary inlet feed water flow rate: 62.85 kg/s
%%Secondary outlet steam pressure:  5.8Mpa
%%Secondary outlet steam temperature:  317.2C
%%Secondary outlet steam flow rate:  62.85 kg/s

W2_nominal=563.0;
T1_nominal=328.5;
T3_nominal=292.0;
T5_nominal=292.0;
W4_nominal=563.0;
T6_nominal=292.0;
W7_nominal=62.85*2.0;
T7_nominal=224.0;
W12_nominal=62.85*2.0;
T12_nominal=317.2;
P1_nominal=15.5;
P6_nominal=15.5+0.072;
P7_nominal=5.8+0.296;
P12_nominal=5.8;

%%%%%%%%%%%%%%% Adjust the data based on the given water/steam table %%%%%%%%%%%%
[mid,H12,mid,mid]=hsh(P12_nominal,T12_nominal);
[mid,H7,mid,mid]=Hsub(P7_nominal,T7_nominal);
[mid,H1,Cpp,mid]=Hsub(P1_nominal,T1_nominal);
[mid,H6,Cpp,mid]=Hsub(P6_nominal,T6_nominal);
H12=H12/1.0E6;
H7=H7/1.0E6;
H1=H1/1.0E6;
H6=H6/1.0E6;

W2_nominal=0.5*W12_nominal*(H12-H7)/(H1-H6);
W4_nominal=W2_nominal;
W1_nominal=2*W2_nominal;
W6_nominal=2*W2_nominal;
%%%%%%%%%%%%%%%     Compute the parameters needed for linearization        %%%%%%%%
HH=[];
TT=[];
for Ttemp=T12_nominal-10:1:T12_nominal+10
  [mid,Htemp,mid,mid]=hsh(P12_nominal,Ttemp);
  HH=[HH,Htemp/1.0E6];
```

```
 TT=[TT,Ttemp];
end;
[Ch12,mid] = POLYFIT(TT,HH,1);

HH=[];
TT=[];
for Ttemp=T7_nominal-10:1:T7_nominal+10
 [mid,Htemp,mid,mid]=hsub(P7_nominal,Ttemp);
 HH=[HH,Htemp/1.0E6];
 TT=[TT,Ttemp];
end;
[Ch7,mid] = POLYFIT(TT,HH,1);

HH=[];
TT=[];
for Ttemp=T1_nominal-10:1:T1_nominal+10
 [mid,Htemp,mid,mid]=hsub(P1_nominal,Ttemp);
 HH=[HH,Htemp/1.0E6];
 TT=[TT,Ttemp];
end;
[Ch1,mid] = POLYFIT(TT,HH,1);

HH=[];
TT=[];
for Ttemp=T6_nominal-10:1:T6_nominal+10
 [mid,Htemp,mid,mid]=hsub(P1_nominal,Ttemp);
 HH=[HH,Htemp/1.0E6];
 TT=[TT,Ttemp];
end;
[Ch6,mid] = POLYFIT(TT,HH,1);
%%%
```

```
xu=     [1  5   4   11  8   9   15   16   17   19   20   21   22  10];
n_xu=length(xu);

%%neq=number of equations.
neq=16;
b=zeros(neq,1);

%%initialization
A1=zeros(neq,n_xm);
A2=zeros(neq,n_xu);
%%%Constraint Equation 1:  W1=W2+W4
A1(1,1)=-1; A1(1,4)=-1;
A2(1,1)=1;
%%%Constraint Equation 2:  W2=W3
A1(2,1)=1; A2(2,2)=-1;
%%%Constraint Equation 3:  W4=W5
A1(3,4)=1; A2(3,6)=-1;
%%%Constraint Equation 4:  W6=W3+W5;
A2(4,4)=1;
A2(4,2)=-1; A2(4,6)=-1;
%%%Constraint Equation 5:  W7=W8+W10;
A1(5,6)=1;
A2(5,7)=-1; A2(5,10)=-1;
%%%Constraint Equation 6:  W8=W9;
A2(6,7)=1;
A2(6,9)=-1;
%%%Constraint Equation 7:  W10=W11;
A2(7,10)=1;
A2(7,12)=-1;
%%%Constraint Equation 8:  W12=W9+W11;
A1(8,9)=1;
A2(8,9)=-1; A2(8,12)=-1;
%%%Constraint Equation 9:  T1=T2;
A1(9,2)=1;
A2(9,3)=-1;
%%%Constraint Equation 10:  T1=T4;
A1(10,2)=1;
A2(10,5)=-1;
%%%Constraint Equation 11:  T7=T10;
A1(11,7)=1;
A2(11,11)=-1;
%%%Constraint Equation 12:  T7=T8;
A1(12,7)=1;
A2(12,8)=-1;
%Measured variables: W2  T1  T3  W4  T6  W7  T7  T9  W12  T12
%No.                 1  2   3   4   5   6   7   8    9    10

%VarName  W1 W3  T2  W6  T4  W5  W8   T8   W9   W10  T10  W11  T11 T5
%        1  2   3   4   5   6   7    8    9    10   11   12   13  14

%%%Constraint Equation 13:  W2*h2-W3*h3=W11*h11-W10*h10
A1(13,3)=-W2_nominal*Ch6(1); A2(13,2)=-H6;  %-W3*dT3-T3*dW3
```

```
A2(13,3)=W2_nominal*Ch1(1); A1(13,1)=H1;   %W2*dT2+T2*dW2
A2(13,13)=-0.5*W12_nominal*Ch12(1); A2(13,12)=-H12; %W11*dT11+T11*dW11
A2(13,11)=0.5*W7_nominal*Ch7(1); A2(13,10)=H7;%W10*dT10+T10*dW10
b(13)=0.5*W7_nominal*Ch7(1)*T7_nominal-0.5*W12_nominal*Ch12(1)*T12_nominal...
   +0.5*W1_nominal*Ch1(1)*T1_nominal-0.5*W6_nominal*Ch6(1)*T6_nominal;

%%%Constraint Equation 14:  W4*h4-W5*h5=W9*h9-W8*h8
A2(14,14)=-W4_nominal*Ch6(1); A2(14,6)=-H6;
A2(14,5)=W4_nominal*Ch1(1); A1(14,4)=H1;
A1(14,8)=-0.5*W12_nominal*Ch12(1); A2(14,9)=-H12;
A2(14,8)=0.5*W7_nominal*Ch7(1);A2(14,7)=H7;
b(14)=0.5*W7_nominal*Ch7(1)*T7_nominal-0.5*W12_nominal*Ch12(1)*T12_nominal...
   +0.5*W1_nominal*Ch1(1)*T1_nominal-0.5*W6_nominal*Ch6(1)*T6_nominal;


%%Constraint Equation 15:  W1*h1-W6*h6=W12*h12-W7*h7

A1(15,5)=-W6_nominal*Ch6(1); A2(15,4)=-H6;
A1(15,2)=W1_nominal*Ch1(1); A2(15,1)=H1;
A1(15,10)=-W12_nominal*Ch12(1); A1(15,9)=-H12;
A1(15,7)=W7_nominal*Ch7(1);A1(15,6)=H7;
b(15)=W7_nominal*Ch7(1)*T7_nominal-W12_nominal*Ch12(1)*T12_nominal...
   +W1_nominal*Ch1(1)*T1_nominal-W6_nominal*Ch6(1)*T6_nominal;

%Measured variables: W2  T1  T3  W4  T6  W7  T7  T9  W12  T12
%No.                1  2   3   4   5   6   7   8    9    10
%VarName  W1 W3  T2  W6  T4  W5  W8   T8   W9   W10  T10  W11  T11 T5
%       1  2   3   4   5   6   7    8    9    10   11   12   13  14
%%%Constraint Equation 15:  W1*h1-W3*h3-W5*h5=W12*h12-W7*h7

A1(16,3)=-0.5*W6_nominal*Ch6(1); A2(16,2)=-H6;
A2(16,14)=-0.5*W6_nominal*Ch6(1); A2(16,6)=-H6;
A1(16,2)=W1_nominal*Ch1(1); A2(16,1)=H1;
A1(16,10)=-W12_nominal*Ch12(1); A1(16,9)=-H12;
A1(16,7)=W7_nominal*Ch7(1);A1(16,6)=H7;
b(16)=W7_nominal*Ch7(1)*T7_nominal-W12_nominal*Ch12(1)*T12_nominal...
   +W1_nominal*Ch1(1)*T1_nominal-W6_nominal*Ch6(1)*T6_nominal;


%Measured variables: W2  T1  T3  W4  T6  W7  T7  T9  W12  T12
%VarName  W1 W3  T2  W6  T4  W5  W8   T8   W9   W10  T10  W11  T11 T5
XX=[W2_nominal, T1_nominal, T3_nominal, W4_nominal,T6_nominal, W7_nominal, T7_nominal, T12_nominal, W12_nominal,
T12_nominal];
UU=[W1_nominal, W2_nominal, T1_nominal,
W6_nominal,T1_nominal,W4_nominal,W7_nominal/2,T7_nominal,W7_nominal/2,W7_nominal/2,...
   T7_nominal,W12_nominal/2,T12_nominal,T5_nominal];

%%%
```

```
ru=rank(A2,1.0E-8);
[n,m]=size(A2);
[Q,R,E]=qr(A2);
ux=E'*u;
Qu1=Q(:,1:ru);
Ru1=R(1:ru,1:ru);
Ru2=R(1:ru,ru+1:end);
Qu2=Q(:,ru+1:end);
Gx=Qu2'*A1;

%the zero columns of Gx corresond to the variables that do not participate in the reconciliation, they are nonredundant.
%the remaining columns correspond to redundant measurements

u1=ux(1:ru);
u2=ux(ru+1:end); %unestimatable
%u1 satisfy u1=-inv(Ru1)*Qu1'*A1*x-inv(Ru1)*Ru2*u2
RIU=inv(Ru1)*Ru2;
%A variable in subset u1 is estimatable if the corresponding row in the RIU matrix is zero
%Otherwise, the variable in the subset is not estimable;



%%%
```

```
%%%
```

```
Gx0=Gx;
bx0=bx;


x=xm';
u=xu';
fprintf('Measured variables\n');
mm=length(x);
for i=1:1:mm
   fprintf('    %s    ',VarNam{x(i)});
end
fprintf('\n');
for jj=1:1:ndata
   for ii=1:1:mm
   fprintf(' %f',XmData(jj,ii));
   end
   fprintf('\n');
end

fprintf('Unmeasured variables\n');
nn=length(u1);
for i=1:1:nn
   fprintf('    %s    ',VarNam{u1(i)});
end
fprintf('\n');
for jj=1:1:ndata
   for ii=1:1:nn
   fprintf(' %f',XuData(jj,ii));
   end
   fprintf('\n');
end


%%%
```

```
    b222=[b111(1:i-1);b111(i+1:m)];
    phiu=diag(b222);
    phic=phim(i,i);
    phi=Au*phiu*Au'+Ac*phic*Ac';
    III=eye(length(Ac));
    phi_n_inv=inv(phi)*(III-Ac*inv(Ac'*inv(phi)*Ac)*Ac'*inv(phi));
    r=Gx0*Xgdata'-bx0;
    temp=r'*phi_n_inv*r;
    JJJ=[JJJ,temp];
end;
%%  End the serial elimination %%

fprintf('Measured variables\n');
mm=length(x);
for i=1:1:mm
    fprintf('     %s    ',VarNam{x(i)});
end
fprintf('\n');
    for ii=1:1:mm
    fprintf(' %f ',JJJ(ii));
    end
    fprintf('\n');

 KKK=JJJ./max(JJJ);

 figure;
 bar(KKK);
%%%
```

```
%% To determine the precision of the estimation  %%
Sigma0=phim;
Sigmac=-phim*Gx0'*inv(Gx0*phim*Gx0')*Gx0*phim;
Sigma_mb=inv(Pb'*inv(Gx0*phim*Gx0')*Pb);
Sigmab=-phim*Gx0'*inv(Gx0*phim*Gx0')*Pb*Sigma_mb*Pb'*inv(Gx0*phim*Gx0')*Gx0*phim;
Sigma=Sigma0+Sigmac+Sigmab;
fprintf('Precision     %f  %f  %f  %f  %f  %f  %f   %f   %f   %f\n', diag(Sigma));
```

Appendix 5 Matlab Code for HCSG Reconstruction PCA based FDI

```
close all;
%%%
```

```
    bvec(ni)=1;
    RPC=PC(:,np+1:m);
    aa=RPC*RPC'*bvec;
    aaa=aa'*covR*aa;
    bbb=(aa'*aa)^2;
    ccc=aaa/bbb;
    dd=PC(:,1:np)*PC(:,1:np)'*bvec;
    ddd=dd'*covR*dd;
    sum=sum+ccc/ddd;
bvec=zeros(m,1);
end;

FaultVar(np)=sum;
end;
%figure;
%plot(FaultVar);
%input('Number of PC for best fault reconstruction=%d');
nPC=find(FaultVar==min(FaultVar));
PCC=PC(:,1:nPC);
RPC=PC(:,nPC+1:m);

%%%
```

```
plot(TrainData(:,1),'b+');
%%%
```

```
figure(2);
plot(t2);
hold on;
line([0 ndata],[tlimit,tlimit]);
hold off;
[q]=qstat(zr,PC,nPC);
figure(3);
plot(q);
hold on;
line([0 ndata],[qlimit,qlimit]);
%%%
```

```
   IdentFreal{ni,nj}.Freal=Freal;
   fprintf ('%d %d\n',[ni,nj]);
   end;
end;
end;

fprintf('Dual fault isolation index\n');
for ni=1:1:m
   fprintf('%d  %f %f %f %f %f %f %f %f \n',[ni,SPEindex(ni,:)]);
end;

fprintf('Dual fault isolation index\n');
for ni=1:1:m
   fprintf('%d  %f %f %f %f %f %f %f %f \n',[ni,IdentRatio(ni,:)]);
end;
figure;
bar3(IdentRatio);

%%%
```

Appendix 6 Matlab Code for HCSG Hybrid PCA Based FDI

```
close all;
%%%
```

```
dzx2=X2;

idm=[1:3,5:8];
dzx2=dzx2(:,idm);
%dmx2=dmx2(idm);
%dstdx2=dstdx2(idm);
[PC,Latent,Explain]=pcacov(dzx2);
ns=1;
model2_PC=PC(:,1:ns);
qlx2=qlim(dzx2,ns);

%%%
```

```
%dzy1=zscore1(Y1,dmx1,dstdx1);
dzy1=Y1;

zy1=dzy1*model1_PC*model1_PC';
%Y1_pred=unscore(zy1,dmx1,dstdx1);
%figure (2);
%plot(Y1_pred(:,idf),'ro');
%hold on;
%plot(Y1_data(:,idf),'b+');

%dzy2=zscore1(Y2,dmx2,dstdx2);
dzy2=Y2;
zy2=dzy2*model2_PC*model2_PC';

idf1=find(idm==idf);

%Y2_pred=unscore(zy2,dmx2,dstdx2);
%figure (3);
%plot(Y2_pred(:,idf1),'r-');
%hold on;
%plot(Y2_data(:,idf1),'b-');

figure (1);
subplot(2,1,1);
plot(X1(:,4),X1(:,1),'r');
hold on;
plot(zr0(1:2:end,4),zr0(1:2:end,1),'b*');
xlabel('Feed water flow rate (scaled)');
ylabel('SG primary outlet temperature (scaled)');

subplot(2,1,2);
plot(X1(:,4),X1(:,6),'r');
hold on;
plot(zr0(1:2:end,4),zr0(1:2:end,6),'b*');
xlabel('Feed water flow rate (scaled)');
ylabel('SG steam outlet temperature (scaled)');

figure (2);
resz=(zy1-dzy1);
SPE=[];
for idk=1:ndata
ttt=resz(idk,:)*resz(idk,:)';
SPE=[SPE;ttt];
end;
subplot(2,1,1);
plot(SPE);
resz=(zy1-dzy1);
reszw=resz.^2;
subplot(2,1,2);
bar(reszw(ndata,:)');
figure (3);
resz=(zy2-dzy2);
```

```
SPE=[];
for idk=1:ndata
ttt=resz(idk,:)*resz(idk,:)';
SPE=[SPE;ttt];
end;
subplot(2,1,1);
plot(SPE);
hold on;
line([0 ndata],[qlx2,qlx2]);
hold off;


reszw=resz.^2;
subplot(2,1,2);
bar(reszw(ndata,:)');
```

Appendix 7 Matlab Code for HCSG Robust Data Driven Model based FDI for Steady State Operation Conditions

```
close all;
%%%
```

```
BB=zeros(msm_output,msm_input);
BB(1,1)=b1';
BB(2,1)=b1';
BB(3,1)=b1';
BB(4,1)=1.0;
BB(5,1)=1.0;
BB(6,1)=b2';
BB(7,1)=b2';
BB(8,1)=b2';
%%%
```

```
AAA=WWt*WWt';
BBB=Mt*Mt';

 [VE,DE]=eig(AAA,BBB,'qz');
ccc=abs(diag(DE));
ddd=sort(ccc);
idhg=find(abs(diag(DE))<1.0E-10);
mmk=length(idhg);

Omega=[];
for ijj=1:1:mmk
npp=find(ccc==ddd(ijj));
if(ccc(npp)>1.0E-10) fprintf('warning\n'); end;
bbb=VE(:,npp);
bbb=bbb/norm(bbb);
Omega=[Omega,bbb];
end;
BBB=orth(Omega);

err=[];
for jjk=1:1:ntest
xtest=zv0(jjk,:);
eee=BBB'*zv0(jjk,:)';
spde=eee'*eee;
err=[err;spde];
end;
figure;
plot(err);
title('Fault Detection without disturbance decoupling');

Ef=eye(mSensor);
Wt=BB;
Mt=Ef;
%Rsv=kron(eye(s+1),Rv);
%Rsd=kron(eye(s+1),Rd);
%Rso=kron(eye(s+1),Ro);
%Rphi=H*Rsv*H'+G*Rsd*G'+Rso;
WWt=[Wt Dbvec];
AAA=WWt*WWt';
BBB=Mt*Mt';

[VE,DE]=eig(AAA,BBB,'qz');
ccc=abs(diag(DE));
ddd=sort(ccc);
idhg=find(abs(diag(DE))<1.0E-10);
mmk=length(idhg);
Omega=[];
for ijj=1:1:mmk
npp=find(ccc==ddd(ijj));
if(ccc(npp)>1.0E-10) fprintf('warning\n'); end;
bbb=VE(:,npp);
bbb=bbb/norm(bbb);
```

```
Omega=[Omega,bbb];
end;
BBB=orth(Omega);

err=[];
for jjk=1:1:ntest
xtest=zv0(jjk,:);
eee=BBB'*zv0(jjk,:)';
spde=eee'*eee;
err=[err;spde];
end;
figure;
plot(err);
title('Fault Detection with disturbance decoupling');

Ef=eye(mSensor);
mhk=1:1:mSensor;
ErrPlot=[];
for ikk=1:1:mSensor
Wt=BB;
Vt=Ef(:,ikk);
isk=find(mhk~=ikk);
Mt=Ef(:,isk);
%Rsv=kron(eye(s+1),Rv);
%Rsd=kron(eye(s+1),Rd);
%Rso=kron(eye(s+1),Ro);
%Rphi=H*Rsv*H'+G*Rsd*G'+Rso;
WWt=[Wt Vt Dbvec];
AAA=WWt*WWt';
BBB=Mt*Mt';

 [VE,DE]=eig(AAA,BBB,'qz');
ccc=abs(diag(DE));
ddd=sort(ccc);
idhg=find(abs(diag(DE))<1.0E-10);
mmk=length(idhg);

Omega=[];
for ijj=1:1:mmk
npp=find(ccc==ddd(ijj));
if(ccc(npp)>1.0E-10) fprintf('warning\n'); end;
bbb=VE(:,npp);
bbb=bbb/norm(bbb);
Omega=[Omega,bbb];
end;
BBB=orth(Omega);

err1=[];
for jjk=1:1:ntest
xtest=zv0(jjk,:);
eee=BBB'*zv0(jjk,:)';
spde=eee'*eee;
```

```
err1=[err1;spde];
end;
ErrPlot=[ErrPlot,err1];
end;

figure;
for ilk=1:1:mSensor
subplot(4,2,1);
plot(ErrPlot(:,1));
ylabel('Res. Gen.dedicated to Signal 1');
subplot(4,2,2);
plot(ErrPlot(:,2));
ylabel('Res. Gen.dedicated to Signal 2');

subplot(4,2,3);
plot(ErrPlot(:,3));
ylabel('Res. Gen.dedicated to Signal 3');
xlabel ('sample');

subplot(4,2,4);
plot(ErrPlot(:,4));
ylabel('Res. Gen.dedicated to Signal 4');
xlabel ('sample');

subplot(4,2,5);
plot(ErrPlot(:,5));
ylabel('Res. Gen.dedicated to Signal 5');
xlabel ('sample');

subplot(4,2,6);
plot(ErrPlot(:,6));
ylabel('Res. Gen.dedicated to Signal 5');
xlabel ('sample');


subplot(4,2,7);
plot(ErrPlot(:,7));
ylabel('Res. Gen.dedicated to Signal 5');
xlabel ('sample');

subplot(4,2,8);
plot(ErrPlot(:,8));
ylabel('Res. Gen.dedicated to Signal 5');
xlabel ('sample');
end;
```

Appendix 8 Matlab Code for HCSG Robust Data Driven Model based FDI for Dynamic Operation Conditions

```
close all;
%%%
```

```
end;

%NormalData=dlmread('MVarNormalData_simm.txt',' ');
[nlen,m]=size(NormalData);
nstart=600;
nlen=2000;
%rawDataP=NormalData(n-1000:1:n,index);
rawDataP=NormalData(1:1:end,[indexout indexinp]);
[n,m]=size(rawDataP);
%rawDataP(nstart:nlen,iii)=rawDataP(nstart:nlen,iii)+mean(rawDataP(:,iii))*0.01;
rawDataP(nstart:nlen,iii)=rawDataP(nstart:nlen,iii);
%[1,2,3,9,6];
GGG1=eye(Nc);
GGG2=zeros(Nc,Nc);
%Thy=[GGG1(:,[1,2,3]),GGG2(:,[4,5])];
Thy=GGG1;
WWW1=eye(Nb);
WWW2=zeros(Nb,Nb);
%Thu=[WWW1(:,[1,2,3]),WWW2(:,[4,5])];
Thu=WWW1;

fff=[];
ggg=[];
for k=nbb+1:1:nlen
   V1=[];
   JJ=[];
   zv=zscore1(rawDataP(k-nbb:1:k,:),meanx,stdx);
   [V1,JJ,eee,Ps]=resgen_noi_mod1(A,B,C,D,zv,Nc,Nb,nbb,V1,JJ,Thu,Thy);
   fff=[fff,eee];
   ggg=[ggg,norm(eee)];
end;
gama=0.90;
ntrain=400;
Rse=1/ntrain*fff(:,1:ntrain)*fff(:,1:ntrain)';
eta=emwa(fff,gama,Rse,nbb,nx,ny,ntrain,nlen);
figure(1)
subplot(2,1,1);
plot(rawDataP(nbb+1:nlen,2));
ylabel('steam pressure (Mpa)');
subplot(2,1,2);
plot(eta);
ylabel('fault detection index');
xlabel('sample');

figure(2);
for iii=1:1:Nc+Nb;
GGG1=eye(Nc);
GGG2=zeros(Nc,Nc);
%Thy=[GGG1(:,[1,2,3]),GGG2(:,[4,5])];
WWW1=eye(Nb);
WWW2=zeros(Nb,Nb);
if iii<=Nc
```

```
%Thu=[WWW1(:,[1,2,3]),WWW2(:,[4,5])];
Thy1=[GGG1(:,1:1:iii-1),GGG2(:,iii),GGG1(:,iii+1:1:end)];
Thu1=WWW1;
Thy2=[GGG2(:,1:1:iii-1),GGG1(:,iii),GGG2(:,iii+1:1:end)];
Thu2=WWW2;
else
iis=iii-Nc;
Thy1=GGG1;
Thu1=[WWW1(:,1:1:iis-1),WWW2(:,iis),WWW1(:,iis+1:1:end)];
Thy2=GGG2;
Thu2=[WWW2(:,1:1:iis-1),WWW1(:,iis),WWW2(:,iis+1:1:end)];
end;

fff=[];
ggg=[];
for k=nbb+1:1:nlen
   V1=[];
   JJ=[];
   zv=zscore1(rawDataP(k-nbb:1:k,:),meanx,stdx);
   [V1,JJ,eee,Ps]=resgen_noi_mod3(A,B,C,D,zv,Nc,Nb,nbb,V1,JJ,Thu1,Thy1,Thu2,Thy2);
   fff=[fff,eee];
   ggg=[ggg,norm(eee)];
end;
gama=0.90;
ntrain=400;
Rse=1/ntrain*fff(:,1:ntrain)*fff(:,1:ntrain)';
eta=emwa(fff,gama,Rse,nbb,nx,ny,ntrain,nlen);
subplot(5,2,iii);
plot(eta);
ylabel(['variable ', int2str(iii)]);
if iii==9 | iii==10 xlabel('sample'); end;
end;

%%%
```

```
  Ht=[];
  Wt=[];
  Lt=[];
  Mt=[];
  Gt=[];
  for ii=s:-1:0   %loop over stack
  y=[y;outputy(s-ii+1,:)'];  %stacked output vector with dimension=number of outputs*(stack number+1)
  u=[u;inputx(s-ii+1,:)'];   %stacked input vector with dimension=number of inputs*(stack number+1)
  Wt=[Wt;C*A^(s-ii)];   %extended observability matrix with dimension=number of outputs*(stack number+1) by number of states
  Lrow=[];
  Mrow=[];
  Hrow=[];
  Grow=[];
  irow=s-ii+1;
  for jcol=1:1:s+1
     if irow>jcol
        irow1=irow-2;
     Hrow=[Hrow,(C*A^(irow1-jcol+1))*B];
     Grow=[Grow,(C*A^(irow1-jcol+1))*Bp];
%     Lrow=[Lrow,(C*A^(irow1-jcol+1))*E1];
%     Mrow=[Mrow,(C*A^(irow1-jcol+1))*R1];

     elseif irow<jcol
     Hrow=[Hrow,zeros(nd,md)];
     Grow=[Grow,zeros(nd,nx)];
%     Lrow=[Lrow,zeros(ncc,me)];
%     Mrow=[Mrow,zeros(ncc,mf)];

     elseif irow==jcol
     Hrow=[Hrow,D];
     Grow=[Grow,Dp];
%     Lrow=[Lrow,E2];
%     Mrow=[Mrow,R2];
     end;
  end;
  Ht=[Ht;Hrow];   %Extended Hankel matrix with dimension= number of outputs*(stack number+1) by number of inputs*(stack
number+1)
  Gt=[Gt;Grow];
%  Lt=[Lt;Lrow];
%  Mt=[Mt;Mrow];
end;
H=Ht;
G=Gt;
Hbar=[eye(Nc*(s+1)),-H];
Th11=kron(eye(s+1),Thy1);
Th12=zeros(Nc*(s+1),(s+1)*Nb);
Th21=zeros(Nb*(s+1),(s+1)*Nc);
Th22=kron(eye(s+1),Thu1);
ThetaP1=[Th11,Th12;Th21,Th22];
Mt=Hbar*ThetaP1;
Th11=kron(eye(s+1),Thy2);
Th12=zeros(Nc*(s+1),(s+1)*Nb);
```

```
Th21=zeros(Nb*(s+1),(s+1)*Nc);
Th22=kron(eye(s+1),Thu2);
ThetaP2=[Th11,Th12;Th21,Th22];
Vt=Hbar*ThetaP2;

%Rsv=kron(eye(s+1),Rv);
%Rsd=kron(eye(s+1),Rd);
%Rso=kron(eye(s+1),Ro);
%Rphi=H*Rsv*H'+G*Rsd*G'+Rso;
WWt=[Wt Vt];
Rphi=eye(Nc*(s+1));
Rphio=chol(Rphi);
AAA=WWt*WWt';
BBB=Mt*Mt';
[VE,DE]=eig(AAA,BBB,'qz');
ccc=abs(diag(DE));
ddd=sort(ccc);
Omega=[];
for ijj=1:1:(Nc-1)*(s+1)-nx
npp=find(ccc==ddd(ijj));
if(ccc(npp)>1.0E-10) printf('warning\n'); end;
bbb=VE(:,npp);
bbb=bbb/norm(bbb);
Omega=[Omega,bbb];
end;
BBB=orth(Omega);
WWW=BBB'*inv(Rphio');
eee=WWW*Hbar*[y;u];
Ps=WWW*Hbar;
%Rse=WWW*Rphi*WWW';
%optresd=eee'*inv(Rse)*eee;
optresd=eee;
return;
```

Vita

Ke Zhao was born in Sichuan, China on May 3,1969. He received the Bachelor of Science degree in Physics at Sichuan University, China, in July 1989, and the Master of Science degree in Nuclear Engineering at the University of Tennessee, Knoxville, USA, in November 2002.

In July 1989, Ke Zhao was employed by Nuclear Power Institute of China. He became an engineer in radiation safety and environmental influence assessment in 1994. He was promoted to be a senior engineer in reactor safety analysis and probabilistic risk assessment in 1998. He did research on failed fuel behavior analysis in Atomic Energy Commission, Cadarache, France, from July 1998 to February 1999.

Ke Zhao came to the United States and entered The University of Tennessee as a graduate student in Nuclear Engineering Department in August 2000. He is advised by Dr. B.R. Upadhyaya in the field of reactor simulation, control, and fault diagnosis.

During the graduate study, K. Zhao completed the following publications:

[1] K. Zhao and B. R. Upadhyaya, "Robust Subspace Based Dynamic Fault Diagnosis of IRIS Helical Coil Steam Generator Systems," Nuclear Technology (submitted), 2004.

[2] K. Zhao and B. R. Upadhyaya, "Adaptive Fuzzy Inference Causal Graph Approach to Fault Diagnosis of Nuclear Power Plants," Progress in Nuclear Energy, 2005.

[3] A. Sawyer, M. Williamson, K. Zhao, and A. Ruggles, "RELAP5-3D Validation Study using MB-2 Prototypical Steam Generator Steady State Data," Nuclear Technology (Accepted), 2004.

[4] B.R. Upadhyaya and K. Zhao, "Thermal-Hydraulic Analysis of a Helical Coil Steam Generator for Level Monitoring," ANS Transaction, 2003:

[5] M.G. Na, Y.R. Sim, K.H. Park, B.R. Upadhyaya, K.Zhao, and B.Lu, "Sensor Monitoring using a Fuzzy Neural Network with an Automatic Structure Constructor," IEEE Transactions on Nuclear Science, 50, 241-250, 2003.

[6] B.R. Upadhyaya, K. Zhao, and B. Lu, "Fault Monitoring of Nuclear Power Plant Sensors and Field Devices," Progress in Nuclear Energy, Vol. 43, pp. 337-342, 2003.

[7] M.G. Na, Y.R. Sim, K.H. Park, B.R. Upadhyaya, B. Lu, and K. Zhao, "Failure Detection using a Fuzzy Neural Network with an Automatic Input Selection Algorithm," Power Plant Surveillance and Diagnotics, (ed) D. Ruan and P.F. Fantoni, Springer, 221-242, 2002.

[8] K. Zhao and B.R. Upadhyaya, "Design of a Fault Diagnosis System for Next Generation Nuclear Power Systems," Proceeding of ICAAP Conference, Pittsburgh, 2004.

[9] K. Zhao and B.R. Upadhyaya, "A Hybrid PCA Approach to Joint Sensor and Process Fault Diagnosis," Proceeding of NPIC Conference, Columbus, 2004.

[10] K. Zhao, B.R. Upadhyaya, and R. T. Wood, "Data reconciliation and Gross Error Detection for IRIS Helical Coil Steam Generators," Transactions of the American Nuclear Society, 2004.

[11] K. Zhao, B.R. Upadhyaya, and R. T. Wood, "Modeling and Fault Detection and Isolation of IRIS Helical Coil Steam Generators," Proceedings of Global 2003, pp. 2059-2068, New Orleans, November 2003.

[12] B.R. Upadhyaya and K. Zhao, "Robust Techniques for Monitoring and Fault Diagnosis of IRIS Helical Coil Steam Generators," GENES4/ANP2003, Kyoto, Japan, September 2003,

[13] B.R. Upadhyaya, K. Zhao, B. Lu, J.M. Doster, M.G. Na, Y.R. Sim, and K.H. Park, "Nuclear Plant System Monitoring Under Process Transients and Multiple Fault Conditions," Transactions of the American Nuclear Society, Vol. 86, pp. 482-484, June 2002.

[14] B.R. Upadhyaya, K. Zhao, B. Lu, and M. Doster, "Fault Detection and Isolation of Sensors and Actuators in a Nuclear Plant Steam Generator," Transactions of the American Nuclear Society, Vol. 85, pp. 350-351, November 2001.